SCALING TEMPERATURE DEPENDENCE OF DISEASE DYNAMICS FROM INDIVIDUALS TO POPULATIONS

by

JAMES EDWARD NOELKER

A dissertation submitted in partial fulfillment of the
requirements for the degree of

DOCTOR OF PHILOSOPHY IN BIOLOGICAL AND BIOMEDICAL SCIENCE

2025

Oakland University
Rochester, Michigan

Doctoral Advisory Committee:

Thomas R. Raffel, Ph.D., Chair
Scott D. Tiegs, Ph.D.
Bruce Pell, Ph.D.

For Angela and Oliver.

ACKNOWLEDGEMENTS

To my advisor, Dr. Thomas Raffel, thank you for bringing me into your lab and for your advice, guidance, and mentorship during my doctoral studies. I have learned so much during my time in your lab and have grown personally and as a scientist.

To my committee members, Dr. Scott Tiegs and Dr. Bruce Pell, thank you for your guidance and support during my doctoral studies these last five years.

To all my past and present graduate student colleagues in the Raffel Lab, Dr. Jason Sckrabulis, Dr. Hunter Craig, Vitoria Abreu Ruozzi, Andrea Nadjarian, Travis Multhaupt, and Sergio Bermudez, thank you for your advice, support, and friendship. To all the undergraduate students without whom this work would not have been possible, thank you. I especially thank Jacob Heabeart, Kyle Spengler, Lutfi Abu-Shanab, Faris Mahjoub, Declan McCrary, Besjana Ahmetaj, Sebastian Taulbee, Gina Ghose, Vanessa Six, Alejandro Pimentel Hernandez, Margaret Marchioni, Alana Sandomierski-Stellman, Onil Potris, and Fareha Hossain. To Mark Vassallo and Michael Andrus at Detroit Zoo, thank you for your support and assistance. To the Oakland University Department of Biological Sciences faculty and staff for their support and assistance.

Thank you to Angela and Oliver, with all my love, and to my parents-in-law for your continuous love and support.

Funding for this work was provided by the National Science Foundation (IOS-1651888) and Oakland University's Provost Graduate Student Research award.

James Edward Noelker

ABSTRACT

SCALING TEMPERATURE DEPENDENCE OF DISEASE DYNAMICS FROM INDIVIDUALS TO POPULATIONS

By

James Edward Noelker

Advisor: Thomas R. Raffel, Ph.D.

There is growing interest among ecologists to develop mechanistic models that can generate generalizable predictions across multiple levels of biological organization. A key question is whether and how host and parasite contributions to infection can be disentangled, and to what degree these separate contributions affect population level transmission dynamics. The Metabolic Theory of Ecology (MT) provides a framework to investigate physiological processes such as metabolism, reproductive rates, host defenses, and parasite infectivity. The amphibian fungal pathogen *Batrachochytrium dendrobatidis* (Bd) is a popular host-parasite system to experimentally investigate temperature dependent infection dynamics. In Chapter 2, I validated methods for decontaminating nitrile and cotton gloves after handling Bd infected *Xenopus laevis*. In Chapter 3, I conducted two Bd infection experiments to quantify temperature-dependent infection on individual *X. laevis* and found persistent acclimation effects and increased infection loads on frogs following a drop in temperature, consistent with the Temperature Variability Hypothesis (TVH). In Chapter 4, I quantified MT-based thermal performance curves (TPC) to estimate a key metabolic parameter (activation energy, E_A) for 60 amphibian

species, allowing me to investigate taxonomic and environmental predictors of species specific E_A. Temperate species had wider thermal breadths than tropical species and E_A was positively correlated with mean environmental temperature within order Caudata, consistent with the Climate Variability Hypothesis (CVH). To test whether MT-based thermal mismatch models can successfully describe individual infections, I built and parameterized models using independent proxies for host and parasite metabolic performance. These models successfully captured the individual infection dynamics observed in Chapter 3 and provided new insights into the thermal biology of this infection. To investigate population-level transmission dynamics, I conducted a controlled temperature outdoor mesocosm Bd transmission experiment with small populations of *X. laevis* and tracked infections via weekly skin swabs (Chapter 6). Frog populations at 10 °C had dramatically higher infection loads compared to individually housed frogs at the same temperature. In Chapter 7, I developed and fully parameterized an Individual Based Model (IBM) that nested individual level MT-based mismatch models within population level transmission dynamics, successfully predicting the higher infection loads and mortality rates observed in the population level experiment.

TABLE OF CONTENTS

LIST OF TABLES

LIST OF TABLES – Continued

LIST OF FIGURES

LIST OF ABBREVIATIONS

AccTemp	Acclimation temperature
AIC	Akaike Information Criterion
ASW	Artificial spring water
BA	Boltzmann-Arrhenius
Bd	*Batrachochytrium dendrobatidis*
Bsal	*Batrachochytrium salamandrivorans*
B_{T0}	Metabolic performance at a standardization temperature
B_{10}	Metabolic performance at 10 °C
B_{20}	Metabolic performance at 20 °C
B_{30}	Metabolic performance at 30 °C
BSA	Bovine serum albumin
Bsal	*Batrachochytrium salamandrivorans*
CT_{max}	Critical thermal maximum
CT_{min}	Critical thermal minimum
CVH	Climate variability hypothesis
DayOfExpo	Exposure Day
DNA	Deoxyribonucleic acid
DT	Daily switch temperature treatment
c.i.	Confidence interval
df	Degrees of freedom
E_A	Activation energy

E_p	Activation energy for a given performance metric
E_p^H	High temperature deactivation energy
E_p^L	Low temperature deactivation energy
HI	High temperature treatment
IACUC	Institutional Animal Care and Use Committee
IBC	Institutional Biosafety Committee
IBM	Individual based model
IPM	Integral projection model
IRB	Institutional Review Board
JOAT	Jack-of-all-temperatures hypothesis
k	Boltzmann constant
LnBdLoad	log Bd load
LnFilterBd.rate	log Bd load from filters for zoospore production
LnSwabBd	log Bd load from skin swabs
LO	Low temperature treatment
LORACS	Laboratory for Outdoor Research Agriculture Conservation & Sustainability
MD	Middle temperature treatment
MT	Metabolic Theory
MTE	Metabolic Theory of Ecology
na	Not applicable
NaOCl	Sodium hypochlorite

NSF	National Science Foundation
O_2	Oxygen
ODE	Ordinary differential equation
OU	Oakland University
qPCR	Quantitative polymerase chain reaction
PDE	Partial differential equation
PerfTemp	Performance temperature
P_{T0}	Performance rate
R1	Short-time random switch temperature treatment
R2	Long-time random switch temperature treatment
s.d.	Standard deviation
s.e.	Standard error
SIR	Susceptible-infected-recovered
SS	Sharpe-Schoolfield
SVL	Snout-vent length
TimeSinceExposure	Time since exposure
T_{opt}	Thermal optimum
TPC	Thermal performance curve
T_P^H	High temperature for enzyme deactivation
T_P^L	Low temperature for enzyme deactivation
TVH	Temperature Variability Hypothesis
Z_e	Zoospore equivalent

CHAPTER ONE

BACKGROUND AND SIGNIFICANCE

1.1 Introduction

Climate change will inevitably have dramatic effects on ecosystems and species distributions, leading to changes in species interactions with potentially dramatic effects on host-parasite interactions and disease (Gehman et al., 2018; Lafferty, 2009; J. Li et al., 2024). Climate change could also affect the health of individual organisms as well as the stability of populations due to shifts in mean temperatures and changes in temperature variability (Cohen et al., 2020; Epstein, 2001; Lafferty, 2009; Raffel et al., 2013). Ectotherms are especially sensitive to changes in environmental temperature because they allow their body temperatures to vary with external conditions, resulting in direct effects of temperature on physiological processes (Brattstrom & Lawrence, 1962; Feder & Burggren, 1992). Many ectotherms respond to temperature fluctuations with adaptive plasticity (i.e., thermal acclimation responses; Bower et al., 2019; Raffel et al., 2013, 2015; Rohr et al., 2013). Both temperature and thermal acclimation responses of hosts can have important effects on parasitic infections (S. E. Greenspan et al., 2017; Raffel et al., 2006, 2013). Current modeling approaches to describe ectotherm infections often use phenomenological descriptions of temperature dependent infections, rather than describing temperature dependence of host and parasite thermal responses as separate thermal performance curves (Cohen et al., 2020; Kirk et al., 2022; Rohr et al., 2013). An important question is, can we develop more mechanistic models to predict changing patterns of climate-disease interactions based on processes that occur at lower scales of

biological organization (i.e., scaling from molecular to organismal scales or from organismal to population scales; (Kirk et al., 2022; Wilber et al., 2021))?

Thermal performance curves (TPC) based on the Metabolic Theory of Ecology (MTE) can help bridge the gap from molecular to organismal processes by using equations derived from enzyme kinetics (J. H. Brown et al., 2004; Dell et al., 2011). Metabolic theory (MT)-based thermal mismatch models, as proposed by Rohr et al. (2013), provide a potential pathway for disentangling the contributions of host and parasite in the infection process (Sckrabulis et al., 2022). Individual based models can then be used to scale from infection dynamics within individual hosts up to transmission dynamics in host populations (Briggs et al., 2005, 2010).

In this dissertation, I use chytridiomycosis in amphibians as a model system to explore the use of MT-based thermal mismatch models to describe ectotherm infections, scaling from molecular to population scales.

1.2 Study system

The amphibian disease chytridiomycosis is an extensively studied skin disease of amphibians caused by the fungal pathogen *Batrachochytrium dendrobatidis* (Bd) (Blaustein et al., 2018; Bower et al., 2017; Fisher et al., 2009; Longcore et al., 1999; Searle et al., 2011; Stuart et al., 2004; Van Rooij et al., 2015; Voyles et al., 2009) or its relative *Batrachochytrium salamandrivorans* (Bsal; Martel et al., 2013). First described by Longcore et al. (1999), Bd is responsible for declines and extinctions of amphibian populations around the globe (Stuart et al., 2004; Voyles et al., 2009). Bd is a microparasite, meaning the pathogen can reproduce within a single host (Anderson & May, 1979; Longcore et al., 1999; Van Rooij et al., 2012; Voyles et al., 2009), or in this

instance on the surface of a single host's skin (Van Rooij et al., 2012). Bd's potential for within-host reproduction can result in a variety of temperature dependent outcomes affecting both the health of the infected host and transmission dynamics via the zoospore, Bd's infectious stage (Van Rooij et al., 2012; Vredenburg et al., 2010). The disease dynamics unique to individual and population level dynamics make chytridiomycosis a prime study system for investigating and modeling the differences between these two scales (Kirk et al., 2022; Wilber et al., 2016).

The experiments for my dissertation used the Bd strain JEL423 originally isolated from *Peltophryne lemur* in Guabal, Panama (Farrer et al., 2011) and is part of the global pandemic lineage of chytrid (Farrer et al., 2011). The host system I used is the fully aquatic the African clawed frog, *Xenopus laevis*, native to temperate regions of southern Africa (Weldon et al., 2004). This host species is valuable to many fields of research as a model organism and is useful here due to its susceptibility to and tolerance of Bd infection (Van Rooij et al., 2012; Weldon et al., 2004). Introduced populations of *X. laevis* frogs are known to serve as a reservoir species for Bd (Fisher & Garner, 2007; Van Rooij et al., 2015). *X. laevis'* tolerance of Bd infection allows for better long-term observations and measurements of infection loads within populations for lengths of time that might otherwise kill the host before the population dynamics of the disease transmissibility are revealed (Cohen et al., 2017; Weldon et al., 2004). A common approach to studying temperature effects on disease in individual amphibians is to conduct laboratory experiments measuring the time course of infection load at different temperatures following a discrete exposure event (Andre et al., 2008; Bradley et al., 2019; Cohen et al., 2017; Raffel et al., 2013, 2015). Other studies have investigated

temperature dependence of infection at population scales by conducting field studies of prevalence or mean infection load in areas with different environmental temperatures (Bosch et al., 2007; Carvalho et al., 2024; Cohen et al., 2020; K. M. Kriger et al., 2007). However, comparing post-exposure dynamics of infection in a controlled temperature experiment to observations of infection in field studies is like comparing apples to oranges, especially when the variables quantified (i.e., infection load versus infection prevalence) are not directly comparable. Although other studies have investigated experimental chytridiomycosis transmission dynamics at a single temperature (Malagon et al., 2020), my dissertation uses controlled temperature experiments at multiple spatial scales to directly compare temperature dependence of individual infection dynamics to population level transmission dynamic. The fully aquatic *X. laevis* species was useful for my experimental designs because it allowed me to house individual frogs and populations of hosts in similar fully aquatic conditions (see Chapters 3 and 6). A unified, controlled temperature experimental approach allowed me to compare similar temperature conditions for individuals and small populations of the same species (and similar ages) of frogs. This allowed me to develop and validate models that provide a more mechanistic description of how temperature affects Bd infection dynamics at individual (within-host) and population (among-host transmission) scales (see Chapters 5 and 7).

1.3 Reducing waste and ensuring data integrity in experimental infections

To investigate effects of climate change on ecological systems, scientists are in need of experimental studies at multiple scales that can help to establish causality for the effects of temperature on disease dynamics (Kirk et al., 2022). One important aspect of these studies is the need to reduce waste and minimize resource utilization while still

maintaining rigorous standards for sample collection throughout such empirical studies. A major source of waste during such studies is frequent changing of disposable gloves. In prior studies, researchers typically changed gloves between every animal despite this leading to excessive waste (Gray et al., 2017). One potential solution is to validate methods for glove reuse by sanitizing gloved hands after handling individual frogs (S. Cashins et al., 2008; Gray et al., 2017; Raffel et al., 2013, 2015). Furthermore, disposable gloves can be slippery and provide inadequate grip when handling aquatic organisms. To address these issues, Chapter 2 of my dissertation is an experimental validation of glove decontamination techniques. In this study, we tested the efficacy of sanitizing nitrile gloves using either ethanol or bleach rinse, conducting a series of two experiments to validate methods for glove decontamination after handling individual animals. We also validated a previously untested cotton glove approach to improving grip on slippery frog species. These methods expedited animal swabbing times and reduced glove waste while retaining rigorous standards for preventing cross contamination between individuals. Results from this chapter were published in the journal *Diseases of Aquatic Organisms* (J. E. Noelker, Abreu Ruozzi, Craig, et al., 2024).

1.4 Effects of thermal acclimation and temperature variability on individual Bd infections

With climate change altering temperature variability in addition to increased mean temperatures, it is important to determine if sudden temperature shifts have effects on infection dynamics that couldn't be predicted based solely on mean temperature experiments. The temperature variability hypothesis of Rohr and Raffel (2010) postulates that parasitism and disease will increase in variable-temperature environments, due to parasites acclimating to new temperatures more quickly than hosts following sudden

shifts in temperature (Raffel et al., 2013; Rohr & Raffel, 2010). This hypothesis assumes that host acclimation to a new temperature takes time, during which the parasite might have an advantage (Raffel et al. 2013). The infection dynamics that occur on individual hosts exposed to parasite infection immediately following a temperature shift have been studied in several species including Bd in juvenile eastern newts (*Notophthalmus viridescens*; Raffel et al., 2015), adult Cuban treefrogs (*Osteopilus septentrionalis*; (Raffel et al., 2013), and spring peepers (*Pseudacris crucifer*; Altman, 2018), green frog tadpoles (*Lithobates clamitans*; Altman & Raffel, 2019) and *Ribeiroia ondatrae* infection in green frog tadpoles (*L. clamitans*; Altman et al., 2016). These studies were designed to investigate the effects of past (acclimation) temperature, after a shift to a new (performance) temperature. However, these studies all exposed their amphibian hosts to parasite infection immediately within hours after the temperature shift, to detect effects of a host's past acclimation status before they become fully acclimated to the new temperature. Less is known about chytridiomycosis disease outcomes for hosts exposed to Bd multiple days before or after a shift in temperature, and timing-of-exposure experiments would be useful to help determine how long it takes for host anti-parasite resistance to become fully acclimated following a temperature shift. In Chapter 3, I tested for thermal acclimation effects on Bd infection in individual *X. laevis*, including timing of exposure treatments to investigate the timing of thermal acclimation responses. I conducted a series of two experiments in 2021 (experiment 1) and 2022 (experiment 2). For each experiment, my team and I designed fully replicated individual infection experiments where frogs were housed at one of two acclimation temperatures (10 or 20 °C for experiment 1 and 10, 15, or 20 °C for experiment 2) and then shifted to a new,

performance temperature (10, 15, 20, or 25 °C). In experiment 1, I also included a timing-of-exposure treatment where frogs were exposed to Bd zoospore either one week before the temperature shift, on the day of, or one week after the temperature shift. These experiments add to the number of species testing the temperature variability hypothesis first described by Rohr & Raffel (2010). These experiments were successfully published in the journal *Royal Society Open Science* (J. E. Noelker, Abreu Ruozzi, Spengler, et al., 2024).

1.5 Scaling metabolic performance from molecules to individual organisms

An interesting research question among ecologists is whether and how molecular processes can be scaled up to predict whole organism performance or fitness under different conditions (Allen & Gillooly, 2007; J. H. Brown et al., 2004; Dell et al., 2013; Stark et al., 2024). Metabolic Theory of Ecology (MTE) has been proposed as one potential mechanistic framework for scaling molecular processes up to the organism (Allen & Gillooly, 2007; J. H. Brown et al., 2004). How mechanistic MTE-based models truly are has been questioned by O'Connor et al. (2007), who point out that MTE use of Boltzmann relationships to model physiological variables (i.e., a metabolic proxies) may be an oversimplification of biochemical pathways and that the models themselves are statistically fit to the observed patterns and not fully rooted in biologically meaningful mechanisms. However, MTE still provides a useful framework for trying to understand the mechanistic underpinnings of organism TPC's. One physiological trait that can be measured across a range of temperatures is an organism's rate of whole body oxygen (O_2) consumption, which provides arguably the most direct measurement of metabolic rate for aerobic organisms (Dell et al., 2011; McWhinnie et al., 2021).

There are many types of mathematical models that can be used to describe the thermal performance curve (TPC) of an organism (Angilletta, 2006; DeLong et al., 2017; Molnár et al., 2013, 2017; Mordecai et al., 2013). Angilletta (2006) reviewed several modeling approaches that can be used to describe species' thermal performance curves (e.g., quadratic, Gaussian, and others). While these models are useful in describing the phenomenological shape of any number response variables, they lack specific mechanistic ties to physiological processes such as metabolism (Angilletta, 2006; Molnár et al., 2017). Additionally, some phenomenological models such as quadratic and Gaussian curves do not have the flexibility to capture some of the more typical data patterns observed in physiological processes, such as the typical leftward skew of empirical TPC's for most organisms. Many of these models are phenomenological and as such do not generate biologically meaningful parameter values that could lead to generalizable insights into the mechanisms underlying species performance (Molnár et al., 2017). MT-based models of thermal performance, such as the Boltzmann-Arrhenius (BA) equation (Arrhenius, 1889) and the more complex Sharpe-Schoolfield (SS) equation (Schoolfield et al., 1981), were originally developed to model temperature dependence of enzyme-assisted chemical reactions. The BA and SS frameworks for modeling ectotherm thermal performance provide a more mechanistic option because they represent the temperature dependence of the underlying enzyme-assisted chemical reactions that comprise metabolism (DeLong et al., 2017; Molnár et al., 2017; O'Connor & Bernhardt, 2018). This means that the key model parameter, the activation energy for metabolism (E_A), can be interpreted as weighted average of E_A's for rate-limiting metabolic enzymes (Molnár et al., 2017). It also means that TPC's for physiological

processes that are linked to an organism's metabolic rate, such as running performance, should have E_A values similar to that of whole-body metabolism, making BA and SS models particularly useful for modeling the shape of TPC's for metabolism-limited processes (Molnár et al., 2017).

In Chapter 4 I investigated the metabolic thermal performance of five amphibian species by measuring the O_2 consumptions of individuals across relevant temperature ranges. For these experiments, my team and I collected oxygen consumption data from *Osteopilus septentrionalis*, *Pseudacris crucifer*, and *Anaxyrus americanus* at Oakland University, and *Atelopus varius* and *Atelopus zeteki* at Detroit Zoo. To accomplish this, we developed an updated version of the respirometry device first published by McWhinnie et al. (2021). We conducted fully replicated trials for these experiments and then fit thermal performance models based on Metabolic Theory of Ecology (J. H. Brown et al., 2004). Although a variety of metabolic proxies can be used such as locomotor performance, heart rate, or carbon dioxide production, we measured oxygen consumption as this is one of the direct measurements of an organism's metabolic rate (Dell et al., 2011).

In addition to conducting oxygen consumption experiments for new species, I also lead a team where we compiled O_2 consumption data from prior studies with at least three temperature treatments (the minimum number of temperatures required to test for high-temperature deactivation in the SS model; (Molnár et al., 2017; Schoolfield et al., 1981). For this expanded analysis, I also made use of unpublished data collected by other members of the Raffel Lab in theses or dissertations. This brought the total number of species that we were able to fit metabolic thermal performance curves to 60 (including

the 5 from my own experiments). After fitting MT-based BA or SS models to each of the 60 species, I collected environmental data from each species home range to test for environmental predictors of key metabolic parameters (i.e., E_A and P_{T0}).

1.6 Metabolic Theory-based thermal mismatch models to describe ectotherm infection

MT-based thermal performance curves have become popular for describing temperature dependent processes for individual organisms, but MT-based approaches to describe species interactions have proven to be more difficult (but see Dell et al. 2014). A possible way to disentangle the separate effects of temperature on host and parasite performance is to develop models that explicitly describe parasite growth or survival on hosts as thermal mismatches between host and parasite performance curves (Rohr et al., 2013; Sckrabulis et al., 2022). Rohr et al. (Rohr et al., 2013) proposed that parasite growth rates in or on hosts could be modeled as the difference (or "mismatch") between parasite infectivity – defined as the parasite growth rate in the absence of host resistance – and host resistance, defined as the ability of the host to reduce parasite growth rates. However, these two processes are difficult to distinguish with empirical infection experiments, because any temperature treatment must be applied to both host and parasite simultaneously (Sckrabulis et al., 2022). MT-based mismatch models provide a possible solution to this parameter identifiability problem (Sckrabulis et al. 2022). A core postulate of MT is that all physiological and ecological rates processes are fundamentally limited by organism metabolic rates, which means it may be possible to predict the temperature dependence of host or parasite performance (i.e., resistance or infectivity) by estimating key metabolic parameters based on the temperature dependence of host or parasite metabolic rates (Rohr et al., 2013; Sckrabulis et al., 2022).

Prior studies have investigated hypothesized patterns in temperature dependence of ectotherm infections that assume thermal mismatches between host and parasite TPCs (Cohen et al., 2017, 2020, 2020; Kirk et al., 2022; Neely et al., 2020; Venesky et al., 2022). However, these studies have largely focused on qualitative predictions based on additional assumptions, such as that parasites have broader TPC's than their hosts, or that parasite and host TPC's can be boiled down to single numbers such as the temperature for peak infection, the host's thermal optimum (T_{opt}) or the host or parasite's critical thermal maximum (CT_{max}) (Carvalho et al., 2024; Cohen et al., 2020; Kirk et al., 2022). Another limitation of past studies is that they have typically identify the T_{opt} for peak infection on individual hosts by fitting phenomenological models (e.g., quadratic or Briere curves) to infection data. These models lack a mechanistic basis, so their parameters largely lack biological meaning that could be used to derive general insights into how temperature affects host-parasite relationships.

In Chapter 5, I developed and validated MT-based thermal mismatch models fit to data from my empirical studies (Chapter 3). These models demonstrate the power of thermal mismatch models rooted in metabolic theory to predict individual infection dynamics across temperatures and to yield potentially generalizable insights into the thermal biology of host-parasite interactions.

1.7 Scaling temperature dependent infection dynamics from individuals to populations

A common question among ecologists is whether and how individual processes and dynamics scale to larger levels of organization, such as population dynamics or interactions with other species (Codling & Dumbrell, 2012; Denny & Benedetti-Cecchi, 2012; Tao et al., 2021). Designing studies that incorporate empirical data to investigate

smaller scale processes and then compare those responses to observations at the population level is an important goal for ecologists (Melbourne & Chesson, 2005; Petersen & Englund, 2005; Underwood et al., 2005). Studies investigating infectious disease dynamics could provide important insights into the scalability of observations and patterns from individual dynamics to the dynamics of disease within a population of hosts (Tao et al., 2021).

Many studies of chytrid in amphibian populations have focused on infection prevalence (Carvalho et al., 2024; Cohen et al., 2017, 2019, 2020), rather than infection load, which is often quantified in individual infection experiments (J. E. Noelker, Abreu Ruozzi, Spengler, et al., 2024; Raffel et al., 2013, 2015). However, comparing these dissimilar response variables (infection prevalence in the field versus infection load in experimental infections) is comparing apples to oranges, because they are quantified differently and may represent different stages in the infection process (e.g., initial infection dynamics of an experimentally infected host versus presumably equilibrium infection levels in field-sampled hosts).

To test if Bd infection dynamics on individual hosts can be used to predict transmission dynamics in host populations, I conducted a controlled temperature outdoor mesocosm Bd infection experiment tracking Bd transmission in small populations of *X. laevis*. This large-scale outdoor mesocosm experiment was conducted during Winter 2020-2021. To explore how the acclimation effects from my individual infection experiments (Chapter 3) scale up to population level transmission dynamics, I included three variable temperature treatments in this mesocosm experiment, in addition to three

constant temperature treatments. This study has potentially important implications for the Temperature Variability Hypothesis of Rohr & Raffel (Rohr & Raffel, 2010).

1.8 Predicting population-level transmission dynamics with MT-based mismatch models

Of particular interest to ecologists, conservation biologists, and land managers is the ability to predict disease progressions through population models in order to better understand the outcomes of population level disease outbreaks (Tao et al., 2021). Furthermore, modeling infection dynamics with more mechanistic foundations is a desirable target for ecologists and conservation biologists looking to better understand the processes underlying disease outbreaks (Kirk et al., 2022; Mideo et al., 2008). One approach to developing more mechanistic population-level disease models is to root the population dynamics to dynamics occurring at an individual level (Kirk et al., 2022; Mideo et al., 2008; Wilber et al., 2016, 2017, 2021). Several popular population disease modeling approaches have been used in the literature including susceptible-infected-recovered (SIR) models, integral projection models (IPMs), and individual based models (IBMs) with varying strengths and weaknesses (Anderson & May, 1979; Briggs et al., 2005, 2010; Metcalf et al., 2016; Wilber et al., 2016, 2021). Models based on ordinary differential equations (ODE) have been used with great success to model the population dynamics of micro- and macroparasite dynamics (Anderson & May, 1979; May & Anderson, 1979). Anderson and May's macroparasite models accounted for among-host variation in individual infection intensities by assuming parasite abundance in individual hosts approximates a negative binomial distribution (Anderson & May, 1979). However, to make this ODE-based approach work for microparasite dynamics, Anderson and May modeled Susceptible and Infected hosts as discrete populations in which all Infected hosts

were assumed to have identical transmission potential (SIR models; Anderson & May, 1979). Modeling dynamics of individual infection loads in populations using ODE-based models is less mathematically tractable due to microparasite abundances tending to be lognormally distributed. Tadiri et al. (2019) got around this problem by assuming normally distributed microparasite loads, but this assumption disagrees with observed microparasite distributions. IPMs can predict dynamics of log-distributed individual infection loads within populations (Wilber et al., 2016, 2021), but these are complex models to develop that might not be practical for land managers to implement (Metcalf et al., 2016). Furthermore, existing IPMs assume that internal infection dynamics of individual infected hosts is not affected by continued transmission (Wilber et al., 2016, 2021), which might not be true for all disease systems.

In contrast, IBMs explicitly model the infection load of every individual within the population being modeled (Briggs et al., 2005, 2010), and can mechanistically root population dynamics to individual-level dynamics by nesting the individual dynamics within the population-level model (Mideo et al., 2008). However, these models, which generate a matrix of infection loads for every individual through time, can be computationally cumbersome (Breckling, 2002). In Chapter 7 of my dissertation, I leveraged the MT-based thermal mismatch model parameterized from my individual infection experiments to develop an individual based model (IBM) predicting among-host transmission dynamics. An important feature of this model was that it assumes frogs can continue to receive additional transmission-derived infections from other frogs, even after they have become infected, opening up the possibility of positive feedback loops between individual infection intensities and among-host transmission dynamics (i.e.,

"transmission intensity feedbacks"; TIF). I used data from my mesocosm experiment (Chapter 6) to validate model predictions from an individual based model (IBM), which I was able to entirely parameterize based on individual level experiments due to nesting the MT-based thermal mismatch model for individual host dynamics within the broader context of among-host transmission dynamics. Despite being parameterized entirely from individual-level infection data and measurements of Bd characteristics in culture, these models predicted both the temperature dependent dynamics and the dramatically higher infection loads observed on individual frogs when housed together in populations of 4–6 animals. This result suggests that transmission-intensity feedbacks (TIF) might play an important role for chytridiomycosis outcomes in populations of *X. laevis*. More broadly, this work shows that MT-based thermal mismatches nested within IBM population models provide a potentially powerful tool for understanding and predicting the outcomes of disease outbreaks among ectothermic hosts and vectors.

1.9 Significance

This dissertation offers several novel contributions to science with societal or conservation implications. In Chapter 4, my results suggest that salamanders have evolved metabolic adaptations to their local thermal environments, but this pattern was not reflected in anurans. Shifting global temperatures will be important evolutionary pressures for amphibians and their parasites, making it important to identify patterns of amphibian thermal evolution if we want to protect these at-risk animals (Fisher & Garner, 2020; J. Li et al., 2024). In chapter 3, I found results consistent with the temperature variability hypothesis of Rohr & Raffel (2010), with frogs exhibiting more severe infections following a sudden drop in temperature. This result is consistent with past

studies suggesting that variable temperature conditions associated with climate change can exacerbate infectious diseases of amphibians (Fisher & Garner, 2020; J. Li et al., 2024). However, I also found that the transmission potential of Bd infected frogs seemed to be less affected by variable temperatures, suggesting the individual-level effects of temperature variability might not scale up to strongly affect transmission dynamics in amphibian populations (Chapter 3). This result has potentially important implications for interpreting results from past studies reporting effects of temperature shifts on Bd infection in individual hosts. Consistent with this finding, I did not observe increased Bd infection loads in frog populations experiencing variable temperatures in a mesocosm-scale experiment, further suggesting Bd transmission dynamics in populations is less affected by shifts in temperature than individual-level infections (Chapter 6). However, frog populations had substantially higher infection loads at the temperature for peak parasite growth (10 °C) compared to individually housed frogs (Chapter 6), resulting in significant infection-induced frog mortality at 10 °C despite *X. laevis* being widely reported as highly tolerant of Bd based on individual-level experimental infections (including in Chapter 3). This demonstrates the importance for understanding how environmental conditions (e.g., temperature) influence infectious diseases and how those conditions could subsequently contribute to mortality rates (Chapter 6). Individual mortality probabilities in the mesocosm experiment were directly proportional to Bd infection loads and exhibited an exponential probability distribution, contrary to past studies that concluded Bd only causes mortality above a threshold infection intensity of ~10,000 zoospore equivalents (on swab samples; Kinney et al., 2011; Vredenburg et al., 2010).

In Chapter 5, I developed and validated MT-based thermal mismatch models that successfully predicted infection dynamics of individual frogs (Chapter 5). These MT-based thermal mismatch models provide a new way to more mechanistically describe the dynamics of microparasite infection (Chapter 5). These models provide new possibilities for understanding the dynamics of ectotherm diseases including important vectors of human disease in a changing climate. When I scaled these MT-based mismatches to predict population dynamics (Chapter 7), the individual based model (IBM) we developed successfully captured the strikingly higher infection loads we observed from our mesocosm transmission experiment (Chapter 6). A key feature of this IBM was that it allowed continued transmission from other frogs to boost the infections of already-infectious individuals, resulting in a positive feedback loop between transmission and infection intensity that we refer to as transmission-intensity feedbacks (TIF or TI feedbacks; Chapter 7). This finding is contrary to assumptions of most prior models of microparasite transmission dynamics. If TI feedbacks are important drivers of infection intensity in other disease systems, this could have major ramifications for our approaches to managing human and animal health (e.g., co-housing of infected individuals; Chapter 7).

In general, this dissertation offers insights into amphibian evolution, disease interactions, and novel modeling approaches to describe temperature dependent diseases of ectotherm hosts. By using controlled experimental conditions to quantify differences in individual- versus population-level disease dynamics, I was able to make direct comparisons and test for causal relationships between temperature, temperature variability, host population size, and infectious disease dynamics. However, caution is

warranted in extrapolating these findings beyond the scope of the conditions investigated. Natural ponds and populations of hosts are more complex and dynamic than the relatively static conditions designed for these experiments. Together with additional laboratory and field studies, the findings of my dissertation could lead to a deeper understanding of disease outcomes for populations in the context of climate change.

CHAPTER TWO

GLOVE DECONTAMINATION PROCEDURES TO PREVENT PATHOGEN AND DNA CROSS-CONTAMINATION AMONG FROGS

2.1 Introduction

Professionals in many disciplines handle aquatic animals on a regular basis (e.g., field researchers, conservation biologists, land managers, zookeepers, and aquarists), potentially causing unintended transmission of infectious diseases between animals or populations (Gray et al., 2017, 2018). When the purpose of animal handling is to collect samples (e.g., skin swabs for DNA analysis), it is important to prevent cross-contamination by non-infectious material (e.g., intact DNA) that might reduce the integrity of data collection (Gray et al., 2017; Raffel et al., 2013). Researchers often address this problem by changing gloves between handling animals in field studies, especially when working with species threatened by emerging infectious diseases (Gray et al., 2017). This approach is widely considered the gold standard, especially when biosecurity is a major concern (Gray et al., 2017; Havlíková et al., 2015). However, disposing of gloves between individuals is costly and results in excessive waste (Gray et al., 2017), and needing to pull disposable gloves over wet hands can increase processing time when handling large numbers of animals in experimental studies or surveys (T. R. Raffel & J. E. Noelker, personal observation). Hence, there is a need for validated methods to decontaminate gloved hands between handling individual animals.

Pathogen and DNA cross-contamination are of particular concern for researchers studying amphibian chytridiomycosis, a skin disease caused by the fungal pathogen

Batrachochytrium dendrobatidis (Gray et al., 2017, 2018; Havlíková et al., 2015; Raffel et al., 2013, 2015). Some researchers have addressed this issue via chemical sanitization of gloves (S. Cashins et al., 2008; Gray et al., 2017; Raffel et al., 2013, 2015). Several chemical agents have been shown to effectively kill the infectious stages of chytrid fungi (Becker & Gratwicke, 2017; M. Johnson et al., 2003; Van Rooij et al., 2017; Webb et al., 2007). Some of the most effective disinfectants are ethanol and bleach (active ingredient: sodium hypochlorite = NaOCl), both of which killed Bd within 30 seconds at high concentrations (70% ethanol and ≥ 1% NaOCl; Johnson et al., 2003). Ethanol dries within seconds, leaving no toxic residue behind that might affect the health of subsequent animals. However, ethanol is commonly used to preserve DNA samples and may not prevent DNA cross-contamination. Bleach may prevent DNA cross-contamination by denaturing Bd DNA (S. Cashins et al., 2008). However, bleach may also irritate researchers' skin, damage clothing and equipment, or leave behind chloride residues that may be toxic to amphibians (Green, 2009). Raffel et al. (2013) addressed the latter concern by rinsing bleach-decontaminated gloves with a commercial dechlorinating agent. However, to our knowledge the effectiveness of this procedure to prevent DNA cross-contamination has not been formally tested.

The choice of gloves is also important. Nitrile gloves and even bare hands have fungicidal properties (Mendez et al., 2008; Thomas et al., 2020), but nitrile or latex gloves may be directly toxic to amphibians (S. D. Cashins et al., 2008; Gutleb et al., 2001). Nitrile exam gloves add a further complication when working with slippery aquatic organisms such as *Xenopus laevis*, by preventing researchers from securely gripping the animal (Green, 2009). Researchers can improve their grip on slippery

organisms (and add separation between animals and potentially toxic nitrile gloves) by using a dampened cloth or cotton glove (Horsberg, 1994; Reed, 2005). However, cotton gloves are more expensive to replace than nitrile exam gloves, increasing the incentive to decontaminate gloves for reuse. Here we validated procedures for decontaminating nitrile and cotton gloves following contamination with a Bd broth culture or after handling Bd infected *X. laevis*.

2.2 Materials and methods

2.2.1 Experiment 1 – decontaminating cotton & nitrile gloves directly contaminated with cultured Bd

We compared the effectiveness of various methods to remove detectable Bd DNA from 100% cotton (Uline Cotton Inspection Gloves S-19283) or nitrile (Syngaurd Nitrile Exam Gloves NGPF 7002) gloves following direct contamination with a Bd broth culture. Experimental nitrile gloves were worn alone (without cotton gloves), and experimental cotton gloves were worn over nitrile gloves that were not swabbed for this test. To contaminate gloves, we pipetted 1 mL of a Bd broth culture (strain JEL423, grown for 18 days at 20 °C) across the palm and fingers of each glove. Four replicate cotton gloves were swabbed immediately following each of four randomly assigned treatments: (1) negative control (1 mL ultrapure water), (2) Bd contamination, (3) autoclave sterilization; or (4) laundry sanitization (see section 2.2.5). Four replicate nitrile gloves were swabbed immediately following one of four randomly assigned treatments: (1) negative control, (2) Bd contamination, (3) bleach sanitization, or (4) ethanol sanitization (see sections 2.2.3–2.2.4).

2.2.2 Experiment 2 – decontaminating gloves after handling a Bd-infected frog

As part of a larger Bd transmission experiment in 2020, we tested the efficacy of using either a bleach or ethanol procedure to decontaminate nitrile gloves worn under cotton gloves while handling twelve Bd infected *X. laevis*. Frogs had been individually exposed to 3×10^6 Bd zoospores (strain JEL423) and held for four weeks at 8 °C in groups of 10 frogs housed in plastic bins containing 4 L of dechlorinated tap water, on a 12:12 hour light cycle with weekly water changes. When collecting swab samples, one researcher swabbed while a second researcher served as the animal handler (Fig. 2.1A). We first swabbed each frog, with the animal handler wearing a pair of cotton gloves over nitrile gloves (see section 2.2.6). Next, we swabbed the contaminated cotton glove (Step 1). The animal handler then removed the outer cotton glove, and we swabbed the underlying nitrile glove (Step 2). The animal handler then decontaminated their nitrile gloved hands using either the bleach or ethanol sanitization procedure (see sections 2.2.3 & 2.2.4), followed by a third swab sample (Step 3). The animal handler then donned a fresh pair of cotton gloves over the decontaminated nitrile gloves, followed by a final swab sample (Step 4). All animal use was conducted under Institutional Animal Care and Use Committee (IACUC) protocol 18011 and Institutional Biosafety Committee (IBC) protocol 2759-13.

2.2.3 Bleach decontamination of nitrile gloves

We tested a bleach-dechlorinate-rinse procedure to decontaminate nitrile gloves using 50% bleach (3% NaOCl; Fig. 2.1B). To sanitize contaminated nitrile gloves, the researcher immersed their gloved hands in 50% Pure Bright Liquid Germicidal Bleach (50% water; 0.11% NaOCl) solution for at least 30 seconds, an exposure time known to

be 100% lethal to Bd (Becker & Gratwicke, 2017). To deactivate chlorines remaining on the gloves following decontamination, gloved hands were immersed for 20 seconds in 30% dechlorination solution (300 mL Kordon AmQuel Plus Ammonia Detoxifier mixed with 700 mL water). This is >2000 times the manufacturer's recommended concentration to dechlorinate tap water. This was followed by a final rinse in aged tap water (Fig. 2.1B).

2.2.4 Ethanol decontamination of nitrile gloves

With goals of preventing cross-contamination by live Bd and reducing cross-contamination by Bd DNA, we tested a glove sanitization procedure using 70% ethanol (30% water). To sanitize contaminated nitrile gloves, the researcher used a squirt bottle to apply sufficient ethanol to fully wet their gloved hands, then lathered their hands for 20 seconds and dried them with an unbleached paper towel (Fig. 2.1C). Drying with a paper towel shortened the drying time and was hypothesized to physically reduce the amount of DNA-containing material.

2.2.5 Decontaminating cotton gloves

For the autoclave procedure, we used a liquid cycle with a 20 minute sterilization period (Model 3AV-ADVPRO Consolidated Sterilizer Systems). For the laundry procedure, we used a Giantex Model FW35-1508 laundry machine (30 L high volume setting) with 400 mL concentrated bleach (final NaOCl concentration: 0.08%) and 72 mL laundry sanitizer (Lysol Laundry Sanitizer Additive; 2.4% quaternary ammonium compounds). This NaOCl concentration is sufficient by itself to kill Bd within 1 minute (Becker & Gratwicke, 2017). Washing involved three cold water cycles (Wash: 17

minutes; Soak: 15 minutes; Rinse: 16 minutes; Spin: 7 minutes). Gloves were air dried before reuse.

2.2.6 Swabbing procedures and Bd qPCR

We sampled each Bd infected *X. laevis* following methods adapted from Raffel et al. (2013), by stroking a rayon fine-tip urethra swab (MW113, Medical Wire & Equipment Company) five times along the ventral side of each thigh and foot. We sampled each glove by stroking a swab across the hand five times, starting at the palm and running down the length of each digit. We analyzed each swab by qPCR, using methods adapted from Hyatt et al. (2007). We generated a standard curve using serially diluted positive control plasmid DNA (Pisces Molecular LLC, Boulder, CO) and calculated the number of zoospore genome equivalents (Z_e) per swab based on a published conversion factor for strain JEL423 (63.5 gene copies per zoospore; Altman & Raffel 2019). Assays were run in duplicate (one well each at 1:10 and 1:100 dilution) for Experiment 1, to guard against the possibility of qPCR inhibition at 1:10 dilution. We did not detect inhibition for Experiment 1. We therefore assayed in singlicate at 1:10 dilution for Experiment 2 to reduce costs (K. Kriger et al., 2006). We defined a positive result as ≥ 0.1 Z_e based on the reported detection limit for this assay (Boyle et al. 2004). Results were analyzed in R (ver. 4.1.3) using the base package as well as *Hmisc* and *effsize* (Harrell & Dupont, 2022; R Core Team, 2022; Torchiano, 2020). We log transformed Bd qPCR data prior to statistical analyses to normalize model residuals ($\ln[Z_e + 1]$; $p > 0.05$ based on Shapiro-Wilk test).

2.2.7 Nitrile glove decontamination cost-benefit analysis

To explore potential benefits of disinfecting gloves, we conducted an informal cost-benefit analysis for the mesocosm experiment referenced in Section 2.2.2. Within this study, a total of 180 frogs were each swabbed weekly over nine weeks. During each swabbing session, one animal handler and one swabber each used a single pair of nitrile gloves for each of six experimental blocks, using the bleach-dechlorinate-rinse procedure between individual animals. We calculated the total number, mass, and cost of nitrile gloves, and costs of materials used for the disinfection procedure (bleach, AmQuel, and paper towels), in comparison to what would have been needed if the animal handler changed gloves between individual frogs (costs based on vendor prices January 3, 2024).

2.3 Results

All negative control gloves tested negative for both experiments. For Experiment 1, contaminated swab samples from nitrile gloves exhibited 25 times higher Bd DNA levels (ln Bd load ± 95% c.i. = 11.51 ± 0.54) than swab samples from cotton gloves (8.29 ± 0.61). The autoclave sterilization and laundry sanitization procedure successfully eliminated all detectable DNA from culture-contaminated cotton gloves, as did the bleach-dechlorinate-rinse procedure for nitrile gloves. However, culture-contaminated nitrile gloves retained detectable DNA following ethanol decontamination (8.29 ± 0.76). For Experiment 2, frogs with higher Bd loads tended to result in greater contamination of cotton gloves, though a Pearson's correlation test was nonsignificant ($r = 0.49$, $t_9 = 1.70$, $p = 0.123$). The level of Bd DNA contamination was reduced by each step of either the bleach or ethanol decontamination procedure (Fig. 2.2). Paired t-tests assuming unequal variances showed that removing contaminated cotton gloves significantly reduced the

level of Bd contamination (Fig. 2; $t_8 = 6.17$, $p < 0.001$; Cohen's $d \pm 95\%$ c.i. $= 2.61 \pm 1.36$), as did the bleach decontamination procedure (Fig. 2.2; $t_{10} = 3.21$, $p = 0.009$; Cohen's $d = 1.37 \pm 0.99$). There were no detections of Bd DNA above our detection threshold ($Z_e \geq 0.1$) for nitrile gloves following the ethanol decontamination procedure or (fresh) cotton gloves pulled over decontaminated nitrile gloves (Fig. 2.2; Table 2.1). One out of six nitrile gloves had a low positive result (0.57 Bd Z_e) following the bleach decontamination procedure (Fig. 2.2; Table 2.1). Two-sample t-tests revealed no significant differences between gloves in the bleach versus ethanol decontamination treatments at any of the four stages of the glove decontamination procedure (Fig. 2.2; all $p > 0.3$).

Cost-benefit analysis found that using the bleach-dechlorinate-rinse procedure in our mesocosm experiment reduced nitrile glove waste by ~93.5% (0.68 kg vs. 10.5 kg) and overall decontamination costs by ~75.4% ($118 vs. $481), relative to if we had changed gloves between individual frogs.

2.4 Discussion

We verified that cotton and nitrile gloves could be successfully decontaminated from Bd DNA using multiple procedures. Either autoclaving or laundry sanitization succeeded at eliminating detectable Bd DNA from cotton gloves, as did a bleach-dechlorinate-rinse procedure for nitrile gloves. An ethanol decontamination procedure reduced but did not eliminate Bd DNA from directly contaminated nitrile gloves; however, the ethanol rinse succeeded at lowering Bd DNA below the detection limit of our assay for nitrile gloves worn underneath contaminated cotton gloves. This appears to be because DNA-containing material was absorbed by the cotton gloves, resulting in

decreased detectability of Bd DNA on contaminated cotton gloves relative to similarly contaminated nitrile gloves (Experiment 1), and a great reduction in Bd DNA contamination for underlying nitrile gloves following removal of a contaminated cotton glove (Experiment 2).

Our results show that removal of cotton gloves between handling animals can reduce DNA cross-contamination to subsequently handled animals, to the point where even a 70% ethanol rinse followed by drying hands with a paper towel was sufficient to reduce DNA below the 0.1 Z_e detection limit of a standard qPCR assay. The latter reduction was most likely due to physical removal of DNA by wiping with the paper towel, given that ethanol does not denature DNA. Future investigations could test these procedures with species that might be more sensitive to Bd infection than *X. laevis*, to ensure that no transmission occurs following repeated handling with decontaminated gloves.

Cotton gloves may be useful for handling slippery aquatic animals and, like nitrile gloves, are generally considered safe for human use. However, researchers should consider potential negative effects of handling amphibians with fabric, which could possibly abrade skin or disrupt mucus coats (Horsberg, 1994; Reed, 2005). Researchers should certainly avoid overly thick, dry, or rough cotton gloves (Reed, 2005). Fabric gloves should be avoided for smaller species that might be disproportionately at risk for injury (Horsberg, 1994), or really any species that can be adequately handled with regular nitrile gloves. Nevertheless, the improved grip of cotton gloves may be worthwhile in certain circumstances, such as experimental settings where dropping a particularly slippery animal might cause injury or loss of biocontainment.

We have successfully used the bleach-dechlorinate-rinse procedure for decontaminating gloves in Bd infection experiments with multiple species (Raffel et al., 2013, 2015), including with cotton gloves for experiments with *X. laevis*, and observed no apparent negative health effects on individuals over several weekly swabbing sessions (T. R. Raffel & J. E. Noelker personal observation). These procedures resulted in substantial waste reduction and cost savings. We did not notice any problems with glove deterioration, consistent with a prior study that found minimal deterioration of nitrile gloves after twenty disinfection cycles with either bleach or ethanol (Esmizadeh et al., 2021). These procedures may be useful for researchers interested in preventing cross-contamination by pathogens or DNA while working with aquatic organisms and wish to reduce costs and waste produced from experiments or surveys. Nevertheless, we believe changing gloves between animals (or populations) should remain the preferred option when biosecurity is a significant concern, such as when sampling multiple ponds or working with endangered species in a zoo setting.

2.5 Data availability

Code and data can be accessed here:

https://github.com/jaynoelker/Noelker_etal_GloveDecontamination

2.6 Acknowledgements

Jacob T. Heabeart, Melissa D. Ostrowski, and Amanda McKeon assisted with the experiment and qPCR assays. This work was supported by an NSF grant to T.R.R. (CAREER: IOS-1651888). All authors helped conceive the project, complete experiments, and edit the manuscript; J.E.N., V.A.R., and T.R.R. conducted analyses; J.E.N. and T.R.R. wrote the manuscript.

This chapter was published in *Diseases of Aquatic Organisms*:

Noelker, J. E., Abreu Ruozzi, V., Craig, H. M., Sckrabulis, J. P., & Raffel, T. R. (2024). Glove decontamination procedures to prevent pathogen and DNA cross-contamination among frogs. *Diseases of Aquatic Organisms*, *158*, 173–178. https://doi.org/10.3354/dao03793

CHAPTER TWO TABLES

Table 2.1: Detection of *Batrachochytrium dendrobatidis* (Bd) DNA on contaminated cotton or nitrile gloves from Experiment 2, before or after each step of the decontamination procedure. We (1) swabbed 12 frog-contaminated cotton gloves (1 swab was removed due to a labeling error); (2) swabbed the underlying nitrile glove after removing the cotton glove (2 swabs were misplaced prior to qPCR); (3) swabbed the nitrile glove again after decontamination with either bleach or ethanol ("Treatment"; 6 gloves each); and (4) swabbed a fresh cotton glove after placing it over the decontaminated nitrile glove. We also swabbed 6 negative control gloves that were never exposed to Bd contamination (3 nitrile and 3 cotton). Swabs were counted as "positive" if we detected ≥ 0.1 zoospore equivalents (Z_e) of Bd DNA. na: not applicable

Glove type	***Procedure step***	***Status***	***Treatment***	***Positive***	***Negative***
Cotton	1	Contaminated	na	9	2
Nitrile	2	Contaminated	na	3	7
Nitrile	3	Decontaminated	Bleach	1*	5
Nitrile	3	Decontaminated	Ethanol	0	6
Cotton	4	Fresh glove	Bleach	0	6
Cotton	4	Fresh glove	Ethanol	0	6
Cotton	na	Negative control	na	0	3
Nitrile	na	Negative control	na	0	3

*This sample returned a value of 0.57 Z_e and could be a false positive

CHAPTER TWO FIGURES

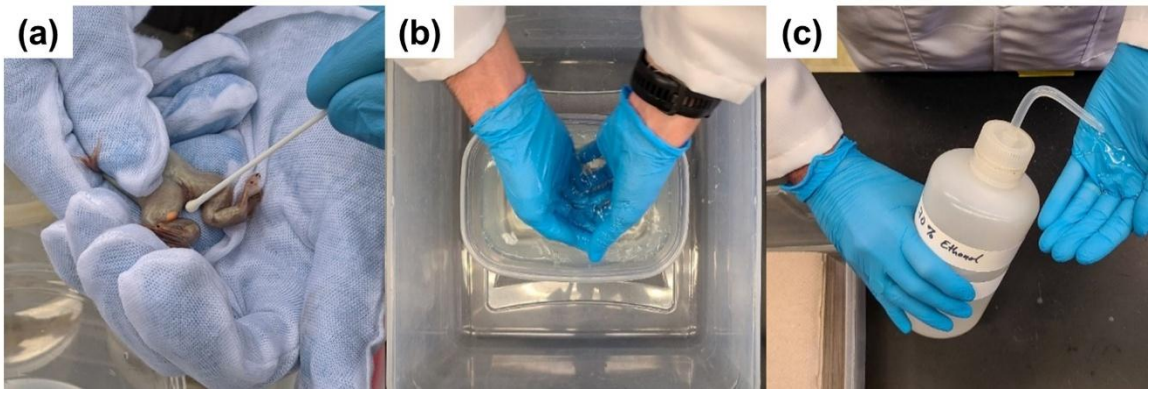

Figure 2.1: Swabbing and decontamination procedures. (a) Collecting a skin swab with cotton over nitrile gloves. (b) Bleach-dechlorinate-rinse procedure, showing immersion of nitrile gloves in double-contained bleach. (c) Ethanol procedure. Photo credit: Andrea R. Nadjarian (a) and Declan S. McCrary (b, c).

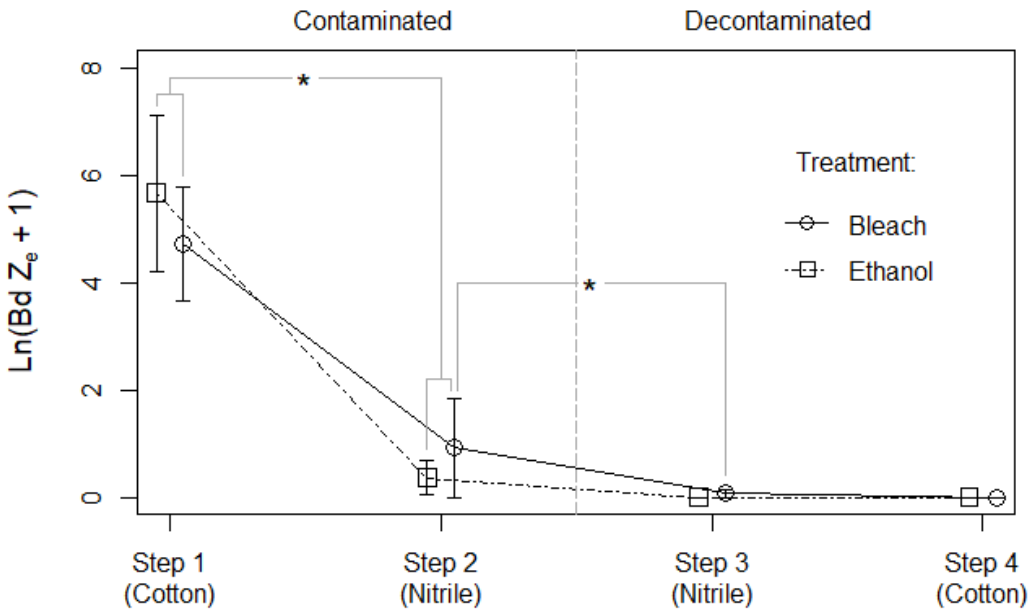

Figure 2.2: *Batrachochytrium dendrobatidis* (Bd) zoospore equivalents (Z_e) detected on cotton and nitrile gloves before and after the bleach (circles) or ethanol (squares) decontamination procedure in Experiment 2. Error bars indicate standard error and asterisks (*) mark a significant reduction ($p < 0.05$).

CHAPTER THREE

DYNAMIC EFFECTS OF THERMAL ACCLIMATION ON CHYTRIDIOMYCOSIS INFECTION INTENSITY AND TRANSMISSION POTENTIAL IN *XENOPUS LAEVIS*

3.1 Introduction

A global reduction of amphibian populations has been partially attributed to the emergence of chytridiomycosis, a fungal skin disease caused by *Batrachochytrium dendrobatidis* (Bd) and the related species *Batrachochytrium salamandrivorans* (Bsal) (Bower et al., 2017; Fisher et al., 2009; Fisher & Garner, 2020; Longcore et al., 1999; Searle et al., 2011; Voyles et al., 2009). Like many diseases of ectothermic hosts, chytridiomycosis is strongly temperature dependent, with most amphibian species becoming more infected at cooler temperatures (Z. Li et al., 2021; Raffel et al., 2013, 2015) but see (Cohen et al., 2017). In addition to these mean-temperature effects on Bd infection, some amphibian species have been found to exhibit periods of increased susceptibility following a sudden temperature shift, due to delays in host acclimation to the new temperature (Raffel et al., 2013, 2015). As climate variability increases and becomes less predictable under the threat of climate change, it is ever more important to understand how temperature and host thermal acclimation responses affect Bd infection and transmission dynamics (Bosch et al., 2007; Raffel et al., 2013).

The temperature variability hypothesis (TVH) of Rohr and Raffel (Rohr & Raffel, 2010) postulates that intra-annual temperature variability increases susceptibility of ectotherm hosts to infectious diseases, due to delays in host thermal acclimation following unanticipated shifts in temperature. This hypothesis assumes that: (1) host

acclimation increases resistance to infection following extended exposure to a new temperature (i.e., "beneficial acclimation"; (Raffel et al., 2015)) and (2) parasites acclimate to new temperatures more rapidly than their hosts (Raffel et al., 2013). A shorter time scale for parasite acclimation is predicted by metabolic theory due to much higher metabolic rates and shorter process time in smaller organisms (J. H. Brown et al., 2004; Gillooly et al., 2001). Beneficial acclimation effects are commonly observed for measures of thermal tolerance (e.g., critical thermal maximum or CT_{max}; (Rohr et al., 2018)); however, other types of thermal acclimation such as "cooler is better" or "optimal temperature" responses are commonly observed when measuring aspects of thermal performance within an organism's normal temperature range (Wilson & Franklin, 2002). Beneficial acclimation effects on susceptibility to Bd infection have been observed in adult Cuban treefrogs (*Osteopilus septentrionalis*) and juvenile red-spotted newts (*Notophthalmus viridescens*), consistent with the TVH (Raffel et al., 2013, 2015); however, studies in other amphibian species found no acclimation effects or evidence contradicting beneficial acclimation (Altman & Raffel, 2019; Bradley et al., 2019; S. E. Greenspan et al., 2017). Additional measurements for more host species and life stages would help to determine if there are general patterns in acclimation effects on host resistance to infection. Here we add to the taxonomic and geographic diversity of species investigated by measuring effects of temperature and thermal acclimation on Bd infection in *X. laevis*.

If delays in host thermal acclimation influence susceptibility to infection, then it is important to determine the time scale over which these acclimation responses occur. One approach to studying the time scale of acclimation responses is to measure how long it

takes for effects of past (acclimation) temperatures to dissipate, following an experimental shift to a new temperature. Full acclimation of amphibian thermal traits like CT_{max} can occur on time scales of hours to days, depending on the species examined and the direction of a temperature shift (typically longer following a temperature decrease) (Hutchison, 1961; Hutchison & Maness, 1979; Hutchison & Michael R. Ferrance, 1970; Nietfeldt et al., 1980). However, changes in ectotherm immune parameters, such as complement activity or blood leukocyte profiles, might sometimes occur on longer time scales of days to weeks (Bly & Clem, 1991; Maniero & Carey, 1997; Raffel et al., 2006). Prior studies found significant acclimation effects on Bd infections up to 2 weeks after amphibians were exposed to infection at new performance temperatures, but these effects dissipated and became non-significant at later time points (Bradley et al., 2019; Raffel et al., 2013, 2015). These results seem to indicate that it took at least two weeks for many of these host species to fully acclimate their parasite resistance mechanisms to a new temperature; however, it is possible that host acclimation occurred on a shorter time scale. Even if the delay in host acclimation is brief (e.g., < 1 week), this short window of parasite opportunity could result in significant differences in infection intensity at later time points. This is because infection is a dynamic process, such that early infection states can have carry-over effects on infection at later time points (Zipkin et al., 2010). It is especially plausible that severe early infections might be self-perpetuating for pathogens like Bd that can suppress host immune responses (Grogan et al., 2018; Rollins-Smith & Le Sage, 2021). In the current study, we sought to distinguish between the timing of host acclimation (i.e., a slow-acclimation hypothesis) and the presence of carry-over effects (i.e., a carry-over effect hypothesis) by experimentally varying the timing-of-

exposure relative to the timing of a temperature shift. We hypothesized that acclimation of *X. laevis* resistance to infection occurs on relatively short time scale (i.e., < 1 week), but that acclimation effects on Bd infection would still be detectable at later time points due to carry-over effects of early infection dynamics.

Another important question about how host thermal acclimation affects Bd infection is whether and how individual-level acclimation effects translate into population-level transmission dynamics. We know thermal acclimation status can influence subsequent development of Bd infection on an individual host, at least in terms of Bd load as measured via skin swab qPCR (Altman & Raffel, 2019; Raffel et al., 2013, 2015). However, it is unclear to what extent gene copies on a skin swab represent a host's potential to transmit the infection to other hosts, for multiple reasons. First, skin swabs only collect DNA from a subsample of a frog's skin surface and might not accurately represent the true infection burden (Clare et al., 2016). Second, qPCR skin swab assays quantify Bd DNA from any source including immature zoosporangia and motile infectious stages (zoospores) left over from experimental inoculations (Boyle et al., 2004; Porco et al., 2024; Van Rooij et al., 2012), contrary to a common assumption that chytrid skin swab assays only measure zoospores released from the host's skin by mature zoosporangia (Clare et al., 2016). Zoospores move via flagellar or amoeboid motility (Longcore et al., 1999) and can survive for multiple days in water (M. L. Johnson & Speare, 2003; Woodhams et al., 2008). At cooler temperatures (4-14.5 °C), low exponential death rates (~0.003 per hour (Woodhams et al., 2008)) might result in up to 40% zoospore survivorship one week post-inoculation, though the vast majority of zoospores should have encysted by this time point (Woodhams et al., 2008). Once they

locate a host, zoospores adhere to and penetrate into the host's skin, where they develop into mature zoosporangia capable of producing zoospores (S. Greenspan et al., 2012; Longcore et al., 1999). However, at 10 °C this process can take 6-13 days in frogs like *X. laevis* (Woodhams et al., 2008), during which time many immature zoosporangia remain on or close to the skin surface (Longcore et al., 1999; Van Rooij et al., 2012). This delay means that at any given time point, qPCR quantification of Bd DNA from skin swabs represents some combination of immature zoosporangia and live or dead zoospores from prior times points, in addition to zoospores released from mature zoosporangia. These various sources of genetic material make it unclear whether Bd DNA detected via skin swabs accurately reflects the release of infective zoospores (Porco et al., 2024; Van Rooij et al., 2012) and thus potential for transmission to other hosts (Woodhams et al., 2018). Since prior studies of acclimation effects on Bd infection focused on skin swab qPCR (Bradley et al., 2019; S. E. Greenspan et al., 2017; Raffel et al., 2013, 2015), it remains uncertain whether thermal acclimation effects on infection will translate into thermal acclimation effects on transmission potential.

A more direct indicator of transmission potential than qPCR of skin swabs is the rate at which a Bd-infected host releases zoospores into the water column, which can be measured by filtering zoospores out of the water and conducting qPCR on the filter (Briggs et al., 2005; Shin et al., 2014; Van Rooij et al., 2012). Shin et al. (Shin et al., 2014) suggested that filtered water samples might be a superior method for detecting infection than skin swabs because it samples the entire skin surface of the frog. Zoospore production rates have been measured in several species and have tended to positively correlate with skin swab measurements, though the degree of correlation varied among

species (DiRenzo et al., 2014, 2018; Maguire et al., 2016; Reeder et al., 2012; Shin et al., 2014). However, it remains unclear whether Bd load on a swab will always reflect zoospore production, especially early in an experimental infection (i.e., the time scale of thermal acclimation effects observed in prior studies). We hypothesized that zoospore production from Bd-infected *X. laevis* would correlate with Bd load on skin swabs and thus exhibit similar responses to temperature and thermal acclimation treatments.

To address questions about the magnitude and timing of host acclimation effects following a temperature shift (i.e., the slow-acclimation hypothesis versus the carry-over effect hypothesis) and their potential implications for Bd transmission, we performed two controlled-temperature infection experiments with *X. laevis*. To quantify the strength and timing of acclimation effects, we exposed *X. laevis* individuals to infection at different time points before and after a temperature shift and tracked infection levels at weekly intervals using qPCR of skin swabs. To evaluate how acclimation effects influence transmission potential, we quantified zoospore production rates from infected frogs in the second experiment for comparison with swab measurements.

3.2 Methods

3.2.1 Experiment 1A – thermal acclimation effects on Bd infection

We investigated the timing of acclimation effects using an individual Bd infection experiment with *X. laevis* in 2021, in which we varied the timing of Bd exposure relative to a shift in temperature. As in prior studies (Raffel et al., 2013, 2015), the experiment started with a 35 day acclimation period, during which frogs were acclimated to one of two temperatures (10 °C or 20 °C). Frogs were then shifted to new "performance" temperatures (10, 15, 20, or 25 °C), followed by a 35 day period at their new constant

temperatures (Fig. 1). The day of the temperature shift was defined as "day zero". To avoid potential for thermal shock, each frog's container was moved to its new "performance" incubator and allowed to equilibrate to the new temperature over the course of approximately 30 minutes. Forty "zero day exposure" frogs (20 per acclimation temperature) were inoculated with Bd zoospores on day zero, as soon as frogs had equilibrated to their new temperatures (similar to prior studies; (Raffel et al., 2013, 2015)). This resulted in a fully crossed 2×4 experimental design testing for interactive effects of acclimation temperature (10 or 20 °C) and performance temperature (10, 15, 20, or 25 °C) on *X. laevis* susceptibility to Bd infection, with five animals per treatment combination which was sufficient to detect hypothesized acclimation effects on Bd infection in a prior study (Raffel et al., 2015). Unlike in prior studies (Raffel et al., 2013, 2015), we chose to omit an unexposed (Bd−) control treatment to maximize sample sizes of Bd+ frogs to detect temperature effects on infection dynamics. Uninfected control frogs are essential to draw valid conclusions about how Bd infection affects frog mortality or morbidity (Raffel et al., 2013, 2015); however, results from a prior experiment suggested that Bd infection would not cause detectable mortality for individually held *X. laevis* at these experimental temperatures (Abreu Ruozzi, 2021). Bd inoculation procedures are described in a separate section below.

3.2.2 Experiment 1B – varying the day of Bd exposure relative to a temperature shift

We ran an additional experiment concurrently with Experiment 1A with overlap in temperature treatments. To minimize animal use, twenty of the forty "0 day exposure" frogs from Experiment 1A – those with performance temperatures of 10 or 20 °C (ten frogs each) – were also analyzed as the "0 day" treatment for Experiment 1B. In this

experiment, we simultaneously tested for carry-over effects and timing of thermal acclimation effects by adding an "exposure day" treatment, inoculating twenty "−7 day" frogs with Bd zoospores seven days prior to the temperature shift and inoculating twenty "+7 day" frogs seven days after the temperature shift (Fig. 3.1). Within each of five spatial blocks, four frogs (one for each combination of 2 performance × 2 acclimation temperatures) were exposed to Bd seven days prior to the temperature shift (−7 exposure day) and four frogs were exposed to Bd seven days after the temperature shift (+7 exposure day; Fig. 1). All frogs were shifted to 10 or 20 °C performance temperatures on the same day of the experiment ("day 0"). Combined with the "0 day" frogs from Experiment 1A, this resulted in a 2×2×3 experimental design testing for interactive effects of acclimation temperature (10 or 20 °C), performance temperature (10 or 20 °C), and timing of exposure relative to the temperature shift (−7, 0, or +7 days). We conducted the entire experimental design in five replicated spatial blocks of 8 incubators per block (2 incubators per temperature). Each block included one frog per treatment combination (16 frogs per block). Frogs were swabbed for quantification of Bd infection once per week throughout the entire experiment (described in a separate section below).

3.2.3 Experiment 2 – temperature dependence of Bd load versus zoospore production

We conducted a second individual infection experiment with *X. laevis* in 2022, to evaluate the replicability of acclimation effects observed in Experiment 1 and to investigate temperature effects on rates of zoospore production. We followed similar procedures to the first experiment by adding an intermediate temperature treatment to make it possible to test for curvilinearity of acclimation temperature effects. Similar to Experiment 1, frogs (N = 96) were housed at one of three acclimation temperatures (10,

15, or 20 °C) for 35 days, shifted to one of four performance temperatures (10, 15, 20, or 25 °C), exposed to Bd infection, and held at these new temperatures for another 35 days. Experiment 2 had no timing-of-exposure treatment (i.e., all animals were exposed on the day of the temperature shift, "day zero"). At 7 days post-exposure, we briefly placed each frog in clean water prior to swabbing to collect zoospores released into the water (described in a separate section below). For a subset of frogs (10 or 20 °C acclimation), we repeated this zoospore-collection procedure at 35 days post-exposure.

3.2.4 Frog maintenance and handling procedures

As soon as frogs were received from the source company (wild type, random sex, post-metamorphosis SVL to 3.81 cm, Xenopus 1 Corp. Dexter, MI), we treated them for potential preexisting Bd infection with a combination of a 7 day high-temperature incubation (30 °C) and a soak in 0.005% itraconazole solution in Amphibian Ringer's Solution for five minutes on each of six consecutive days (Brannelly, 2014). Prior to the start of each experiment, frogs were maintained in plastic bins with 4 L of dechlorinated and continuously aerated tap water in our animal care room, which is maintained at 18–20 °C on a 12:12 light cycle. Frogs used in Experiment 1 had an average initial mass of 6.07 ± 0.17 g while frogs used in Experiment 2 had an average initial mass of 9.17 ± 0.20 g (mean ± SE). Frogs exhibiting signs of severe Bd pathology including loss of righting reflex (Voyles et al., 2009) were removed from the study and euthanized via benzocaine overdose (0.5% solution in water) according to our Institutional Animal Care and Use Committee (IACUC) protocol.

During Bd infection experiments, frogs were housed in 1 L deli cups with ventilated lids and 500 mL of dechlorinated tap water (using Kordon AmQuel following

manufacturer recommendations; Kordon, LLC, Hayward, CA), placed within custom built Styrofoam incubators with transparent lids to let in room light (12:12 cycle). Incubators were constructed as described by McWhinnie et al. (McWhinnie et al., 2021). Frog water was not bubbled during each experiment, but preliminary experiments indicated that dissolved oxygen remained above 50% between water changes. Once per week, frogs received water change and were fed 3–4 g of live black worms (*Lumbriculus variegatus*). To ensure consistency of water temperatures throughout the experiment, source water was brought to the target experimental temperature prior to each water change. All experiments and animals were used following IACUC protocol 18011 and IBC protocol 2759-13.

3.2.5 Bd inoculation procedure

To prevent possible adaptation to culture conditions, we cultured Bd from cryopreserved culture stocks (stored at −80 °C; (Boyle et al., 2003)) less than one month prior to each experiment (strain JEL423 isolated in 2004 from *Peltophryne lemur* in Guabal, Panama (Boyle et al., 2003; Farrer et al., 2011)). We grew initial cultures in 1% tryptone broth at room temperature (~18 °C) until there was significant visible growth (~14 days) and then spread 1 mL of the culture broth onto 100 mm 1% tryptone agar plates. Plates were then grown for 10-14 days at room temperature with staggered start dates, starting 8-10 plates per day to ensure we had enough plates producing viable zoospores to generate sufficient inoculate on each scheduled Bd exposure day. To collect zoospores, we pipetted 1 mL of artificial spring water (ASW) onto the agar surface and spread the water around by tilting the plate back and forth for 1-2 minutes. Zoospores were quantified using a hemocytometer and the inoculate was diluted with ASW to 10^6

zoospores/mL. We inoculated frogs with Bd after a water change at the acclimation temperature. We moved each frog and its new housing water to the new performance temperature, waited 3 hours to allow the water to equilibrate to the new temperature, held the frog over its housing water with a vinyl-gloved hand, and pipetted 1 mL of inoculate (10^6 zoospores) over the frogs' dorsal side, allowing excess inoculate to drip into the water.

3.2.6 Swabbing procedure

To quantify levels of Bd infection on each animal throughout the experiment, we swabbed the animals once per week just prior to each water change. For each swabbing session, one researcher held the frog, and a second researcher brushed a fine-tip rayon urethra swab (MW113, Medical Wire & Equipment Company) five times along the ventral surface of each thigh and foot. Animal handlers wore cotton gloves over nitrile gloves to improve their grip when handling frogs (J. E. Noelker, Abreu Ruozzi, Craig, et al., 2024). Cotton gloves were removed after handling each individual frog and sanitized for later reuse by washing with quaternary disinfectant and bleach (J. E. Noelker, Abreu Ruozzi, Craig, et al., 2024). Within a spatial block (~14 frogs), nitrile gloves were sanitized with 70% ethanol, dried with a paper towel, and covered with a fresh pair of cotton gloves before handling the next frog. This procedure effectively prevents cross-contamination by Bd DNA while greatly reducing glove waste (J. E. Noelker, Abreu Ruozzi, Craig, et al., 2024). Nitrile gloves were removed and replaced before moving on to the next spatial block.

Swabs were frozen at −20 °C for later analysis using a standard qPCR assay as described by Altman and Raffel (Altman & Raffel, 2019). To hedge against possible

reaction inhibition at 1:10 dilution or failure to detect low levels of Bd DNA at 1:100 dilution, we ran each swab sample at both levels (1 well each).

3.2.7 Quantifying zoospore production (zoospore filtering procedure):

We used methods adapted from DiRenzo et al. (DiRenzo et al., 2014) to quantify the rate of zoospore production by each infected frog in Experiment 2. Frogs were placed into a fresh deli cup containing 100 mL of dechlorinated collection water for a target period of 15 minutes (the precise time was recorded for each frog). The frog was then swabbed and transferred to another new container with 500 mL fresh water (i.e., the regular water change procedure). After removing the frog, we mixed in 100 µL of bovine serum albumin (BSA) to the zoospore collection water before collecting a 10 mL sample using a 50 mL syringe. We filtered each sample using a 0.45 µm syringe filter (Cytiva Whatman GD/X 13, 6880-1304, 13 mm diameter) and methods adapted from DiRenzo et al. (DiRenzo et al., 2014). To expedite the filtering process, we used a modified caulk gun fitted with hydraulic pinch pressure gauge to ensure we never exceeded the syringe filters' maximum pressure of 75 p.s.i. (517.11 kPa), meaning no more than 51.8 lbs (230.4 N) of force on the syringe plunger (Fig. S1). Filters were capped, stored, and refrigerated for no more than 4 days until extraction. We extracted DNA by adding 200 µL of a 1:1 mixture of PrepMan Ultra and 0.25x TE buffer (diluted 1x solution TE Buffer, Tris-EDTA, pH 8.0, Fisher BioReagents) to the filters using a 1 mL syringe. Filters were then capped and dry incubated at 100 °C for 10 minutes. We then pushed air through the filter with a 1 mL syringe to push the extract out of the filter. The supernatant was collected and stored at – 20 °C. Samples were later analyzed by qPCR assay using the same procedure as for skin swabs (described above).

3.2.8 Replication of temperature treatments

To ensure true replication of temperature treatments, we used an array of 40 incubators for Experiment 1 and 44 incubators for Experiment 2. Each incubator included a spare deli cup containing 500 mL of tap water that held a HOBO temperature logger (Onset, Bourne, Massachusetts, USA) that tracked the temperature throughout the acclimation and performance periods (Fig. 3.1). We also checked the calibration of each incubator each day using an aquarium thermometer. Deli cups containing frogs and HOBO loggers were shuffled weekly to control for possible within-incubator variation in temperature.

Frogs were assigned to incubators using a type of split-plot design, similar to that described by Altman et al. (Altman et al., 2016). Each incubator contained multiple frogs, but each acclimation incubator contained only one frog for a given performance temperature or timing-of-exposure treatment, and each performance incubator contained only one frog from a given acclimation temperature (Fig. 3.1). This allowed us to treat incubator as the unit of replication for acclimation and performance temperature treatments (see Statistical Analysis section).

3.2.9 Statistical Analysis

Analyses were conducted using R statistical software (v. 4.1.3; R Core Team, 2022). The number of gene copies detected on each swab or filter was converted to zoospore equivalents (Z_e) using the conversion factor for JEL423 described by Altman and Raffel (Altman & Raffel, 2019). The zoospore production rate per 15 minutes was calculated by dividing each filtered-Bd quantity by the amount of time the frog spent soaking (appx. 15 min), multiplying by 15, and multiplying again by 10 to account for

taking a 10 mL subsample out of the 100 mL total collection water volume. To improve normality of model residuals, we log transformed all Bd quantities prior to analysis ($\ln[\text{Bd } Z_e + 1]$). To analyze Bd infection status, we categorized swab samples as positive if Bd load $\geq 0.1\ Z_e$. To test for effects of acclimation temperature, performance temperature, time since exposure, and exposure day (for Experiment 1B) on log Bd load, we ran linear mixed effects models that included random effects for the acclimation incubator, performance incubator, and individual frog identity (function *lmer* in R package *lme4*; (Bates et al., 2015). We used the *Anova* function from the *car* package to conduct Type II F tests with Kenwood-Rogers degrees of freedom (Fox & Weisberg, 2019). For each analysis, we collected unstandardized coefficients from models with marginal interaction terms removed, to make sure each coefficient's sign (+ or −) represented the directionality of effect detected by a Type II test. We also ran versions of these analyses with Bd infection status as a response variable, using the *glmmTMB* function from the *glmmTMB* package (Brooks et al., 2017) to generate generalized linear mixed effects models with binomial error and the same random effects as in the log Bd load models.

To test specific predictions about the relative strength of acclimation effects with the direction or magnitude of a temperature shift, we analyzed subsets of the day 7 & 14 data from Experiments 1A & 2, with time since exposure as a covariate. To compare the magnitude of acclimation effects for a temperature increase versus a temperature decrease, we quantified differences between 10 and 20 °C acclimation treatments for a 10 °C performance temperature (20→10 vs. 10→10) or a 20 °C performance temperature (10→20 vs. 20→20). To compare the magnitude of acclimation effects following a larger

or smaller temperature shift, we quantified the magnitude of acclimation effects in Experiment 2 for a 5 °C temperature decrease (15→10 vs. 10→10) to compare with a 10 °C temperature decrease (20→10 vs. 10→10). We made the same comparison for different magnitudes of temperature increase (15→20 vs. 20→20 and 10→20 vs. 20→20).

To analyze log Bd zoospore production, we ran linear regressions to compare log Bd zoospore production, log Bd load, acclimation temperature, and performance temperature. We also used variance partitioning to analyze the amount of shared variance in Bd zoospore production accounted for by both performance temperature and log Bd load.

3.3 Results

3.3.1 Temperature and thermal acclimation effects – Day 0 exposures (Expt. 1A & Expt. 2)

Frogs in Experiment 1A (2021) became overall more infected than frogs in Experiment 2 (2022; Fig. 3.3). Nevertheless, there were similar effects of performance and acclimation temperature in both experiments (Table 3.2). Bd infection load significantly decreased with time since exposure in Experiment 2 and had a nearly significant decreasing trend in Experiment 1A (Fig. 3.2, 3.3, Table 3.2). There was no mortality during either experiment except for one frog in Experiment 2 that was euthanized on day 14 after exhibiting signs of severe Bd-induced pathology (loss of righting reflex (Voyles et al., 2009)). No other frogs exhibited signs of severe Bd pathology (>2 pathology score as described by Voyles et al. (Voyles et al., 2009)).

There was a highly significant interaction between performance temperature and acclimation temperature in both experiments, in both cases primarily driven by high Bd infection loads in warm-acclimated frogs that were exposed to Bd at cooler performance temperatures (Fig. 3.3, Table 3.2). There was also a visible but less consistent trend towards cool-acclimated frogs having higher Bd loads than warm-acclimated frogs when exposed to Bd at warmer temperatures (Fig. 3.3). There were also highly significant negative main effects of performance temperature in both experiments and significant positive main effects of acclimation temperature in both experiments (Fig. 3.3, Table 3.2). This main effect of acclimation temperature became reduced with time since exposure (i.e., time since the temperature shift), based on a significant interaction between acclimation temperature and time since exposure in Experiment 1A (Table 3.2). The interaction between acclimation temperature and performance temperature was highly significant at day 7 of both experiments and persisted till the end of each experiment, remaining significant on day 35 in Experiment 1A and nearly significant in Experiment 2 (Table D.1). We found no curvilinear effects of acclimation temperature with the addition of the 15 °C acclimation treatment in Experiment 2. Instead, the 15 °C group exhibited intermediate Bd loads relative to 10 and 20 °C acclimated frogs, indicating a monotonic effect of acclimation temperature on host resistance to Bd infection (Fig. 3.3). Binomial mixed effects models revealed similar effects of temperature treatments on Bd infection status but with lower levels of significance (Table D.3).

3.3.2 Direction and magnitude of temperature shifts

There were stronger acclimation effects on Bd infection intensity following a decrease in temperature from 20 to 10 °C (Experiment 1A: $F_{1,8} = 31.4$, $p < 0.001$; Experiment 2: $F_{1,5} = 8.5$, $p = 0.033$) than for an increase in temperature from 10 to 20 °C (Experiment 1A: $F_{1,7.6} < 0.1$, $p = 0.855$; Experiment 2: $F_{1,5} = 2.1$, $p = 0.207$). In Experiment 2, a larger (10 °C) decrease in temperature resulted in a significant acclimation effect on Bd infection intensity whereas a 5 °C decrease only resulted in a nonsignificant trend (20→10: $F_{1,5} = 8.5$, $p = 0.033$; 15→10: $F_{1,11.3} = 3.3$, $p = 0.097$). There were no significant acclimation effects on Bd infection intensity following a temperature increase to a 20 °C performance temperature, regardless of the magnitude of the temperature shift (15→20: $F_{1,11} = 1.2$, $p = 0.299$; 10→20: $F_{1,5} = 2.1$, $p = 0.207$).

3.3.3 Timing-of-exposure effects (Experiment 1B)

The full analysis of Experiment 1A (above) provided a complete picture of how acclimation and performance temperatures influenced Bd infection in the Day 0 frogs for this experiment. For comparison with the Day −7 and Day +7 treatments, we conducted a follow up analysis of the subset of Day 0 frogs with acclimation or performance temperatures of 10 or 20 °C. This analysis was restricted to the first two weeks post-exposure, to maximize the chances of detecting short-term effects of thermal acclimation. We found significant main and interactive effects of acclimation and performance temperatures for this subset of temperature treatments that were consistent with the findings for the full Day 0 dataset (Fig. 3.4, Table 3.3). There were no significant main or interactive effects of time since exposure in this model, indicating that acclimation and performance temperature effects remained consistent for the first two weeks post-

exposure (Fig. 3.4, Table 3.3; Table D.2). No frogs died or exhibited signs of severe Bd pathology during this experiment.

For frogs exposed to Bd on Day −7 (i.e., 7 days prior to the temperature shift), there was a highly significant main effect of acclimation temperature on log Bd load, a negative effect of time since exposure, and significant interactions with time since exposure for both acclimation temperature and performance temperature (Fig. 3.4, Table 3.3). When time points were analyzed separately, there was a highly significant negative effect of acclimation temperature at 7 days post-exposure (Table D.2), at which point these frogs had not yet experienced their performance temperature treatments (Fig. 3.1). By 14 days post-exposure, these frogs had low levels of infection across all treatments and there were no detectable main or interactive effects of either acclimation or performance temperature (Table D.2). These low levels of infection persisted through the remainder of the experiment (Fig. 3.4).

For frogs exposed on Day +7, we found highly significant main effects of performance temperature on Bd load during the first two weeks post-exposure but no significant main or interactive effects of acclimation temperature or time since exposure (Fig. 3.4, Table 3.3). This performance temperature effect was only significant in the second time point after Bd exposure (Table D.2), though there was a nonsignificant trend in the first week towards higher Bd levels at the cooler performance temperature, consistent with the performance temperature effect observed for Day 0 frogs (Fig. 3.4, Table D.2). Binomial generalized linear mixed effects models failed to converge when trying to test for timing of exposure effects on Bd infection status.

3.3.4 Zoospore production (Experiment 2)

Log Bd zoospore production was significantly higher on day 7 than day 35 (Fig. 3.2, 3.5), by which time both Bd load (swab samples) and Bd production were almost reduced to zero in this experiment (Fig. 3.2, 3.4). We therefore focused our analysis of Bd zoospore production on the day 7 time point. Regardless of performance temperature treatment, zoospore production over a 15 minute collection period yielded higher Bd quantities in qPCR than standard swab samples (Fig 3.5). This resulted in positive detections of Bd infection even in frogs that tested negative based on swab samples, especially for the warmer temperature treatments (Fig. 3.2, 3.5).

There was no significant effect of host acclimation temperature on log zoospore production at either time point (day 7: $F_{7,88} < 0.1$, $P = 0.834$; day 35: $F_{3,41} = 2.1$, $P = 0.151$). As a single predictor (i.e., simple linear regression), log swab Bd had a highly significant positive effect on zoospore production on day 7 post-exposure ($F_{1,94} = 15.7$, $P > 0.001$) and accounted for 14.3% of the variance in log zoospore production. Performance temperature was an even more significant positive predictor of zoospore production ($F_{1,94} = 70.2$, $P < 0.0001$), explaining 42.7% of the variance in log zoospore production. Variance partitioning revealed that these two correlated variables explained much of the same variation in zoospore production, with performance temperature explaining 98.0% of the log swab Bd effect whereas log swab Bd only explained 32.7% of the performance temperature effect. In multiple regression with both predictors, performance temperature continued to have a highly significant negative effect on zoospore production ($F_{1,93} = 47.0$, $P < 0.0001$) but log swab Bd became non-significant ($F_{1,93} = 0.5$, $P = 0.491$).

3.4 Discussion

Both experiments revealed negative effects of current (performance) temperature on Bd infection in *X. laevis* and reduced Bd loads over time, consistent with temperature dependence of Bd infection observed in other species (Bradley et al., 2019; Raffel et al., 2013, 2015; Turner et al., 2021; Van Rooij et al., 2015) and a prior study showing that *X. laevis* mounts an acquired immune response to Bd infection (McMahon et al., 2014). There was also consistently strong evidence for beneficial acclimation effects on host resistance to Bd infection, as revealed by an interactive effect of acclimation and performance temperatures on frogs exposed to Bd on the day of the temperature shift. In both experiments, cool-acclimated frogs were more resistant to Bd infection at cooler performance temperatures than warm-acclimated frogs, and this effect was stronger following a greater decrease in temperature. Our finding of greater acclimation effects on Bd infection following a temperature decrease than for a temperature increase was similar to results from prior studies of *O. septentrionalis* and *N. viridescens* (Raffel et al., 2013, 2015). This provides further support for the temperature variability hypothesis of Rohr and Raffel (Rohr & Raffel, 2010), adding to a growing list of species found to have increased susceptibility to Bd infection following a recent drop in temperature (Raffel et al., 2013, 2015). As with these other species, *X. laevis* may benefit from experiencing lower levels of individual Bd infection through time if intraannual temperature shifts occur slowly or infrequently enough to allow frogs to remain fully acclimated to current temperatures for a greater fraction of each year. However, zoospore production measurements from Experiment 2 suggest that temperature variability effects on individual infection intensities may have less impact on Bd transmission dynamics than

we previously assumed, given our inability to detect thermal acclimation effects on zoospore production (discussed further below).

The strong effects of frog acclimation status on Bd infection persisted for at least five weeks following the temperature shift (and Bd exposure) in both Experiment 1A and Experiment 2, in contrast to prior studies where acclimation effects on Bd infection were detectable two weeks post-exposure (also 2 weeks following the temperature shift) but had dissipated by four weeks post-exposure (Bradley et al., 2019; Raffel et al., 2013). We used a timing-of-exposure treatment to help distinguish between two alternative hypotheses to account for acclimation effect persistence: the slow-acclimation hypothesis and the carry-over effect hypothesis. Contrary to the slow-acclimation hypothesis, which postulates extended delays in the acclimation of frog immune systems to a new performance temperature, frogs exposed to Bd one week following a temperature shift (Day +7) exhibited no acclimation effects on Bd infection. This suggests that the frogs became fully acclimated to their new temperatures within the 7 days following the temperature shift, at least in terms of their ability to fight off Bd infection. A thermal acclimation time of less than 7 days for resistance to Bd infection is consistent with measurements of thermal acclimation times for other aspects of amphibian thermal performance (e.g., CT_{max}), which have usually been in the range of 1–11 days (Blem et al., 1986; H. Craig et al., 2024; Dunlap, 1969; Feder, 1985).

The lack of acclimation effects in Day +7 frogs is, however, consistent with the carry-over effect hypothesis. This finding suggests that the delay in *X. laevis* acclimation following a temperature shift is relatively brief (i.e., less than 7 days), but that Bd can take advantage of this brief window of opportunity to establish higher infection

intensities in warm-acclimated frogs that then carry over into later time points (Fig. 3.4). Our results suggest that this carry-over effect is strong enough to result in persistently higher infection levels for at least four weeks after frogs become fully acclimated to the new temperature. Infection is a dynamic process, and it is hardly surprising that current Bd infection intensities should be affected by Bd infection intensities in the recent past. However, effects of past events (e.g., exposure to a past acclimation temperature) are typically assumed to dissipate through time, and four weeks is longer than it took in past studies for acclimation effects on Bd infection dynamics to dissipate (Raffel et al., 2013, 2015). One way that early acclimation effects on infection dynamics could persist for more than four weeks is if high Bd infection intensities are self-perpetuating in *X. laevis,* perhaps due to Bd suppression of immune responses (Fites et al., 2013). Further research would be needed to confirm that Bd immune suppression is responsible for these effects and under what circumstances carry-over effects result in persistently high infections.

The carry-over hypothesis also predicts that high infection levels prior to a temperature shift should carry over to high infection levels following the shift, regardless of the performance temperature treatment. However, we did not find evidence for this in frogs exposed to Bd infection 7 days prior to a temperature shift (day −7). When these frogs were exposed to Bd at the cooler acclimation temperature, they developed higher infection intensities by the time of the temperature shift (day 0), but these higher infection intensities did not carry over to the next time point (day 7). The low levels of Bd infection by day 7 can be partly explained based on the strong negative effect of warm performance temperatures, given that three of the temperature treatments (warm-warm, warm-cold, cold-warm) involved at least one week of exposure to 20 °C. Nevertheless,

the lack of persistent high infections in five frogs that experienced the cold-cold treatment is inconsistent with the carry-over effect hypothesis. A second inconsistency is that cold-acclimated frogs exposed to Bd on day 0 did not get heavily infected when exposure occurred at the cold performance temperature, unlike frogs exposed to ostensibly identical (cold-cold) temperature conditions after Bd exposure on day −7 (Fig. 3.4). The reason for this inconsistency is unclear, though it may simply highlight the importance of random variation when dealing with small sample sizes (five animals per treatment combination). Another possible difference is that the Day −7 and Day 0 exposure frogs were exposed to separately prepared Bd inoculates. We made every effort to maintain consistent inoculate quality by standardizing culture methods and concentrations of live (moving) zoospores, but we cannot rule out the possibility that random effects of inoculate quality might have resulted in different levels of infection. Random effects on inoculate quality might also account for differences in overall infection levels between Experiments 1 and 2, though this could also be due to other random effects, such as working with *X. laevis* juveniles with different size distributions.

Zoospore production data from Experiment 2 ("filter Bd") provided us with an opportunity to evaluate how an aquatic frog's infection intensity, as measured via DNA quantification of skin swabs, relates to their transmission potential. Our findings were consistent with prior studies of terrestrial frogs that observed higher detectability of Bd zoospores from filtered-water samples than from swab samples, but with a positive correlation between filter Bd and swab Bd (DiRenzo et al., 2014, 2018; Maguire et al., 2016; Reeder et al., 2012; Shin et al., 2014). However, we failed to detect an effect of host acclimation temperature on Bd zoospore production, despite detecting a significant

acclimation effect on Bd skin swabs. These conflicting results suggest the possibility these two response variables are biologically distinct from each other, such that production of Bd zoospores might not always be directly proportional to Bd infection intensity. This is contrary to a common assumption of disease models (Briggs et al., 2010). A result reinforcing this conclusion was that the negative effect of performance temperature on filter Bd remained significant after controlling for its relationship with swab Bd load, due to frogs at cool temperatures having high zoospore production relative to their swab Bd loads. The latter result may suggest that individual zoosporangia have higher zoospore production rates at cooler temperatures, consistent with high per-sporangium zoospore production rates in culture reported by Woodhams et al. (Woodhams et al., 2008). However, this does not account for the lack of acclimation effects on Bd zoospore production in our experiment. Another plausible reason why Swab Bd and Filter Bd might generate different patterns is if temperature has different effects on development or survival of immature zoosporangia than on zoospore production by mature zoosporangia. In this case, acclimation temperature might have different effects on swab Bd versus filter Bd, especially in the first several days following an experimental infection, assuming that immature zoosporangia make a significant DNA contribution to Bd swab measurements. This assumption seems plausible given that immature zoosporangia remain on or near the epidermal surface of a frog's skin for multiple days following Bd exposure (Van Rooij et al., 2012).

The mechanisms driving different acclimation effects on Swab Bd versus zoospore production may be unclear, but the implications of these differences could be consequential. Prior studies of host acclimation effects on Bd infection focused solely on

Swab Bd, a common measure of individual infection intensity that correlates with individual health outcomes (e.g., probability of death; (Vredenburg et al., 2010)). However, zoospore production should provide a better indication than Swab Bd of a host's ability to transmit Bd to other individuals. Our results do not call into question the individual-level consequences of delays in host acclimation, as postulated by the Temperature Variability Hypothesis, but they do warrant caution in extrapolating these results to variable-temperature effects on population-level transmission dynamics. If acclimation effects only influence individual infection intensity, without subsequent effects on transmission to other animals, then the overall effect of variable temperatures on population level disease dynamics might be less important than suggested by prior studies. One caveat is that our zoospore production results focused on a single time point in Experiment 2 (7 days post-exposure), and it is possible that the persistent acclimation effects observed in Experiment 1A might have led to unobserved acclimation effects on zoospore production at later time points. Nevertheless, our findings demonstrate the importance of examining multiple aspects of Bd infection (e.g., Swab Bd and Filter Bd) when considering effects of environmental factors on both individual and population level disease processes.

3.5 Data availability statement

Data and R code are available here: (J. Noelker et al., 2024)

https://doi.org/10.5061/dryad.k3j9kd5gv

3.6 Acknowledgments

Jason P. Sckrabulis and Andrea R. Nadjarian provided feedback on the experimental design and provided experimental assistance. Graziella V. DiRenzo provided valuable

insights that helped us adapt our methods for measuring zoospore production. Multiple undergraduate researchers assisted with experiments, animal care, and qPCR assays: Jacob T. Heabeart, Nicole Wanis, Michael Manuel, Lutfi Abu-Shanab, Faris Mahjoub, Declan S. McCrary, Gina Ghose, Alana Sandomierski-Stellman, Carson Evans, Besjana Ahmetaj, Sebastian Taulbee, and Onil Potris. Financial support was provided by a NSF grant to TRR (IOS 1651888), an Honors College grant to KDS, and a Provost Award grant to JEN, and the OU Research Excellence Fund. JEN, VAR, and HMC were also supported by graduate assistantships from the OU Department of Biological Sciences.

This chapter was published in *Royal Society Open Science*:

Noelker, J. E., Abreu Ruozzi, V., Spengler, K. D., Craig, H. M., & Raffel, T. R. (2024). Dynamic effects of thermal acclimation on chytridiomycosis infection intensity and transmission potential in *Xenopus laevis*. *Royal Society Open Science*, *11*(9), 240789. https://doi.org/10.1098/rsos.240789

CHAPTER THREE TABLES

Table 3.1: Response variable abbreviations and their definitions used for statistical model fitting.

Variable	***Abbreviation***	***Definition***
Acclimation temperature	AccTemp	The temperature a frog experienced during the (earlier) acclimation period of the experiment (°C).
Infection status	BdStatus	A frog's infection status as either infected (1) or uninfectied (0)
Day	Day	Time within the experiment relative to the day of the temperature switch (Day 0).
Exposure day	DayOfExpo	Timing of Bd exposure for each frog, relative to the day of the temperature switch (Day 0).
log Bd zoospore production	LnFilterBd.rate	Natural log of Bd zoospore equivalents produced over 15 minutes (ln[Bd Z_e +1])
log Bd load	LnSwabBd	Natural log of Bd zoospore equivalents detected from a swab sample (ln[Bd Z_e +1])
Performance temperature	PerfTemp	The temperature a frog was exposed to during the (later) performance period of the experiment (°C).
Time since exposure	TimeSinceExposure	Number of days elapsed since the timing of Bd exposure for each swab or filter sample

Table 3.2: Interactive effects of performance temperature, acclimation temperature, and time since exposure on LnSwabBd, only for frogs exposed to Bd immediately after the temperature shift ("Day 0" exposure day). Predictor variables included AccTemp (acclimation temperature), PerfTemp (performance temperature), and TimeSinceExposure (days since Bd exposure). Variable abbreviations are defined in Table 3.1. Statistical tests were based on Kenward-Rogers degrees of freedom (df), which may be non-integers in mixed effects models.

Experiment	*Predictor*	*Coefficient*	*F*	*df*	*P*
1A	**Acclimation temperature**	**0.1142**	**6.9**	**1, 17.1**	**0.017**
	Performance temperature	**−0.2340**	**33.3**	**1, 29.6**	**< 0.001**
	Time since exposure	−0.0232	3.8	1, 154.3	0.052
	AccTemp × PerfTemp	**−0.0289**	**12.8**	**1, 29.6**	**0.001**
	AccTemp × TimeSinceExposure	**−0.0052**	**4.8**	**1, 154.3**	**0.030**
	PerfTemp × TimeSinceExposure	−0.0001	< 0.1	1, 154.1	0.947
	AccTemp × PerfTemp × TimeSinceExposure	< 0.0001	< 0.1	1, 154.1	0.955
2	**Acclimation temperature**	**0.0584**	**6.2**	**1, 18.9**	**0.022**
	Performance temperature	**−0.0736**	**13.4**	**1, 21.3**	**0.001**
	Time since exposure	**−0.0214**	**23.8**	**1, 380.8**	**< 0.001**
	AccTemp × PerfTemp	**−0.0174**	**16.9**	**1, 53.0**	**< 0.001**
	AccTemp ×TimeSinceExpo	−0.0004	0.1	1, 381.9	0.734
	PerfTemp × TimeSinceExposure	**0.0039**	**25.0**	**1, 381.5**	**< 0.001**
	AccTemp × PerfTemp × TimeSinceExposure	0.0003	2.1	1, 383.6	0.146

Table 3.3: Interactive effects of performance temperature, acclimation temperature, and time since exposure for Experiment 1B. Analysis of temperature effects (PerfTemp & AccTemp) at 7 and 14 days since exposure. Variable abbreviations are defined in Table 3.1. Statistical tests were based on Kenward-Rogers degrees of freedom (df), which may be non-integers in mixed effects models. Note: for day of exposure treatments −7 and +7, only a single frog was housed per incubator for these treatments resulting in no df decimals.

Day of exposure	***Predictor***	***Coefficient***	***F value***	***Df***	***P***
−7	**Acclimation temperature**	**−0.2679**	**52.1**	**1, 16**	**< 0.001**
	Performance temperature	0.0456	1.5	1, 16	0.237
	Time since exposure	**−0.3157**	**99.4**	**1, 16**	**< 0.001**
	AccTemp × PerfTemp	−0.0053	0.5	1, 16	0.489
	AccTemp × TimeSinceExposure	**0.0576**	**82.8**	**1, 16**	**< 0.001**
	PerfTemp × TimeSinceExposure	**−0.0337**	**28.4**	**1, 16**	**< 0.001**
	AccTemp × PerfTemp × TimeSinceExposure	**0.0043**	**11.5**	**1, 16**	**0.004**
0	**Acclimation temperature**	**0.2568**	**14.9**	**1, 10.7**	**0.003**
	Performance temperature	**−0.3143**	**21.3**	**1, 10.6**	**0.001**
	Time since exposure	0.0199	< 0.1	1, 15.2	0.861
	AccTemp × PerfTemp	**−0.0521**	**15.3**	**1, 10.8**	**0.003**
	AccTemp × TimeSinceExposure	−0.0087	0.2	1, 15.5	0.669
	PerfTemp × TimeSinceExposure	−0.0040	0.1	1, 15.5	0.798
	AccTemp × PerfTemp × TimeSinceExposure	−0.0049	1.8	1, 15.7	0.199
+7	Acclimation temperature	0.0198	< 0.1	1, 16	0.835
	Performance temperature	**−0.3064**	**10.7**	**1, 16**	**0.005**
	Time since exposure	−0.0894	0.7	1, 16	0.405
	AccTemp × PerfTemp	0.0039	< 0.1	1, 16	0.837
	AccTemp × TimeSinceExposure	0.0002	< 0.1	1, 16	0.993
	PerfTemp × TimeSinceExposure	−0.0294	2.0	1, 16	0.178
	AccTemp × PerfTemp × TimeSinceExposure	−0.0023	0.3	1, 16	0.592

CHAPTER THREE FIGURES

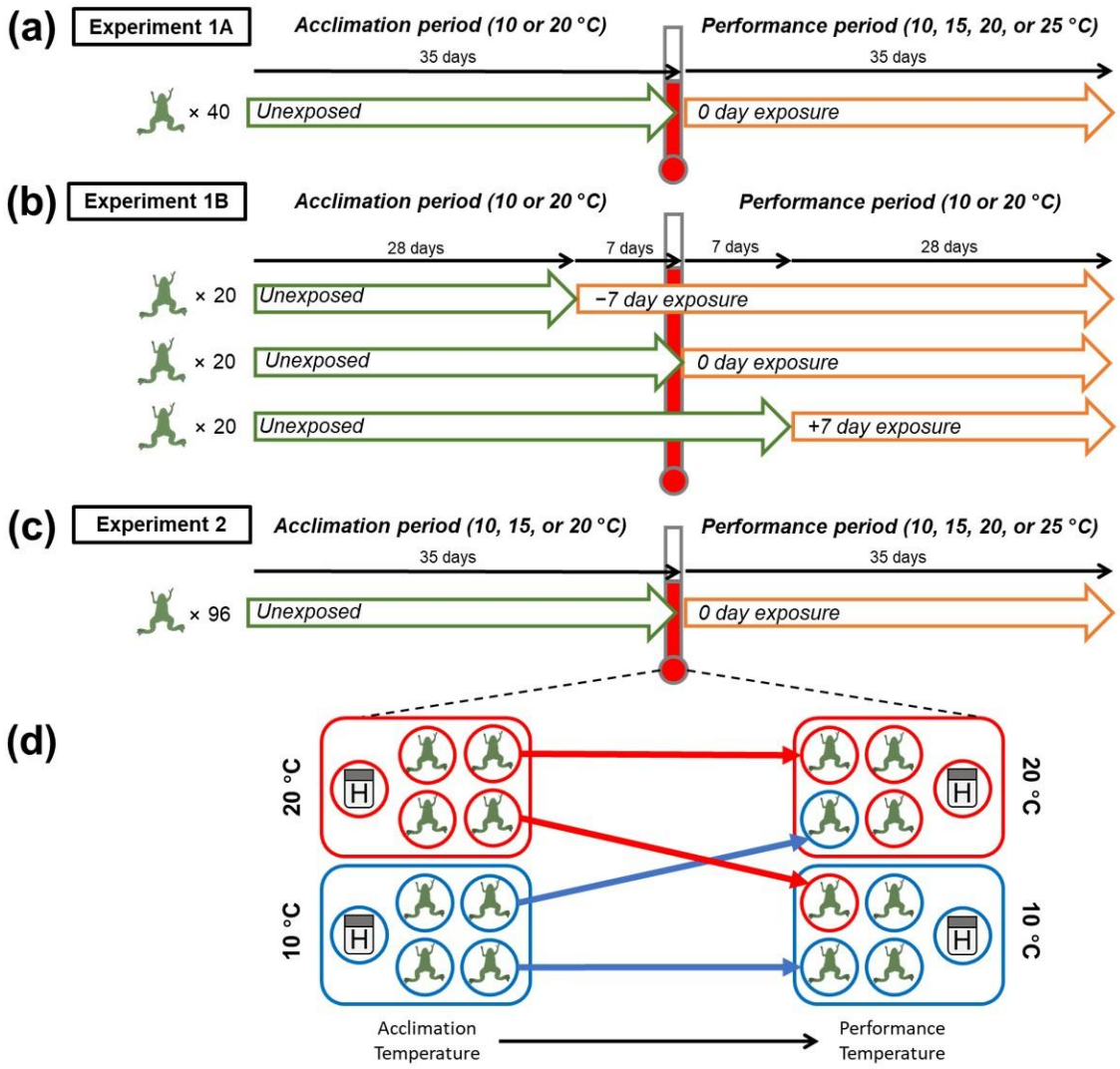

Figure 3.1: Experimental timelines for (a) Experiment 1A, (b) Experiment 1B, and (c) Experiment 2, summarizing the timing of Bd exposure (green→orange arrows) relative to a temperature shift (thermometer) for each exposure-day treatment. (d) Illustration of how frogs assigned to warm (red) or cold (blue) acclimation incubators were all transferred to randomly assigned performance incubators within the same spatial block. Each incubator also contained a "blank" deli cup with a HOBO temperature logger (represented by the icon with "H") and the same water volume as cups housing frogs, to verify temperatures achieved within each incubator.

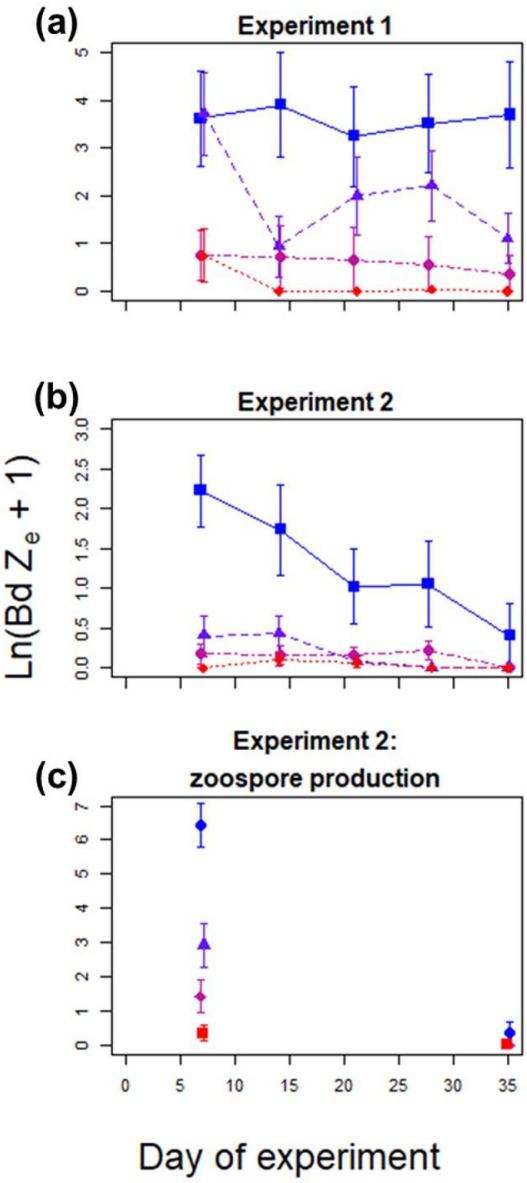

Figure 3.2: Overall effects of performance temperature on Bd infection dynamics throughout the performance period for "day 0" frogs (i.e., frogs exposed to Bd on the day of the temperature shift). (a) Experiment 1A dynamics based on skin swabs (LnSwabBd). (b) Experiment 2 dynamics based on skin swabs. (c) Zoospore production over 15 minutes from Experiment 2 as measured by water filtration (LnFilterBd.rate). 10 °C: blue solid squares and solid lines; 15 °C: purple solid triangles and dashed lines; 20 °C: solid magenta circles and dot-dashed lines; 25 °C: solid red diamonds and dotted lines. Points have been jittered on the x-axis. Error bars indicate standard error.

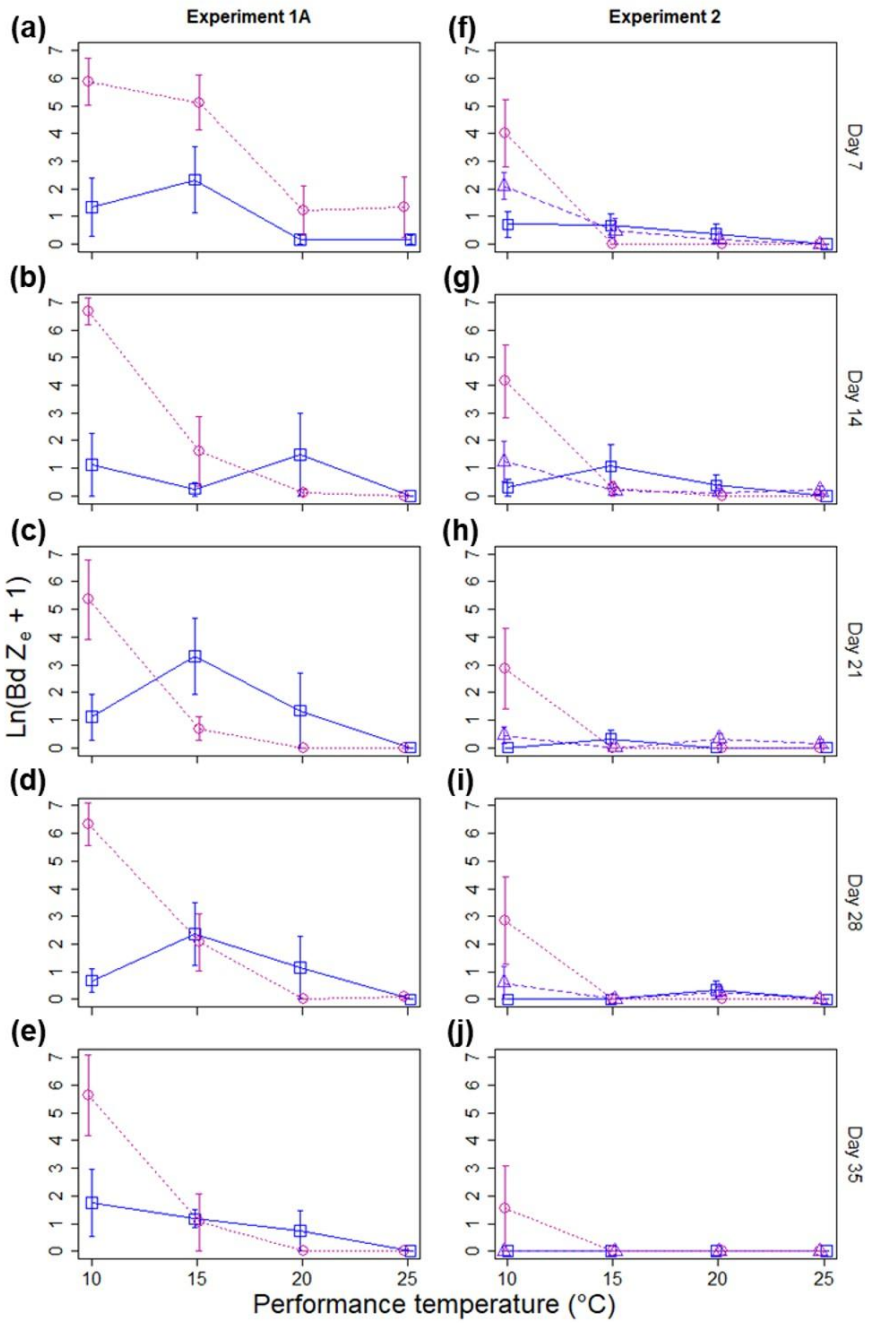

Figure 3.3: Acclimation and performance temperature effects for (a–e) Experiment 1A and (f–j) Experiment 2. Acclimation temperatures were 10 °C (open blue squares and solid lines), 15 °C (open purple triangles and dashed lines), or 20 °C (open magenta circles and dot-dashed lines). Each row represents a different week during the performance period of the experiment, with "days" indicating the time since the temperature shift and Bd exposure occurred. Points are jittered on the x-axis. Error bars indicate standard error.

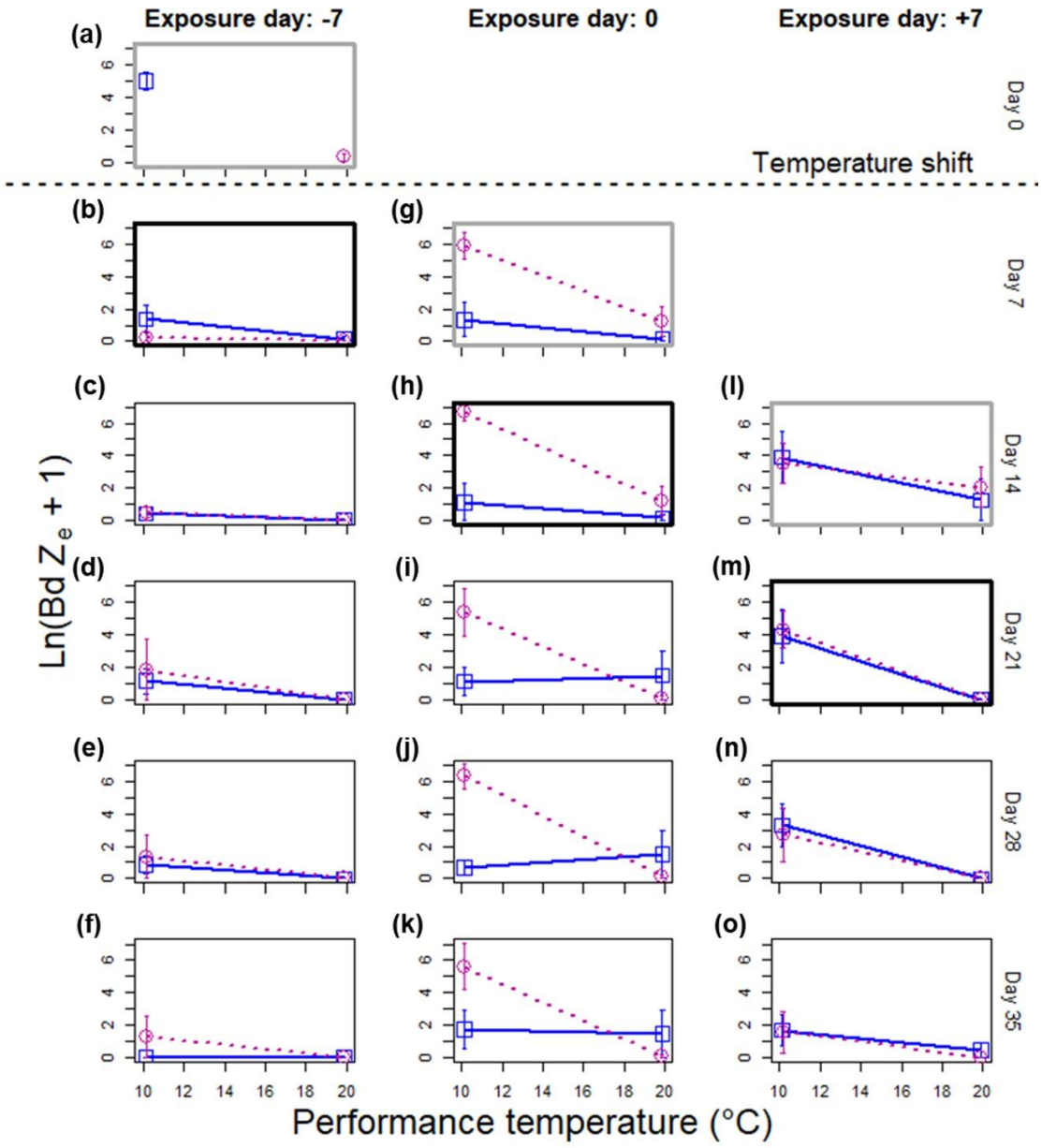

Figure 3.4: Acclimation effects for timing of exposure treatments from Experiment 1B. Panels (a–f) are frogs that were exposed one week prior to the temperature shift (Day −7). Panels (g–k) are frogs exposed on the day of the temperature shift (Day 0). Panels (l–o) are frogs exposed one week after the temperature shift (Day +7). Acclimation temperatures were 10°C (blue squares and solid lines) or 20°C (magenta circles and dotted lines). Plots outlined in thick grey boxes indicate the time point 7 days after Bd exposure. Plots outlined with thick black boxes indicate time points 14 days after Bd exposure. Frogs in panel A had not yet experienced performance temperature treatments and are therefore shown at their acclimation temperatures. Error bars indicate standard error.

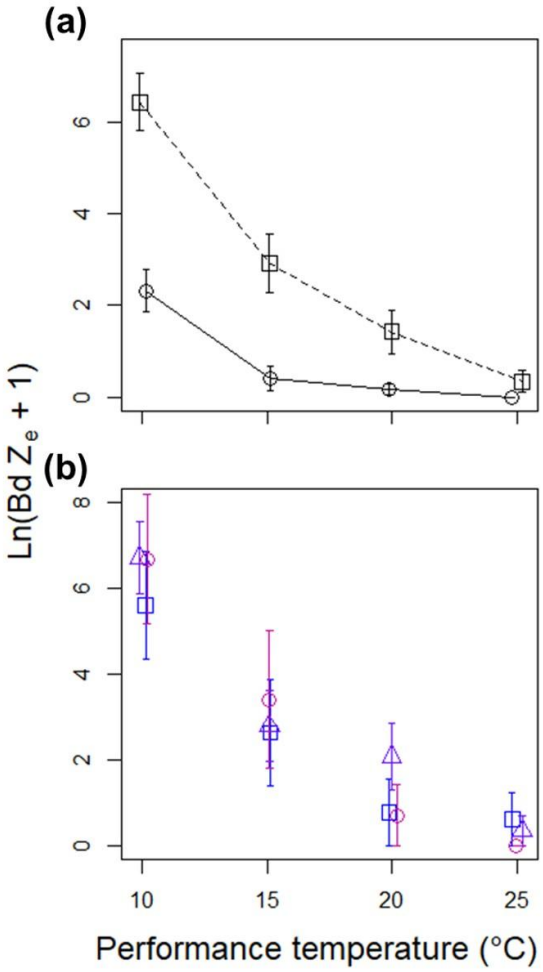

Figure 3.5: Bd zoospore production over 15 minutes (LnFilterBd.rate) as a function of performance temperature on day 7 of Experiment 2. (a) Comparison of zoospore production (open squares and dashed line) to Bd load from skin swabs (LnSwabBd; open circles and solid line). (b) Comparison of zoospore production by frogs acclimated to 10 °C (open blue squares), 15 °C (open purple triangles), or 20 °C (open magenta circles). Points are jittered on the x-axis. Error bars indicate standard error.

CHAPTER FOUR

GLOBAL ENVIRONMENTAL PREDICTORS OF METABOLIC THERMAL PERFORMANCE AMONG AMPHIBIANS

4.1 Introduction

The Metabolic Theory of Ecology (MTE) postulates that an organism's metabolism has directly scalable implications across multiple biological and ecological levels (J. H. Brown et al., 2004; Gillooly et al., 2001; Stark et al., 2025). According to MTE, ecological rate processes are driven by the rates of organism-level physiological and metabolic rates, which are in turn driven by rates of chemical reactions within their component cells (J. H. Brown et al., 2004; Dell et al., 2011). Since the introduction of MTE (Brown et al., 2004), researchers have become increasingly interested in better understanding the implications of metabolism for a variety of biological systems (Stark et al., 2025). Ectotherm metabolic rates depend on a variety of variables including life history strategies, activity, and environmental temperature (Carter et al., 2023; DeLong et al., 2018; Deluen et al., 2022; Mineo & Schaeffer, 2015; Vasseur et al., 2014; Wells et al., 1996). Temperature in particular directly impacts organism metabolic rates by affecting the rates of enzyme-assisted chemical reactions within cells (Gillooly et al., 2001), and a species' thermal tolerances are important determinants of their geographic ranges (Deluen et al., 2022; Mineo & Schaeffer, 2015; Wells et al., 1996). The broader thermal breadths of ectotherms living in temperate regions farther from the equator compared to the narrower breadths of species found near the tropics (Sunday et al., 2011)

is one piece of evidence that highlights an important question of whether and how organisms evolve metabolic adaptations to temperature.

MTE generates clear predictions for organism metabolic rates and physiological performance based on body mass and body temperature (Angilletta, 2006; Dell et al., 2011). MTE-based thermal performance curve (TPC) models, i.e., models describing the temperature dependence of organism physiological processes, are typically derived from the Arrhenius equation that describes temperature dependence of chemical reactions (Arrhenius, 1889; Molnár et al., 2017). Two key parameters of MTE-based TPCs are the metabolic activation energy (E_A) and the metabolic performance at a specified standardization temperature (B_{T0}; Molnár et al., 2017).

Early MTE modeling efforts used broad among-species comparisons of metabolic rates to estimate E_A values, implicitly making the simplifying assumption that E_A is approximately constant across aerobic organisms or at least across broad taxonomic groupings (J. H. Brown et al., 2004; Gillooly et al., 2001, 2002). However, variation among species for these key parameters exists (e.g., Dell et al., 2011). Relatively few studies have examined species specific estimates of core MTE parameters E_A or B_{T0} values (e.g., McWhinnie et al., 2021), and the most prominent comparative studies of species-specific E_A have relied mostly on indirect proxies of metabolic rate such as locomotor performance (e.g., burst speed or jumping distance; Dell et al., 2011, 2013, 2014). Even fewer studies of among-species variation in species-specific E_A have focused on the most direct proxy for the whole-body metabolic rate of aerobic organisms, i.e., the resting rate of oxygen consumption (indeed, I was unable to find an example in the primary literature). If we allow for the fact that there is among-species variation in core

MTE parameters like E_A, and perhaps even within-species plasticity in the value of E_A (Sckrabulis et al., 2022), then an important question becomes whether and to what extent species exhibit adaptive evolution in metabolic parameters such as E_A and B_{T0} in response to environmental temperature. This question will become increasingly important as climate change continues to alter patterns of temperature and temperature variability in the future.

One way to address questions about metabolic thermal adaptation is by conducting comparative analyses of thermal parameters across many species (Huey & Kingsolver, 1989). For example, DeLong et al. (2018) tested four alternative hypotheses about how cold versus warm adaptation affects the relationship between an organism's thermal optimum (T_{opt}) and its maximum resting metabolic rate (i.e., Metabolic Cold Adaptation, Hotter is Better, Colder is Better, and Peak Matching hypotheses; DeLong et al., 2018). However, these four hypotheses do not generate clear predictions for among-species variation in metabolic E_A.

Multiple evolutionary hypotheses have been proposed that predict patterns of thermal adaptation involving changes in thermal breadth or the rate of metabolic increase in temperature, both of which could relate to among-species variation in metabolic E_A. In general, prior authors have postulated that within-generation temporal variation in climate (e.g., seasonal) should be the dominant selection pressure for the evolution of thermal breadths (Huey & Kingsolver, 1989). Based on this idea, the Climate Variability Hypothesis (CVH) posits that ectotherms in temperate regions will have broader thermal breadths than species in tropical regions, due to the need to tolerate a wider range of seasonal temperatures (Dewenter et al., 2024). This prediction has been supported by

comparative studies of thermal tolerances (critical thermal maximum [CT_{max}] and minimum [CT_{min}]; $CT_{max} - CT_{min}$) in various ectotherm taxa (Dewenter et al., 2024; Sunday et al., 2011), but to our knowledge potential implications of the CVH for E_A variation remains untested. The "Jack-Of-All-Temperatures" (JOAT) hypothesis posits that constraints on energetics or efficiency of enzyme function prevent maximal metabolic performance in all thermal environments, leading to a specialist-generalist trade-off between maximal thermal performance and performance breadth (Dewenter et al., 2024; Huey & Kingsolver, 1989; Vasseur et al., 2014; Visher & Boots, 2020). Assuming temperate organisms have broader thermal breadths (i.e., the CVH; Dewenter et al., 2024), JOAT predicts that warm-temperature thermal specialists should have higher maximal metabolic rates than temperate thermal generalists, with T_{opt} at the upper end of the TPC (Fig. 4.1).

In this study, we used metabolic TPCs for adult amphibians, derived from direct metabolic measurements (resting O_2 consumption), to test predictions of evolutionary hypotheses for among-species variation in key metabolic parameters. We hypothesized that species-level E_A values evolve adaptively in response to the historic temperatures that species experienced in their native geographic ranges. We further hypothesized that lower metabolic E_A corresponds to both higher metabolic performance at lower temperatures and broader thermal breadths, based on collision theory which predicts less temperature dependence of chemical reactions and faster reactions at lower temperatures (i.e., the Arrhenius equation; Arrhenius, 1889). Based on a combination of the CVH and JOAT hypotheses, we predicted temperate species would be thermal generalists with lower E_A values and higher metabolic performance at cool temperatures than tropical

species (Fig. 4.1). This should lead to a negative among-species relationship between E_A and metabolic performance when measured at a cool temperature (i.e., ≤ 10 °C), and it should also result in lower E_A for species that historically experienced colder seasonal temperatures in their geographic range. We further predicted that tropical species would be warm-temperature specialists, leading to a higher thermal maximum than temperate species and thus a positive among-species relationship between E_A and metabolic performance at warmer temperatures (Fig. 4.1).

4.2 Methods

4.2.1 Species selection for respirometry experiments

To test these hypotheses, it is especially important for biologists conducting respirometry trials to be able to ensure data integrity and robust experimental design that, ideally, include replicated temperature treatments and multiple measurements across a range of temperatures. To achieve this, we developed an updated, user-friendly and cost-effective version of the respirometry device first described by McWhinnie et al. (2021). McWhinnie et al. (2021) presented an Arduino based respirometry system that utilizes readily available electronic components to capture the percent difference in the amount of oxygen (O_2) available in ambient air compared to air from a chamber housing a frog. This system was validated with and successfully captured the total O_2 consumption of *Xenopus laevis* across temperatures to generate a TPC (McWhinnie et al., 2021). We tested an updated version of this Arduino respirometry system by quantifying the O_2 consumption of five additional species. We provide an updated version of the Arduino based system presented by McWhinnie et al. (2021) that utilizes a 3D printed circuit

board (which we named the "*Bufo Breathalyzer 2.0*") that provides reliable data at a fraction of the cost of traditional or manufactured systems.

We collected data for *Pseudacris crucifer, Osteopilus septentrionalis, Anaxyrus americanus, Atelopus zeteki* and *Atelopus varius*. These species were selected based on local availability (*P. crucifer* and *A. americanus*) or to broaden the geographic regions represented in our study (*O. septentrionalis, A. zeteki*, and *A. varius*). We collaborated with the Detroit Zoo (Detroit Zoological Society; DZS), which houses breeding populations of *A. zeteki* and *A. varius*. The primary goal of our proposed collaborative project with DZS is to measure temperature dependence of O_2 consumption in these and potentially additional amphibian taxa, allowing us to estimate key metabolic parameters for each species (e.g., E_A). DZS staff provided support and input in the design of respirometry trials and experiments as needed to ensure animal welfare standards at DZS.

4.2.2 Literature data collection

To obtain literature values for published adult amphibian resting O_2 consumption data, we narrowed the compiled dataset in Chapter 12 of *Environmental Physiology of the Amphibians* (Feder & Burggren, 1992; Gatten, Jr. et al., 1992) to species with data from at least three temperatures, the minimum number of temperature treatments needed to detect nonlinear TPC patterns. I also included data collected for *Notophthalmus viridescens* (H. M. Craig, 2024) and *Ambystoma mexicanum* (Brady, 2019) from prior Raffel Lab students.

4.2.3 Respirometry methods

For terrestrial species, we used either flow-through respirometry or intermittent-flow respirometry. For larger species, we conducted flow-through respirometry (Fig. 4.2)

to allow continuous air flow to the animal. This method allowed us to compare the O_2 concentration of ambient air compared to air flowing through the animal chamber. For smaller species which were particularly challenging to quantify, we used intermittent-flow respirometry similar to strategies used for fish (Svendsen et al., 2016). This allowed us to measure the O_2 consumption rate of an animal over the time when the air flow was directed to the bypass airline (Fig. 4.3).

We achieved each method (flow-through or intermittent flow) using 3-way stopcock valves into the air hoses downstream from the Drierite chambers to direct either the airflow from the frog or the bypass line. The frog chamber itself was modified to meet the needs of each focal species (Fig. 4.4) and measured O_2 concentrations from ambient air and air passed through the animal chamber using custom-built *Bufo Breathalyzer 2.0* respirometry devices based on the open source Arduino system (Fig. 4.4) first presented in McWhinnie et al. (2021). Depending on the species, we customized the size of respirometry chambers to accommodate each species and pose minimal risk to each frog.

For each species, we constructed custom respiration chambers using a variety of plastic containers such as 50 mL centrifuge tubes and locking Rubbermaid containers (Fig. 4.4) with ports for airflow from the air pump. We inserted damp, unbleached paper towel (enough to cover the bottom of each chamber) to ensure animals remained hydrated during the trials. We removed excess water vapor from the airlines prior to O_2 measurement in the *Bufo Breathalyzer* by passing the air through a secondary chamber filled with approximately 52 g of Drierite (Fig. 4.2). We quantified O_2 consumption for each species across at least 5 ecologically relevant temperatures for each species, using

an array of reptile incubators and re-randomized incubator temperature assignments for each temporal block to ensure true replication of treatments. All respirometry trials were completed in compliance with Oakland University IACUC #2022-1193.

For each species, we adjusted our experimental approach to ensure animals were relaxed with minimal activity, since our variable of interest was resting metabolic rate. For *O. septentrionalis*, we used 50 mL centrifuge tube modified with air nozzles on either end. *P. crucifer* was more difficult due to their particularly small size. To accommodate *P. crucifer*, we further modified 50 mL centrifuge tubes by removing the middle portion of the tube and gluing the two ends together to produce a chamber with an even smaller internal volume (Fig. 4.4). *A. varius* and *A. zeteki* were quite comfortable in our chambers made from Rubbermaid containers. For *A. americanus* individuals were more active once enclosed in the respirometry chamber and needed a longer acclimation period to relax to a resting state (> 4 hours) similar to what was observed for other relatively large toad species such as *Rhinella marina* (Overgaard et al., 2012). To assess species activity levels, we collected observational data during each trial every 15 minutes and recorded scores of whether the animal had not moved (score = 0), shifted in place (score = 1), moved its entire body 2-3 times (score = 2), moved its entire body 3-4 times (score = 3), or moved its entire body > 4 times (score = 4) allowing us to remove trials where frogs were overly active (average score for each trial > 1.5).

4.2.4 *Bufo breathalyzer 2.0* performance

We tested verified an updated version of the Arduino based respirometry system first presented in McWhinnie et al. (2021) using a new 3D printable circuit board (designed by Matthew Bruer, Oakland University Engineering). We also upgraded to a

new air flow sensor (MEMS Flow Sensor D6F-P, Omron Corp.) and confirmed that they produce accurate and precise data by conducting simultaneous measurements of the same air flow stream at several different flow rates with a bubble flow sensor (Soap Film Bubble Flowmeter Model 20136, Restek Corp., Bellefonte, Pennsylvania, USA). We then plotted the data against each other and performed a Pearson's correlation test. We also tested the precision of the O_2 sensors by comparing the O_2 concentration in two airlines, one with ambient air and the other with 100% Nitrogen gas.

The new *Bufo Breathalyzer 2.0* system provided highly accurate and precise airflow measurements (Pearson's correlation $P < 0.01$; Fig. 4.5) when compared with measurements based on the bubble flow meter (Fig. 4.5). Our tests validating the O_2 sensors found that although the O_2 sensors varied with age, they consistently measured O_2 concentration in the Nitrogen gas stream at very close to 0% O_2 (all < 1 %; Fig. 4.5). This allowed us to make calibration adjustments to the O_2 concentrations measured compared to the known atmospheric O_2 concentration. To do this for each run, we multiplied each O_2 measurement by the known atmospheric O_2 concentration (20.946% O_2) divided by the average O_2 measurement during ambient-air periods. This calibration provides an important update to the potential precision of our measurements compared to the original device presented in McWhinnie et al. (2021).

4.2.5 Fitting MTE-based TPCs to respirometry data

After sufficient data had been collected for all species across at least three temperatures (to determine curvilinearity), we fit mass-corrected O_2 consumption data to thermal performance curves using the Boltzmann-Arrhenius (BA) equation (Arrhenius, 1889; Sckrabulis et al., 2022):

$$B_T = B_{T0} e^{-\frac{E_A}{k}\left(\frac{1}{T}-\frac{1}{T_0}\right)} \quad \text{Eq. 4.1}$$

and the more complex Sharpe-Schoolfield (SS) equation simplified for high-temperature enzyme deactivation (Schoolfield et al., 1981):

$$B_T = B_{T0} e^{-\frac{E_A}{k}\left(\frac{1}{T}-\frac{1}{T_0}\right)} \cdot \left[1 + e^{\frac{E_D^H}{k}\left(-\frac{1}{T_P^H}+\frac{1}{T}\right)}\right]^{-1}. \quad \text{Eq. 4.2}$$

We compared model fits with all four combinations of simple BA versus more-complex SS models and normal versus lognormal error distributions. Trying both normal and lognormal error is important for fitting MTE-based thermal performance curves (Xiao et al., 2011). In this case, we expected most O_2 consumption data to be lognormally distributed, except for datasets based aggregated data that had been averaged across multiple individuals which were more likely to be normally distributed due to the Central Limit Theorem (Gotelli & Ellison, 2013). We used Akaike information criterion (AIC) to select the model of best model for each species (Angilletta, 2006; Xiao et al., 2011). All results were analyzed in R (version 4.1.3) using packages *deSolve* (ver. 1.35), *Hmisc* (ver. 4.6.0), *minpack.lm* (ver. 1.2.3), and *simecol* (ver. 0.8.14) (Elzhov et al., 2023; Harrell & Dupont, 2022; Petzoldt & Rinke, 2007; R Core Team, 2022; Soetaert et al., 2010). We then compiled two sets of metabolic parameter estimates for each species, including activation energy (E_A) and metabolic performance at 10, 20, and 30 °C (B_{10}, B_{20}, and B_{30}). The first were estimates from the model of best fit based on AIC comparisons (Table 4.1, 4.2), while the second was based on parameter estimates from only the best SS model for each species.

SS models can have trouble converging on a reasonable estimate for the high temperature deactivation energy (E_D^H) if there is insufficient data above the T_{opt} for a particular TPC (Molnár et al., 2017), resulting in relatively few estimates of E_D^H in the primary literature and the need to sometimes estimate E_D^H based on outside sources of information (Molnár et al., 2013). In this study, there were only three species that readily converged on reasonable values for E_D^H as a free parameter (*Atelopus zeteki*, *Ambystoma maculatum*, *Anaxyrus woodhousii*). For all other species, we fixed E_D^H to the mean value for these three species to achieve SS model convergence for use in among-model and among-species comparisons (Table 4.1, 4.2).

4.2.6 Collecting climate and environmental predictors from amphibian native ranges

To quantify species environmental and climatic data from the geographic ranges where species evolved, we downloaded species occurrence data from the Global Biodiversity Information Facility (*GBIF*, 2024). I then removed duplicate observations based on identical latitude and longitude locations and subset the occurrence data to locations only within the native range of each species based on map data from the International Union for Conservation of Nature and Natural Resources (IUCN; Fig. 4.9; *The IUCN Red List of Threatened Species*, 2024). Species occurrence latitude and longitude locations from GBIF were matched to values for standard bioclimatic variables within the WorldClim map layers between 1970-2000, which has been used in past studies as a standard timeframe for establishing historic climate conditions (Fick & Hijmans, 2017; *WorldClim*, 2024). These environmental variables were then averaged for each species using R statistical software (v. 4.1.3) and R packages *maptools* (ver. 1.1.3), *raster* (ver. 3.6.20), *dismo* (ver. 1.3.9), *sf* (ver. 1.0.12) and *ggplot2* (ver. 3.3.5; Bivand &

Lewin-Koh, 2022; Hijmans, 2023; Hijmans et al., 2022; Pebesma, 2018; R Core Team, 2022; Wickham, 2016). We also obtained elevation data for each observation location for all species based on the Global Multi-resolution Terrain Elevation Data (GMTED2010) database (Danielson & Gesch, 2011).This resulted in a weighted average for each bioclimatic variable and elevation across each species native range, weighted according to the number of times each species was observed in a particular location. We then combined the bioclimatic and elevation data into a single summary dataset along with metabolic parameter estimates (E_A, B_{10}, B_{20}, and B_{30}) taken from the best model (lowest AIC overall for BA or SS models) for each species as well as the estimates from the best SS model (lowest SS AIC) for each species.

4.2.7 Analyzing among-species variation in MTE parameters

To look for relationships between activation energy (E_A) and performance at 10, 20, or 30 °C (B_{10}, B_{20}, or B_{30}), we conducted linear regression models (function *lm*) with log transformed B_{10}, B_{20}, or B_{30} as response variables, and E_A as the predictor variable with log of mass (g) and Family taxa as covariates. To investigate the effects of environmental variables on amphibian E_A, we explored possible relationships by running a Pearson's correlation between each environmental variable and our E_A estimates. We then conducted forward selection with linear regression models (function *lm*). We tested all amphibian E_A estimates against environmental variables before testing subsets of the dataset by Family (Anura, Caudata). Gymnophiona had only one species represented in the dataset which was insufficient for this analysis. We then repeated the final statistical tests using metabolic parameter estimates taken from the best SS model for each species.

4.3 Results

In total, we obtained metabolic parameters for 60 adult amphibian species with North and Central America being the regions with the greatest representation. In total, our dataset included 36 North American, 1 Caribbean, 10 Central American, 2 South American, 4 European, 2 African, 3 Asian, and 2 Australian (Fig. 4.9). Results from our respirometry experiments and literature data generated species level E_A values that fell within the expected range of 0.2 – 1.2 eV as described by Dell et al. (2011; Fig. 4.6, 4.7, 4.8, 4.10; Table 4.1, 4.2). We also found significant negative effects of mass on performance at 10, 20, and 30 °C (B_{10}, B_{20}, and B_{30}; Table 4.3).

The model with the lowest AIC (e.g., BA, SS, log[BA], vs. log[SS]) varied depending on the species dataset. For most species (33 species; 55%), models assuming normally distributed error provided a better fit compared to species with models assuming lognormal errors (27 species; 45%). Of the 52 species where models were based solely on aggregated data, 35 species (92.1%) had lower AIC assuming lognormal error whereas 17 (77.3%) had lower AIC assuming normal error. For the 8 species with models based on individual data points, 3 species had lower AIC assuming lognormal error and the remaining 5 had lower AIC assuming normal error.

There was a significant negative relationship between species-level E_A and B_{10}, a nonsignificant negative trend towards a relationship between E_A and B_{20} , and a significant positive relationship between E_A and B_{30} (Fig. 4.11; Table 4.3). We found similar patterns for B_{10} and B_{20} when compared with E_A estimates from only SS models, however for B_{30}, the relationship was not significant and was, in fact, a negative trend (Fig. 4.11). When testing environmental predictors of E_A estimates (BA or SS) across all

amphibian species, there were no significant predictors of E_A. When we conducted a separate analysis of species in Family Anura, there were again no significant environmental predictors of E_A. However, three models resulted in significant environmental predictors of E_A for Caudata. In two separate single-predictor models, there was a significant positive effect of mean annual temperature on salamander E_A and a significant positive effect of mean temperature of the coldest quarter on salamander E_A (Fig. 4.12; Table 4.4). However, together, mean elevation and mean distance from the equator (absolute value of the latitude) explained more variation (i.e., greater R^2 values) among salamander E_A than either single predictor model (Fig. 4.12; Table 4.4). The results for these final environmental analyses found the same significant predictors of E_A estimates from Caudata and Anura when conducted using parameter estimates from only SS models.

4.4 Discussion

Our study adds to the growing number of adult amphibian datasets for which resting O_2 consumption has been quantified (Fig. 4.6, 4.7, 4.8; Table 4.1, 4.2). Additionally, the MTE-based TPC models we fit to our compiled datasets provided E_A estimates within the expected range for aerobic organisms (0.2 – 1.2 eV; Fig. 4.10; Table 4.1, 4.2; Dell et al., 2011). We found metabolic parameters for *Xenopus laevis* consistent with McWhinnie et al. (2021)'s analysis of the same dataset, though the estimates were not identical. This is because we used a different mass-scaling coefficient ($O_2 \cdot g^{-1}$ compared to $O_2 \cdot g^{-0.75}$ for McWhinnie et al. 2021) to allow comparisons with published studies that presented only mg $O_2 \cdot g^{-1}$ data (Gatten, Jr. et al., 1992). Our results also found significant negative effects of body mass on metabolic rate at 10, 20, and 30 °C (B_{10}, B_{20},

and B_{30}; Table 4.3), consistent with Metabolic Theory predictions for mass scaling effects on metabolism (J. H. Brown et al., 2004; Gillooly et al., 2001).

When comparing all amphibian species, we found a significant negative relationship between metabolic E_A and metabolic performance at 10 ˚C (B_{10}) regardless of when we used parameters from lowest AIC models (BA or SS), or estimates from only SS models. At 20 ˚C, the relationship between E_A and B_{20} was nonsignificant but retained a negative trend for both analyses. However, at 30 °C (B_{30}), this relationship became significantly positive for model parameters taken from the best overall model (BA or SS) but remained a nonsignificant negative trend when we used parameters from only SS models. The patterns we observed from both versions of the analysis (best model or best SS) are consistent with the wider thermal breadths (and lower E_A) predicted for temperate generalists as predicted by CVH, however, only the analysis that used parameters derived from the best model overall (i.e., a mix of BA or SS models for any given species), was consistent with the generalist-specialist tradeoffs postulated by the JOAT hypothesis. The significant negative relationship between E_A and metabolic performance at cool temperatures (B_{10}) and positive relationship at warm temperatures (B_{30}) is consistent with the idea that temperate species evolved lower E_A values. If there the significant positive relationship between E_A and metabolic performance at warm temperatures (B_{30}) is accurate, that would suggest that generalist-specialist trade-offs led to reduced performance of temperate species at warmer temperatures. However, the strength of these patterns is questionable considering they were nonsignificant and trended negative when we used only parameters from SS models. These results generally support the idea that

warm-temperature thermal specialists tend to have higher activation energies and thermal generalists tend to have lower activation energies.

Based on CVH, we also predicted that species that experience cooler seasonal temperatures (i.e., temperate species) should have lower activation energies. We found no significant environmental predictors of E_A for all amphibian species. Subsequent forward selection, even with nonsignificant trends of various environmental predictors, continually returned nonsignificant results. We then posited that there could be important taxonomic differences between amphibian families. When we analyzed our results according to separate amphibian families, we found significant predictors of E_A across global latitudinal and elevation gradients for Caudata. We found no such effects of environmental predictors on anuran E_A. These results were true for both compilations of parameter estimates (BA or SS, or only SS), so from here I will discuss results based on the analysis using parameters from the lowest overall model AIC (BA or SS).

Temperature is an important driver of ectotherm performance and our study suggests that, at least for family Caudata, there are important selective pressures of thermal environment on evolution of metabolic activation energies. Our results found strong effects of the average minimum temperature on E_A for salamanders. Further analysis identified that elevation and absolute latitude (north or south relative to the equator) explained more variation among salamander E_A. This finding is consistent because elevation and latitude are strong geographic drivers of the minimum temperature experienced at a given location. These results suggest that the climate could be an important selective pressure for salamander metabolism.

In contrast to salamanders, we did not identify any significant environmental predictors of anuran E_A, despite having a comparable sample size. Why would frogs exhibit so little evidence of adaptive evolution in metabolic E_A, when there was such a strong pattern in salamanders? We speculate that the lack of environmental predictors of anuran E_A might relate to dissimilarities between salamanders and frogs in their ability to regulate body temperature via behavioral thermoregulation. Most salamanders are either fully aquatic or have fossorial lifestyles, and most terrestrial salamanders are largely nocturnal (Duellman & Trueb, 1986; Petranka, 1998). This might limit opportunities for salamanders to regulate their body temperatures via behavioral thermoregulation, leading to strong selection pressure to evolve metabolic adaptations to optimize performance at a given temperature. In contrast, many anuran species have terrestrial or arboreal lifestyles and actively forage for food during daytime, providing increased opportunities for thermoregulatory behaviors such as basking (Duellman & Trueb, 1986). This capacity of anurans to respond to temperature variation with behavioral adaptations might reduce selection pressure to evolve metabolic thermal adaptations, relative to salamanders. Future investigations could further test this idea by expanding the analysis to include additional taxa, including non-amphibians, to determine if organisms with aquatic, fossorial, or nocturnal lifestyles are more likely to exhibit relationships between metabolic E_A and environmental temperatures.

We compared model fits assuming normal or lognormal error distributions. MTE tends to predict that metabolic processes should be lognormally distributed, due to exponential effects of body mass and temperature on metabolic rates (Gillooly et al., 2001; Gotelli & Ellison, 2013). Xiao et al. (2011) reported that most (68.6%) of

physiological and morphological allometric datasets they investigated approximated a lognormal error distribution, but 16.6% fit better with a normal error distribution. One possible reason for datasets to approximate a normal distribution, despite the MTE prediction, is because much data from published studies consists of pooled means from measurements of multiple individuals rather than individual data points. According to the Central Limit Theorem, datapoints based on means of aggregated data should become more normally distributed as the sample size per datapoint increases (Gotelli & Ellison, 2013). In our study, 22 of the 60 species-specific datasets had best fit models with normally distributed error, and 17 out of those 22 datasets were based on aggregated sample means rather than individual datapoints. Five of the eight datasets with individual measurements had lognormal error distributions according to AIC comparisons. It would be interesting to compare normal versus lognormal model fits for individual versus aggregated data from the sample sets to better test if data aggregation was an important source of (apparently) normal error distributions in the published datasets.

Our findings also highlight how the open source Arduino system first described by McWhinnie et al. (2021) can successfully capture the whole body O_2 consumed from a variety of amphibian species and further validates the capabilities of the system to collect reliable data for a variety of taxa with species of variable sizes. Additionally, the updates provided in our study make this system more accessible to research groups by providing 3D-printable schematics for the electronic circuit board and oxygen sensor covers (Fig. 4.4). This system could provide a valuable resource to researchers seeking an inexpensive alternative to manufactured systems. The *Bufo breathalyzer 2.0* system's small size, portability, and low cost to construct many devices also allows for greater

flexibility in experimental design and replication of temperature treatments compared to more traditional systems. For example, it can facilitate experimental designs seeking to investigate thermal performance nested within other experimental treatments (e.g., looking for performance differences between parasite infected versus uninfected individuals). In addition to amphibian respirometry, this system may also be useful in collecting O_2 consumption data for other taxa including small reptiles. An important consideration when using this system for measurements of resting metabolic rate is selecting a respirometry chamber where animals will remain comfortable throughout the trial. For example, hylid species often choose to inhabit small spaces (e.g., pipe samplers) and appear to be comfortable in smaller chambers fashioned from centrifuge tubes, whereas bufonids appeared to be more relaxed when tested in larger Rubbermaid containers (Fig. 4.4). Smaller chambers tended to provide more precise respirometry measurements in our trials, though the need for this is reduced with a flow-through respirometry approach during which measurement precision depends more on the rate of air flow (Fig. 4.2).

4.5 Conclusion

Our findings support the broad adaptationist hypothesis that environmental pressures shape the evolution of metabolic thermal performance curves of amphibians, revealing a negative correlation between E_A and metabolic performance at cool temperatures (B_{10}). Results from analyses consider parameters from BA or SS models found a positive correlation between E_A and metabolic performance at warm temperatures (B_{30}) that are consistent with predictions of the Climate Variability Hypothesis (CVH) and the Jack-Of-All-Temperatures (JOAT) hypotheses. The same final analysis using

only SS model parameters also supported the broader thermal breadths expected for generalists as predicted by CHV. This small difference in results shows that there is still some uncertainty surrounding amphibian performance at warm temperatures, depending on model selection. For salamanders, our analysis also revealed a positive effect of environmental temperatures on metabolic E_A, as predicted by the Climate Variability Hypothesis (CVH). However, for anurans we observed no significant relationships between environmental predictors and E_A, contrary to our prediction. Further investigation is needed to further elucidate potential drivers of among-species variation in metabolic E_A of anurans. There is substantial bias towards North American species in the available data for amphibian respirometry TPCs, highlighting the need for further investigations into additional species from around the world to obtain a more representative sample. We also present updates to the open source Arduino respirometry system presented by McWhinnie et al. (2021) and highlight its effectiveness and experimental flexibility to make respirometry measurements across temperatures and taxa.

4.6 Acknowledgements

Vanessa Six, Declan McCrary, and Alejandro Pimentel Hernandez provided experimental assistance with amphibian respirometry experiments and modeling. Mark Vassallo and Michael Andrus provided valuable access and assistance with animals at Detroit Zoo. Jason Sckrabulis provided helpful feedback for updating the Arduino device and compiling our species distribution database. Matthew Bruer was the engineer who designed the 3D printable circuit board files.

CHAPTER FOUR TABLES

Table 4.1: Table of metabolic parameters for 32 Anurans species using either the Boltzman-Arrhenius (BA) model or modified Sharpe-Schoolfield (SS) model for O_2 consumption and log-normal O_2 consumption for each species. Listed is the activation energy (E_A), performance temperature at 10 ˚C (B_{10}), and high temperature in Kelvin (T_H) for those with best fit SS models. Standard error (s.e.) is given where possible estimates without s.e. values are due to models with ≤ 3 data points.

Taxon	***Species***	***Best Fit***	E_A	B_{10}	T_H
Order Anura					
Bufonidae	*Anaxyrus americanus*	ln BA	0.34 ± 0.13	0.04 ± 0.010	—
	Anaxyrus boreas	ln BA	0.53 ± 0.11	0.07 ± 0.018	—
	Anaxyrus cognatus	ln SS	0.71	0.07	297
	Anaxyrus terrestris	BA	1.04 ± 0.10	0.02 ± 0.006	—
	Anaxyrus woodhousii	ln SS	1.26 ± 0.27	0.03 ± 0.003	294 ± 1.7
	Atelopus varius	BA	0.49 ± 0.09	0.07 ± 0.016	—
	Atelopus zeteki	ln SS	0.55 ± 0.08	0.06 ± 0.008	307 ± 1.8
	Bufo bufo	ln BA	0.48 ± 0.25	0.08 ± 0.058	—
	Rhinella marina	BA	0.60 ± 0.07	0.05 ± 0.010	—
Hylidae	*Acris crepitans*	BA	0.74 ± 0.02	0.06 ± 0.002	—
	Dryophytes chrysoscelis	SS	0.77	0.05	311
	Dryophytes cinereus	SS	0.69	0.08	304
	Dryophytes gratiosus	ln SS	0.37	0.10	315
	Dryophytes versicolor	BA	0.41 ± 0.07	0.12 ± 0.015	—
	Osteopilus septentrionalis	ln SS	0.64 ± 0.12	0.04 ± 0.007	309 ± 2.7
	Pseudacris crucifer	ln BA	0.53 ± 0.09	0.07 ± 0.011	—
	Pseudacris triseriata	SS	0.43	0.24	306
Phyllomedusidae	*Phyllomedusa sauvagii*	ln BA	0.66 ± 0.02	0.04 ± 0.002	—
Myobatrachidae	*Crinia parinsignifera*	BA	0.55 ± 0.03	0.13 ± 0.010	—
	Crinia signifera	ln BA	0.56 ± 0.03	0.13 ± 0.007	—
Ranidae	*Hylarana erythrae*	BA	0.84 ± 0.10	0.02 ± 0.005	—
	Lithobates catesbeianus	SS	0.96	0.01	305
	Lithobates clamitans	ln SS	0.70	0.04	300
	Lithobates pipiens	ln BA	0.62 ± 0.06	0.05 ± 0.008	—
	Lithobates virgatipes	BA	0.76 ± 0.04	0.04 ± 0.003	—
	Pelophylax lessonae	SS	1.15 ± 0.44	0.02 ± 0.006	294 ± 2.3
	Rana arvalis	SS	0.80 ± 0.02	0.08 ± 0.003	311.± 1.7
	Rana temporaria	BA	0.78 ± 0.01	0.06 ± 0.001	—
Scaphiopodidae	*Scaphiopus couchii*	ln BA	0.45 ± 0.05	0.04 ± 0.004	—
Dicroglossidae	*Fejervarya cancrivora*	ln BA	0.70 ± 0.06	0.03 ± 0.004	—
	Occidozyga martensii	ln SS	0.48 ± 0.13	0.04 ± 0.012	311 ± 2.6
Pipidae	*Xenopus laevis*	ln BA	0.51 ± 0.06	0.09 ± 0.007	—

Table 4.2: Table of metabolic parameters for 27 Caudata and a single Gymnophiona species using either the Boltzman-Arrhenius (BA) model or modified Sharpe-Schoolfield (SS) model for O_2 consumption and log-normal O_2 consumption for each species. Listed is the activation energy (E_A), performance temperature at 10 ˚C (B_{10}), and high temperature in Kelvin (T_H) for those with best fit SS models. Standard error (s.e.) is given where possible estimates without s.e. values are due to models with ≤ 3 data points.

Taxon	*Species*	*Best Fit*	E_A	B_{10}	T_H
Order Caudata					
Plethodontidae	*Aneides hardii*	ln BA	0.37 ± 0.06	0.05 ± 0.004	—
	Batrachoseps attenuatus	BA	0.64 ± 0.12	0.04 ± 0.010	—
	Bolitoglossa occidentalis	BA	1.02 ± 0.35	0.02 ± 0.013	—
	Bolitoglossa subpalmata	SS	0.93 ± 0.16	0.02 ± 0.002	295 ± 1.7
	Desmognathus fuscus	BA	0.45 ± 0.09	0.04 ± 0.004	—
	Desmognathus ochrophaeus	ln BA	0.66 ± 0.07	0.03 ± 0.002	—
	Desmognathus quadramaculatus	BA	0.36 ± 0.07	0.03 ± 0.005	—
	Eurycea bislineata	SS	1.15 ± 0.20	0.04 ± 0.003	292 ± 1.8
	Eurycea multiplicata	BA	0.78 ± 0.08	0.02 ± 0.003	—
	Gyrinophilus porphyriticus	BA	0.78 ± 0.01	0.02 ± 0.000	—
	Plethodon cinereus	ln BA	0.55 ± 0.03	0.03 ± 0.008	—
	Plethodon dorsalis	ln SS	0.72 ± 0.30	0.03 ± 0.006	296 ± 3.1
	Plethodon glutinosus	BA	0.64 ± 0.04	0.03 ± 0.003	—
	Plethodon jordani	BA	0.64 ± 0.05	0.03 ± 0.002	—
	Plethodon neomexicanus	SS	0.20 ± 0.05	0.07 ± 0.003	303
	Pseudoeurycea gadovii	BA	0.70 ± 0.07	0.03 ± 0.004	—
	Pseudoeurycea goebeli	BA	0.85 ± 0.08	0.02 ± 0.003	—
	Pseudotriton ruber	SS	0.88	0.02	301
	Thorius spilogaster	BA	0.78 ± 0.16	0.02 ± 0.008	—
Cryptobranchidae	*Cryptobranchus alleganiensis*	ln SS	0.61	0.02	300
Ambystomatidae	*Ambystoma maculatum*	ln SS	0.67 ± 0.10	0.07 ± 0.007	302 ± 1.5
	Ambystoma mexicanum	ln SS	1.05 ± 0.12	0.03 ± 0.003	300 ± 1.5
	Ambystoma tigrinum	ln BA	0.40 ± 0.09	0.08 ± 0.013	—
Amphiumidae	*Amphiuma means*	ln BA	0.75 ± 0.09	0.01 ± 0.001	—
Proteidae	*Necturus maculosus*	BA	0.60 ± 0.04	0.01 ± 0.001	—
Salamandridae	*Notophthalmus viridescens*	ln BA	0.40 ± 0.04	0.07 ± 0.005	—
	Taricha granulosa	BA	0.43 ± 0.02	0.08 ± 0.002	—
Order Gymnophiona					
Herpelida	*Boulengerula taitana*	SS	0.54	0.04	390

Table 4.3: Linear regression model with log(Performance) at 10, 20 or 30 °C (B_{10}, B_{20}, or B_{30}) as the response variable and activation energy (E_A), log(mass [g]), and Family as predictor variables. Results from analyses that used parameters derived from TPC models with the overall lowest AIC (i.e., BA or SS models) are listed first. Results from analyses that used only parameters derived from the best (lowest AIC) SS models are listed second.

TPC model	***°C***	***Predictor***	***Coefficient***	***F-value***	***d.f.***	***p***
Lowest AIC (BA or SS)	10	Activation energy (E_A)	−1.36	34.7	1, 42	< 0.001
		log(mass [g])	−0.11	3.8	1, 42	0.058
		Family		8.2	13, 42	< 0.001
	20	Activation energy (E_A)	−0.35	3.1	1, 42	0.087
		log(mass [g])	−0.10	4.5	1, 42	0.039
		Family		11.2	13, 42	< 0.001
	30	Activation energy (E_A)	0.96	23.0	1, 42	< 0.001
		log(mass [g])	−0.10	4.5	1, 42	0.039
		Family		11.2	13, 42	< 0.001
Lowest AIC (SS only)	10	Activation energy (E_A)	−1.50	37.9	1, 42	< 0.001
		log(mass [g])	−0.09	2.3	1, 42	0.137
		Family		7.1	13, 42	< 0.001
	20	Activation energy (E_A)	−0.43	4.0	1, 42	0.053
		log(mass [g])	−0.09	2.7	1, 42	0.111
		Family		9.4	13, 42	< 0.001
	30	Activation energy (E_A)	−0.57	1.2	1, 42	0.281
		log(mass [g])	−0.14	1.2	1, 42	0.271
		Family		2.6	13, 42	0.009

Table 4.4: Environmental predictors of amphibian E_A based on parameters from the best SS model for each species. Mean annual temperature and mean temperature of the coldest quarter were each significant predictors of E_A for amphibian species in Family Caudata. However, together, mean elevation and distance from the equator (mean absolute value of latitude) explained the greatest amount of variation among salamander E_A. There were no significant environmental predictors of anuran E_A.

Model	***Order***	***R^2***	***Predictor***	***Coefficient***	***F-value***	***d.f.***	***p***
1	Caudata	0.304	Mean annual temperature	0.032	10.9	1, 25	0.002
2		0.254	Mean temperature of the coldest quarter	0.016	8.5	1, 25	0.007
3		0.483	Mean elevation	-1.65×10^{-4}	11.8	1, 24	0.002
3			Mean absolute value of latitude	−0.024	22.4	1, 24	< 0.001
1	Anura	< 0.001	Mean annual temperature	4.90×10^{-4}	5.7×10^{-3}	1, 30	0.941
2		< 0.001	Mean temperature of the coldest quarter	-9.16×10^{-5}	5.0×10^{-4}	1, 30	0.983
3		0.005	Mean elevation	$1.295.7 \times 10^{-5}$	1.5×10^{-3}	1, 29	0.927
3			Mean absolute value of latitude	0.001	0.2	1, 29	0.698

CHAPTER FOUR FIGURES

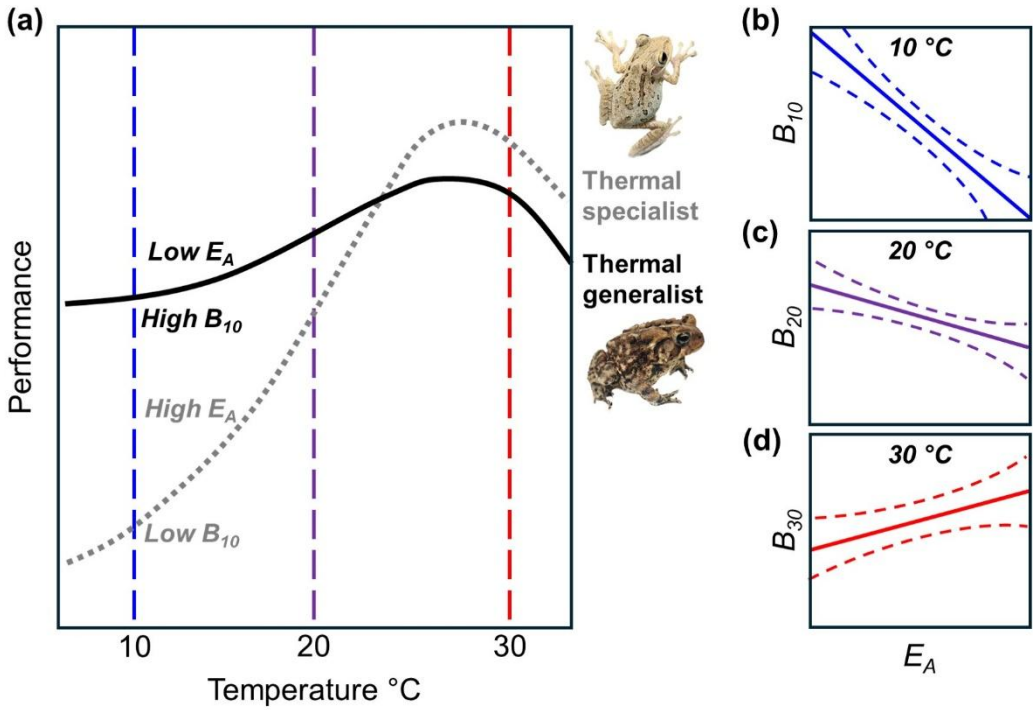

Figure 4.1: Hypothetical predictions for amphibian metabolic TPCs based on specialist-generalist tradeoffs, as predicted by a combination of the Jack-Of-All-Temperatures hypothesis (JOAT) and the Climate Variability Hypothesis (CVH). (a) A hypothesized thermal generalist (e.g., *Anaxyrus americanus*) should have a lower metabolic activation energy (E_A) and higher performance at cooler temperatures (B_{10}) while the hypothesized thermal specialist (e.g., *Osteopilus septentrionalis*) should have higher E_A and higher performance at warmer temperatures. (b), (c), and (d) show the predicted negative relationship between B_{T0} and E_A at cooler temperatures and positive relationship after the thermal performance curves cross at warmer temperatures.

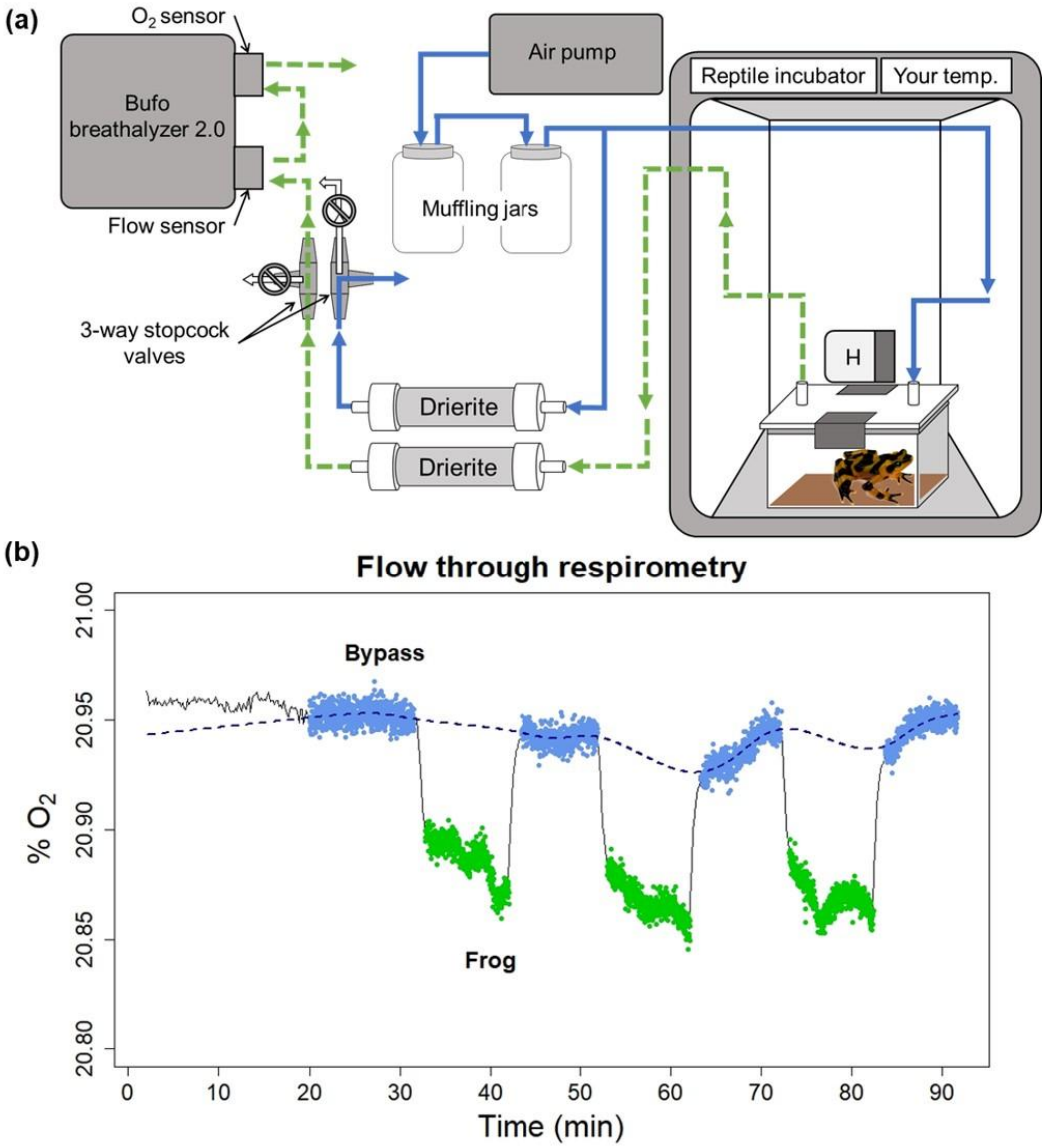

Figure 4.2: Experimental design setup for flow through respirometry. Three-way stopcock valves were used to direct the airflow measured at any given time allowing continuous flow. (a) shows the path of air flow from the air pump then split into either an ambient air line (blue arrows) or the animal chamber line (green arrows). (b) shows a sample respirometry trace (blue points are ambient air; green points are animal air).

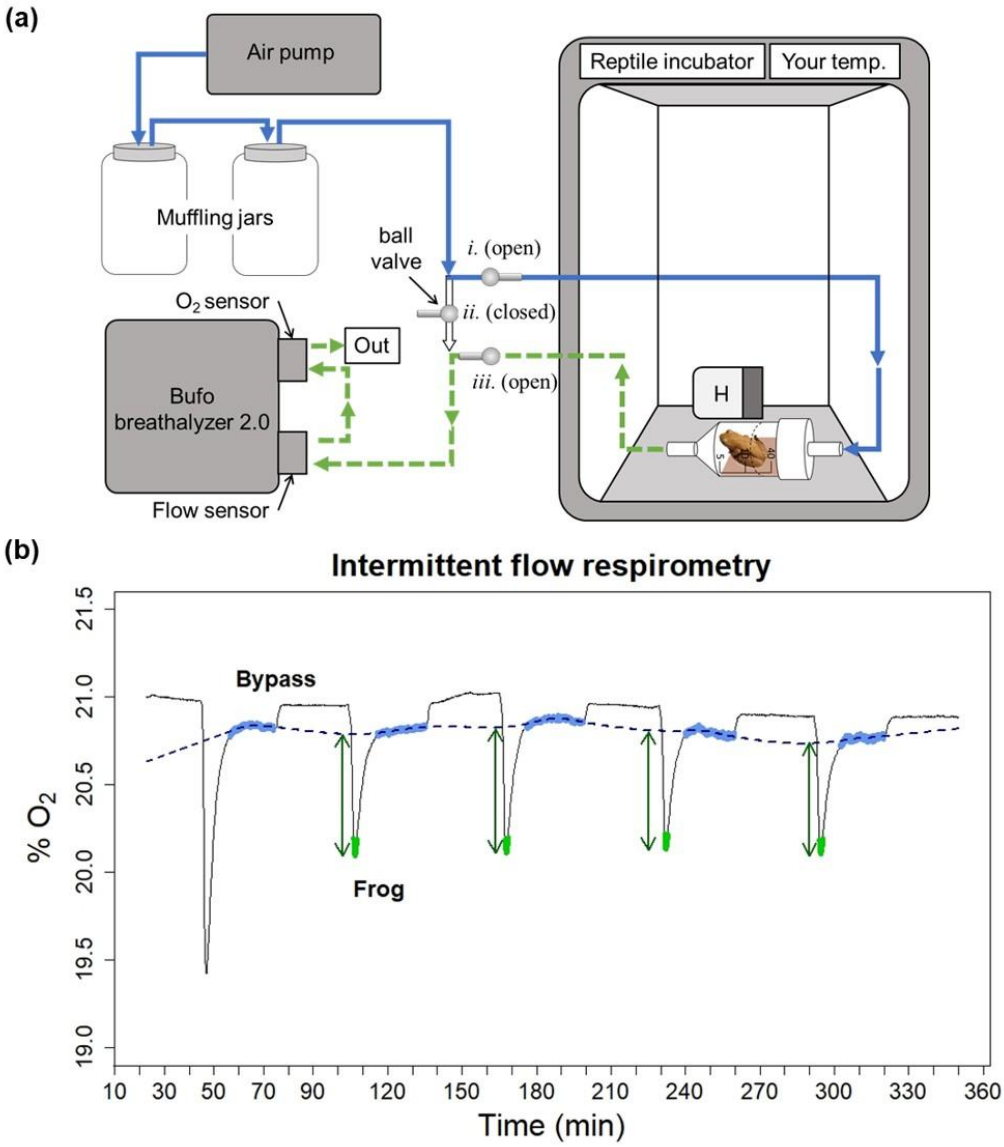

Figure 4.3: Experimental design for intermittent flow respirometry. (a) shows the path of air to the Bufo breathalyzer (ambient; blue arrows) or the animal chamber line (green arrows). Ball valves were used to close the animal chamber for specified periods (i. and iii.) or allow air flow directly to the Bufo breathalyzer (ii.). (b) shows a sample trace (blue points are internal control ambient air; green points are animal air immediately after air flow was restored after a period of closed respirometry).

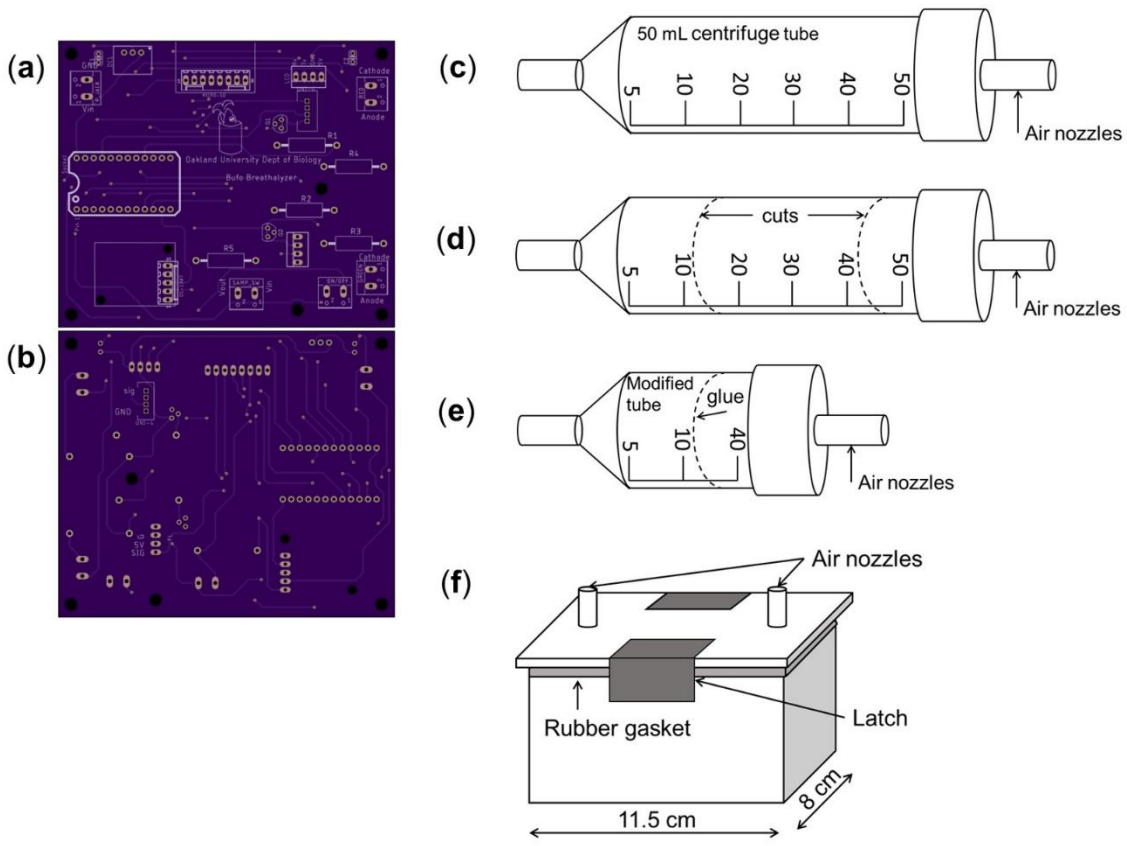

Figure 4.4: Components for assembling the Arduino based respirometry system. The new, 3D-printable circuit board (a–b) designed by Matthew Bruer (Oakland University Engineering) and respirometry chamber designs (c–f). 50 mL centrifuge tubes (c) can be used as a larger chamber or modified by cutting the ends (d) and gluing them together to form (e) a smaller chamber and (f) a larger chamber made by fitting air nozzles to a Rubbermaid container.

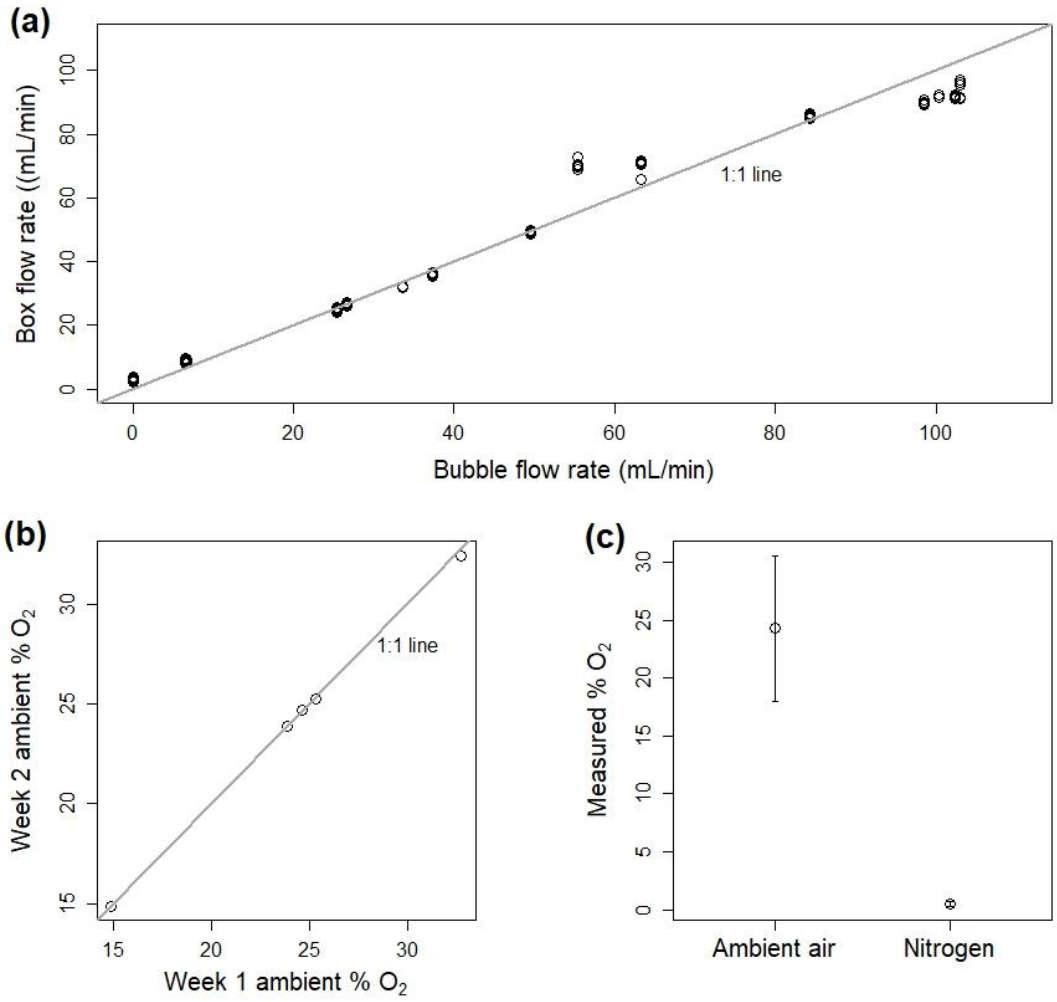

Figure 4.5: Results from our *Bufo breathalyzer 2.0* box flow rate and O_2 concentration verification. (a) is the flow rate verification between the rate measured by the sensor and our bubble flow meter with a 1:1 line. (b) shows how little the oxygen sensors vary in their measurements from week 1 to week 2 with a 1:1 plotted over. (c) shows the concentration of O_2 measured from ambient air compared to an air line with 100% Nitrogen.

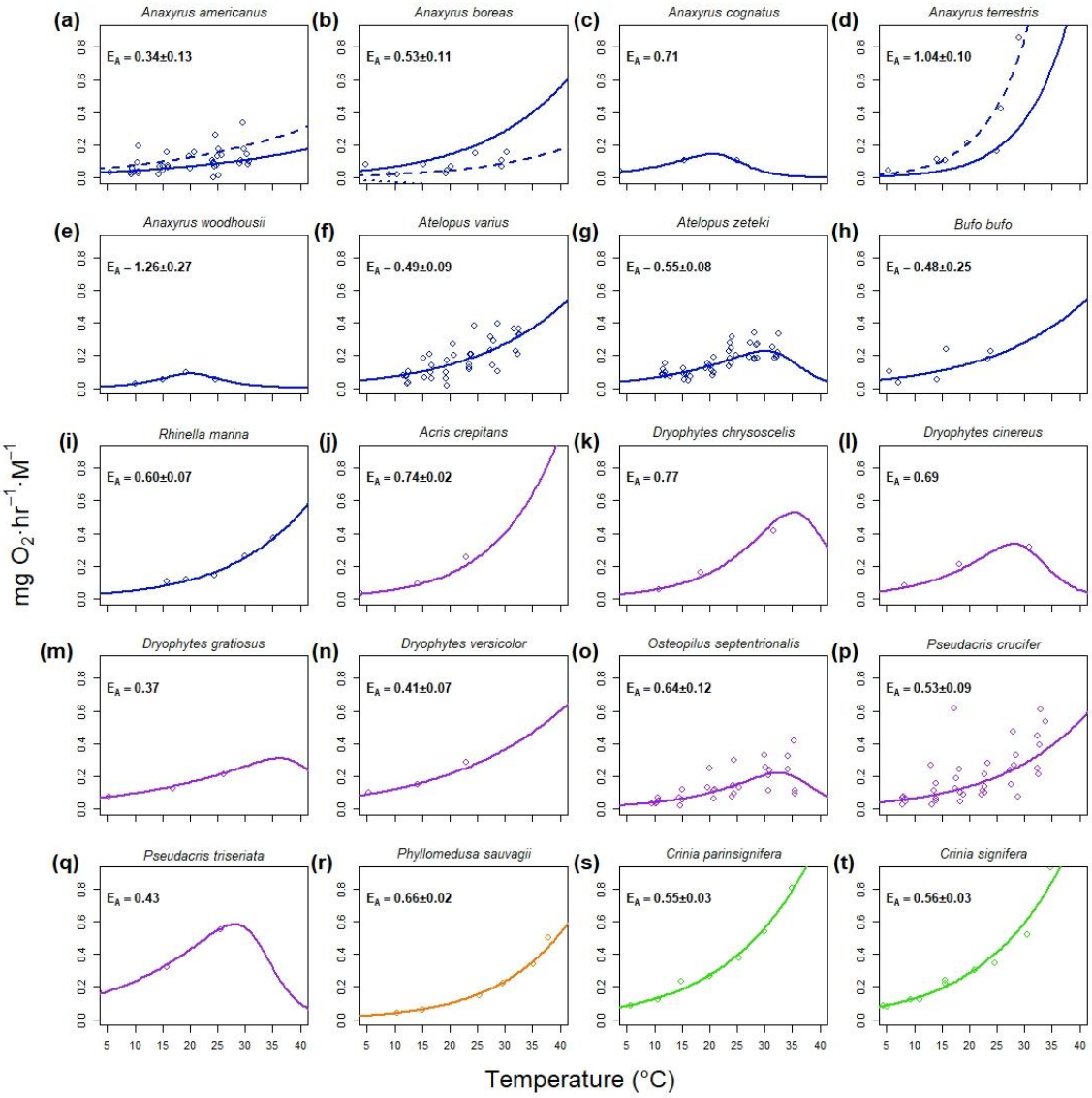

Figure 4.6: Thermal performance curves for 20 species as either BA or SS models. Species within each family are indicated by color (a–i: Bufonidae [royal blue]; j–q: Hylidae [purple], r: Phyllomedusidae [dark orange]; s–t: Myobatrachidae [green]). Species with 2+ lines indicate multiple studies were used for model fits. Activation energy (E_A) is displayed ± s.e. for each species.

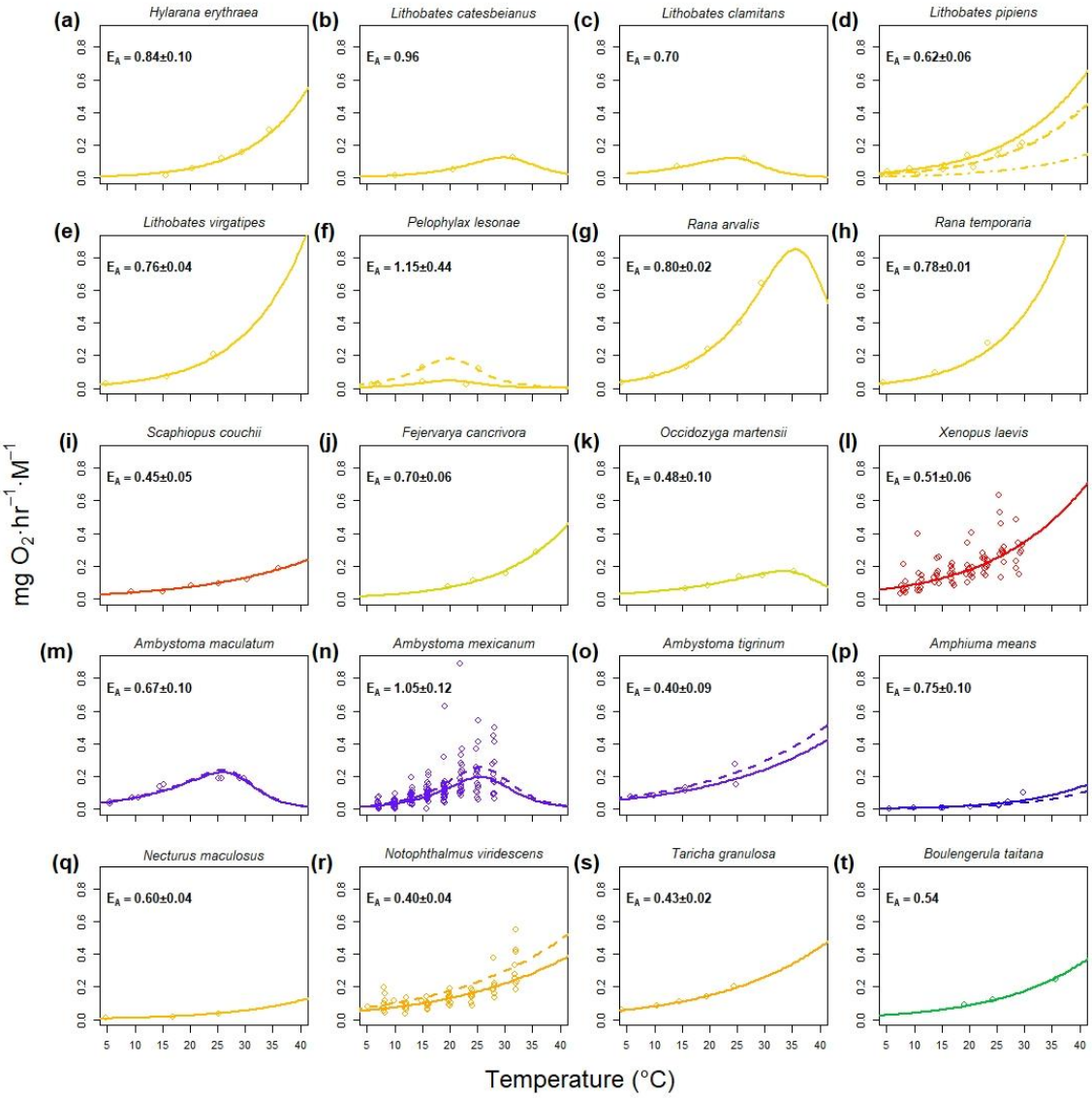

Figure 4.7: Thermal performance curves for 20 species as either BA or SS models. Species within each family are indicated by color (a–h: Ranidae [gold]; i: Scaphiopodidae [red orange]; j–k: Dicroglossidae [lime]; l: Pipidae [red]; m–p: Ambystomatidae [purple]; q: Proteidae [light orange]; r–s: Salamandridae [orange]; t: [dark green]). Species with 2+ lines indicate multiple studies were used for model fits. Activation energy (E_A) is displayed ± s.e. for each species.

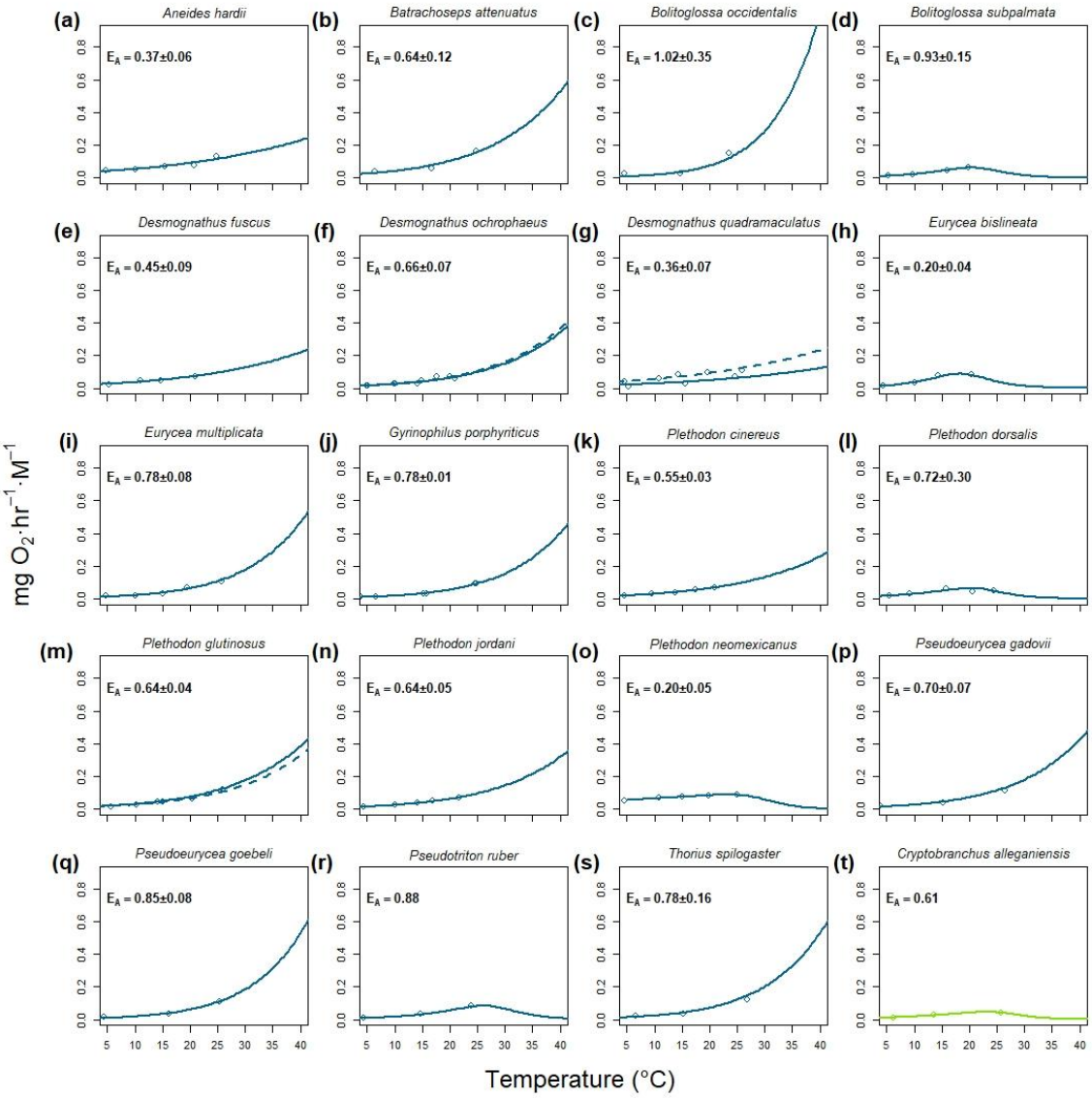

Figure 4.8: Thermal performance curves for 20 species as either BA or SS models. Species within each family are indicated by color (a–s: Plethodontidae [teal]; t: Cryptobranchidae [light green]). Species with 2+ lines indicate multiple studies were used for model fits. Activation energy (E_A) is displayed ± s.e. for each species.

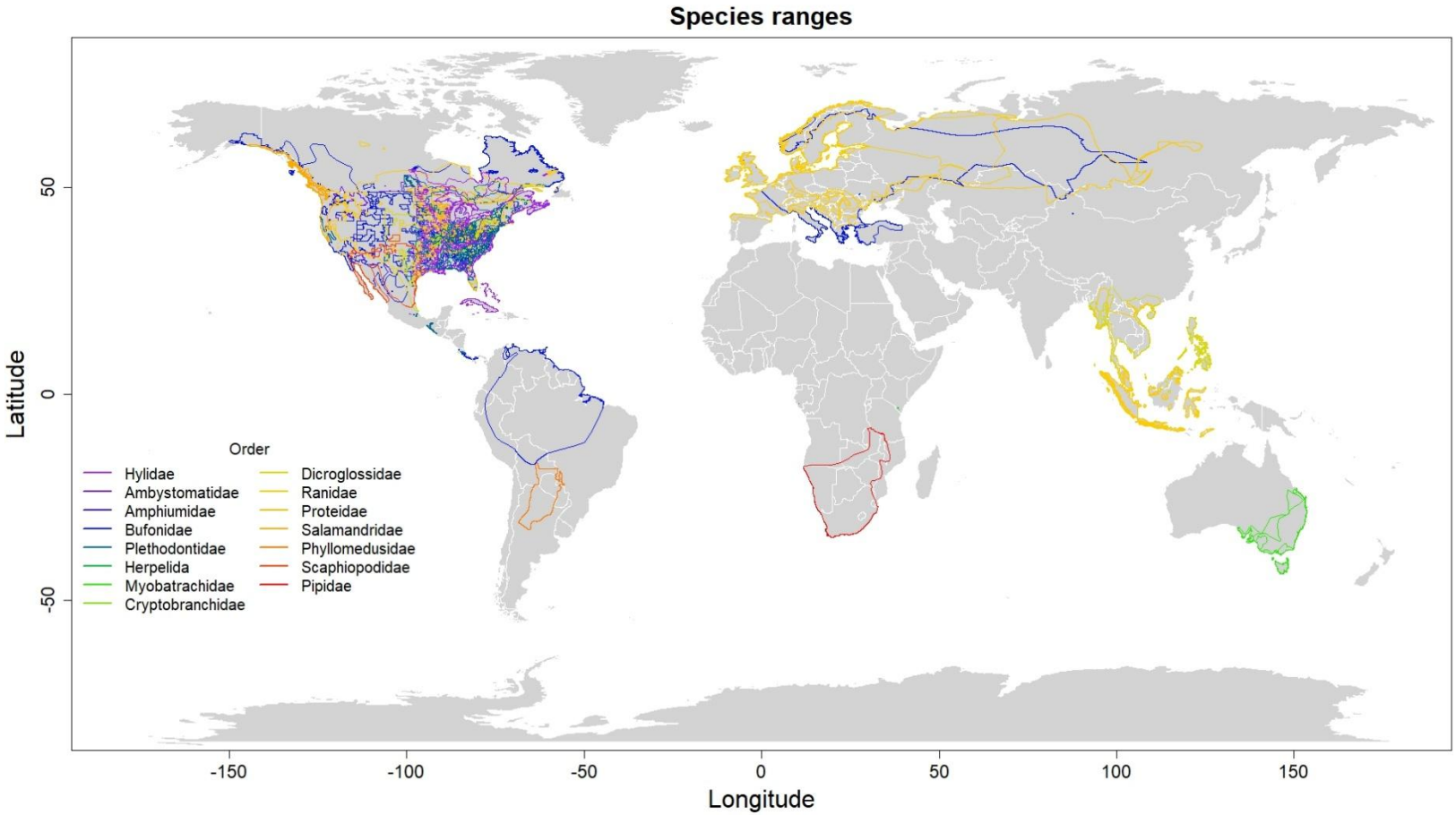

Figure 4.9: Species native ranges. Each species' native range was sourced from the IUCN database and used to collect occurrence data from the GBIF database. These locations were used to compile environmental predictors for each species' metabolic parameters.

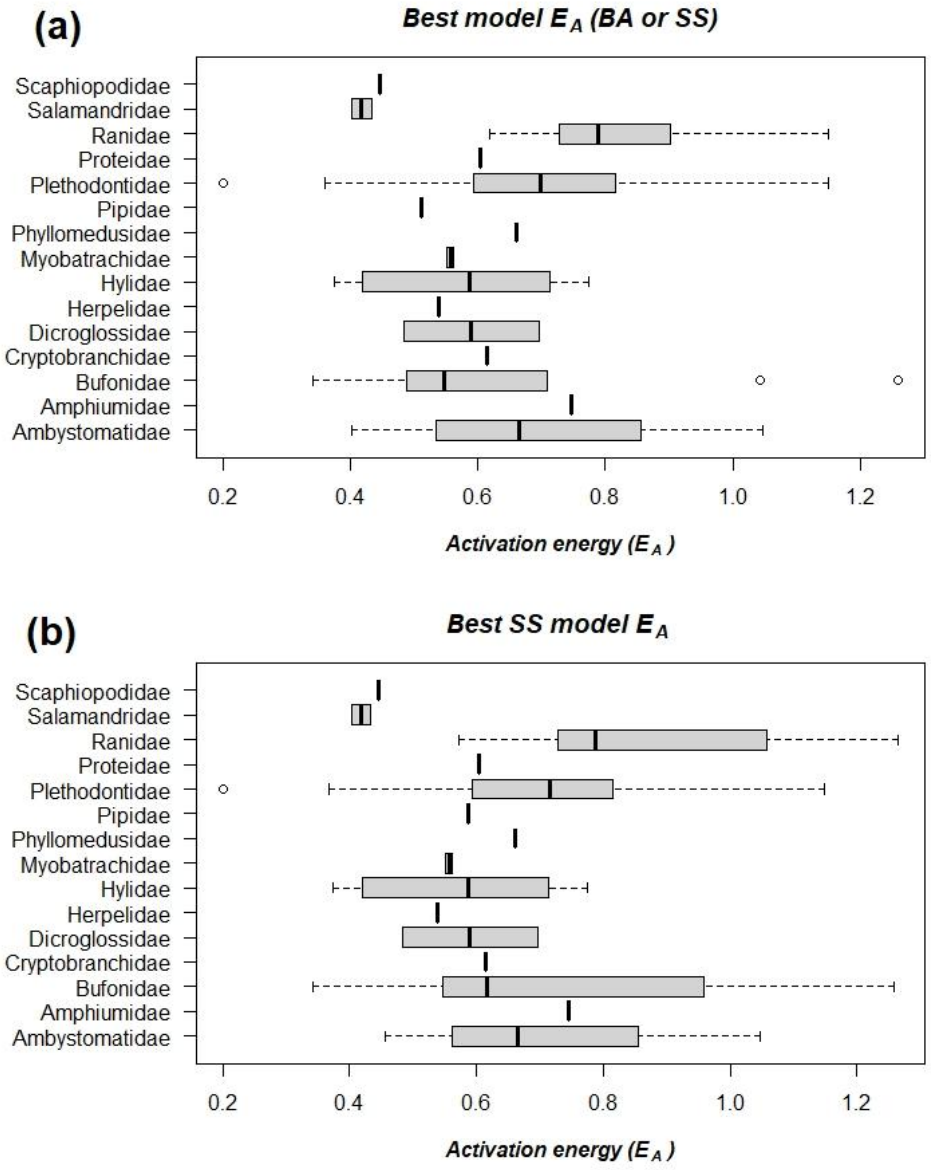

Figure 4.10: Box plot showing the distribution of activation energies (E_A) for 15 families of amphibians based on experimental respirometry and published literature data. (a) shows the distribution of E_A parameters derived from TPC models based on lowest AIC for BA or SS models. (b) shows the distribution of E_A parameters derived from TPC models based only on lowest AIC SS models.

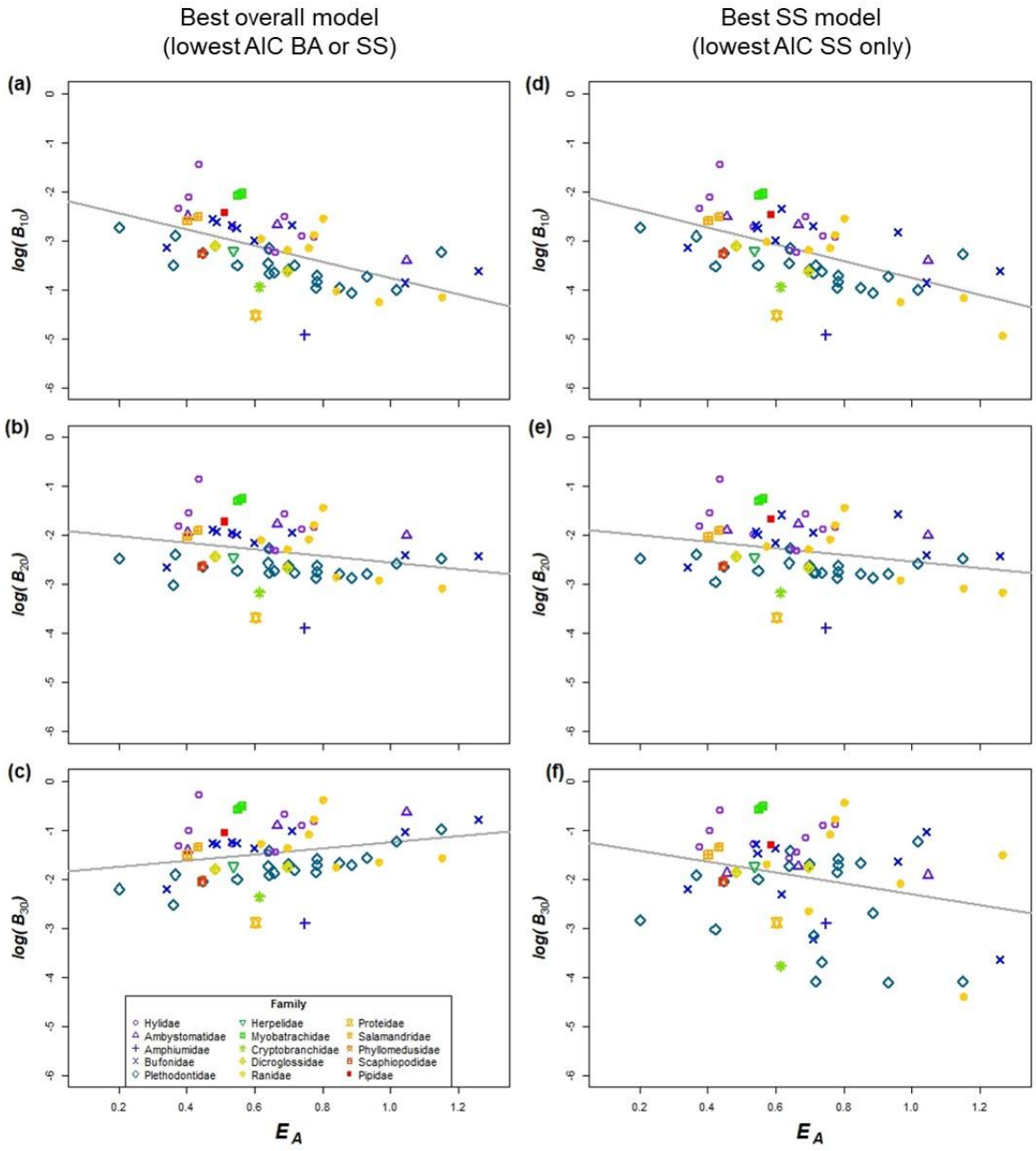

Figure 4.11: Linear regression testing activation energy (E_A) versus the log of performance at 10, 20, and 30 °C. (a) shows the significant negative effect of B_{10} on E_A. (b) shows the nonsignificant, negative trend between B_{20} and E_A, and (c) the significant positive effect of B_{30} on E_A. The same final model was run using parameter estimates from only the best (lowest AIC) SS model for each species. (d) shows the significant negative effect of B10 on E_A, and (e) and (f) were non-significant negative trends.

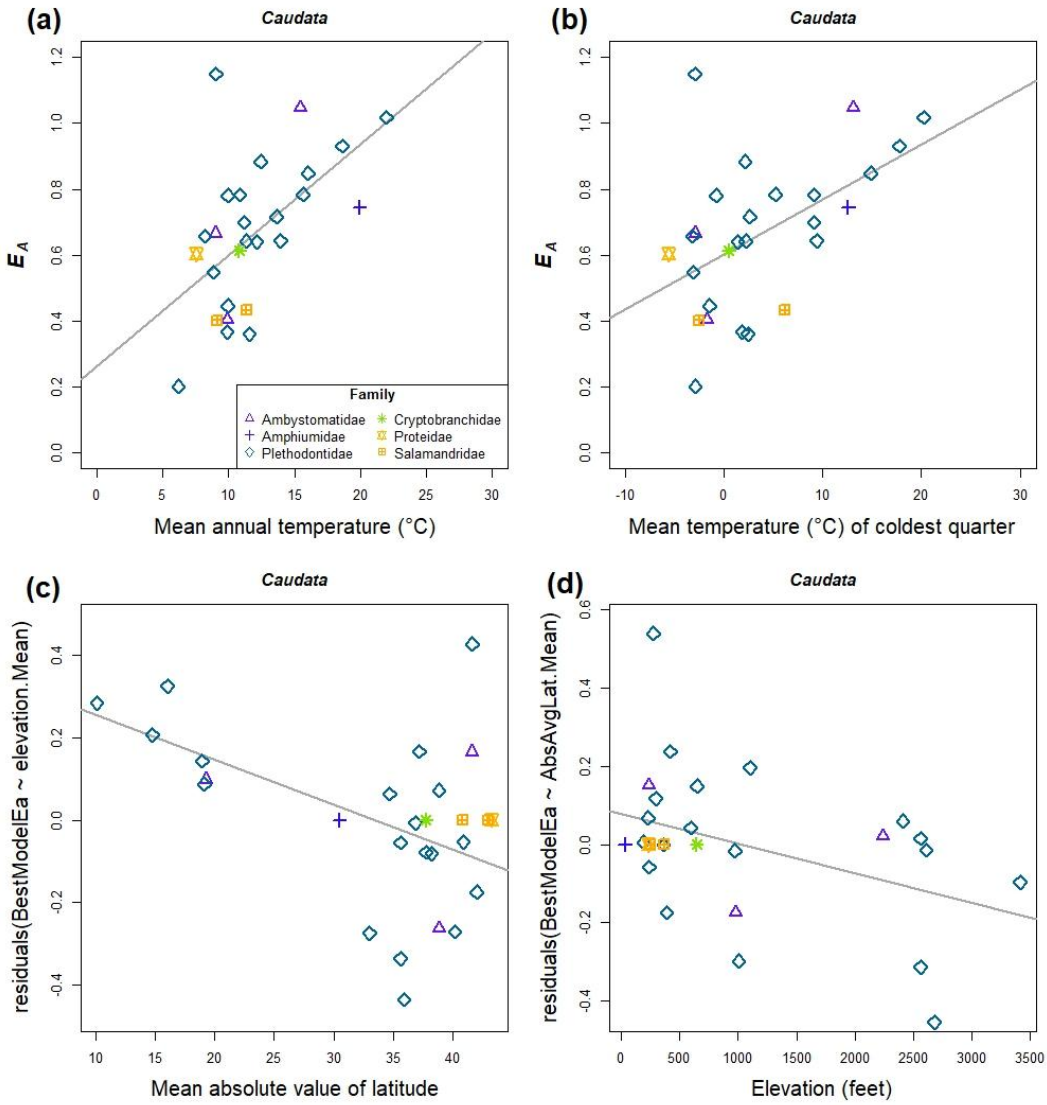

Figure 4.12: Three models found significant environmental predictors of salamander (Caudata) E_A. (a) There was a significant positive effect of mean annual temperature on E_A. (b) There was a significant positive effect of mean temperature of the coldest quarter on E_A. In the bottom two graphs (c) and (d) are residual plots showing the significant effects of mean elevation and distance from the equator (absolute value of latitude) on salamander E_A, each after accounting for the effect of the other predictor.

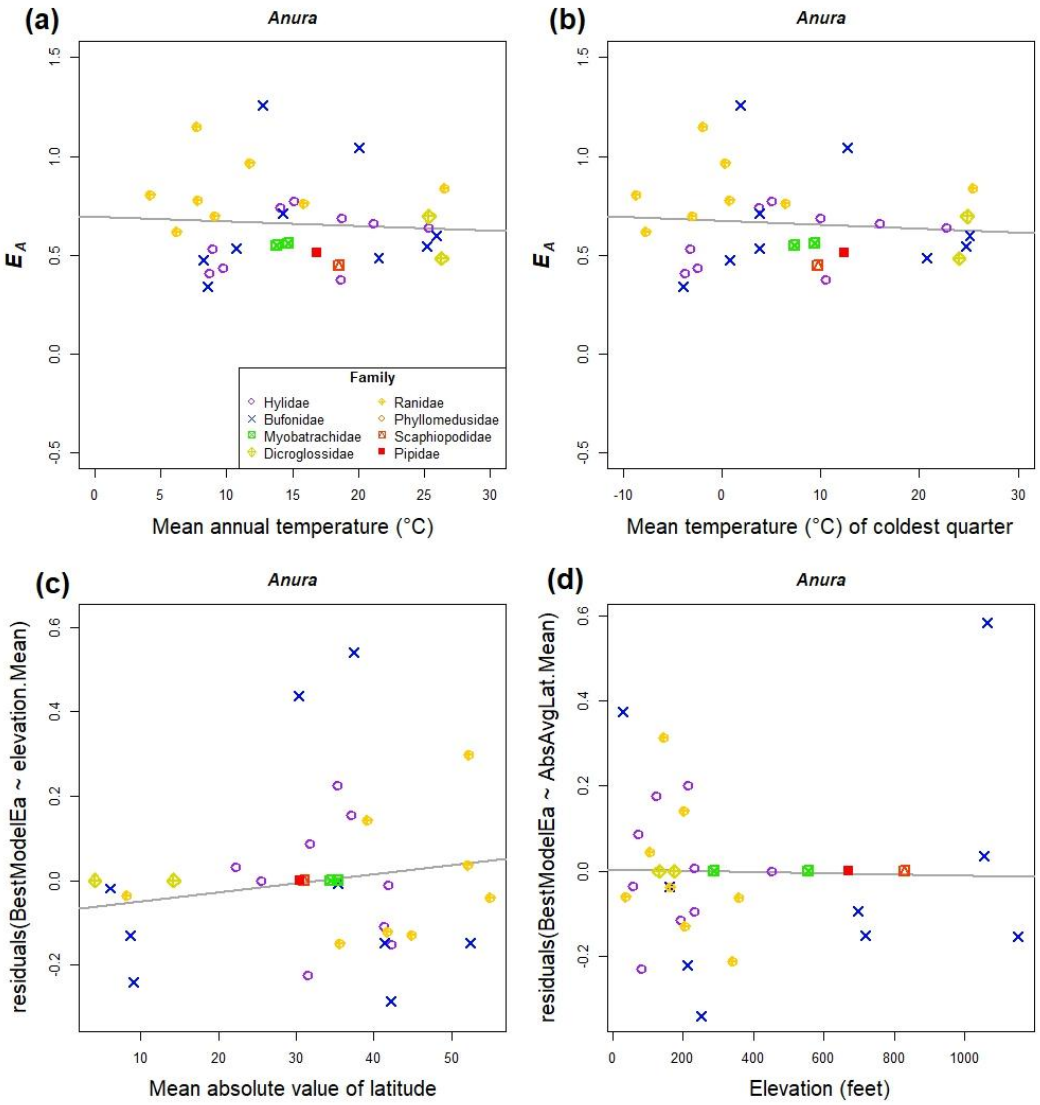

Figure 4.13: A replication of the three models that found significant environmental predictors of salamander (Caudata) E_A, were nonsignificant for frogs and toads (Anura). (a) There was no significant effect of mean annual temperature, (b) mean temperature of the coldest quarter, or (c) and (d) effects of mean elevation and distance from the equator (absolute value of latitude).

CHAPTER FIVE

USING METABOLIC THEORY-BASED THERMAL MISMATCH MODELS TO DESCRIBE INDIVIDUAL INFECTION DYNAMICS

5.1 Introduction

Climate change affects the emergence of human and wildlife diseases, making it ever more important to develop modeling frameworks to predict temperature-dependent disease dynamics (Cohen et al., 2017, 2019; Molnár et al., 2017; Raffel et al., 2013). Predictive modeling is especially important for understanding diseases of ectotherms whose changes in body temperature directly impact parasite growth rates, in contrast to parasites of endotherms that experience constant host body temperatures (Molnár et al., 2017; Raffel et al., 2013; Rohr & Cohen, 2020). A challenge with understanding the thermal biology of infection is that parasites and hosts each have their own independent responses to temperature (Molnár et al., 2017; Raffel et al., 2006, 2013). For example, the disease chytridiomycosis is typically more severe at cooler temperatures (Forrest & Schlaepfer, 2011; Turner et al., 2021), but it has been unclear whether this is due to higher parasite infectivity or lower host resistance at cooler temperatures (Raffel et al., 2013). These two processes are difficult to disentangle due to their inherent confoundment in experimental infection studies (Molnár et al., 2017; Sckrabulis et al., 2022). As a result, even sophisticated modeling studies that combined multiple thermal performance curves (TPCs) to predict infection have typically described internal infection dynamics within ectotherm hosts using a single combined TPC (e.g., “parasite population

growth rate" in Kirk et al., 2018; "vector competence" in Mordecai et al., 2019; "snail infection rate" in Nguyen et al., 2021).

One potential solution to this problem is thermal mismatch models, which quantitatively describe host and parasite contributions to infection outcomes as separate thermal performance curves (Molnár et al., 2017; Sckrabulis et al., 2022). For example, Rohr et al. (2013) defined "parasite infectivity" (i_T) as the temperature-dependent exponential growth rate of a parasite in the absence of host resistance and "host resistance" (here represented as h_T) as the host's ability to reduce pathogen growth at a particular temperature (i.e., $r_T = i_T - h_T$). A challenge with this approach is that parasite infectivity and host resistance have similar effects on measurable infection outcomes, leading to serious problems with parameter separability (a.k.a. "identifiability") that make it difficult to obtain statistical model convergence when estimating parameters based solely on infection data (Molnár et al., 2017; Sckrabulis et al., 2022). Rohr et al. (2013) suggested a possible solution to this problem, by modeling parasite infectivity and host resistance TPC's derived from Metabolic Theory of Ecology (MTE; Brown et al., 2004). MTE postulates that all physiological and ecological rate processes (including infectivity and resistance) are governed by organism metabolic rates (J. H. Brown et al., 2004; Gillooly et al., 2001). Based on this principle, Rohr et al. (2013) suggested that physiological rate processes of hosts and parasites could be used as metabolic proxies to partially parameterize MTE-based TPC models of host resistance and parasite infectivity (Molnár et al., 2017; Sckrabulis et al., 2022). For example, it might be possible to estimate key MTE model parameters like the activation energy host resistance (E_h) or

parasite infectivity (E_i) by measuring temperature dependence of host O_2 consumption or parasite infective-stage velocities (e.g., Sckrabulis et al., 2022).

Sckrabulis et al. (2022) showed that this approach could be used to successfully describe the temperature dependence of initial infection success and subsequent survival of a larval macroparasite in tadpoles, across a discrete time interval. However, this approach has yet to be rigorously tested for a microparasitic infection, despite the original proposal being inspired by Bd infection dynamics on a frog host (Rohr et al., 2013). Modeling the internal dynamics of a microparasitic infection poses additional challenges due to their ability to reproduce within a single host (Anderson & May, 1979). In this study, I collaborated with other members of the Raffel Lab team to investigate whether a MT-based thermal mismatch model could successfully describe temperature dependent infection dynamics of chytridiomycosis in individual *X. laevis*. We compared models for a variety of host and parasite metabolic proxies, including frog breath rate, frog oxygen consumption, Bd maximum zoospore swimming velocity, and Bd growth rate in culture. We also tested the (predicted) maximum lifetime distance traveled by Bd zoospores as a composite proxy for pathogen infectivity, by combining MT-based equations for zoospore velocity and zoospore mortality.

5.2 Methods

5.2.1 MT-based thermal mismatch models – describing Bd dynamics in individual hosts

Rohr et a. (2013) described the parasite's infectivity (i_T) as the hypothetical growth rate of a parasite on a host in the absence of host resistance (h_T). Pathogen infectivity ($i_T \equiv i\{T\}$) and host resistance ($h_T \equiv h\{T\}$) are each defined as separate functions of temperature in Kelvin (T) utilizing MTE-based models of thermal

performance (Sckrabulis et al., 2022). The difference between i_T and h_T is then defined as the pathogen's intrinsic growth rate on the host for a particular temperature:

$$r_T = i_T - h_T \quad \text{Eq. 5.1}$$

We converted this model into a continuous time equation for the growth rate of the parasite on the host through time using an ordinary differential equation, with *P* defined as the number of parasites (in Bd zoospore equivalents on a skin swab sample; Z_e) in or on a host at time *t* (days):

$$\frac{\delta P}{\delta t} = (i_T - h_T)P \quad \text{Eq. 5.2}$$

Integrating this equation results generates an exponential growth model that predicts parasite burden for a given time point ($P\{t\}$), depending on an initial population size P_0:

$$P\{t\} = P_0 e^{(i_T - h_T)t}. \quad \text{Eq. 5.3}$$

To allow parasite dynamics to come to an equilibrium on a given host, we incorporated an additional parameter (K_P) representing the parasite's carrying capacity on a single host in the absence of host resistance:

$$\frac{\delta P}{\delta t} = \left[i_T \left(1 - \frac{P}{K_P}\right) - h_T \right] P; \quad \text{Eq. 5.4}$$

This model generates logistic growth of a microparasite population in or on a host, with an equilibrium burden at a given temperature of $P_T{}^* = K_P(1 - h_T/i_T)$.

$$P\{t\} = \frac{K_P(1 - h_T/i_T)}{1 - (1 - K_P(1 - h_T/i_T)/P_0)e^{-(i_T - h_T)t}}. \quad \text{Eq. 5.5}$$

5.2.2 Metabolic proxy thermal performance curves (TPCs)

Here "metabolic proxy" refers to a measurement of host or parasite physiological performance. We described all TPC's for host or parasite metabolic proxies using either the Boltzmann-Arrhenius (BA) equation (Arrhenius, 1889; Sckrabulis et al., 2022):

$$p_T = p_{T_0} e^{-\frac{E_P}{k}\left(\frac{1}{T}-\frac{1}{T_0}\right)} \quad \text{Eq. 5.6}$$

or a more complex Sharpe-Schoolfield equation to account for reversible enzyme deactivation at very low or high temperatures (Schoolfield et al., 1981):

$$p_T = p_{T_0} e^{-\frac{E_p}{k}\left(\frac{1}{T}-\frac{1}{T_0}\right)} \cdot \left[1 + e^{\frac{E_p^L}{k}\left(\frac{1}{T}-\frac{1}{T_p^L}\right)} + e^{\frac{E_p^H}{k}\left(-\frac{1}{T}+\frac{1}{T_p^H}\right)}\right]^{-1}. \quad \text{Eq. 5.7 (SS.full)}$$

In each model, E_p represents the activation energy for a given performance metric, scaling constant p_{T_0} represents BA-predicted performance at standardization temperature T_0 (T_0 = 10 °C = 283.15 K throughout this chapter), k is Boltzmann's constant (k = 8.62 $\times 10^{-5}$ eV·K^{-1}), performance is reduced by 50% (relative to BA-predicted performance) at deactivation temperatures T_p^L & T_p^H, and deactivation energies E_p^L and E_p^H determine the rate of deactivation at low or high temperatures. All temperatures are converted to Kelvin for modeling purposes.

The SS equation can also be simplified to only have performance deactivated at either cooler or warmer temperatures (Molnár et al., 2017; Sckrabulis et al., 2022), resulting in one of two reduced SS models:

$$p_T = p_{T_0} e^{-\frac{E_p}{k}\left(\frac{1}{T}-\frac{1}{T_0}\right)} \cdot \left[1 + e^{\frac{E_p^H}{k}\left(-\frac{1}{T}+\frac{1}{T_p^H}\right)}\right]^{-1}; \quad \text{Eq. 5.8 (SS.high)}$$

$$p_T = p_{T_0} e^{-\frac{E_p}{k}\left(\frac{1}{T}-\frac{1}{T_0}\right)} \cdot \left[1 + e^{\frac{E_p^L}{k}\left(\frac{1}{T}-\frac{1}{T_p^L}\right)}\right]^{-1}. \quad \text{Eq. 5.9 (SS.low)}$$

The full SS equation is useful because it models expected decreases in performance at high or low temperature extremes. However, BA and reduced SS models

are simpler, making them preferable in cases where the sampled temperature range is insufficient to detect low or high temperature deactivation, or where deactivation only occurs at ecologically irrelevant temperature extremes (Sckrabulis et al., 2022). These models allowed us to capture the TPC for each proxy of host or parasite thermal performance, with a slight modification for zoospore mortality rate (see below). When referring to MTE-based models for specific proxies of host or parasite metabolic performance, we replace each lowercase *p* with a symbol representing the metabolic proxy (e.g., E_v is the activation energy for maximum Bd zoospore velocity). Modeling parameters, definitions, and units are provided in Table 5.1.

5.2.3 Composite proxy TPC – maximum travel distance for Bd zoospores

We combined TPC's for Bd zoospore maximum velocity (v_T) and Bd zoospore mortality rate (ω_T) to generate a TPC predicting the maximum distance (D_T) a zoospore could travel in its expected lifespan (ignoring zoospores that sporulate or find a host prior to death; Woodhams et al., (2008). We fit MTE based TPCs to maximum zoospore velocity data from Craig et al. (2024) and Bd zoospore mortality rate estimates at four temperatures from Woodhams et al. (2008). We generated two alternative TPC formulations for D_T based on the BA or SS.high models for zoospore velocity, which were within ΔAIC < 6 of each other:

$$v_T^{BA} = v_{T_0} e^{-\frac{E_v}{k}\left(\frac{1}{T}-\frac{1}{T_0}\right)}; \qquad \text{Eq. 5.10}$$

$$v_T^{SS} = v_{T_0} e^{-\frac{E_v}{k}\left(\frac{1}{T}-\frac{1}{T_0}\right)} \cdot \left[1 + e^{\frac{E_v^H}{k}\left(-\frac{1}{T}+\frac{1}{T_v^H}\right)}\right]^{-1}. \qquad \text{Eq. 5.11}$$

SS models describing mortality use a similar formulation to Eq. 5.6, except that the SS term has a positive rather than negative exponent because enzyme deactivation translates to higher rather than lower mortality rates (Molnár et al., 2013). The best fit TPC for Bd zoospore mortality was the SS.full model:

$$\omega_T^{SS} = \omega_{T_o} e^{-\frac{E_\omega}{k}\left(\frac{1}{T}-\frac{1}{T_0}\right)} \cdot \left[1 + e^{\frac{E_\omega^L}{k}\left(\frac{1}{T}-\frac{1}{T_\omega^L}\right)} + e^{\frac{E_\omega^H}{k}\left(-\frac{1}{T}+\frac{1}{T_\omega^H}\right)}\right]. \quad \text{Eq. 5.12}$$

We assumed Bd zoospores have a mortality rate that follows an exponential distribution, such that a zoospore's life expectancy is the inverse of its mortality rate and $D_T = v_T \omega_T^{-1}$. We combined the BA components of the two TPCs together resulting in single parameters for D_{T_0} and E_D ($D_{T_0} = v_{T_0}\omega_{T_0}^{-1}$; $E_D = E_v - E_\omega$). This generated two projected TPCs for D_T: D_T^{BA} (based on v_T^{BA}) and D_T^{BA} (based on v_T^{SS}).

$$D_T^{BA} = D_{T_0} \cdot e^{-\frac{E_D}{k}\left(\frac{1}{T}-\frac{1}{T_0}\right)} \cdot \left[1 + e^{\frac{E_\omega^L}{k}\left(\frac{1}{T}-\frac{1}{T_\omega^L}\right)} + e^{\frac{E_\omega^H}{k}\left(-\frac{1}{T}+\frac{1}{T_\omega^H}\right)}\right]^{-1} \quad \text{Eq. 5.13}$$

$$D_T^{SS} = D_{T_0} \cdot e^{-\frac{E_D}{k}\left(\frac{1}{T}-\frac{1}{T_0}\right)} \cdot \left[1 + e^{\frac{E_v^H}{k}\left(-\frac{1}{T}+\frac{1}{T_v^H}\right)}\right]^{-1} \cdot \left[1 + e^{\frac{E_\omega^L}{k}\left(\frac{1}{T}-\frac{1}{T_\omega^L}\right)} + e^{\frac{E_\omega^H}{k}\left(-\frac{1}{T}+\frac{1}{T_\omega^H}\right)}\right]^{-1} \quad \text{Eq. 5.14}$$

5.2.4 Fixing TPC parameters to allow convergence of some SS models

We set E_p and p_{T_0} as free parameters in all TPC optimizations for metabolic proxies but sometimes selected fixed values for T_p^L, T_p^H, E_p^L, or E_p^H to achieve model convergence. Even fitting a single TPC to data sometimes requires holding one or more parameters constant, especially if the range of temperatures sampled is narrow relative to the thermal breadth of the TPC (Molnár et al., 2013). We set T_p^H and T_p^L as free parameters for all SS models except those for zoospore mortality. No metabolic proxies

had data from sufficiently low temperatures to estimate E_P^L as a free parameter, so we set a constant value of $E_P^L = 3.25\ eV$ as suggested by Molnar et al. (2013). The zoospore mortality TPC was derived based on a single mean mortality rate estimate for each of four temperatures, but we obtained convergence for SS models by assuming fixed values for T_ω^H and E_ω^H based on zoospore velocity model outputs (i.e., $T_\omega^H = T_v^H$ and $E_\omega^H = E_v^H$). Two metabolic proxies (maximum zoospore velocity v_T and Bd growth rate in culture G_T) had sufficient high-temperature data for E_P^H to converge as free parameters, but we set E_P^H = 3.25 eV to achieve model convergence for *X. laevis* O_2 consumption and breath rate. To decide which version(s) of each metabolic proxy TPC to use in thermal mismatch models, we preferred simpler BA models unless one of the SS models generated lower AIC. In these cases, we considered both the lowest-AIC SS model and the simpler BA model if $\Delta AIC < 8$.

5.2.5 Sources of metabolic proxy data

To partially parameterize host resistance TPC's, we fit BA or SS models to measurements of temperature dependent total oxygen consumption and ventilation (breath) rates from *X. laevis* respirometry experiment conducted by McWhinnie et al. (2021). To partially parameterize pathogen infectivity TPC's, we used zoospore swimming speed data collected by Craig et al. (H. Craig et al., 2024) and growth rate in culture data collected by Sheets et al. (2021). The combined Bd lifetime distance traveled TPC was parameterized using Bd zoospore velocity data from Craig et al. (H. Craig et al., 2024) and zoospore mortality rate measurements from Woodhams et al. (2008).

5.2.6 Statistical methods for modeling MT-based thermal mismatches

All statistical analysis and model implementation was conducted in program R (version 4.1.3; R Core Team, 2022). I used the *nlsLM* function in the *minpack.lm* package (version 1.2.3; Elzhov et al., 2023) to fit the TPC models to each metabolic proxy and to fit thermal mismatch models to Bd infection data. I used the *Anova* function from package *car* for statistical tests (version 3.0.12; Fox & Weisberg, 2019). I also used packages *deSolve* (version 1.35; Soetaert et al., 2010) and *simecol* (version 0.8.14; Petzoldt & Rinke, 2007) for modeling MT-based thermal mismatches. I used package *Hmisc* for generating plots (version 4.6.0; Harrell & Dupont, 2022).

For each metabolic proxy, I fit each of the four TPC model variations (BA, SS.low, SS.high, & SS.full) to proxy data using the *nls.lm* function, setting the experimental ("performance") temperature as the primary predictor variable. I set activation energy upper bounds to 1.5 eV, close to the upper limit observed for whole organism activation energies (Dell et al., 2011). For activation energy estimates based on a single metabolic proxy, I set the lower bound to 0 eV because negative activation energies are typically considered chemically and biologically unreasonable (Atkins & De Paula, 2010; Dell et al., 2011). However, models based on maximum lifetime travel distance for Bd zoospores sometimes yielded negative activation energy estimates, which is possible because this is a combined process where the overall activation energy (E_D) equals the difference between activation energies for two separate processes (i.e., $E_D = E_v - E_\omega$). This is analogous to complex multi-step chemical reactions, which can sometimes yield negative activation energy estimates (Atkins & De Paula, 2010). For this, I set the lower bound for E_D estimates to −1.5 eV. For each metabolic proxy, I also ran a version

of each model assuming either a normal or lognormal error distribution. To implement a lognormal error distribution with a function based on least squares optimization (*nls.lm*), I applied a natural transformation to both sides of the model. Transforming the response variable results in *nls.lm* model AIC's that are not comparable between the normal versus lognormal model fits. To generate comparable AIC values for normal vs. lognormal model fits to each metabolic proxy, I calculated log-likelihoods for each model's predictions relative to data on a natural scale and recalculated AIC values as described by Xiao et al. (2011). I selected the best model for each metabolic proxy using model AIC (Table 5.2).

I fit thermal mismatch models to experimental Bd infection data for *Xenopus laevis* collected by Noelker et al. ("Experiment 1A"; 2024). To reduce the number of free parameters to be estimated by any given model, we set a fixed value for parasite infectivity at the standardization temperature based on the maximum growth rate of Bd strain JEL197 observed by Woodhams et al. ($i_{T0} = 0.55$; Woodhams et al., 2008). JEL197 is a highly virulent Bd strain that belongs to the same global pandemic lineage as JEL423, the Bd strain used in the current study (Greener et al., 2020). We compared fits for multiple MT-based mismatch model formulations, using either (1) fixed values for key TPC parameters based on various host or parasite metabolic proxies (e.g., E_p, E_p^H, or T_p^H; Table 5.2) or (2) alternative model formulations with either the host or parasite activation energy set as a free parameter (Figure 5.1, 5.2). In some cases, we compared multiple versions of models based on the same metabolic proxy because BA and SS model fits for that proxy had $\Delta AIC < 8$ (see above). Initial infection load (P_0), parasite carrying capacity (K_P), and host resistance at the standardization temperature (h_{T0}) were

free parameters in every model. Upper and lower bounds for the initial infection load (P_0) were 1 to 1,000,000 zoospore equivalents because frogs in the Bd infection experiment were each inoculated with 1,000,000 zoospores (J. E. Noelker, Abreu Ruozzi, Spengler, et al., 2024). Upper and lower bounds for carrying capacity (K_P) and host resistance (h_{T0}) were set to 0–1,000,000 and 0–10 respectively.

5.3 Results

5.3.1 Metabolic proxy TPCs

Individual metabolic proxies all had lognormal error distributions based on AIC and generated activation energy estimates consistent with the expected range of 0.2–1.2 eV (Table 5.2; Dell et al., 2011). Results from the best model for each proxy (lowest AIC) along with the simplest BA model are reported in Table 5.2. The best models for *X. laevis* O_2 consumption and breath rate generated E_h estimates of 0.51 and 0.44 eV (respectively), each slightly higher than values identified by McWhinnie et al., (2021) based on the same dataset (O_2 E_h = 0.458 ± 0.03 eV; Breath rate E_h = 0.365 ± 0.06 eV). The best model for zoospore velocity (v_T) was SS.high (ΔAIC = 6.3) with peak performance at ~24 °C (Fig. 5.1) and an activation energy of E_v = 0.69 ± 0.74 eV (Table 5.2), higher than the activation energy from the simpler BA model but with a higher standard error (E_v = 0.21 ± 0.02 eV; Table 5.2). The best model for Bd growth rate in culture was SS.full by a large margin (ΔAIC = 298.3), with peak performance at ~24 °C (Fig. 5.1) and an activation energy estimate of E_G = 0.29 ± 0.10 eV (Table 5.2). The best model for zoospore mortality (ω_T) was SS.full by a large margin (ΔAIC = 35.4), with maximum survivorship predicted at ~8 °C (Fig 5.1) and an activation energy estimate of E_ω = 0.83 ± 0.01 eV (Table 5.2). The SS.full model for ω_T suffered from overfitting due

to the small number of available datapoints, limiting our ability to draw inferences about parameter values. However, the BA model fit generated a similar estimate of E_ω = 0.82 ± 0.23 eV (Table 5.2). Combining the two ν_T TPC's with the SS.full version of ω_T generated two TPC's for zoospore lifetime travel distance with peak performance at ~8–9 °C (Fig. 5.1), with in negative activation energy estimates for both model formulations (E_D = −0.14 for Distance SS; E_D = −0.62 for Distance BA; Table 5.2).

5.3.2 Fitting MT-based thermal mismatch models to individual infection dynamics

Most versions of MTE-based thermal mismatches successfully converged on biologically reasonable parameter values (i.e., within the set boundaries) and captured patterns of temperature dependent Bd infection dynamics, even for model variations with either E_h or E_i set as free parameters (Table 5.3, 5.4; Fig. 5.3). However, lower-AIC models tended to generate more biologically reasonable parameter estimates, with some higher-AIC models hitting the upper or lower bounds of certain parameters (Table 5.3, 5.4). Mismatch models predicted greater $i_T - h_T$ mismatches and higher equilibrium levels of Bd infection at cooler temperatures (at least within the 10–25 range of the infection experiment), except for some models based on G_T that failed to converge on reasonable parameter estimates (Figure 5.3). Models whose E_h estimates were derived from host oxygen consumption had consistently lower AIC values than similar models based on E_h from host breath rate (Table 5.3, 5.4).

Out of models with both E_i and E_h derived from metabolic proxies, the best (lowest AIC) model was based on a combined proxy representing the maximum lifetime distance traveled for a Bd zoospore (Distance BA/Oxygen BA; Table 5.3), followed closely by the BA model for Bd zoospore velocity (Velocity BA/Oxygen BA; Table 5.3).

The infectivity TPC for all five top models, which had similar model fits (delta-AIC < 2), were all based on either Velocity BA, Distance BA, or Distance SS (Table 5.3). All these top 5 models had i_T and h_T TPCs that crossed around T = 12–13 °C, predicting $i_T - h_T > 0$ at cooler temperatures and $i_T - h_T < 0$ at warmer temperatures (Fig. 5.3). These five models also consistently generated P_0 estimates between 17-24 Z_e (Table 5.3). The four top models based on Distance BA or Distance SS generated h_{T0} estimates between 0.13–0.17 and K_P estimates between 70–140 Z_e, whereas the Velocity BA model generated higher estimates of h_{T0} = 0.5 and K_P = 406 Z_e (Table 5.3); however, all five predicted similar equilibrium dynamics at 10 °C of $P_T^* \approx \exp[3.5]$ (Fig. 5.3). Models based on Velocity SS both had relatively high AIC and hit the upper parameter boundary of $K_P = 10^6$, and models based on the Growth SS both had very high AIC and hit the lower parameter boundary of h_{T0} = 0 (Table 5.3).

When we ran new versions of each thermal mismatch model with either E_i or E_h as a free parameter, models converged on activation energy estimates between -1.5 and +1.5 eV unless they were parameterized based on the G_T TPC (Table 5.4). The top two models for estimating E_h (derived from Distance BA & Velocity BA) converged on values of E_h = 0.63 ± 0.34 eV and E_h = 0.54 ± 0.15 eV (Table 5.4), close to the *X. laevis* metabolic activation energy of 0.46 ± 0.03 eV described by McWhinnie et al. (2021) based on total O_2 consumption. Estimates for E_i nearly always converged on negative numbers, albeit with large error bars (Table 5.4). The top two models for estimating E_i, according to model AIC, generated estimates of $E_i = -0.55$ (Predict BA/Breath BA) and $E_i = -0.85$ (Predict BA/Oxygen BA), close to the $E_D = -0.62 \pm 0.02$ eV estimate from the Distance BA TPC (Table 5.2, 5.4). Among the five models for estimating E_i that were

based on Oxygen BA, only one had a positive E_i estimate (Predict SS with high or low temperature deactivation based on Distance; Table 5.4) that corresponded to an increasing i_T TPC at temperatures below 10 °C (Fig. 5.3). All five of these models predicted a decreasing i_T TPC in the 10–25 °C range (Fig. 5.3).

5.4 Discussion

This investigation highlights the potential power of MT-based thermal mismatch models to mechanistically describe infection dynamics of microparasites in individual hosts. This approach provides a possible path towards disentangling host and parasite contribution to the temperature dependence of ectotherm infection, something once thought impossible by many disease researchers. Prior to the current study, MT-based thermal mismatch models had only been applied to describe discrete-time dynamics of a trematode parasite in tadpoles, whose specific life cycle characteristics (e.g., dormant metacercariae) allowed simplifying assumptions to reduce problems with parameter separability (Sckrabulis et al., 2022). Despite clear problems with parameter separability in the current study (e.g., similar effects of h_{T0} and K_P on P_T*), we were able to achieve model convergence for MT-based mismatch models of Bd infection in *X. laevis* using TPC's for various aspects of host and parasite physiological performance. Some proxies generated better model fits than others, with the best mismatch models being derived from host whole-body O_2 consumption and aspects of parasite locomotory performance (i.e., zoospore velocity v_T and maximum travel distance D_T). Host breath rate, which had a slightly lower activation energy than host O_2 consumption, consistently generated less predictive mismatch models of Bd infection. These findings show that MT-based TPC's can help us solve the parameter separability problems inherent in thermal mismatch

models, to the extent where we were able to distinguish that some proxies of host or parasite performance were more predictive of Bd infection than others. These results highlight the importance of selecting metabolic proxies that are closely related to the infection process. Despite the core MT assumption that various aspects of physiological performance are fundamentally limited by whole-organism metabolism, it is well documented that different physiological rate processes within the same organism including immune parameters can have different temperature dependencies (Dell et al., 2011; Raffel et al., 2006; Sckrabulis et al., 2022). This might be because certain processes are more tied to whole-body metabolic rates than others (Sckrabulis et al., 2022). Whole-body O_2 consumption is a more direct measurement of host metabolism than breath rate, which might make O_2 consumption a better proxy to predict a host's overall ability to resist infection.

Our three direct proxies of parasite performance (v_T, G_T, and ω_T) also provide opportunities to evaluate the assumption that different physiological rate processes should have similarities in their MT based TPC's. For all three, the best-fit TPC was an SS model that included high-temperature deactivation (Table 5.2). SS models for zoospore velocity (v_T) and Bd growth in culture (G_T) had similar thermal optima, but G_T had a more rapid decline in performance above T_{opt} that resulted in greater AIC difference from the BA model and a higher deactivation energy estimate (Table 5.2, Fig. 5.1). The SS models for v_T and w_T converged on relatively high activation energy estimates of 0.69 and 0.83 eV (Table 5.2). In contrast, the SS model for G_T converged on a lower estimate of 0.29, closer to the E_V = 0.21 eV estimate derived from the BA model fit for v_T (Table 5.2). It is unclear whether the SS or BA model provides a better description of the Bd

zoospore velocity TPC, in part because the shape of this TPC appears to vary depending on the thermal acclimation status of Bd zoospores. Craig et al. (2024) found that Bd acclimated to 15 or 20 °C produced zoospores with a unimodal TPC that might be best described using an SS curve, whereas Bd acclimated to 10 °C produced zoospores whose velocity TPC increased throughout the range of test temperatures and might be best described using a BA model.

MT-based mismatch models were also surprisingly successful at estimating activation energies for parasite infectivity (i_T) or host resistance (r_T) by using one of the more-successful metabolic proxies from the opposing organism. This provides a novel way to independently estimate host and parasite activation energies. For example, we estimated E_h by fitting a MT-based mismatch model to infection data and partially parameterizing the model based on the TPC for zoospore velocity (v_T), all of which is independent of activation energy estimates derived from measurements of host O_2 consumption. Consistent with the core assumption of our modeling approach, mismatch models based on either zoospore velocity (v_T) or maximum travel distance (D_T) both generated E_h estimates (0.54 & 0.63 eV, respectively) near the activation energy for whole-organism O_2 consumption of *X. laevis* (0.46 eV; McWhinnie et al., 2021). Similarly, the two simplest (and lowest AIC) mismatch models to estimate E_i generated values (−0.55 & −0.85 eV) near the E_D = −0.62 eV for maximum travel distance when calculated from the BA model for zoospore velocity (Table 5.3, 5.4; Fig. 5.4). Interestingly, many of the mismatch models that used host TPC's to predict parasite E_i converged on negative values (Table 5.3, 5.4). This pattern is consistent with a TPC for Bd infectivity that decreases with temperature and has a correspondingly negative

activation energy, and it is close to the E_D estimates generated by combining ν_T and ω_T into a single TPC predicting the maximum travel distance of Bd zoospore. This suggests that the common observation of more-severe Bd infections at cooler temperatures (Forrest & Schlaepfer, 2011; Turner et al., 2021) might be caused in part by Bd being inherently more infective at cooler temperatures, contrary to a common assumption that this pattern is primarily driven by lower host resistance to infection (h_T) at cooler temperatures (e.g. Raffel et al., 2013).

It is counterintuitive to consider the possibility of negative activation energies, since activation energies represent the energy needed to initiate a chemical reaction and seem to be definitionally positive. However, it has long been understood that complex multi-step chemical reactions can have overall negative activation energies, for example if the activation energy of a reverse chemical reaction exceeds the combined activation energies of the forward reactions (Atkins & De Paula, 2010). Our TPC for D_T was derived by combining TPCs for two metabolic proxies, one of which (ω_T) inversely affects lifetime distance traveled by reducing zoospore longevity. Since E_ω was greater than either estimate of E_ν (Table 5.2), $E_D = E_\omega - E_\nu$ generated negative values for E_D. This is analogous to negative activation energies for some complex chemical reactions. Kirk et al. (2018) also reported a negative activation energy for the part of their MT-based model of parasitic infection describing equilibrium parasite abundance, which they modeled as a sort of temperature-dependent carrying capacity. Carrying capacities can have negative temperature dependence due to elevated metabolic rates and thus higher energy usage at higher temperatures, leading to negative activation energies when fit directly to a TPC model (Kirk et al., 2018; Savage et al., 2004). Our study highlights an

additional reason why MT-based models might sometimes predict negative activation energies.

Parasite growth rate in culture consistently generated poor fits to MT-based mismatch models, despite being the original suggestion of a potential metabolic proxy for parasite infectivity (Rohr et al., 2013). Bd growth in culture has also been widely cited as a potential proxy for parasite infectivity when generating qualitative predictions for thermal mismatch hypotheses (Cohen et al., 2017; Raffel et al., 2013; Rohr et al., 2013). This highlights our relatively poor knowledge of which physiological processes are the most important drivers of Bd infection and the dangers of assuming organism responses to culture conditions can be extrapolated to field conditions. It is possible that zoospore swimming velocity and survival are more important factors during actual Bd infections than they are under culture conditions. Zoospore performance is important for both the transmission process and for the spread of Bd infection across an amphibian's skin (Longcore et al., 1999), with greater velocities and longevities potentially helping zoospores to locate a new host or to swim across an amphibian's skin in search of a new encystment location (Briggs et al., 2010; Wilber et al., 2021).

Overall, this study contributes to the expanding use of thermal mismatch frameworks to predict climate effects on infectious diseases, based on hypothesized differential responses of hosts and parasites to temperature. Other groups have largely used thermal mismatch hypotheses to generate qualitative predictions about climate-disease interactions. For example, Raffel et al. (2013) showed that temperature dependence of Bd growth in culture was qualitatively different from that of Bd growth on frogs, highlighting the importance of accounting for host thermal responses to explain

thermal biology of host-parasite interactions. Several studies have tested predictions of the "thermal mismatch hypothesis" of Cohen et al. (2017, 2020), which postulates that climatic warming should lead to increased infection in cool-adapted hosts relative to warm-adapted hosts if we assume parasites have greater TPC breadths than their hosts or faster adaptation to new thermal conditions (Carvalho et al., 2024; Cohen et al., 2017, 2019, 2020; Neely et al., 2020; Venesky et al., 2022). Kirk et al. (2022) explored the potential use of mismatches between host and parasite thermal optima to predict population-level infection patterns, and Nowakowski et al. (2017) explored the potential importance of mismatches between host and parasite high-temperature thermal tolerances as a driver of among-host differences in Bd infection. Palmer-Young et al. (2018) showed that mismatches between TPC's of parasites versus beneficial microbes helped to explain reduced bumblebee infections at warmer temperatures, whereas Palmer-Young et al. (2023) found that temperature dependence of a viral infection in bees was better described as being directly limited by host metabolic rate rather than being described by a thermal mismatch framework. These studies have yielded important insights into qualitative patterns of temperature dependent infections in ectotherm hosts, and into the potential strengths and limitations to thermal mismatch frameworks to predict infectious disease outcomes. Our study shows that thermal mismatches can also be used as a quantitative framework to predict dynamics of microparasite infection in or on an ectotherm host.

5.5 Conclusion

This study shows that proxies for whole organism metabolism are useful for disentangling host and parasite contributions to infection and highlight the power of MT-

based mismatch models to develop more mechanistic quantitative models of temperature dependent infection dynamics in ectotherms. This modeling approach could be particularly useful for multi-host parasites, such as Bd, if it is possible to describe infection in more than one host species using a single shared TPC for parasite infectivity. MT-based mismatch models might allow researchers to develop predictive models of infection dynamics in host species for which infection experiments might be difficult or impossible to perform, by deriving TPC's for host resistance based on proxies for h_T such as whole organism O_2 consumption. However, much work is needed to test the generality of this approach, and to determine which metabolic proxies (or combinations of proxies, e.g., maximum travel distance) are most closely related to the specific processes that determine infectivity or resistance in each host-parasite system. Future investigations attempting to fit MT-based thermal mismatches with additional hosts will allow us to look for generalities in the infection dynamics between amphibian hosts and Bd.

CHAPTER FIVE TABLES

Table 5.1 Parameter definitions used in modeling Metabolic Theory-based thermal mismatches.

Parameter	***Definition***	***Unit***
E_p	Activation energy for a given performance metric ("*p*" can be substituted for any given performance metric)	eV
E_p^L	Deactivation energy at low temperatures for a given performance metric	eV
E_p^H	Deactivation energy at high temperatures for a given performance metric	eV
T_p^H	High temperature of enzyme deactivation for a given performance metric	K
T_p^L	Low temperature of enzyme deactivation for a given performance metric	K
t	Time	days (d)
T	Temperature	K
T_0	Standardization temperature (10 °C = 283.15 K)	K
E_i, E_h	Activation energy for parasite infectivity and host resistance	eV
h_T	Host resistance at temperature T	d^{-1}
i_T	Parasite infectivity at temperature T	d^{-1}
k	Boltzmann's constant (8.617×10^{-5} eV/K)	eV/K
K_P	Parasite carrying capacity on a single host	Bd Z_e
P	Parasite population size at time t	Bd Z_e
P_0	Parasite population size at time $t = 0$	Bd Z_e
P_T*	Equilibrium P at temperature T ($P_T^* = K_P \times [1 - h_T/i_T]$)	Bd Z_e
p_{T0}	Performance at temperature T_0	performance metric unit
r_T	Parasite intrinsic growth rate on the host at temperature T	d^{-1}
v_T	Maximum zoospore velocity at temperature T	μm/s
ω_T	Bd zoospore mortality rate at temperature T	hr^{-1}
D_T	Bd maximum distance traveled at temperature T	m
G_T	Pathogen Growth rate in culture at temperature T	d^{-1}
E_G, E_v, E_ω, E_D	Activation energies for Bd growth rate in culture, Bd zoospore maximum velocity, zoospore mortality rate, and maximum zoospore distance traveled	eV

Table 5.2: Metabolic Theory-based thermal performance model outputs for host O_2 consumption and breath rate, and parasite zoospore maximum velocity, growth rate in culture, zoospore mortality, and potential lifetime distance traveled. P_{T0} estimates have the same unit as the metabolic proxy. AIC values were calculated for comparison of normal versus lognormal model fits as described by Xiao et al. (2011); AIC values should only be compared among models for a given metabolic proxy. The model with the lowest AIC was used for MT-based mismatch models unless the simpler BA model had ΔAIC < 8.

Organism	***Proxy***	***Model***	E_A	p_{T0}	E_p^H	T_p^H	T_p^L	***AIC***
Host	O_2 consumption [1] ($mg \cdot hr^{-1} \cdot g^{-0.75}$)	BA	0.51 (0.06)	0.09 (0.01)	---	---	---	98.96
	Breath rate [1] ($breaths \cdot hr^{-1}$)	BA	0.44 (0.12)	15.27 (2.87)	---	---	---	217.3
Parasite	Maximum zoospore velocity [2] (v_T)	SS.high	0.69 (0.74)	63.98 (62.25)	0.85 (0.23)	16.03 (27.0)	---	−72.9
		BA	0.21 (0.02)	45.92 (1.19)	---	---	---	−66.3
	Growth rate in culture [3] (G_T)	SS.full	0.29 (0.10)	0.36 (0.06)	7.66 (1.20)	26.5 (0.2)	10.0 (1.6)	−1644.7
		BA	0.11 (0.03)	0.37 (0.04)	---	---	---	−1346.4
	Zoospore mortality [4] (ω_T)	SS.full	0.83 (0.01)	1.1×10^{-3} (1.2×10^{-5})	0.85†	16.03†	6.75 (0.05)	−25.3
		BA	0.82 (0.23)	3.9×10^{-3} (1.4×10^{-3})	---	---	---	10.1
	Lifetime distance traveled [4] (D_T)	SS.high	−0.14	207.89	0.85†	16.03†	---	---
		BA	−0.62	149.19	0.85†	16.03†	---	---

Data Source: [1] McWhinnie et al., 2021; [2] Craig et al., 2024; [3] Sheets et al., 2021; [4] Woodhams et al., 2008
†Fixed parameter based on SS.high for v_T.

Table 5.3: Outputs from MT-based thermal mismatch models, with fixed parameter values for parasite infectivity (E_i) and host resistance (E_h). Fixed parameter estimates were derived from thermal performance curves for parasite or host metabolic proxies. All models had a fixed value of $i_{T0} = 0.55$. "Distance SS" and its associated parameters (E_i^H, T_i^H) refers to the velocity component of the D_T TPC; all parameters associated with the mortality component of D_T TPC's were derived from the ω_T TPC (E_ω^L, T_ω^L, E_ω^H, T_ω^H). Standard errors are provided for all free parameters in parentheses (± s.e.).

Parasite Source	***Host Source***	E_i *(eV)*	E_i^H *(eV)*	T_i^H *(°C)*	h_{T0} *(d^{-1})*	E_h *(eV)*	K_P *(Z_e)*	P_0 *(Z_e)*	*AIC*
Distance BA	Oxygen BA	−0.62	---	---	**0.16** (0.03)	0.46	**73.5** (30.5)	**19.3** (13.9)	879.73
Velocity BA	Oxygen BA	0.21	---	---	**0.50** (0.02)	0.46	**406.0** (350.9)	**23.8** (14.8)	879.94
Distance BA	Breath BA	−0.62	---	---	**0.17** (0.03)	0.37	**80.3** (34.9)	**17.1** (11.6)	880.07
Distance SS	Oxygen BA	−0.14	0.85	16.0	**0.13** (0.02)	0.46	**111.1** (65.4)	**18.4** (11.2)	880.59
Distance SS	Breath BA	−0.14	0.85	16.0	**0.14** (0.02)	0.37	**137.0** (95.0)	**17.0** (9.8)	881.24
Velocity BA	Breath BA	0.21	---	---	**0.53** (0.02)	0.37	**1×10^6** (2×10^9)	**19.0** (9.5)	882.25
Velocity SS	Oxygen BA	0.69	0.85	16.0	**0.38** (0.03)	0.46	**1×10^6** (4×10^9)	**25.0** (13.29)	885.53
Velocity SS	Breath BA	0.69	0.85	16.0	**0.40** (0.03)	0.37	**1×10^6** (7×10^9)	**22.6** (12.9)	898.75
Growth SS	Oxygen BA	0.33	8.44	26.5	**0.00** (0.44)	0.46	**3.9** (4.6)	**509.0** (4×10^5)	943.04
Growth SS	Breath BA	0.33	8.44	26.5	**0.00** (0.39)	0.37	**3.7** (3.6)	**104.8** (2×10^4)	943.15

Table 5.4: Outputs from MT-based thermal mismatch models, with the activation energy for either parasite infectivity (E_i) or host resistance (E_h) set as a free parameter. Fixed parameter estimates were derived from thermal performance curves (TPC) for parasite or host metabolic proxies. All models had a fixed value of $i_{T0} = 0.55$. "Distance SS" and its associated parameters (E_i^H, T_i^H) refers to the velocity component of the D_T TPC; all parameters associated with the mortality component of D_T TPC's were derived from the ω_T TPC (E_ω^L, T_ω^L, E_ω^H, T_ω^H). For models with E_i as a free parameter (top table), the metabolic proxy source of any SS model parameters (e.g., E_p^L, T_p^L, E_p^H, T_p^H) is indicated in parentheses. Standard errors are provided in parentheses for all free parameters.

Models with parasite activation energy (E_i) as a free parameter

Parasite Source	*Host Source*	E_i *(eV)*	E_i^H *(eV)*	T_i^H *(°C)*	h_{T0} *(d^{-1})*	E_h *(eV)*	K_P *(Z_e)*	P_0 *(Z_e)*	*AIC*
Predict BA	Breath BA	**−0.55**	---	---	**0.31**	0.37	**79.7**	**27.2**	881.32
		(2.37)			(0.50)		(163.7)	(27.4)	
Predict BA	Oxygen BA	**−0.85**	---	---	**0.23**	0.46	**61.6**	**29.3**	881.32
		(1.48)			(0.23)		(44.8)	(41.9)	
Predict SS	Oxygen BA	**−0.16**	0.85	16.0	**0.21**	0.46	**85.4**	**23.5**	881.50
(Distance)		(1.44)			(0.20)		(115.6)	(20.9)	
Predict BA	Oxygen BA	**−0.23**	---	---	**0.21**	0.46	**101.6**	**23.7**	881.59
(Distance)		(1.18)			(0.16)		(149.9)	(18.9)	
Predict SS	Breath BA	**−0.13**	0.85	16.0	**0.23**	0.37	**100.8**	**20.6**	881.71
(Velocity)		(1.53)			(0.24)		(198.2)	(16.2)	
Predict SS	Breath BA	**−1.05**	8.44	26.5	**0.23**	0.37	**246.1**	**24.3**	881.82
(Growth)		(0.67)			(0.11)		(734.4)	(15.0)	
Predict BA	Breath BA	**−0.19**	---	---	**0.23**	0.37	**130.6**	**21.4**	881.85
(Distance)		(1.18)			(0.19)		(295.9)	(15.2)	
Predict SS	Oxygen BA	**0.32**	0.85	16.0	**0.18**	0.46	**314.1**	**22.2**	882.26
(Distance)		(0.92)			(0.11)		**(2×10^4)**	(12.9)	
Predict SS	Breath BA	**0.31**	0.85	16.0	**0.20**	0.37	**1992.0**	**20.7**	882.84
(Distance)		(0.83)			(0.12)		**(7×10^4)**	(11.1)	
Predict SS	Oxygen BA	**−1.5**	8.44	26.5	**0.11**	0.46	**33.1**	**11.5**	886.67
(Growth)		(0.83)			(0.07)		(16.4)	(10.1)	

Models with host activation energy (E_h) as a free parameter

Parasite Source	***Host Source***	E_i *(eV)*	E_i^H *(eV)*	T_i^H *(°C)*	h_{T0} *(d^{-1})*	E_h *(eV)*	K_P *(Z_e)*	P_0 *(Z_e)*	*AIC*
Distance	**Predict BA**	−0.62	---	---	**0.14**	**0.63**	**63.6**	**24.2**	881.49
BA					(0.04)	(0.34)	(31.5)	(22.8)	
Velocity	**Predict BA**	0.21	---	---	**0.46**	**0.54**	**206.5**	**30.7**	881.62
BA					(0.07)	(0.15)	(219.7)	(30.2)	
Velocity	**Predict BA**	0.69	0.85	16.0	**0.21**	**1.24**	**69.9**	**1×10^6**	881.67
SS					(0.22)	(1.30)	(100.7)	**(8×10^{10})**	
Distance	**Predict BA**	−0.14	0.85	16.0	**0.11**	**0.77**	**71.5**	**24.1**	881.71
SS					(0.04)	(0.33)	(43.0)	(18.8)	
Growth SS	**Predict BA**	0.33	8.44	26.5	**0.23**	**1.5**	**163.4**	**56.9**	883.08
					(0.12)	(0.56)	(363.9)	(97.7)	

CHAPTER FIVE FIGURES

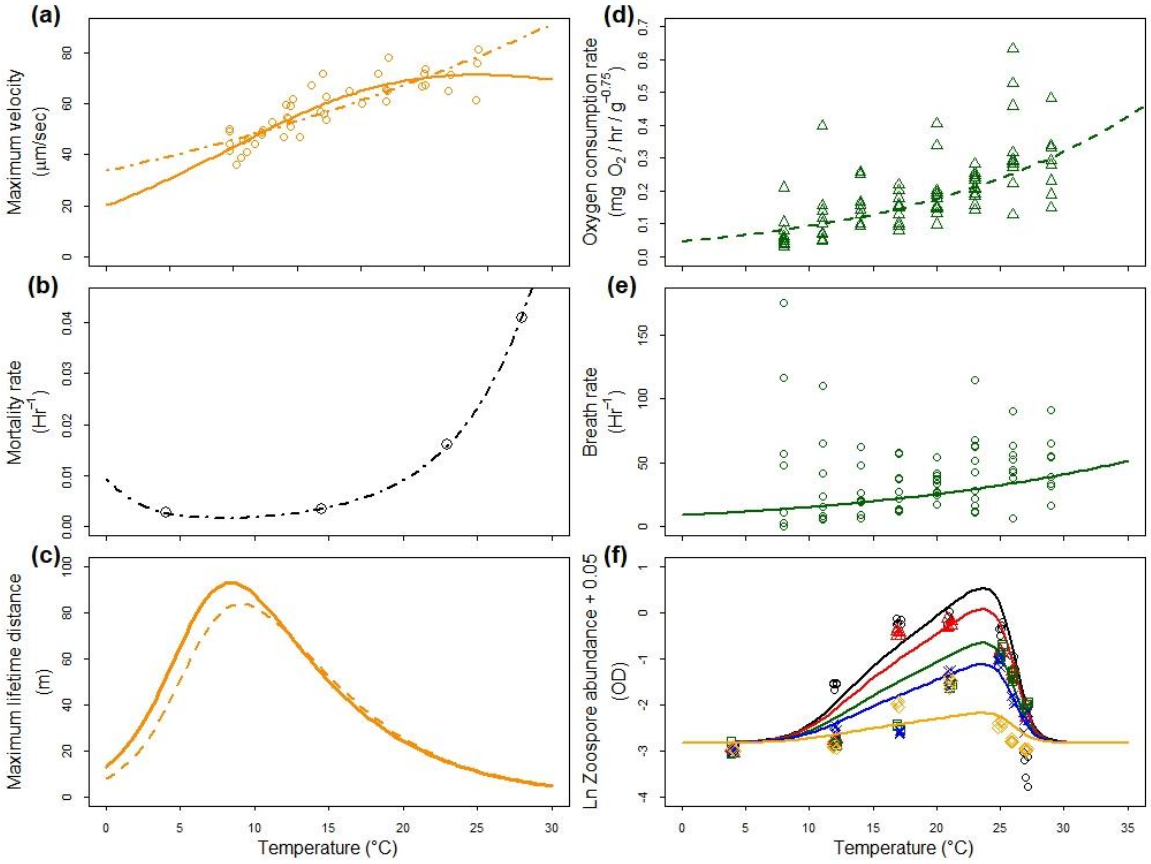

Figure 5.1: Metabolic Theory-based thermal performance curves for host (*X. laevis*) and parasite (Bd). (a) the maximum zoospore velocity (H. Craig et al., 2024), (b) zoospore mortality rate (Woodhams et al., 2008), (c) the maximum potential lifetime distance traveled (m) based on combined proxy measurements for maximum zoospore velocity (H. Craig et al., 2024) and mortality rate (Woodhams et al., 2008), (d) whole body oxygen consumption (McWhinnie et al., 2021), (e) breath rate (McWhinnie et al., 2021), and (f) Bd growth rate in culture (Sheets et al., 2021).

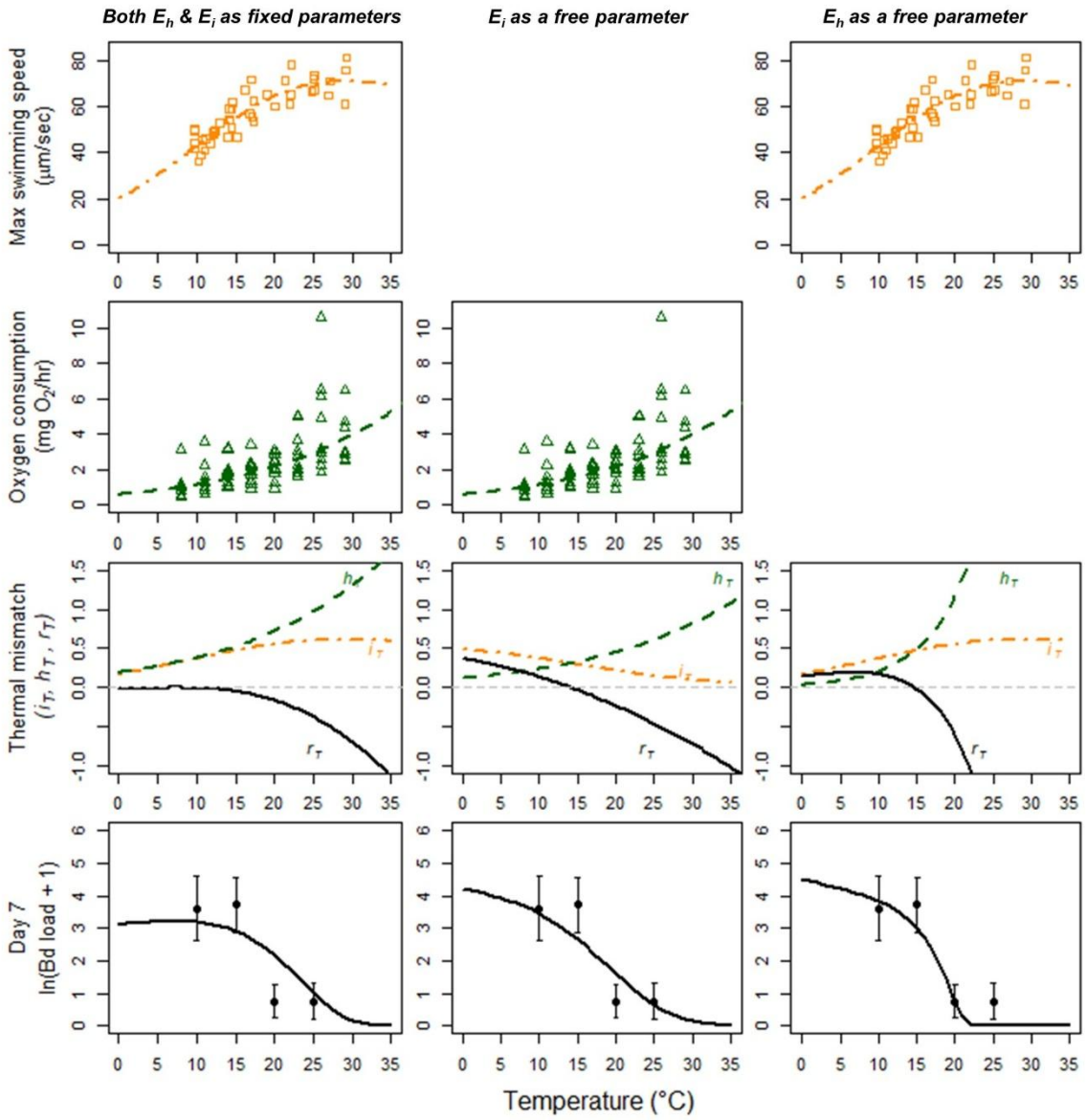

Figure 5.2: Example approach for modeling MT-based thermal mismatches. In the first column of plots, the parasite (orange squares) proxy (Velocity SS) and host (green triangles) proxy (Oxygen BA) are used to quantify the difference ($i_T - h_T$) between each organism's thermal performance (row four, thermal mismatch curves) resulting in the predicted infection loads across temperatures (row five plots). MT-based thermal mismatches models can also be used to estimate parasite (column 2 plots) or host (column 3 plots) metabolic parameters and infection outcomes.

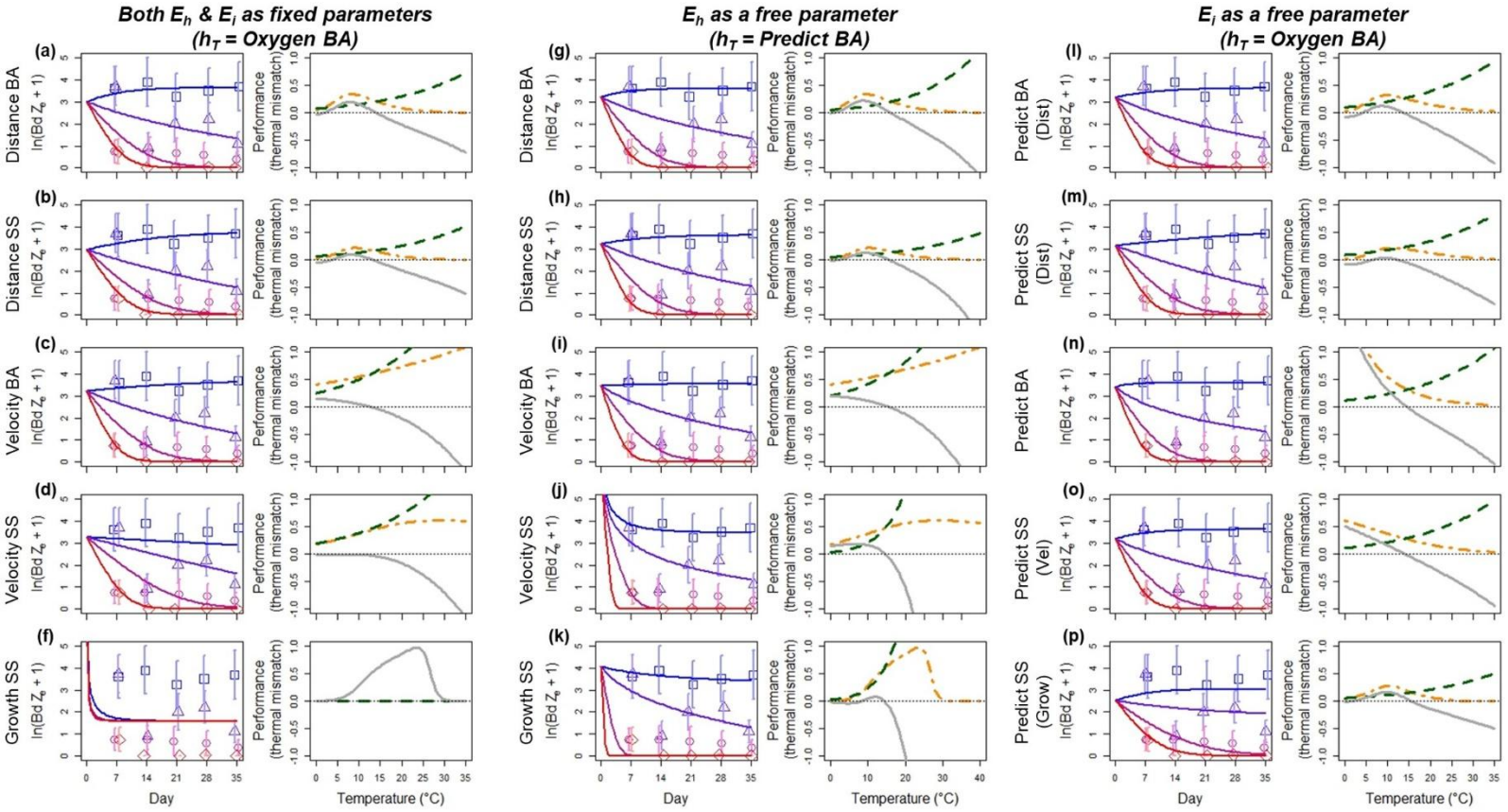

Figure 5.3: Model outputs from MT-based thermal mismatches for models where host and parasite metabolic proxies were both fixed (a–f) or were held constant for either the parasite (g–k) or host (l–p) allowing the other to be estimated as a free parameter. The first plot for each panel is the model's predicted infection load plotted with the actual infection data. The second plot in each panel is the MT-based thermal mismatch from each host-parasite combination. Columns 1 and 3 only include models with E_h derived from host O_2 consumption, since comparable models based on host breath rate had consistently higher AIC.

CHAPTER SIX

HOW DOES TEMPERATURE VARIABILITY AFFECT DISEASE TRANSMISSION IN AQUATIC FROG POPULATIONS? AN EXPERIMENTAL APPROACH.

6.1 Introduction

Climate change will inevitably lead to stronger within-year temperature fluctuations (P. T. Brown et al., 2017; Räisänen, 2002), with potentially important implications for host susceptibility to infectious diseases (Bradley et al., 2019; Dowell, 2001; Krichel et al., 2023; Paaijmans et al., 2010; Raffel et al., 2006, 2015; Rohr & Raffel, 2010). Developing a better understanding of the population-level consequences of these fluctuations is especially important for managing emerging diseases that threaten wildlife populations, such as ranavirus and chytridiomycosis infections of amphibians (Blaustein et al., 2018; Bower et al., 2017, 2019). Chytridiomycosis is a temperature dependent fungal skin disease of amphibians caused by the chytrid fungus *Batrachochytrium dendrobatidis* (Bd), for which frogs tend to become more infected at cooler or more variable temperatures (Carvalho et al., 2024; Cohen et al., 2019; Fisher et al., 2009; Raffel et al., 2013; Rohr & Raffel, 2010). Several studies investigating the effects of variable temperatures on individual Bd infection loads have shown increases in infection intensity (J. E. Noelker, Abreu Ruozzi, Spengler, et al., 2024; Raffel et al., 2013, 2015); however, this is not the only possible outcome for variable-temperature effects on infectious disease dynamics (Krichel et al., 2023; Paaijmans et al., 2010; Shocket et al., 2024).

There have now been several laboratory studies in multiple amphibian species for how temperature variability and sudden temperature shifts affect Bd infection in individual animals (Altman & Raffel, 2019; Bradley et al., 2019; J. E. Noelker, Abreu Ruozzi, Spengler, et al., 2024; Raffel et al., 2013, 2015). However, less is known about population level effects of temperature and temperature variability on among-host transmission of Bd and other infectious diseases. Population-level studies have so far largely taken advantage of natural variation in the field to test hypotheses about how temperature and temperature variability affects Bd and Bd-induced population declines (Briggs et al., 2005, 2010; Rohr & Raffel, 2010). However, an important knowledge gap exists concerning how temperature-dependent disease dynamics in laboratory settings relates to observational studies of Bd in natural populations. Although a wealth of observational data has accumulated for Bd infection in wild-caught individuals, most available data (e.g., amphibiandisease.org; Koo et al., 2021) and most field studies of climate-Bd relationships have focused on disease occurrence or prevalence (e.g., Carvalho et al., 2024; Cohen et al., 2017; but see Kriger et al., 2007; Vredenburg et al., 2010). This is in contrast to most laboratory Bd-infection studies, which tend to focus on longitudinal changes in Bd load following experimental infection of an individual animal (Cohen et al., 2017; J. E. Noelker, Abreu Ruozzi, Spengler, et al., 2024; Raffel et al., 2013, 2015; Venesky et al., 2022). Comparing snapshots of Bd prevalence in natural populations to dynamics of Bd infection intensities in laboratory experiments has yielded important insights by revealing qualitatively similar patterns of temperature dependence (Cohen et al., 2017, 2020). However, these apples-to-oranges (e.g., prevalence-to-intensity) comparisons are limited in their ability to test quantitative predictions for

whether and how Bd dynamics change when we move from individual to population scales. Epidemiological models for microparasites typically assume that among-individual variation in infection intensity is either unimportant (i.e., most Susceptible-Infected-Recovered models, Anderson & May, 1979) or independent of the presence of other host individuals (e.g., Wilber et al., 2016, 2017, 2021), but this assumption is rarely tested. Testing this assumption is vital to understanding potential conservation or management implications of these laboratory-scale infection studies of individual infection dynamics.

A potential way to address this question is to conduct controlled-temperature infection experiments at both individual and population scales, using experimental mesocosms to approximate natural frog densities. However, experimental mesocosm studies of population-level chytrid transmission have largely focused on effects of host density and habitat complexity (Malagon et al., 2020; Wilber et al., 2017). Additionally, past large-scale mesocosm investigations that manipulated temperature have done so by increasing variability or heating mesocosms relative to ambient temperatures, rather than fully controlling temperature conditions (Hamilton et al., 2012; Yvon-Durocher et al., 2011). This lack of controlled-temperature experimental studies at larger population scales makes it difficult to say whether or how variable-temperature and thermal acclimation effects observed on individual hosts will scale up to influence population-level transmission dynamics. Experiment designs that utilize controlled temperature treatments are critical to further test the effects of variable temperatures on population Bd infection intensities.

Multiple theoretical frameworks have been proposed to predict different infectious disease outcomes in variable-temperature environments, relative to a constant mean temperature. The temperature variability hypothesis (TVH) of Rohr and Raffel (2010) proposed that shifts in temperature would favor parasites due to their faster acclimation times compared to hosts, resulting in higher infection loads after each unpredictable shift to a new temperature. Several laboratory and field studies have found support for this hypothesis, including increased rates of disease-induced amphibians extinctions in years with greater month-to-month temperature shifts (Rohr & Raffel, 2010) and laboratory studies documenting the hypothesized delays in host thermal acclimation following a sudden increase or decrease in temperature (Altman et al., 2016; Altman & Raffel, 2019; Bradley et al., 2019; J. E. Noelker, Abreu Ruozzi, Spengler, et al., 2024; Raffel et al., 2013, 2015). Also consistent with the TVH, Bd zoospores have been found to have relatively short thermal acclimation times (mere minutes) compared to those observed for various amphibian species (usually multiple days; Craig et al., 2024). Noelker et al. (2024) found that delayed thermal acclimation in individual *X. laevis* following a sudden drop in temperature had positive effects on Bd load that persisted for at least five weeks, despite evidence that hosts became fully acclimated to the new temperature within a week of the temperature shift. However, Noelker et al. (2024) found no evidence that these delays in host thermal acclimation affected rates of zoospore production by infected *X. laevis* individuals, implying that these variable-temperature effects might be more important for the health of individual frogs than for subsequent transmission from infected frogs to other frogs (J. E. Noelker, Abreu Ruozzi, Spengler, et al., 2024). Thus, it is unclear whether or how the acclimation effects

observed in individual infection experiments will affect population-level Bd dynamics where among-individual transmission is likely to be an important factor.

In addition to testing the TVH, Raffel et al. (2013) explored potential implications of predictable diurnal variation versus unpredictable (e.g., random daily) variation for infection dynamics in ectotherms. Raffel et al. (2013) postulated that diurnal temperature effects should be less affected by the relative rates at which host and parasite respond to changing conditions and should instead favor whichever organism is better at using circadian rhythms to anticipate and adaptively respond to diurnal fluctuations. Raffel et al. (2013) found substantially reduced Bd infection in Cuban treefrogs (*Osteopilus septentrionalis*) exposed to diurnal fluctuations (15–25 °C) compared to random daily fluctuations (also 15–25 °C, despite observing an opposite (positive) effect of diurnal temperature variation on Bd growth in culture. In combination, these results suggest that both the pathogen and the host possess adaptive responses to diurnal temperature variation, which is unsurprising given that circadian rhythms are essentially ubiquitous in eukaryotic organisms (Lincoln, 2019; Reddy & Rey, 2014), but that host thermal adaptations overcame parasite adaptations in this case (Raffel et al., 2013). In contrast, Rohr and Raffel (2010) found a positive relationship between mean diurnal temperature range and rates of disease-associated amphibian extinctions. To our knowledge, no experimental study has yet experimentally tested whether or how adaptive responses to diurnal fluctuations influence Bd transmission dynamics in amphibian populations.

A third theoretical framework often used to predict responses to variable environments is nonlinear averaging, sometimes referred to as “rate summation”, in which predictions are generated by averaging TPC-predicted rates of a temperature

dependent process over time (Krichel et al., 2023; Shocket et al., 2024). Predictions based on nonlinear averaging depend on whether a performance curve is concave-up or concave-down, due to Jensen's inequality which posits that the secant line of a concave-down function always lies below the curve (Denny, 2017; Jensen, 1906; Martin & Huey, 2008; Sinclair et al., 2016; Vasseur et al., 2014). Due to Jensen's inequality, nonlinear averaging predicts reduced or heightened infection loads in variable temperature conditions, relative to a constant mean temperature, depending on if the TPC infection TPC is concave-down or concave-up (respectively). Our best-fit MTE-based models for temperature dependent Bd exponential growth rates on individual *X. laevis* all exhibited concave-down nonlinearity between 10 and 20 °C (Chapter 5), so nonlinear averaging predicts that *X. laevis* individuals exposed to temperatures fluctuating between 10 and 20 °C will have lower infection loads compared to hosts held at a constant 15 °C. This is opposite the TVH prediction for this system. Prior studies have found mixed evidence that nonlinear averaging generates improved predictions for infectious disease outcomes in variable-temperature conditions, relative to predictions based on mean temperatures (e.g., Krichel et al., 2023; Paaijmans et al., 2010; Shocket et al., 2024). For example, Krichel et al. (2023) observed elevated infection loads in the *Daphnia magna-Ordospora colligata* host-parasite system under variable-temperature conditions, despite predicting reduced infections based on nonlinear averaging from a concave-down infection TPC. It is possible that biological responses to temperature variability, such as the delays in thermal acclimation postulated by the TVH, sometimes outweigh negative effects of temperature variability predicted by Jensen's inequality for pathogens with concave-down infection TPCs.

To determine how temperature dependence of Bd transmission dynamics at population scales compares to Bd load dynamics on individual frogs (i.e., Noelker, Abreu Ruozzi, Spengler, et al., 2024), and to test how predictable diurnal temperatures influence Bd infection relative to unpredictable fluctuations or a constant mean temperature, we conducted a large-scale controlled temperature experiment with small populations of *X. laevis* held in heated outdoor mesocosms. I hypothesized that *X. laevis* populations would have similar temperature dependent infection loads (ln[Bd Z_e +1]) across a range of temperatures similar to infection dynamics observed on individual frogs (i.e., Noelker, Abreu Ruozzi, Spengler, et al., 2024). I further hypothesized that delays in host thermal acclimation observed in individual Bd infections (i.e., Noelker, Abreu Ruozzi, Spengler, et al., 2024) would manifest as increased infection loads (ln[Bd Z_e + 1]) in frog populations exposed to unpredictable temperature fluctuations, as predicted by the temperature variability hypothesis (Raffel et al., 2013; Rohr & Raffel, 2010), and that diurnal temperature variation would tend to favor the host as observed at the individual-infection level in *O. septentrionalis* (Raffel et al., 2013).

6.2 Methods

6.2.1 Mesocosm design and replication of temperature treatments

Our experimental design was inspired by the one used by Raffel et al. (2013) to test for effects of unpredictable versus diurnal temperature variation on Bd infection. Raffel et al. (2013) compared constant low, mean, or high temperature treatments (15, 20, and 25 °C) to a predictable diurnal temperature treatment (15–25 °C) and a treatment with random daily temperature shifts (also 15–25 °C). In the current study, we similarly included three constant temperature treatments (LO: 10 °C; MD: 15 °C; HI: 20 °C) and

three variable temperature treatments that fluctuated between 10 and 20 °C either diurnally (twice per day) or randomly over shorter time intervals (R1: shifts every 1–3 days) or longer time intervals (R2: shifts every 4–6 days). The experimental units consisted of 36 mesocosms containing susceptible populations of 3 or 5 *X. laevis* frogs randomly assigned to one of the six temperature treatments within six spatial blocks (Fig. 6.1, 6.2). After addition of the infected "source" frog, this resulted in a Density of 4 or 6 frogs per mesocosm, evenly distributed across Block and Treatment. Mesocosms were housed in a hoophouse at the Oakland University LORACS facility (Laboratory for Outdoor Research Agriculture Conservation & Sustainability), which had roll-up sides that allowed us to moderate changes in outside ambient temperatures. Each spatial block had on replicate mesocosm of each treatment resulting in a 6 × 6 experimental design.

Each mesocosm consisted of a 140 L (37 gallon) plastic tub, insulated from the ground with a one inch polystyrene foam board and insulated around the sides with Reflectix® double reflective bubble-wrap insulation. Mesocosms were filled with approximately 71.2 L (20 cm depth) tap water that was bubbled for at least 3 days prior to the addition of frogs to remove chlorine. A large tank of aged tap water was maintained nearby and mesocosm volumes were supplemented as needed to ensure volumes did not drop below 64.1 L (18 cm depth). Each mesocosm was also fitted with a 1/8" plexiglass lid lined with 50% black shade cloth to moderate potential for solar heating. The inside bottom of each mesocosm was coated with white rubberized Plasti Dip paint (Plasti Dip International, Blaine, MN) to provide greater contrast while collecting behavioral data and netting frogs during swabbing sessions. The variable treatment mesocosms lacked

insulated walls to allow for more rapid temperature shifts, especially with the diurnal treatment.

We achieved our target temperatures by conducting the experiment between December 2020 and March 2021 when outdoor temperatures are consistently below 10 °C in this part of Michigan. We used 150 or 300 Watt aquarium heaters to heat each mesocosm up to desired temperature target temperature (Fig. 6.2, 6.4). Heaters were housed within custom-built cylindrical cages constructed from plastic embroidery mesh, including extensions for the shorter 150 W heaters to ensure the cage cylinders had a consistent size across all experimental treatments. We plugged the aquarium heaters into daily timers or manually controlled thermostat boxes to manipulate when the variable temperature treatments switched. We generated a randomly assigned schedule for short- and long-intervals for the R1 and R2 treatments and switched temperature controllers between high and low temperature setpoints as needed. Diurnal fluctuations (DT treatment) were controlled using thermostat boxes rigged to plug-in timer outlets.

6.2.2 Animal handling and swabbing procedures

After they were received from the supplier, all frogs were treated to clear preexisting Bd infection by subjecting them to a four day 30 °C heat treatment. Frogs for this experiment were wild-type, random sex, post-metamorphosis snout-vent length to 3.81 cm (Xenopus 1 Corp. Dexter, MI). Frog masses for this experiment averaged 6.68 ± 0.19 g (mean ± s.e.). To introduce Bd to the population of frogs within each mesocosm, a single infected “source” frog was placed within each mesocosm housing either 3 or 5 susceptible “target” frogs (Fig. 6.3). Target frogs were added to their mesocosms seven days prior to the start of each temporal block of the experiment to allow them to

acclimate to their respective temperature regimens. To track infection loads for all individuals within each population, we swabbed frogs weekly. The first swab sample was taken on the first day of the experiment before the “source” frog was introduced in order to verify the infection status of all “target” frogs. For each swabbing session, animal handlers worked in pairs where one person held the frog and the other swabbed the frog and labeled samples. Both swabbers wore nitrile gloves while the animal handler wore cotton gloves over nitrile to improve grip as described by Noelker et al. (2024). Cotton gloves were changed between handling individual frogs and nitrile gloves were decontaminated using the bleach-decontaminate-rinse procedure described by Noelker et al. (2024). Nitrile gloves were changed between each block of mesocosms. For each mesocosm, a small tub of water was removed to hold frogs after they were swabbed. Individual frogs were then netted and immediately swabbed. Once the entire mesocosm population had been swabbed, the tub of water and frogs were returned to the mesocosm. Frogs were swabbed five times across the ventral side of each thigh and foot weekly to quantify the infection level and prevalence among the mesocosm population, as described by Noelker et al. (2024). Skin swabs were analyzed by qPCR analysis following protocols established protocols (J. E. Noelker, Abreu Ruozzi, Spengler, et al., 2024).

On the first day of “Week 0” one “source” frog was introduce into each population of “target” frogs. Within each mesocosm, the Bd-infected “source” frog was labeled with a small, orange elastomer injection on the ventral side of the right thigh (Fig. 6.3). Susceptible “target” frogs were marked with green elastomer in a coded location on the upper or lower leg to allow us to track each frog’s individual identity for the duration

of the experiment (Fig. 6.3). All experiments and animal use followed Institutional Animal Care and Use Committee (IACUC) protocol 18011 and IBC protocol 2759-13.

6.2.3 Bd preparation and frog inoculation

To prepare Bd infected "source" frogs, individual *X. laevis* needed to be inoculated with Bd zoospores prior to their being added to the mesocosms. First, 3 mL of cryopreserved Bd (stored at −80 °C; Boyle et al., 2003) was thawed, split between six 500 mL bottles with approximately 250 mL 1% tryptone broth, and allowed to grow for eight days before 1 mL of the broth was pipetted onto approximately twenty-four 100 mm 1% tryptone agar plates and housed at room temperature (~21 °C) for a further 18 days. Twenty agar plates were confirmed to have no bacterial contamination and active zoospores, and these were flooded with 3 mL ultrapure water and placed back into 21 °C incubators for 20 minutes to collect as many zoospores as possible. All 20 plates were then poured into a beaker where the collection water was homogenized, zoospore concentration was determined by hemocytometry (with > 90% of zoospores active), and collection water was diluted with ultrapure water to a concentration of 1×10^6 zoospores/mL.

Prior to the start of the outdoor mesocosm experiment, 40 potential "source" *X. laevis* were housed in our cold room facility at 8 °C. Frogs were communally housed with 10 frogs per container in 4 L dechlorinated tap water. These frogs were inoculated with Bd by pipetting 3×10^6 zoospores onto the dorsal side of each frog's body. Excess Bd inoculate was allowed to run off into the communal water, and frogs were placed back into the same housing water. The infected "source" frogs were housed together at 8 °C

for 2 weeks, to ensure infection has time to build up to sufficient levels for use in the transmission phase of the experiment.

6.2.4 Statistical analysis

I conducted statistical analyses using R statistical software (v. 4.1.3; R Core Team, 2022). I converted the number of gene copies detected on each swab sample as analyzed by qPCR to zoospore equivalents (Z_e) using the conversion factor for Bd strain JEL423 described by Altman and Raffel (2019). This method allowed me to track the infection load for each frog within mesocosm populations throughout the experiment. However, for analysis at the mesocosm level and to use mesocosm as the unit of replication for plotting purposes, I averaged the ln(Bd Z_e + 1) for all frogs within a mesocosm (MesoID) prior to calculating means ± s.e. for each week (0 – 7) of the experiment.

Infection results from the entire mesocosm experiment were subdivided into an "Early" phase (Weeks 0-3), during which infection generally continued to spread among uninfected hosts, and a "Late" phase (Weeks 4-7), during which infections among frogs appeared to reach an equilibrium. To test for effects of temperature treatment (Treatment), density, and time (Week), I ran linear mixed effects models that included random effects of block and mesocosm (MesoID; function *lmer* in R package *lme4* (ver. 1.1.36). To conduct Type II F-tests I used the *Anova* function in package *car* (ver. 3.1.3); Bates et al., 2015; Fox & Weisberg, 2019). I also conducted post-hoc tests for all pairwise combinations of temperature treatments, always including Treatment × Week interactions to compare rates of change in ln(Bd Z_e + 1) (slopes) of each pair of

treatments. I corrected p-values for multiple comparisons within each phase of the experiment (early or late) by correcting p-values for the false discovery rate.

To investigate treatment effects on mortality for individual frogs, I generated a dataset of one-week intervals for each frog that included the mean ln(Bd Z_e + 1) over that interval and, whether the frog survived or died by the end of each interval, and the day of death (or end of the experiment if a frog survived to the end). I used this time interval dataset to conduct a time-to-event survival analysis with mean ln(Bd Z_e + 1) for each time interval as a predictor. To avoid pseudoreplication when testing for effects of Treatment and Density on frog mortality, I used cox proportional hazards models (*coxme* function from the R package *coxme* (ver. 2.2.18.1; Therneau, 2022), including a random effect of FrogID nested within MesocosmID. I also used these models to explore the continuous effect of temperature on survival within the three constant-temperature treatments, and to explore how much of the among-Treatment variation was explained by individual variation in ln(Bd Z_e + 1). I generated survival curves for each temperature treatment in the mesocosm experiment using the *survfit* function in the *survival* package (ver. 3.5.5) in R (Therneau & Grambsch, 2000).

I further explored the quantitative effects of Bd load on individual frog mortality rates using survival regression. Models were fit using the *flexsurvreg* function in R package *flexsurv* (ver. 2.2.2; Jackson, 2016) which allows me to use interval censoring to track each individual in the overall time series, while using mean ln(Bd Z_e + 1) across each interval as a predictor variable. I compared models with exponential and Weibull error distributions and found little difference in model AIC. This allowed me to use a relatively simple model with exponentially distributed residual error (ε), which allows

estimation of a baseline mortality rate parameter (β_0) and a coefficient describing the effect of mean ln(Bd Z_e + 1) on mortality (β_1):

$$Mortality\ rate = e^{\beta_0} \cdot e^{\beta_1 \ln (Z_e + 1)} \cdot e^{\varepsilon}. \quad \text{Eq. 6.1}$$

I initially estimated β_1 as a free parameter; however, β_1 was close to 1.0, allowing me to further simplify the model by assuming $\beta_1 = 1$. This simplifies the equation to:

$$Mortality\ rate = e^{\beta_0} \cdot (Z_e + 1) \cdot e^{\varepsilon} \cong \alpha Z_e \cdot e^{\varepsilon}. \quad \text{Eq. 6.2}$$

This is useful because $\alpha = e^{\beta_0}$ is equivalent to the intensity-dependent host mortality rate due to Bd infection as defined in classic macroparasite models (Anderson & May, 1979).

6.3 Results

6.3.1 Initial conditions

We successfully achieved target temperatures for all 6 treatments, with average temperatures for variable treatments close to 15 °C (Fig. 6.4, 6.5). The average infection load for the "source" frogs at the time of addition to the mesocosms were LO = 8.19 ± 0.49, MD = 7.43 ± 0.69, HI = 5.44 ± 1.30 ln(Bd Z_e +1) for the constant temperature treatments and DT = 7.96 ± 0.87, R1 = 5.74 ± 1.22, and R2 = 7.76 ± 0.62 ln(Bd Z_e +1) for the variable treatments (mean ± s.e.). Unfortunately, we discovered that some of the "target" frogs had pre-existing Bd infections despite the precautionary heat treatment. The original source of these infections is unclear but likely relates to a Bd outbreak detected in the lab around the same time (see Abreu Ruozzi, 2021 for additional details). However, 103 of the 146 "target" frogs returning 0 Bd Z_e on their initial swabs and average loads far lower than the "source" frogs (LO = 4.87 ± 0.69, MD = 1.60 ± 0.28, and HI = 1.49 ± 0.37 ln[Bd Z_e + 1] and DT = 2.14 ± 0.56, R1 = 3.22 ± 0.73, and R2 = 2.61 ± 0.72 ln[Bd Z_e + 1]; mean ± s.e.). Overall effects of temperature treatments on

ln(Bd Z_e + 1) were nonsignificant at the start of the experiment (Week 0; Table 6.2, 6.3, Fig. 6.6). Since we were able to document their initial infection levels, we treated these already infected "target" frogs as extra "source" frogs that did not affect our ability to track subsequent effects of temperature treatments on population-level Bd dynamics.

6.3.2 Main effects of temperature and density treatments on ln(Bd Z_e + 1)

There was overall a highly significant main effect of Treatment on ln(Bd Z_e + 1) throughout the experiment (Table 6.2; Fig. 6.6, 6.7). We did not detect a significant effect of frog Density in the full model (Table 6.2). However, when we tested for Density effects within individual temperature treatments and experimental phases, we detected a significant effect of frog Density during the early phase within the LO temperature treatment ($F_{1,3.03}$ = 4.18, hazard ratio (*HR*) = 2.74, p = 0.041). When we tested for the effect of temperature as a continuous predictor across the three constant temperature treatments, there was highly significant negative effect of temperature in both the early and late phases of the experiment (Table 6.2). When we examined individual weeks, we found that this negative effect of temperature on ln(Bd Z_e + 1) was already significant by Week 1 and remained significant through the end of the experiment (Weeks 1-7 all p < 0.001; Fig. 6.6).

During the early phase (Weeks 0–3), mean ln(Bd Z_e + 1) was highest in the LO treatment and significantly different from the MD, HI, and R1 variable treatments (Table 6.3; Fig. 6.7). The HI temperature treatment consistently had the lowest mean ln(Bd Z_e + 1), which was significantly different from the LO, MD, DT, and R2 treatments (Table 6.3; Fig. 6.7). During the late phase (weeks 4–7), qualitative patterns of ln(Bd Z_e + 1) were similar to the Early phase, with all three constant temperature treatments being

significantly different from one another (Table 6.3; Fig. 6.7). All three variable treatments were significantly lower than the LO treatment during the late phase, but none were significantly different from the MD or HI treatment (Table 6.3; Fig. 6.7). The variable treatments (DT, R1, and R2) showed overall similar patterns of Bd load dynamics to each other and to the MD treatment during both phases of the experiment (Fig. 6.6, 6.7). The R1 treatment was consistently lower than the MD and other variable temperature treatments during Weeks 1-4, but even this treatment was not significantly different from the others (Fig. 6.6, 6.7).

6.3.3 Treatment effects on Bd temporal dynamics (Treatment × Week effects)

During the early phase (Weeks 0–3) there was an overall increase in ln(Bd Z_e + 1) through time across all Treatments, with a highly significant Treatment × Week interaction (Table 6.2; Fig. 6.6). The rate of increase through time was significantly higher in the LO treatment than all other treatments during the early phase, based on significant Treatment × Week interactions in pairwise comparisons (Table 6.3; Fig. 6.6, 6.7). Among the remaining temperature treatments (other than LO), the HI treatment had the overall lowest slope through time during the early phase but was only significantly different from the R2 treatment (Table 6.3; Fig. 6.6, 6.7). The variable temperature treatments all had similar slopes through time compared to the MD treatment during this early phase (Fig. 6.6, 6.7). Frogs in the HI treatment experienced an initial increase but peaked in Week 1 at ln(Bd Z_e + 1) ≈ 3 and then steadily decreased, in contrast to the MD and variable-temperature treatments which leveled off between ln(Bd Z_e + 1) ≈ 3–5 by Week 2 (Fig. 6.6).

During the late phase (Weeks 4–7), there was a weakly significant overall decline in ln(Bd Z_e + 1) through time (Table 6.2, Fig. 6.6). The three constant-temperature treatments were essentially level during this time frame (Fig. 6.6), though with a significantly higher slope through time in the LO than the HI treatment after accounting for random effects of Mesocosm and Frog ID (Fig. 6.7, Table 6.3). The DT and R1 treatments were also level during the late phase, but the R2 treatment declined and had a significantly lower slope through time than all other treatments (Fig. 6.6, 6.7, Table 6.3).

6.3.4 Patterns of Bd-induced mortality

A mixed-effects Cox proportional hazards model revealed a highly significant effect of Treatment on frog survival (X_5^2 = 17.52, p = 0.004), driven by high mortality in the LO treatment (Fig. 6.8). All other temperature treatments had low rates of mortality (Fig. 6.8). However, when we added ln(Bd Z_e + 1) to the model as a covariate, Treatment became nonsignificant (X_5^2 = 0.31, p = 0.998), whereas ln(Bd Z_e + 1) significantly increased the individual hazard of frog mortality within a given time interval (X_1^2 = 31.73, p < 0.001). Focusing just on the constant-temperature treatments, there was also a highly significant negative effect of Temperature on frog mortality (X_1^2 = 6.87, p = 0.009, AIC = 110.36). Again, when we added ln(Bd Z_e + 1) to this model, Temperature became nonsignificant (X_1^2 = 0.01, p = 0.910) and ln(Bd Z_e + 1) was very highly significant (X_1^2 = 20.08, p < 0.001). There was no significant effect of frog Density when added to the full survival model testing for Treatment effects (X_1^2 = 0.16, p = 0.687). We were only able to detect a significant (positive) effect of Density on mortality if we focused on Weeks 0–4 of the LO treatment (X_1^2 = 4.18, p = 0.041; Fig. 6.8).

A survival regression model with Weibull distribution and a free β_1 parameter resulted in β_0 *shape* = 0.50 and β_0 *scale* = 10.75 and $\beta_1 = -0.68$ with AIC = 178.7. A survival regression model with exponential distribution and free β_1 parameter resulted in $\beta_0 = -15.59$ and $\beta_1 = 1.15$ with AIC = 179.8. When fitting fully parameterized survival regression models, the AIC for the Weibull fit (178.7) was similar to the AIC for the Exponential fit (179.8; ΔAIC = 1.1), so we focused on a simpler exponential model resulting in a constant parameter of $\beta_0 \approx -15.59$ and a coefficient for the effect of ln(Bd Z_e + 1) of $\beta_1 = 1.15 \pm 0.13$ (s.e.). This β_1 value was not significantly different from 1.0. Holding this coefficient constant ($\beta_1 = 1$) resulted in a lower model AIC (179.1) and a constant parameter of $\beta_0 \approx -13.97$, corresponding to an estimated virulence parameter of $\alpha = \exp(-13.97) = 8.59 \times 10^{-7} \pm 1.75 \times 10^{-7}$ (s.e.).

6.4 Discussion

Qualitatively, the patterns of temperature dependent infection in this population-level transmission experiment were similar to those seen in prior experiments with individual *X. laevis*, with substantially higher infection levels at cooler temperatures (J. E. Noelker, Abreu Ruozzi, Spengler, et al., 2024; Raffel et al., 2013, 2015). However, the infection intensities observed in this experiment were dramatically higher than the infection loads observed on individually infected *X. laevis* in prior laboratory experiments, especially at 10 °C where geometric mean infection intensities in the current study (~44,000 Bd Z_e later in the experiment) were nearly three orders of magnitude higher than equilibrium levels of infection in prior individual-level Bd experiments with *X. laevis* (~35 Bd Z_e; Noelker, Abreu Ruozzi, Spengler, et al., 2024). These much higher infection intensities at 10 °C corresponded to greatly elevated rates of infection-induced

mortality, in contrast to individual-level laboratory infection experiments with *X. laevis* during which no animals died despite being infected at the same temperatures over a 5-week time frame (J. E. Noelker, Abreu Ruozzi, Spengler, et al., 2024). These high levels of Bd infection intensity and Bd-induced mortality were unexpected, because *X. laevis* is widely cited as being Bd-resistant relative to other amphibian species (J. E. Noelker, Abreu Ruozzi, Spengler, et al., 2024; Rollins-Smith, 2009; Weldon et al., 2004).

Contrary to the temperature variability hypothesis (TVH) of Rohr & Raffel (2010), the mean infection loads for our variable temperature treatments were generally similar to infection loads observed at the mean temperature treatment (MD: 15 °C) and far lower than those observed at 10 °C (our LO temperature treatment). The TVH predicts increased infection levels in variable-temperature conditions with frequent unpredictable temperature shifts, due to delays in host thermal acclimation following each shift to a new temperature (Rohr & Raffel, 2010). Noelker et al. (2024) observed higher Bd infection loads in individual *X. laevis* following a sudden temperature decrease, consistent with the delays in host acclimation assumed by the TVH. Based on these prior results, we predicted positive effects of the R1 and R2 treatments on Bd infection levels; the lack of such a positive effect of either treatment was unexpected.

There are multiple possible reasons for this deviation from the TVH prediction. First, it is possible negative effects of nonlinear averaging on $\ln(\text{Bd } Z_e + 1)$ in the R1 and R2 treatments, as predicted by Jensen's inequality, counteracted the effects of delayed host acclimation resulting in similar Bd loads to the MD treatment (Denny, 2017; Jensen, 1906; Krichel et al., 2023). The MT-based mismatch models we developed for individual *X. laevis* infections (see Chapter 5) showed a concave-down thermal performance curve

for Bd population growth rate on the host, so Jensen's inequality predicts reduced infection levels in a variable-temperature environment compared to a constant average temperature. (Fig. 6.6). Another possible explanation is that the thermal acclimation effects on individual-level Bd load dynamics observed by Noelker et al. (2024) are less important for population-level Bd transmission dynamics than originally predicted by the TVH. Noelker et al. (2024) also observed that there were no significant effects of host thermal acclimation status on the rates of Bd zoospore release from infected *X. laevis*, despite there being consistent acclimation effects on Bd load as quantified via qPCR of skin swabs. If host acclimation has no effect on rates of among-host transmission, and if among-host transmission is an important driver of Bd load dynamics, then the variable-temperature effects predicted by the TVH might be unimportant for Bd load dynamics in small populations of *X. laevis*. We also saw no significant differences between predictable diurnal temperature shifts (DT) and treatments with random temperature shifts at unpredictable time intervals (R1 or R2). This implies either: (1) that neither the host nor the parasite possesses adaptive responses to diurnal temperature variation that affect Bd infection dynamics (but see Raffel et al., 2013), or (2) that *X. laevis* possess adaptations to predict and adapt to diurnal variation that approximately compensated for Bd diurnal adaptations within the context of this experiment. Like other eukaryotic organisms, *X. laevis* is known to be sensitive to circadian rhythms and should be capable of anticipating and responding to natural diurnal changes in temperature (Curran et al., 2008). Diurnal temperature ranges of approximately 10 °C are common within the native range of *X. laevis* (mean diurnal temperature range = 12.0 °C; see Chapter 4), so this species could plausibly possess adaptive responses to this level of diurnal temperature

variation. Further investigations would be needed to truly elucidate the potential additive or subtractive effects of TVH, nonlinear averaging across variable temperature treatments, and host or parasite responses to diurnal temperature variation on population-level infection dynamics in this system.

Perhaps the most unexpected result of this experiment was the extraordinarily high infection loads in these small populations of hosts compared to the infection dynamics observed at the same temperatures in isolated individuals (Fig. 6.6; Noelker, Abreu Ruozzi, Spengler, et al., 2024). This was true for every temperature treatment, but especially for the lowest (10 °C) temperature treatment. One possible driver of such high infection intensities with multiple individuals is that continued transmission among already-infected frogs might result in positive feedback loops that allow Bd loads to build up to higher equilibrium levels in small populations of frogs than is possible for a single isolated individual. In Chapter 7, I explore this hypothesis in more detail by using individual-based models (IBMs) to simulate the effects of these "transmission intensity feedbacks" on population-level Bd dynamics. It also remains possible that something else about conditions in the mesocosm experiment led to elevated Bd infection levels, such as (for example) stress-induced immune suppression in response to aggressive behaviors by conspecifics. Further work will be needed to test these alternative hypotheses. In general, however, this unexpected result highlights the value of conducting population-level infection experiments for comparison with more-common individual-level laboratory experiments. These results also highlight the importance of quantifying infection intensities from all individuals in a population-level experiment rather than relying on prevalence data. Prevalence data would not have revealed the far more interesting

changes in the dynamics of Bd load when scaling this disease system from individuals to populations. Prevalence data would also have provided only limited insights into which temperatures resulted in more infections, due to nearly all individuals testing positive for infection by Week 3 of the experiment regardless of temperature treatment. Prevalence data would also been insufficient to draw strong conclusions about whether or how Bd infection was affecting rates of frog mortality in the population-level experiment, due to the ubiquity of positive Bd results on individual animals and the lack of Bd− control mesocosms in this experiment.

The high rates of Bd-induced mortality in the constant 10 °C mesocosms was unexpected, given that prior Bd-infection studies with individual *X. laevis* found little to no infection-induced mortality (J. E. Noelker, Abreu Ruozzi, Spengler, et al., 2024; Rollins-Smith, 2009; Van Rooij et al., 2012; Weldon et al., 2004). Despite the lack of Bd− control mesocosms in this experiment, the survival analyses provided strong evidence that this mortality was induced by high levels of Bd infection, with individual $\ln(\text{Bd } Z_e + 1)$ emerging as a highly significant predictor of frog mortality that fully accounted for among-Treatment differences in mixed-effects models. Only frogs in the constant 10 °C treatment experienced substantial mortality, and this was also the only temperature treatment where mean Bd loads regularly exceeded 10,000 zoospore equivalents (Fig. 6.6, 6.8). On the surface, this result seems to support Vredenburg's "10,000 zoospore rule", which postulates that mortality is unlikely until Bd load per skin swab exceeds this threshold (Kinney et al., 2011; Vredenburg et al., 2010). However, our results indicate that this might not be a true threshold effect in *X. laevis*, but rather an apparent threshold resulting from the non-intuitive nature of exponential dynamics. Bd

loads are lognormally distributed due to exponential population dynamics of Bd on frogs, and ln(Bd load +1) was a highly significant predictor of mortality in our survival models. However, the coefficient representing the effect of ln(Bd load +1) on baseline hazard rate was quite close to $\beta_1 = 1.0$. Mathematically, this means that the daily probability of an individual frog's death was proportional to exp(ln[Bd Z_e + 1]), i.e., directly proportional to its Bd load (+ 1) on a natural scale. This effect appears to entirely explain the among-Treatment differences in mortality rates observed in this experiment, with high mortality in the LO treatment corresponding to exponentially higher Bd loads than in all other temperature treatments. For example, the difference between mean ln(Bd Z_e +1) for the LO and MD treatments might seem modest on a logarithmic scale (LO = 10.7 versus MD = 4.2), but this corresponds to more than a 600-fold difference in geometric mean Bd load (LO ≈ 44,000 versus MD ≈ 66). It is possible that this kind of pattern might account for apparent "threshold" effects of Bd load on amphibian mortality reported by prior studies. If so, our results suggest that Bd-induced mortality in populations of infected frogs could be modeled as a simple intensity-dependent virulence parameter as described by Anderson & May (1979) in their classic models of macroparasite-host dynamics, which would be simpler than model Bd-induced mortality as a threshold response (e.g., Wilber et al., 2016, 2017).

We observed a significant effect of frog density on survival within the LO temperature treatment when focusing the first four weeks of the experiment. There was also a positive though nonsignificant trend (*coef* = 0.49, $p = 0.237$) towards frogs in the higher-density mesocosms having higher Bd loads during the weeks 0–4 of the experiment, suggesting that frogs in higher density populations built up higher infection

loads more quickly. Such an effect might account for higher mortality rates in the higher-density mesocosms, but this interpretation is speculative due to the relatively small sample sizes involved (3 mesocosms per density within the LO treatment).

6.5 Conclusions

This study reveals the potential for groups of hosts to exhibit patterns of infection intensity that differ substantially from isolated infections of individual animals, highlighting the importance of reporting infection intensity data in field studies to allow apples-to-apples comparisons with laboratory studies. Furthermore, this study showed that acclimation effects on infection observed on individual frogs (J. E. Noelker, Abreu Ruozzi, Spengler, et al., 2024) did not translate to higher levels of infection in populations of frogs subjected to repeated temperature shifts, as predicted by the TVH. Instead, we saw infection loads in variable temperature treatments similar to the average temperature (our MD temperature treatment, 15 °C). Much of the evidence for the TVH to date has come from similar observations of acclimation effects on individual-level Bd infections, so the results of the current study call into question the population-level implications of the TVH. Few studies have utilized controlled temperature experiments at both individual and population scales to directly test TVH predictions at a population level. Further investigation is needed to determine if the substantially higher infection loads observed in the LO temperature treatment could possibly be due to positive feedback loops between transmission and individual infection intensities (i.e., “transmission-intensity feedbacks”).

CHAPTER SIX TABLES

Table 6.1: Variables, their abbreviations, and definitions for the experiment and statistical models.

Variable	***Abbreviation***	***Definition***
Temperature treatment	Treatment	Temperature treatments (HI, MD, LO, DT, R1, R2) assigned to mesocosms within replicate experimental blocks
Week of experiment	Week	Week of the experiment (0-7) relative to the introduction of an infected frog which occurred on the first day of Week 0
Mesocosm identification	MesoID	Mesocosm number (1-36)
Block	Block	Replicate spatial block within the experiment (A-F)
Density	Density	Density of frogs within a mesocosm (4 or 6; average of 5)
log Bd load	LnBdLoad	Natural log of Bd zoospore equivalents detected from a swab sample (ln[Bd Z_e +1])
Mean interval log Bd load	LnBdLoad.IntMean	Average of LnBdLoad at the start and end of each weekly interval
Proportion alive	PropAlive	The proportion of frogs alive throughout the mesocosm experiment
High temperature treatment	HI	Highest temperature treatment (20 °C)
Medium temperature treatment	MD	Medium temperature treatment (15 °C)
Low temperature treatment	LO	Low temperature treatment (10 °C)
Diurnal switch	DT	Diurnal temperature shift with average of 15 °C
Short random switch	R1	Random temperature switches between 10 and 20 °C over short time periods (1-3 days) with average 15 °C
Long random switch	R2	Random temperature switches between 10 and 20 °C over long time periods (4-6 days) with average 15 °C

Table 6.2: Interactive linear mixed effect models for Treatment, Week, and Density on LnBdLoad for the early (weeks 0–3) and late (weeks 4–7) phases of the mesocosm experiment. Models also included interactions of Treatment × Week and had random effects of MesoID nested with Block (1|Block/MesoID). Variable definitions are given in Table 6.1.

Phase	***Response***	***Predictor***	***F value***	***Df***	***P***
Early	LnBdLoad	Treatment	14.2	5, 25	< 0.001
		Week	45.8	1, 102	< 0.001
		Density	0.4	1, 4	0.578
		Treatment × Week	9.2	5, 102	< 0.001
Late	LnBdLoad	Treatment	38.9	5, 24.0	< 0.001
		Week	4.0	1, 92.2	0.047
		Density	0.6	1, 4.0	0.489
		Treatment × Week	4.6	5, 93.8	0.001

Table 6.3: Post hoc tests of the full model were also run for all possible combinations of treatment (Treatment 1 compared to Treatment 2 columns). Main effect of treatment on infection load for the early phase and the late phase of the experiment were recorded and adjusted using false discovery rate correction. The P-values of the Treatment × Week interaction indicate whether the two paired treatments had significantly different slopes through time. Variable definitions are given in Table 6.1.

Phase	*Treatment 1*	*Treatment 2*	*Treatment main effect (corrected P)*	*Treatment × Week (corrected P)*
Early	DT	MD	0.368	0.801
	HI	MD	**0.027**	0.052
	LO	MD	**0.014**	**0.003**
	R1	MD	0.495	0.166
	R2	MD	0.257	0.634
	HI	DT	**0.014**	0.075
	LO	DT	0.052	**0.001**
	R1	DT	0.184	0.232
	R2	DT	0.554	0.517
	LO	HI	**0.006**	< **0.001**
	R1	HI	0.257	0.519
	R2	HI	**0.014**	**0.018**
	R1	LO	**0.012**	< **0.001**
	R2	LO	0.061	**0.015**
	R2	R1	0.117	0.063
Late	DT	MD	0.315	0.661
	HI	MD	**0.009**	0.464
	LO	MD	**0.003**	0.303
	R1	MD	0.114	0.979
	R2	MD	0.396	**0.022**
	HI	DT	0.059	0.856
	LO	DT	**0.003**	0.187
	R1	DT	0.117	0.677
	R2	DT	0.776	**0.036**
	LO	HI	< **0.001**	**0.037**
	R1	HI	0.089	0.540
	R2	HI	0.067	**0.030**
	R1	LO	**0.002**	0.521
	R2	LO	**0.005**	**0.022**
	R2	R1	0.130	**0.029**

CHAPTER SIX FIGURES

Figure 6.1: The mesocosm arrangement from my experiment with 36 randomized replicate temperature treatments. There were 6 replicate spatial blocks. Two blocks were started each day the first week to reduce the total number of mesocosms that needed to be swabbed each day of the experiment. Frogs found to cross our endpoint criteria or dead were swabbed at the time of their discovery and removed from the experiment.

Figure 6.2: Each mesocosm consisted of a large, 37-gallon plastic tank. The bottom of each mesocosm was painted with white Plasti Dip paint to provide contrast making it easier to locate each frog. Each mesocosm was equipped with a heater enclosed in a cage designed by our lab to protect frogs from injury by the heating element and to ensure frogs experienced the target water temperature (compared to potentially warmer water found closer to the heater). Heaters were connected to external thermostat control boxes with the probe inserted along the inside edge of the heater cage away from direct contact to the heating element. A HOBOware temperature logger was secured to the cage to track the mesocosm temperatures.

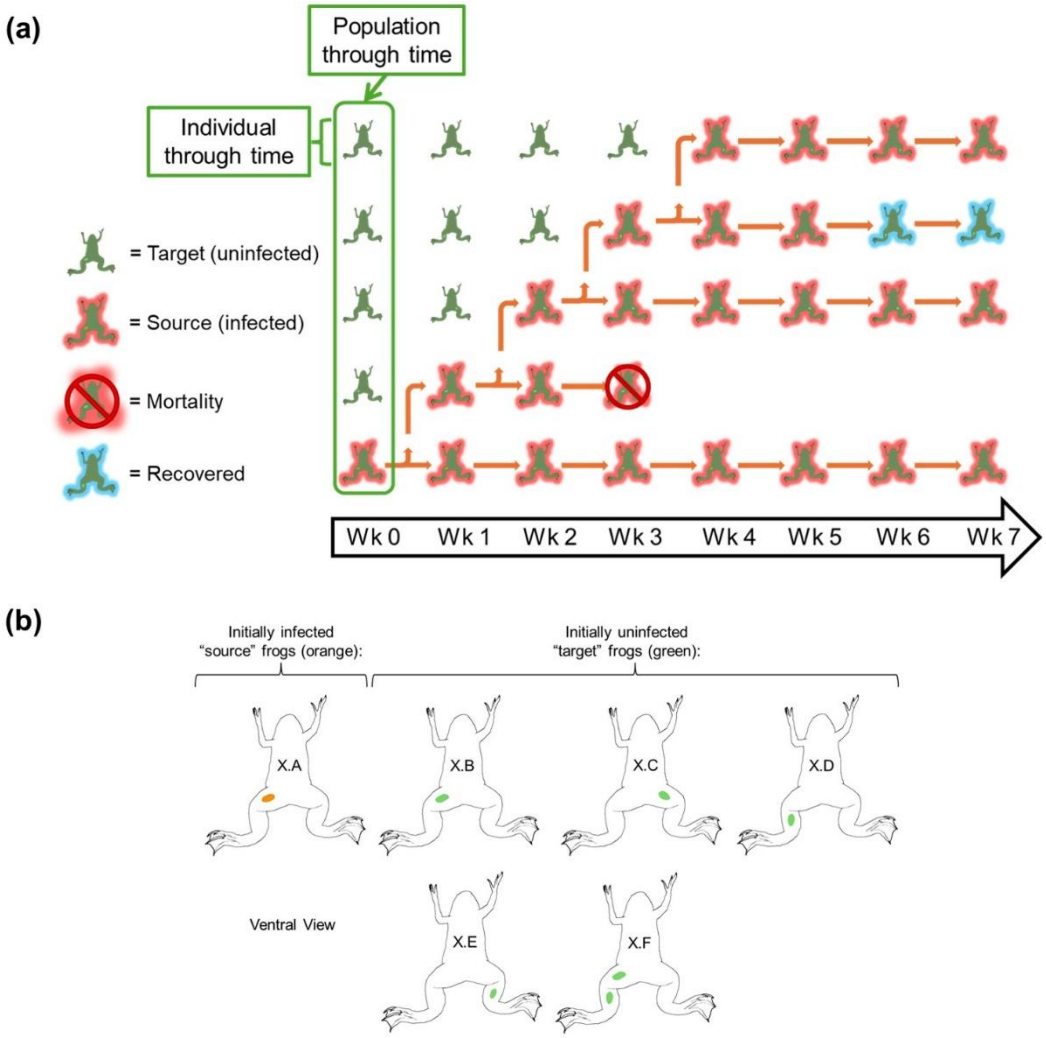

Figure 6.3: (a) Illustration of the hypothesized transmission pattern expected by weekly swabbing of frogs in an uninfected population exposed to Bd via an infected individual. (b) Identification marking pattern used for frogs' populations made using VIE tags. Bd-infected "source" frogs were marked with orange while uninfected "target" frogs were marked with green on the ventral side of the upper or lower leg. In each code, "X" is the mesocosm number and the letter is the individual from that tank to generate a unique identification for each frog throughout the experiment.

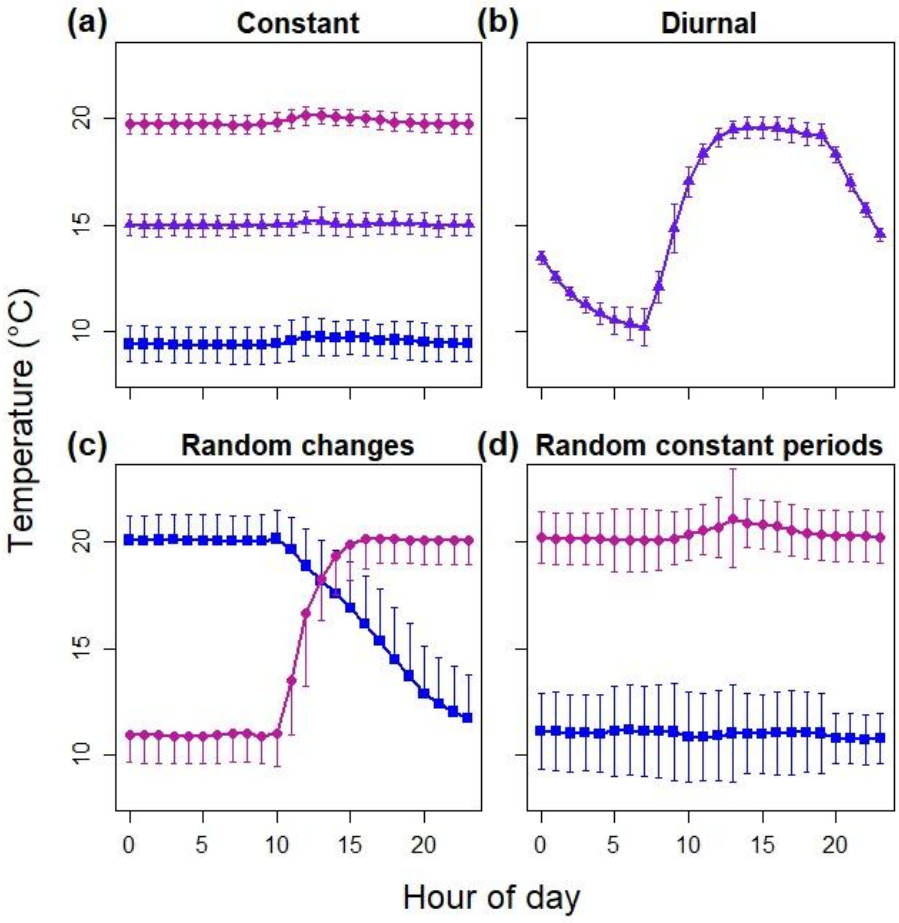

Figure 6.4: Temperature treatments from the outdoor mesocosm experiment as tracked by HOBO temperature loggers. (a) Shows Constant 10, 15, and 20 °C temperature treatments, (b) shows Diurnal fluctuations between 10 and 20 °C, (c) shows Random treatment transitions from 10 to 20 °C (or 20 to 10 °C) on days Random treatment mesocosms changed. One sided error bars were used in panel (c) for clarity to avoid confusion during hours where temperature increases and decreases overlap. (d) shows average temperature for Random treatments when temperature was held constant. Error bars shown are standard deviations.

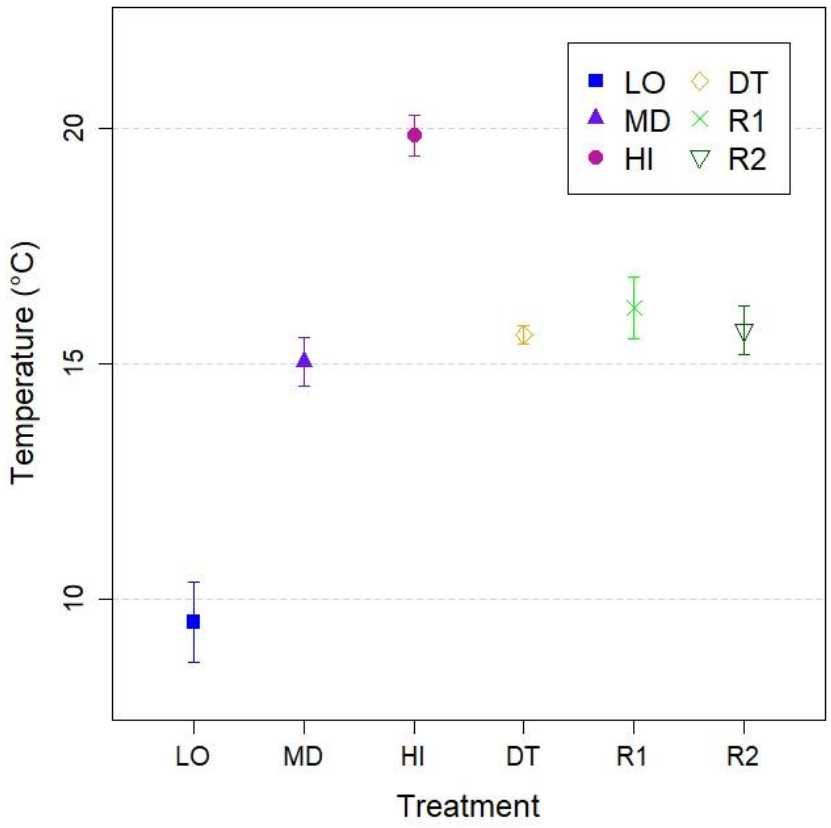

Figure 6.5: Average temperatures for the duration of the experiment for each of the six temperature treatments. Note that the variable temperature treatments were on average slightly higher than the target average temperature of 15 °C. The grey dashed lines are added at each of the lower (10 °C), middle (15 °C), and upper (20 °C) targets. Error bars indicate standard deviations.

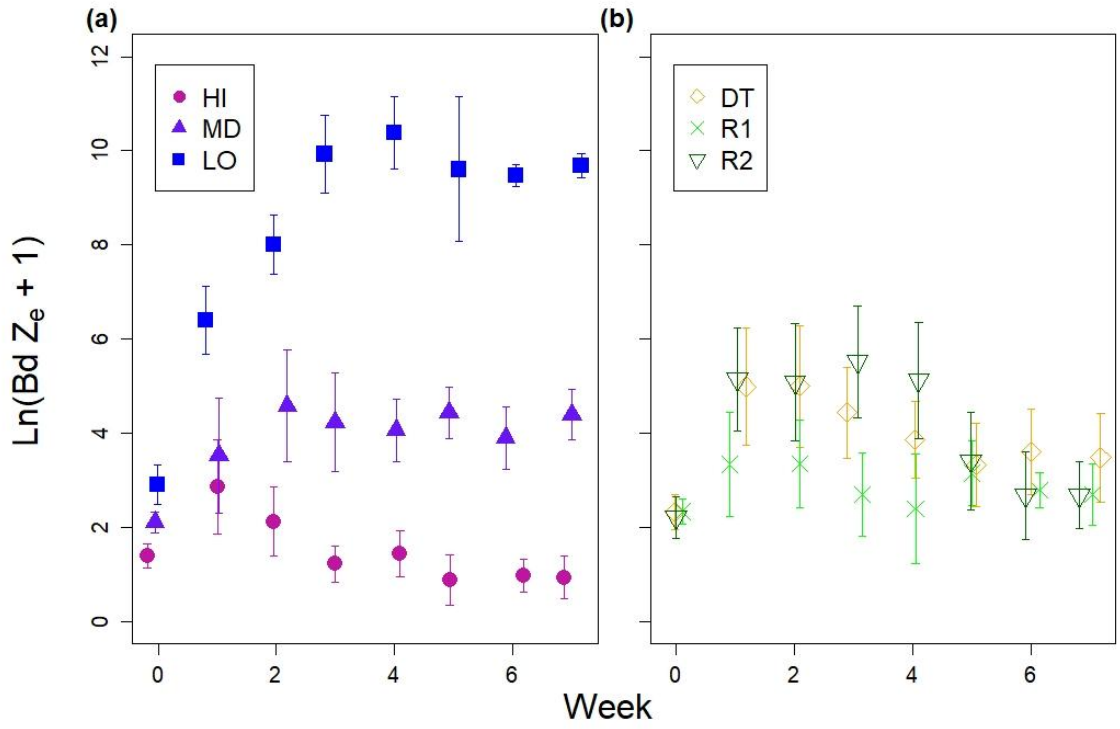

Figure 6.6: (a) Infection loads (Ln [Bd Z_e + 1]) for frog populations in mesocosms exposed to constant temperature treatments (HI: 20 °C; MD: 15 °C; LO: 10 °C) treatment for the seven-week experiment with mesocosms used as replicates. Points are jittered on the x-axis. (b) Infection loads (Ln [Bd Z_e + 1]) for frog populations in mesocosms exposed to variable temperature treatments (DT: diurnal fluctuations; R1: short period random switch; R2: long period random switch; average temperatures for each treatment are given in Fig. 6.5) treatment for the seven-week experiment with mesocosms used as replicates. Error bars show standard error. Points are jittered on the x-axis.

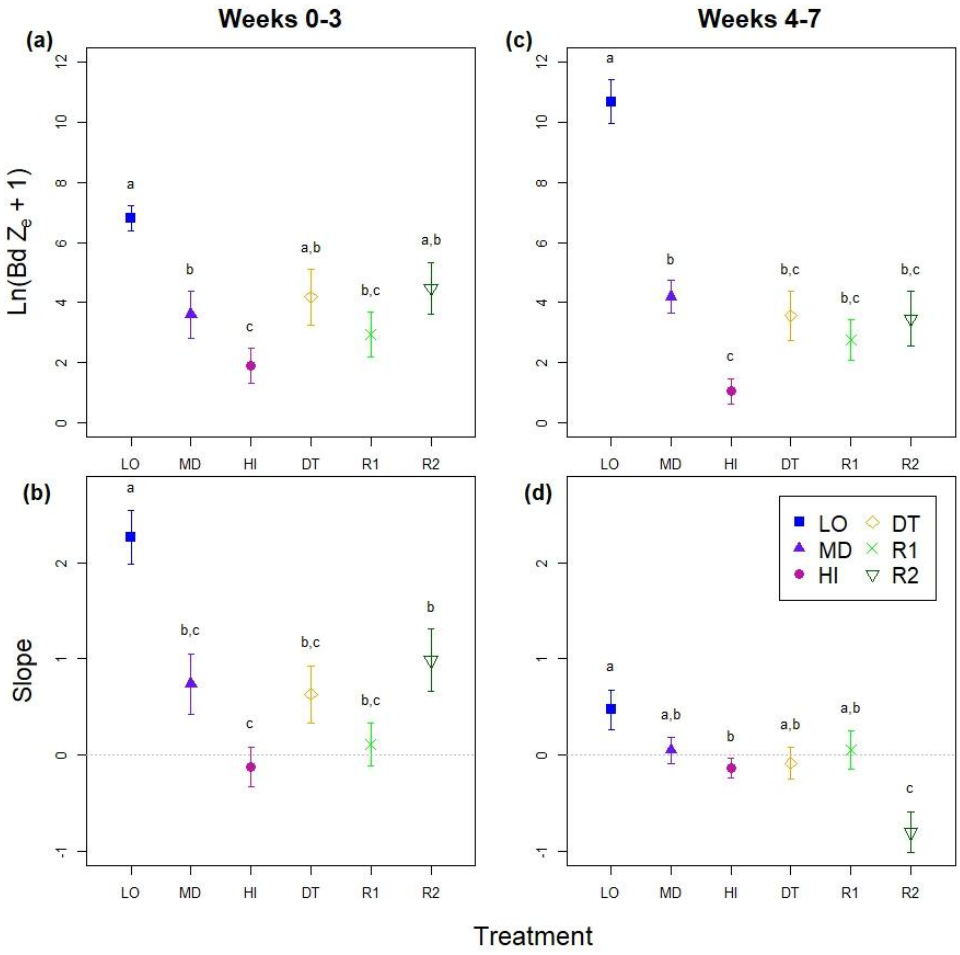

Figure 6.7: Infection loads and slope of infection directionality for two phases of the experiment: the “early” phase (weeks 0–3) and the “late” phase (weeks 4–7).

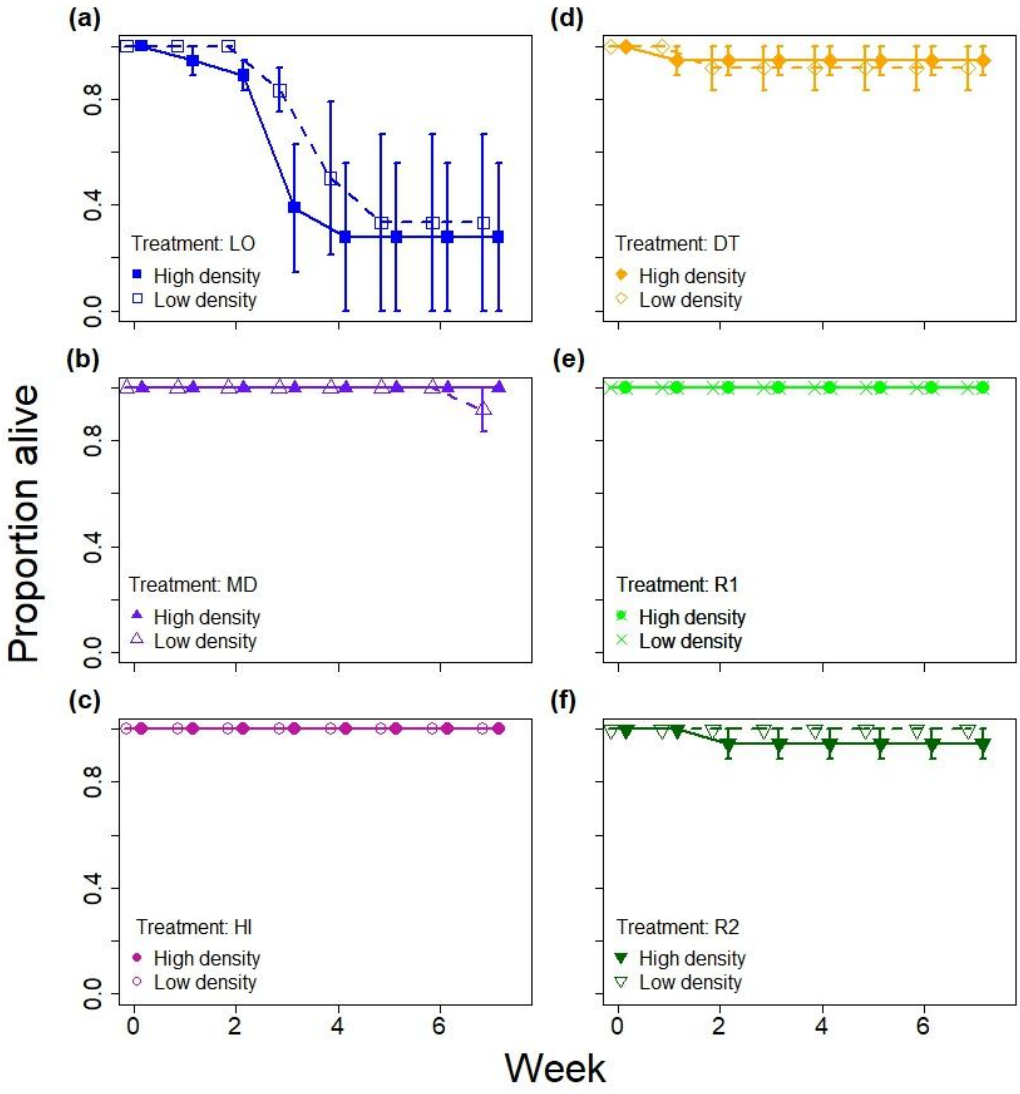

Figure 6.8: High rates of mortality were only observed in (a) the LO (10 °C) mesocosm treatment where there was a significant effect of density on the proportion of frogs alive from weeks 0 to 4. Other mesocosm treatments (b, d, and f) had low levels of mortality while (c) HI (20 °C) and (e) R1 (short random switches) had no mortality.

CHAPTER SEVEN

POSITIVE FEEDBACK LOOPS BETWEEN TRANSMISSION AND INFECTION ACCOUNT FOR HIGH INFECTION LOADS IN CO-HOUSED FROGS

7.1 Introduction

An important question among population and disease ecologists is how to best describe and predict dynamics of climate-dependent infectious diseases in host populations (Anderson & May, 1979; Kirk et al., 2022; May & Anderson, 1979; Tao et al., 2021). A popular model system for investigating temperature dependence of infectious disease is the amphibian microparasite, *Batrachochytrium dendrobatidis* (Bd). Using available field data, researchers have used statistical models to describe climatic predictors of Bd prevalence among amphibian populations (K. M. Kriger et al., 2007), and others have used species distribution models to describe and predict spatial patterns of Bd infection in response to climate variables including temperature (Zumbado-Ulate et al., 2021). However, much of our available information about temperature dependent Bd dynamics comes from experimental exposures of individual animals under laboratory conditions (Cohen et al., 2017; J. E. Noelker, Abreu Ruozzi, Spengler, et al., 2024; Raffel et al., 2013, 2015). It is unclear whether and how the dynamical patterns observed in these individual level experiments will scale up to population-level transmission dynamics (see Chapter 6). Cohen et al. (2017) noted similar qualitative patterns of temperature dependent prevalence in field prevalence data for cool vs warm adapted amphibian species, relative to observed Bd load dynamics in laboratory infection experiments (albeit with a different set of species). However, so far it has not been

possible to directly compare temperature-dependent infection dynamics for isolated individuals versus populations under similar conditions, or to validate modeling approaches that attempt to scale up from individual infections to population level transmission dynamics.

A popular framework to model population-level dynamics of microparasite infections (including for Bd in amphibians) is a susceptible-infectious-recovered (SIR)-style model based on ordinary differential equations (ODE; Anderson & May, 1979). In an SI framework, the host population is divided into categories of susceptible (S) or infectious (I) hosts, or even subcategories of groups to improve heterogeneity (Szapudi, 2020). SI models have been used to successfully predict dynamics of a wide range of infectious diseases (Hudson et al., 2009). One drawback of classic SI models is that they do not account for the distribution of parasite infection intensities within the Infected population, nor do they account for potentially important effects of parasite burden on host mortality (Anderson & May, 1979). This is a problem, because the distribution of parasite burdens among hosts can be an important driver of infection dynamics (Wilber et al., 2017, 2021). Most pathogens and parasites exhibit highly aggregated distributions, with some heavily infected individuals ("superspreaders") being more responsible for maintaining and spreading the infection than other members of the host population (Szapudi, 2020). SIR models also have limited utility to predict dynamic properties of disease systems where infection rapidly spreads throughout the entire host population resulting, resulting in limited variation in the prevalence of infection among populations (i.e., all prevalences ≈ 1). In these cases, it may be preferable to use population-level models that explicitly describe changes in infection intensities.

A variety of mathematical and computational frameworks have been developed to describe population-level infection dynamics while accounting for among-individual variation in infection burdens (here denoted as P_i parasites on a given host i), including ordinary differential equation models (ODE), diffusion models based on partial differential equation models (PDE), integral projection models (IPM), and individual based models (IBM; Foufopoulos et al., 2022; Milner & Patton, 2003). All of these frameworks have positive and negative features. Anderson and May (1979) developed ODE-based microparasite models that assume the distribution of P_i across the full Host population (including hosts with $P_i = 0$) can be approximated using a single negative binomial distribution. This approach has worked well for macroparasites whose offspring must leave and infect a new host to complete their life cycle; however, microparasites that replicate for multiple generations within a single host are likely to exhibit a high distribution of infection intensities ($P_i > 0$) relative to numbers of Susceptible individuals ($P_i = 0$). Tadiri et al. (2019) used an ODE-based model to describe changes in mean parasite burden on within the Infectious host population, but this framework deviates substantially from empirical microparasite distributions by assuming parasites are normally distributed within the Infectious host population. Indeed, microparasite distributions might be expected to be lognormally distributed as a result of exponential population dynamics in or on ectotherm hosts.

Two frameworks that allow microparasite burdens to be described as a non-normal distribution on Infectious hosts are the “diffusion model” framework of Milner and Patton (2003), which uses partial differential equations to improve realism in terms of describing parasite distribution by assuming a continuous distribution of parasites on

Infectious hosts, but does add to model computational complexity and parameter sensitivity, and Integral Projection Models (IPM), which describes dynamics in discrete-time and uses integrals to describe the distribution of parasite intensities across a population of infected hosts (Coulson, 2012; Metcalf et al., 2016; Wilber et al., 2016, 2021). IPMs in particular have been shown to be useful in describing Bd dynamics in populations of amphibians (Wilber et al., 2016, 2017, 2021). The pathogen growth function is a key component of IPM's, describing the dynamics of infection within an individual host (Wilber et al., 2016, 2021). IPMs have an advantage of allowing straightforward incorporation of external factors, such as temperature, by making the pathogen growth function into a linear function of the environmental predictor (Wilber et al., 2016, 2017, 2021). Both diffusion models and IPMs are sophisticated frameworks that have an advantage of not requiring excessive computational power to fit models to data (Metcalf et al., 2016; Milner & Patton, 2003; Wilber et al., 2021). However, these frameworks are also mathematically complex than traditional ODE-based models and require development of custom solvers, making them more difficult to work with (e.g., Milner & Patton, 2003; Tadiri et al., 2019; Wilber et al., 2021). Furthermore, IPM's developed so far have made a simplifying assumption that within-host infection dynamics are determined solely by the parasite's growth function, not allowing for the possibility that ongoing transmission from other infectious animals might influence an already-infected host's internal infection dynamics (Wilber et al., 2017, 2021).

Individual based models (IBM) provide a more flexible modeling framework, compared to more limited SI or more complex IPM models, and have already proven successful at describing Bd dynamics in a population of hosts (Briggs et al., 2005, 2010).

IBMs generate a stochastic simulation of parasite dynamics, tracking the parasite population in each individual host modeled as a separate entity (Briggs et al., 2005, 2010). IBM's can be used to simulate dynamics based on almost any error distribution for the underlying rate processes, with the resulting distribution of Bd loads arising as an emergent property of the model simulation. IBMs also have the advantage of allowing dynamics to be directly scaled up from individual host dynamics, making IBM a highly flexible framework for incorporating existing models that describe individual-level dynamics (e.g., Chapter 5). The primary drawback to IBMs is that they are computationally intensive, making it difficult to optimize parameters by fitting IBM's to data (something more easily accomplished with ODE-based and IPM models; (Breckling, 2002; Wilber et al., 2016).

For this final chapter of my dissertation, I used model simulations to determine whether the unexpectedly high Bd infection intensities I observed in small populations of 4–6 *X. laevis* (Chapter 6) could be explained by scaling up from the individual level Bd infection dynamics described in Chapters 3 & 5. I found qualitatively similar patterns of increased Bd infection at cooler temperatures at both scales, but mean Bd loads were > 10,000 times higher in the population-level experiment, resulting in unexpectedly high levels of Bd-induced mortality in the constant 10 °C treatment. I hypothesized that this difference might be caused by transmission-intensity feedbacks (TIF or "TI feedbacks"), where Bd-infectious frogs continue contributing to each other's ongoing infections by adding to an environmental pool of infectious zoospores, resulting in a positive feedback loop that builds up higher equilibrium infection intensities (Figure 7.1, 7.2). Although this hypothesis is consistent with the known biology of Bd infection, it is potentially

controversial because models of infectious disease dynamics (e.g., SI models & IPM's) routinely assume that continued transmission has no bearing on parasite dynamics within already-infected hosts (Wilber et al., 2017, 2021).

To evaluate whether TI feedbacks were sufficient to account for my observations of elevated infection intensities at the population scale, I developed a discrete time (daily time scale) IBM model of population-level transmission dynamics based on results from my individual Bd infection experiment. I focused on predicting Bd load dynamics in the three constant temperature treatments (10, 15, and 20 °C). I used a previously developed Metabolic Theory (MT) based thermal mismatch model to describe temperature dependence of Bd infection in individual *X. laevis*, describing within-host infection dynamics based on the difference between nonlinear parasite and host thermal performance curves (TPCs; Chapter 5). This MT-based mismatch model provided a good description of temperature dependent infection dynamics on individual *X. laevis*. To scale this model up to describe population-level transmission dynamics, I needed a framework that was flexible enough to: (1) track Bd load dynamics on frogs through time; (2) describe Bd load dynamics in either an isolated individual or in a population; (3) describe among-host transmission via a pool of infectious zoospores; (4) incorporate nonlinear temperature dependence of individual infection dynamics; and (5) support alternative model formulations with and without the hypothesized TI feedbacks. Bd loads were lognormally distributed in both experiments, so I also needed my modeling framework to (6) accommodate a non-normal distribution of infection intensities. I chose to use an individual-based modeling approach (IBM) to accommodate these requirements. The fact that IBM's are computationally intensive was not a serious concern in the current study,

because I was able to estimate all parameters independently of the population-level experiment based on: (1) the MT-based mismatch models described in Chapter 5, (2) rates of zoospore production from infectious hosts (Chapter 3), and (3) published data for temperature dependence of Bd-specific biological rate processes (e.g., zoospore mortality and zoosporangium development time).

7.2 Methods

7.2.1 Establishing initial (boundary) conditions for the model

Initial conditions for frogs within IBM simulations for population-level dynamics (N = 5; see below) were estimated from data collected on or before Day 0 of the mesocosm infection experiment (Chapter 6), including mean ± s.d. log Bd infection loads (ln[Bd Z_e + 1]) for individual "source" or "target" frogs (see Chapter 6). Some "target" frogs pre-existing low infection intensities that were not cleared prior to the start of the mesocosm experiment, with slightly higher Bd loads in the cooler temperature treatments (thought these differences were not significant; Chapter 6). We simulated these starting conditions by sampling initial log infection intensities (P_j) of "target" frogs from a normal distribution (function *rnorm* in R) with mean ± s.d. calculated from the initial ln[Bd Z_e + 1] on Day 0 for frogs in each temperature treatment (10 °C = 1.67 ± 2.64 Z_e, 15 °C = 0.70 ± 0.93 Z_e, 20 °C = 0.39 ± 0.78 Z_e). We also simulated infection history for "source" frogs by sampling random values from a normal distribution (function *rnorm* in R) based on the observed distribution of infection load for "source" frogs on Day 0, i.e., their time of addition to experimental mesocosms (10 °C = 8.19 ± 1.19 Z_e, 15 °C = 7.43 ± 1.69 Z_e, 20 °C = 5.44 ± 3.17 Z_e). Simulation of the Transmission function required retrospective calculations based on each individual's previous exposure history. "target"

frogs were assumed to have exposure levels of $Z[t - \text{tau}] = 0$ zoospores if time t – tau was prior to addition of the "source" frog. However, "source" frogs had been held in groups of H = 10 individuals at a housing temperature of (8 °C) prior to their addition to the experimental mesocosms (Chapter 6). We simulated their exposure histories at each time t − tau by summing 10 P_j values that were randomly sampled from a lognormal distribution based on the overall mean ± s.d. ln(Bd Ze + 1) for "source" animals on Day 0 (mean ln[Bd Ze + 1] = 7.03 ± s.d. = 2.49).

7.2.2 Modeling internal infection dynamics of individual frogs (Growth function)

I used two versions of my MT-based thermal mismatch model (Chapter 5) to describe within-host dynamics in Bd load for infected host individuals from one day to the next. The temperature dependence of parasite infectivity (i_T) and host resistance (h_T) was calculated from Eq. 5.4 (see Chapter 5) and parameterized based on results from individual controlled temperature experimental infection dynamics where i_T and h_T are derived from either the Boltzmann-Arrhenius (BA) equation (Eq. 5.6; see Chapter 5) or the modified Sharpe-Schoolfield (SS) equation (Eq. 5.8; see Chapter 5). These individual TPCs were incorporated into the MT-based thermal mismatch parasite population growth model (see Chapter 5: Eq. 5.9). To test whether results depended on the specific model formulation, I used the two thermal mismatch model combinations with the lowest AIC score from Chapter 5. In these models, the h_T TPC was based on the BA model for *X. laevis* O_2 consumption (Oxygen BA), and the i_T TPC was based on either (1) the BA model for zoospore maximum lifetime travel distance (Distance BA) or (2) the BA model for zoospore velocity (Velocity BA).

In the IBM framework, the growth function predicts the expected number of parasites on a host due to internal (within-host) parasite population growth since over the last time step (P_j'). This growth function was derived by integrating the MT-based thermal mismatch model from Chapter 5 (Ch. 5, Eq. 5.4) over the previous time step:

$$P_j'\{t\} = \frac{K_P(1-h_T/i_T)}{1-\left(1-K_P(1-h_T/i_T)/P_j\{t-1\}\right)e^{-(i_T-h_T)}}, \qquad \text{Eq. 7.1}$$

where t = time in days and T = temperature in Kelvin. Parameters K_P, i_T, and h_T were defined and parameterized as described for the Oxygen BA/Distance BA and Oxygen BA/Velocity BA models in Chapter 5.

7.2.3 Modeling transmission-derived infections (Transmission function)

We assumed transmission among frogs was mediated by an environmental pool of infectious zoospores (Z), released by the suprapopulation of reproductive zoosporangia on infectious hosts at a zoospore production rate of $\lambda \times \sum(P_j[t])$. We assumed zoospores are removed from the environmental pool by zoospore uptake as they are transmitted to hosts (βH) and by the temperature dependent process of zoospore mortality (ω_T; described in detail in Chapter 5). This results in a rate of change for Z according to the following differential equation:

$$\frac{\delta Z}{\delta t} = \lambda \sum(P_j) - \beta H Z - \omega_T Z. \qquad \text{Eq. 7.2}$$

Zoospores have limited lifespans (Woodhams et al., 2008), so we further assumed that the rate of zoospore turnover is rapid enough to ensure the zoospore pool (Z) is approximately in equilibrium with the parasite suprapopulation at any given time point (Briggs et al., 2010; May & Anderson, 1979), such that:

$$Z[t] = \frac{\lambda \sum(P_j[t])}{\omega_T + \beta H[t]}. \qquad \text{Eq. 7.3}$$

However, we recognized that formulating the Growth function based on the individual Bd infection experiment meant that self-reinfection by zoospores produced by a given individual "*j*" is already accounted for as part of the Growth function. We therefore discounted zoospores produced by individual "*j*" in calculating the zoospore pool for transmission to that individual:

$$Z[t] = \frac{\lambda \sum(P_{i \neq j}[t])}{\omega_T + \beta H[t]}. \qquad \text{Eq. 7.4}$$

An advantage of modeling transmission to frogs from an environmental zoospore pool is that we investigated this part of the infection process in Chapters 3 and 5 by exposing individual *X. laevis* to 1 million infectious zoospores and tracking initial infection dynamics at multiple temperatures. This makes it possible to use the initial (exponential) version of our MT-based thermal mismatch model (Chapter 5, Eq. 5.3) to describe the predicted effect of temperature on transmission. However, it takes time for zoospores to develop into reproductive zoosporangia (Woodhams et al., 2008). To predict the number of transmission-derived parasites added to each frog at a given time point ($P_j''\{t\}$), we modeled transmission as a retrospective (time-delayed) process starting at time = $t - \tau'_T$, where τ'_T is the simulated development time for maturation of a Bd zoosporangium at temperature *T*.

$$P_j''\{t\} = \beta \cdot Z\{t - \tau'_T\} \cdot e^{(i_T - h_T)\tau'_T}. \qquad \text{Eq. 7.5}$$

Here β represents the proportion of zoospores that successfully colonized host "*j*" at time $t - \tau'_T$, such that $\beta \cdot Z\{t - \tau'_T\}$ replaces parameter "P_0" from Equation 5.3 (Chapter 5). Like many waiting-time processes, development time is typically non-normal (Mideo et al., 2008). We therefore sampled τ'_T from a gamma distribution for

each frog at each time point. To generate gamma-distributed development times at a given temperature (τ'_T), we sampled from a gamma distribution (function *rgamma* in R) with shape = γ and scale = τ_T/γ, where τ_T is the expected development time at a given temperature based on the following MT-based TPC:

$$\tau_T = \tau_{T0} \cdot e^{\frac{E_A}{k}\left(\frac{1}{T_0}-\frac{1}{T}\right)}. \quad \text{Eq. 7.6}$$

During IBM stochastic simulations, we generated an expected Bd load for each frog at each time point by summing the growth and transmission functions, then generating random variation based on a lognormal error distribution:

$$P_j\{t\} = \left(P'_j\{t\} + P''_j\{t\}\right) \cdot e^{N\{0,\sigma^2\}}. \quad \text{Eq. 7.7}$$

To incorporate effects of parasite-induced host mortality on infection dynamics into the IBM, I removed individual hosts from the model depending on a Bd load-dependent survival probability determined by a virulence parameter (α). I assumed that survival followed an exponential distribution (see Chapter 6) and calculated survival probability of a particular host H_j until the day (t + 1) according to the following equation:

$$Survival\left[H_j\{t+1\}\right] = e^{-\alpha P_j\{t\}}. \quad \text{Eq. 7.8}$$

IBMs were coded, simulated, and visualized in R (v. 4.1.3) using the *minpack.lm*, *deSolve*, and *Hmisc* packages (Elzhov et al., 2023; Harrell & Dupont, 2022; R Core Team, 2022; Soetaert et al., 2010).

7.2.4 Estimating model parameters

We estimated all model parameters independently from the population-level transmission experiment, based on a combination of published data and the individual Bd

infection experiment described in Chapter 3. All model fitting to data was conducted using the *nls* function in base R (R Core Team, 2022). Parameters for MT-based thermal mismatch models were estimated as described in Chapter 5. Parameters estimated in Chapter 5 included those for modeling the zoospore mortality TPC (ω_T), which was based on a Sharpe-Schoolfield model fit to data collected by Woodhams et al. (2008). For IBM modeling on a daily time scale, we used the original ω_T TPC from Chapter 5 (which was parameterized on an hourly time scale) to predict the proportion of zoospores surviving at the end of a 24 hour period at temperature *T*. For each version of the IBM (derived from either of the two MT-based mismatch models), we also estimated the transmission coefficient (β, representing the proportion of available zoospores that successfully establish new infections) by dividing the estimated P_0 in the individual infection experiment by the experimental inoculum size of 10^6 zoospores (Experiment 1A; Noelker et al., 2024). We also estimated σ based on temporal variation in infections from the individual infection experiment (Experiment 1A; Noelker et al., 2024), excluding frogs that never became infected and using the addition rule for error propagation to estimate how much day-to-day variance (σ^2) in individual Bd load would have generated the observed within-individual variances in Bd load through time.

We estimated the rate of zoospore production per Bd load on frogs (λ) using zoospore production data collected by Noelker et al. (2024) in their Experiment 2 (Chapter 3). At two different times during Experiment 2, infected frogs were placed in a fixed volume of water for a specified duration. The zoospores released during this period were filtered from the water and quantified using qPCR (Chapter 3). Immediately after zoospore collection, frogs were also sampled using our standard swabbing procedure to

obtain Bd load measurements (Chapter 3). We assumed a direct relationship between the number of zoospores produced ("FilterBd") and Bd load (FilterBd ~ λ·BdLoad); however, both variables were lognormally distributed and included zeroes. We therefore used nonlinear least squares regression to estimate λ based on a ln(N + 1) transformation of each side of the equation, ln $(FilterBd + 1)$ ~ln $(\lambda \cdot BdLoad + 1)$, resulting in an estimated λ = 311.9 ± 176.0 (s.e.).

We parameterized our MT-based TPC for the temperature dependence of zoosporangium development times (τ_T; Eq. 7.5) based on eight published data points for times to first reproduction of Bd zoosporangia at 10 and 23 °C (Fig. 3B in Woodhams et al., 2008). We fit Eq. 7.5 to these data to estimate τ_{T0} and E_τ, using nonlinear least squares and comparing normal vs. lognormal error distributions as described in Ch. 5.

In baseline model formulations, I made a simplifying assumption of zero host mortality and α = 0 due to not observing any mortality in the individual level Bd infection experiment (Experiment 1A; Noelker et al., 2024). However, I observed highly significant mortality due to Bd infection in the population-level transmission experiment, along with evidence that the mortality rate was exponentially distributed and directly related to Bd load on a natural scale (Chapter 6). This allowed me to use fully parameterized survival regression to estimate a value for the virulence parameter of α = exp(−13.97) (Chapter 6).

Parameter values and their definitions are summarized in Table 7.1.

7.2.5 Baseline IBM formulations

I generated several variations of the IBM transmission model to evaluate the importance of hypothesized processes (e.g., transmission-intensity feedbacks, parasite-

induced host mortality). First I developed a "Baseline–Distance" IBM to simulate population-level infection dynamics. The Growth function for this model was based on a MT-based mismatch model with i_T described by the Distance BA TPC and h_T described by the Oxygen BA TPC; this had the lowest AIC out of the mismatch models we considered when fitting them to data from the individual-level Bd experiment (Chapter 5). The Baseline–Distance IBM assumed no parasite-induced host mortality ($\alpha = 0$), since all hosts survived in the individual level Bd experiment (Chapter 3). The Baseline–Distance IBM also allowed for the possibility of transmission intensity (TI) feedbacks, by allowing transmission to continue adding to the Bd loads of individual frogs even after they become infectious (i.e., $P_j \geq 1$). Next, I developed a second IBM formulation ("Baseline–Velocity"), which was the same as the Baseline–Distance IBM except that the Growth function was based on a MT-based mismatch model with i_T described by the Velocity BA TPC (second-lowest AIC with ΔAIC = 0.21; Chapter 5).

I ran simulations of both Baseline models with populations of N = 5 or N = 1 individuals, with initial conditions based on Day 0 data from the population-level transmission experiment (Chapter 6) or individual-level Bd experiment (Chapter 3), respectively. N = 5 was the average of N = 4 or N = 6 individuals in the population level transmission experiment (Chapter 6). I ran simulations of N = 5 frogs at 10, 15, and 20 °C with populations of N = 5 frogs and simulations of N = 1 frogs at 10, 15, 20, and 25 °C for comparison with experimental data (Chapters 3 and 6). For each IBM, I conducted 1500 simulations at each temperature and calculated mean ln(Bd Z_e + 1) at each time point to generate predictions. I also calculated the standard deviation of among-population variation in ln(Bd Z_e + 1) for each time point and temperature treatment, and

used this to estimate what the among-population standard error should have been for N = 6 populations per temperature treatment (s.e. = sd/sqrt[N]). I then superimposed model predictions over actual infection data from my population or individual level transmission experiments, to compare predictions to observed infection dynamics (Chapter 6). I also calculated likelihood statistics and model AIC for each model, based on deviations of observed data from the mean IBM prediction for each time point and mesocosm.

7.2.6 Alternative IBM formulations

For comparison with each of the baseline models, I developed two alternative model formulations. First, I developed a version of each baseline IBM representing the common assumption that transmission stops contributing to infection after an individual frog has become infectious ($P_j > 1$), which should prevent transmission-intensity feedbacks (TIF) from occurring. I will refer to these as the "NoTIF−Distance" and "NoTIF−Velocity" models. Second, I developed a version of each baseline IBM with nonzero parasite-induced host mortality, estimating α from survival regression analysis of data from the population-level transmission experiment as described in Chapter 6.

7.3 Results

7.3.1 Parameter estimates

The zoospore production from Bd filtered from individually infected frogs resulted in a rate of $\lambda = 312$ zoospores/zoospore equivalents/day (Zsp./Z_e/Day) relative to the infection load of the infected host. The transmission parameter estimated from the individual thermal mismatch model resulted in a value of $\beta = 2.2 \times 10^{-5}$ Zsp./Z_e/Day. We estimated a mean within-individual temporal variance in ln(Bd Z_e + 1) of $\sigma^2 = 0.768$. Our analysis of zoospore development time resulted estimates of $\tau_{T0} = 8.06 \pm 1.10$ and $E_\tau =$

0.36 ± 0.11 eV (± s.e.). All parameter values estimated in the present study and those taken from MT-based thermal mismatches are listed in Table 5.1.

7.3.2 Comparing baseline IBM predictions to the population-level infection experiment

Model simulations generated by the Baseline-Distance IBM, which used host O_2 consumption and zoospore travel distance as proxies and allowed TI feedbacks to occur, returned predictions for means and standard errors of frog Bd loads through time that were at similarly high levels compared to results observed in the population level infection experiment (Fig. 7.4). As in the empirical experiment, the 10 °C predictions from this IBM formulation increased quickly during the first four weeks and continued increasing throughout the 49 day timeline of the model. The 15 and 20 °C predictions were higher than the observed infection loads observed in the mesocosm infection experiment (Fig. 7.4). The AIC for this model was 621.413. I also ran simulations for this model version with N = 1.

7.3.3 Alternative IBM predictions without TI feedbacks or with mortality due to infection

When TI feedbacks were removed from the baseline model, the predicted infection loads were far lower for all three temperature treatments (Fig. 7.4). In this model formulation, the 10 °C simulation never reached infection loads greater than ln(Bd Z_e + 1) ≈ 4, far lower than the observed infection levels at 10 °C in the empirical experiment (Figure 7.4). However, model predictions for 20 °C were more consistent with the empirical data than the baseline model, nearly matching the infection data at each time point (Fig. 7.4). The AIC for this model was 3199.491.

When non-zero mortality due to infection (α) was added to the baseline model, IBM predictions were even more consistent with the empirical population-level

experiment than the baseline model (AIC = 572.811). In particular, the 10 °C model predictions were even closer to the empirical results, leveling off to a similar equilibrium level of infection in roughly the same time frame (Fig. 7.4). The IBM also aligned closely with the individual level infection data with AIC = 828.98 for model fit to this dataset (Fig. 7.4).

7.3.4 IBM predictions using an alternative Growth function (Velocity BA)

An IBM based on an alternative MT-based mismatch model for within-individual infection dynamics, based on host O_2 consumption and Bd zoospore velocity (Velocity BA), were similar to those that used the Bd maximum distance traveled parasite proxy (Distance BA, Fig. 7.5). In an IBM that allowed TI feedbacks to occur, the 10 °C predictions again reached relatively high infection loads close to those observed in the mesocosm experiment (Fig. 7.5) with an AIC = 752.493. Similar to the IBM predictions that used zoospore maximum distance traveled (Distance BA), the 15 and 20 °C predictions were somewhat higher than the infection loads observed in the mesocosm experiment (Fig. 7.5). When transmission was not allowed to continue after a frog became infected (TI feedbacks blocked), IBM predictions were again far lower than the infection loads observed for small populations of frogs (AIC = 2179.378; Fig. 7.5), and the 20 °C predictions were quite similar to the infection loads observed in the warm temperature treatment from the mesocosms (Fig. 7.5). When the non-zero mortality due to infection was added to this IBM formulation, there was not an improvement in model AIC (783.427) relative to the model with $\alpha = 0$. This IBM again reproduced the mortality levels observed in the 10 °C treatment for the population-level infection experiment and predicted a similar turnover in Bd load at later time points (Fig. 7.5). The model

predictions for a single frog were also generally quite close to the infections observed in the individual infection experiment with AIC = 742.61 (Fig. 7.5), which was a slightly better fit compared to using the zoospore maximum distance traveled proxy with a difference in AIC of 86.37.

7.4 Discussion

Some but not all formulations of the IBM model predicted the general patterns of temperature-dependent dynamics of Bd infection observed in small experimental populations of *X. laevis*. IBM's were more successful at predicting the population level infection dynamics, especially the orders of magnitude higher infection levels observed at 10 °C, if they allowed TIF's to occur by allowing transmission to boost the infection intensities of already-infectious individuals ($P_j > 1$). Baseline IBM's generated similar predictions regardless of which MT-based thermal mismatch model was used to parameterize the Growth function, though the IBM whose i_T TPC was based on the Distance BA model provided a somewhat better fit than the one based on the Velocity BA model. These better model fits achieved by IBM formulations with continued transmission suggest that TI feedbacks might indeed be the cause for these exceptionally high infection loads observed in populations of *X. laevis* at 10 °C. Both baseline model formulations also provided good descriptions of individual level Bd infection dynamics, showing that the baseline IBM's provide generalizable predictions for both individual- and population-level Bd infection dynamics.

To evaluate if TI feedbacks were necessary and sufficient to account for elevated Bd loads at 10 °C in the population-level experiment, we used a "models are hypotheses" approach by building alternative versions of mechanistic IBM's and comparing their

ability to predict the observed patterns (Glasser & Feng, 2025). We compared both baseline IBM formulations, in which transmission was allowed to continue to infectious individuals regardless of their Bd load, to similar models where transmission to infectious individuals was halted once a given individual had obtained $P_j > 1$ zoospore equivalents. These alternative IBM formulations, which prevented TI feedbacks from occurring, failed to predict the elevated Bd loads at 10 °C and had overall far worse fits to the observed data (delta-AIC > 1400). This result shows that TI feedbacks accounted for most of the observed elevation in Bd loads observed in *X. laevis* populations at 10 °C, relative to individual infections. However, these population-level models with no TI feedbacks did still predict elevated Bd loads in populations of N = 5 frogs relative to individual-level dynamics, especially in the warmer temperature treatments (15 and 20 °C). This appears to have been caused by "rescue effects", in which host individuals that lost their infections by random chance were recolonized by Bd via transmission from other hosts.

Interestingly, models that prevented TI feedbacks provided more accurate predictions for Bd infection dynamics at 20 °C than baseline models that included TI feedbacks. This result suggests that TI feedbacks are more important at cooler temps in this host-parasite system. It is possible that TI feedbacks are less important at warm temps because zoospores have shorter lifespans and thus shorter lifetime travel distances at warm temperatures (Chapter 5), which might increase the importance of within-host Bd reproduction relative to transmission-derived reproduction.

The baseline IBM's discussed so far represent what McGill (McGill, 2003) called a "strong test" of ecological theory, as it was not an exercise in curve fitting. For the baseline IBM's (with TI feedbacks) and alternative IBM's without TI feedbacks, all

parameters were estimated independently from the population-level transmission experiment, based on published data from individual-level Bd infection experiments or for Bd performance characteristics in culture. However, to incorporate host mortality due to infection into IBM simulations, we needed to make use of information from the population-level transmission study because there was no host mortality in the individual-level Bd infection experiment. When we incorporated a non-zero rate of infection-induced mortality into the model ($\alpha > 0$), we found some improvement of model fit suggesting that infection-induced mortality influenced the Bd load dynamics. However, mortality only affected infection dynamics at 10 °C, since the other temperature treatments never approached Bd infection intensities high enough to cause significant mortality (Chapter 6). This highlights the fact that equilibrium dynamics within the proposed IBM framework are determined by multiple density-dependent factors, and which factors are more important in determining equilibrium dynamics depends on temperature and host density. For example, the equilibrium Bd load for individual-level dynamics is determined by the interplay of K_P, i_T, and h_T ($P_T^* = K_P[1 - h_T/i_T]$; Chapter 5), but this equilibrium setpoint is elevated by rescue effects and TI feedbacks when $H > 1$ (Figure 7.4, 7.5) and becomes limited by infection-induced mortality when Bd loads get to high levels (10 °C treatment; Figure 7.4, 7.5; see Chapter 6).

Our conclusion that TI feedbacks likely drove elevated infection intensities in the population-level transmission experiment is potentially controversial, because most existing models of microparasite transmission dynamics implicitly assume that infection intensity dynamics within individual hosts is unaffected by continued transmission from other hosts. SI models typically account for density dependence in transmission dynamics

(e.g., Anderson & May, 1979), but they largely ignore among-host variation in infection intensities and assume host density has no effect on processes that might depend on infection intensity (e.g., individual infectiousness or parasite-induced host mortality; Anderson & May, 1979). While several population-level models of Bd transmission have been developed to account for among-individual variation in Bd infection intensities, those studies made a simplifying assumption that continued transmission had no effect on internal Bd load dynamics of already-infectious hosts (Briggs et al., 2010; Wilber et al., 2016, 2021). However, we think it is debatable whether blocking continued transmission to infectious hosts should be considered a parsimonious assumption for Bd infection in frog populations. In this system, within-host reproduction occurs when Bd spreads across host skin via flagellar or amoeboid movement of zoospores, i.e., essentially the same process by which Bd transmits among hosts (Berger et al., 2005; Longcore et al., 1999; Van Rooij et al., 2012). Allowing transmission to continue between frogs that are already infectious is thus biologically reasonable, because there is no clear biological mechanism that should stop zoospores from transmitting to already-infectious individuals. Empirical experiments with individual frogs have shown that frogs with low Bd infection can have their infections boosted from additional Bd inoculation (Neely et al., 2020). In the current study, internal infection dynamics of individual hosts was explicitly nested within our IBM describing among-host transmission ("essential nesting"; Mideo et al., 2008). This resulted in baseline IBM's that naturally allowed transmission-derived Bd to boost infection intensities in already-infectious hosts, which is arguably simpler than models that blocked further infections when $P_j > 1$.

Our proposed IBM framework had limitations and simplifying assumptions that likely limit its ability to make general predictions for Bd dynamics in populations of *X. laevis*. For example, none of the IBM's presented here accounted for variation in water volume, despite there being substantial differences in water volume between the individual- and population level Bd infection experiments (Chapter 3; Chapter 6). One might expect Bd transmission rates to decrease at larger water volumes, due to zoospores needing to travel longer distances to search for new hosts (Briggs et al., 2010). It is thus noteworthy that the baseline IBM formulations accurately predicted Bd infection loads in the population-level transmission experiment, despite being formulated based on experiments conducted with much smaller water volumes. One possible explanation is that zoospores seem to be capable of traveling long distances relative to even the container size in population-level transmission experiment (Chapter 5, Chapter 6), especially at cooler temperatures, such that their ability to find other hosts might not be limited by volume at these spatial scales. Another limitation is the artificial nature of containers used in these experiments, which might limit the applicability of these results to more natural settings.

An important unanswered question that deserves future investigation is whether and to what extent TI feedbacks affect equilibrium parasite intensities other host-parasite systems, including Bd infections in other host species and in more natural environments. The potential for continued transmission to boost the infection intensities of already-infectious hosts, resulting in TI feedbacks when multiple host individuals are present, is uncontroversial for macroparasites (DeVore et al., 2020; May & Anderson, 1979) but typically ignored for microparasites. A key difference between macro- and micro-

parasites is that macroparasites are often assumed to require transmission to another host to complete their life cycles, making continued among-host transmission the only source of increased infection intensities in already-infectious hosts (Anderson & May, 1979; Hudson et al., 2009). In contrast, microparasites are defined in modeling studies by the importance of within-host replication (Foufopoulos et al., 2022; Hudson et al., 2009). If within-host replication rates are high relative to parasite reproduction via among-host transmission, such as for pathogens that infect internal organs (e.g., rabies or *Naegleria fowleri*), it might be reasonable to ignore the potential for TI feedbacks when modeling transmission dynamics (e.g., Anderson et al., 1981). However, TI feedbacks could play an important role in driving infection intensities of microparasites for which parasite reproduction via among-host transmission is important relative to reproduction via within-host replication. This might be especially true for parasites like Bd that infect the external body surface of their host, that use similar mechanisms to accomplish both within-host replication and among-host transmission, that transmit readily via water-borne (or aerosol) transmission, or that have motile infectious stages capable of seeking out new hosts (Berger et al., 2005; Longcore et al., 1999). Based on this reasoning, TI feedbacks might help to explain other cases where there is evidence of higher host densities driving higher mean infection intensities, such as high Bd infection intensities in frog populations concentrated into small pools within drying streams (Kupferberg et al., 2022) and *Ichthyophthirius multifiliis* infections in fish (Francis-Floyd et al., 2016). Other parasites that share some of all of these characteristics include other fungal pathogens of plants and animals such as *Batrachochytrium salamandrivorans* (Malagon et al., 2020), American chestnut blight (Van Drunen et al., 2018), sea grass wasting disease (Eisenlord

et al., 2024), white nose syndrome in bats (Hoyt et al., 2021; Isidoro-Ayza et al., 2024), snake fungal disease (Lorch et al., 2016; McCoy et al., 2017), and fungal diseases of coral (Shore & Caldwell, 2019). Our understanding of these important wildlife diseases might benefit from considering TI feedbacks when modeling population-level infection dynamics.

7.5 Conclusion

The IBM presented here successfully predicted elevated infection intensities observed in a population level infection experiment, consistent with the presence of TI feedbacks in this disease system and contrary to assumptions made by common approaches to model microparasite disease dynamics. The potential for TI feedbacks has been largely ignored in epidemiological models of both human and wildlife diseases, including waterborne and aerosol-transmitted pathogens for which among-host transmission might occur at high enough rates to affect internal infection dynamics of already-infectious hosts. It is possible that the potential for TI feedbacks have been overlooked even in well studied disease systems, due to a historical focus on SI frameworks that ignore variation in infection intensities. If this is the case, then IBM's with essential nesting, like the ones described in this study, could provide better predictions of population level disease dynamics and be of potential use for conservation biologists and public health officials seeking stronger modeling tools for understanding population level dynamics driven by individual animal infection loads. If any human pathogens exhibit non-trivial TI feedbacks that result in elevated infection intensities for co-housed individuals, this finding could induce changes in common medical practices (e.g., housing infectious individuals together in the same room).

CHAPTER SEVEN TABLES

Table 7.1: Parameters, values, and definitions used in the IBM model. Parameter values for the individual thermal mismatch model were quantified in Chapter 5. Parameter values for the population level IBM model were quantified in the present chapter using data from individual infection experiments described in previous chapter or from published data.

Scale	***Parameter***	***Estimate***	***Definition***
Individual-level model (MTE-based mismatch; Chapter 5)	$P_j\{t\}$	variable	Bd load on frog "*j*" at time *t*
	P_0	23.1	Bd load on frog "*j*" at $t = 0$
	K_P	7.3×10^5	Bd carrying capacity on frog "*j*"
	T_0	10 °C	Standardization temperature (283.15 K)
	k	8.6×10^{-5}	Boltzmann's constant (eV/K)
Population-level model (IBM)	$H\{t\}$	Variable	Number of live hosts at time *t*
	Pj'		Predicted Bd load based on within host Growth function
	Pj''		Increased Bd load due to transmission-derived infections
	α	$e^{(-13.97)}$	Bd load-dependent host mortality rate
	λ	312	Zoospore production rate (relative to Bd load)
	β	2.2×10^{-5}	Transmission rate constant
	σ^2	0.768^2	Variance in $\ln(P_j)$ on a daily time scale
	γ	2	Gamma shape parameter for sporulation time

CHAPTER SEVEN FIGURES

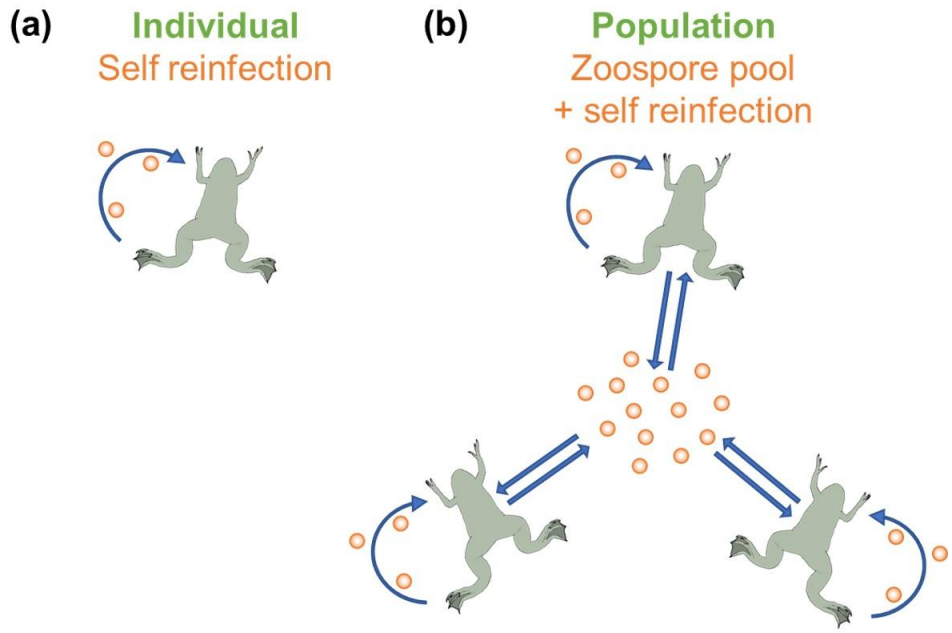

Figure 7.1: Communal zoospore pool from multiple hosts could drive up the equilibrium infection levels on individual hosts, assuming ongoing transmission boosts intensities of already-infected hosts.

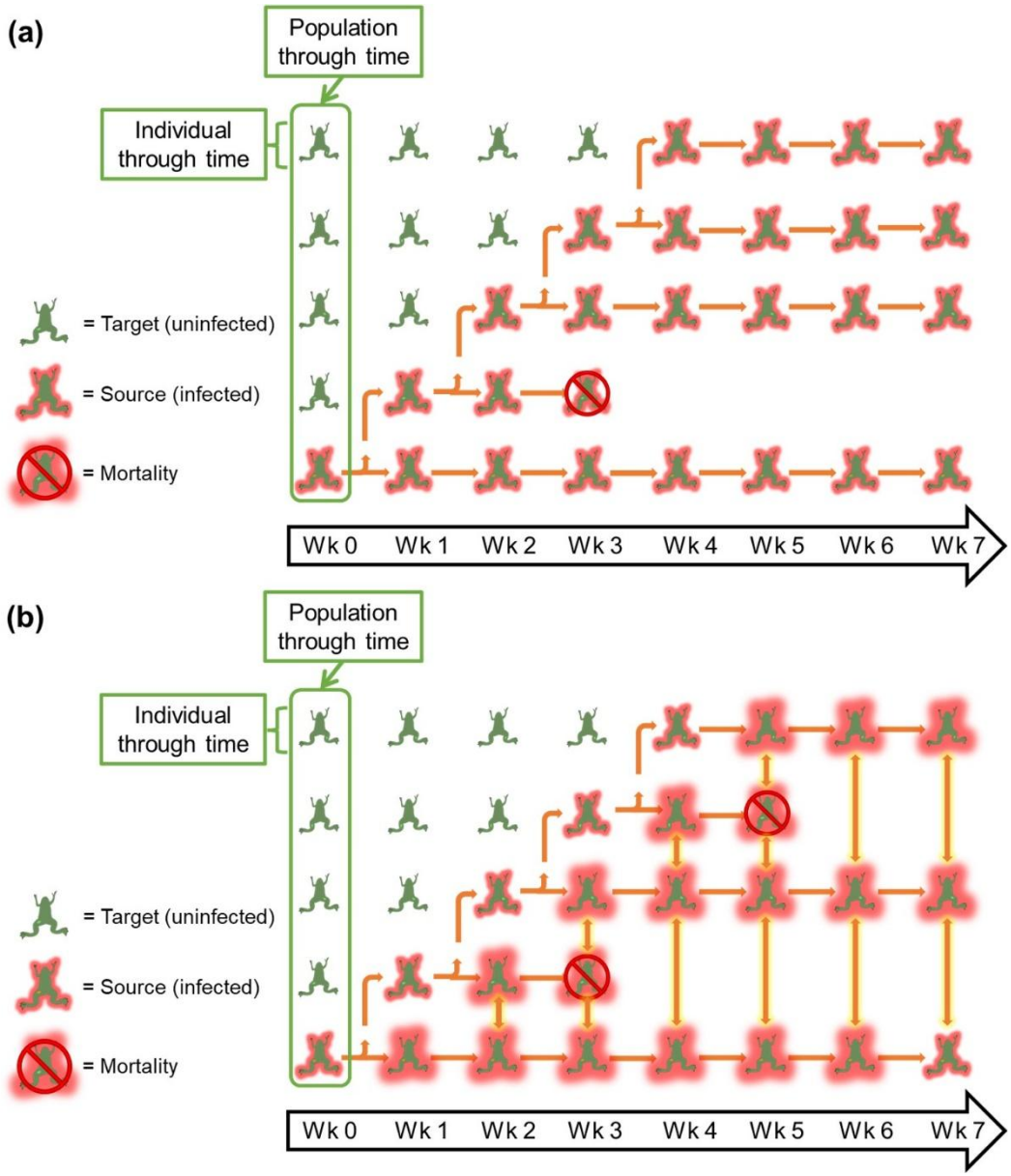

Figure 7.2: Illustrations of Bd transmitting through populations of frogs where (a) transmission to an individual stops after the frog becomes infected compared to (b) a population of hosts where frogs continue to transmit to one another even after becoming infected resulting in transmission intensity feedbacks (orange arrows with yellow highlights) resulting in higher infection loads and higher rates of mortality.

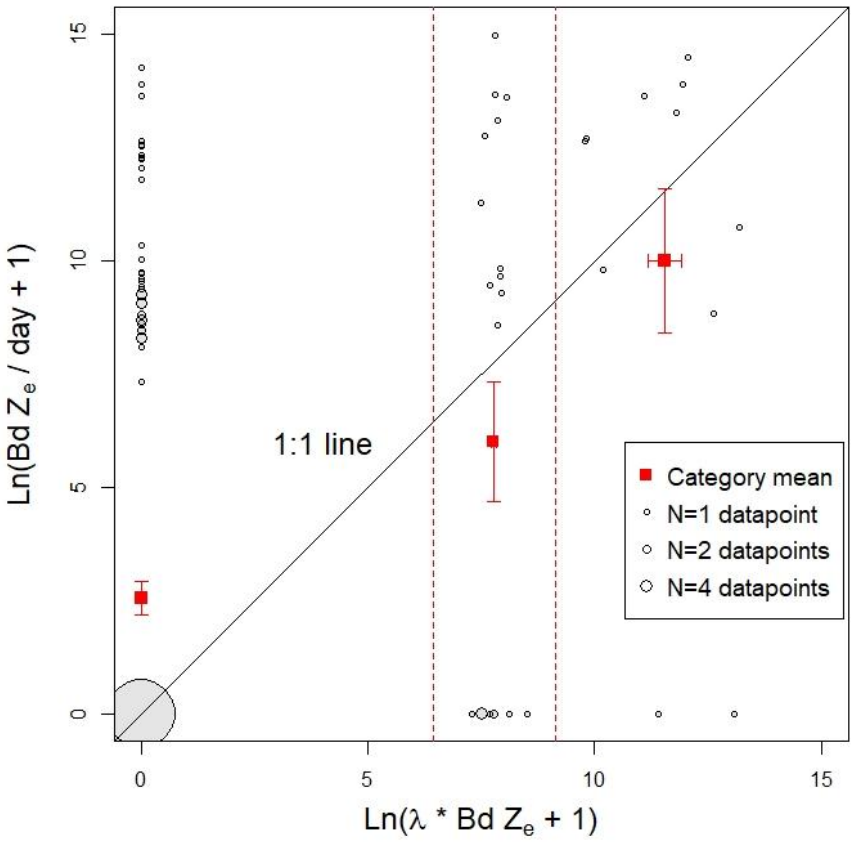

Figure 7.3: Shows the visual for the λ model estimate taken from the rate of zoospore shedding from *X. laevis* individual infection experiments (Chapter 3).

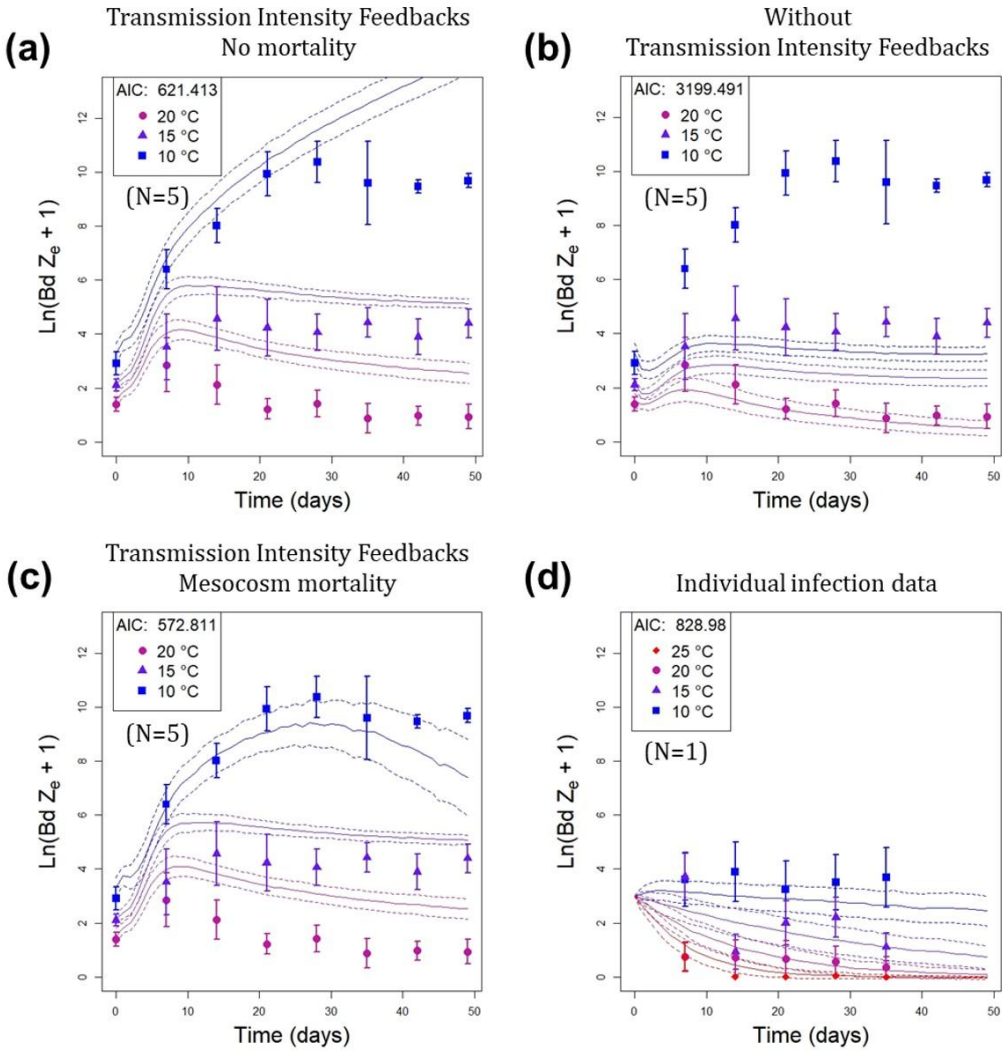

Figure 7.4: IBM model based on the nested thermal mismatch model that uses Bd zoospore maximum distance traveled and host O_2 consumption outputs overlayed onto constant temperature treatment mesocosm data. (a) Transmission intensity feedbacks allow continued transmission between infected frogs. (b) The same IBM where transmission stops after infection. (c) The IBM with a single α parameter estimated from the mesocosm experiment. (d) The IBM with n = 1 overlayed on individual infection data. Simulations = 1500.

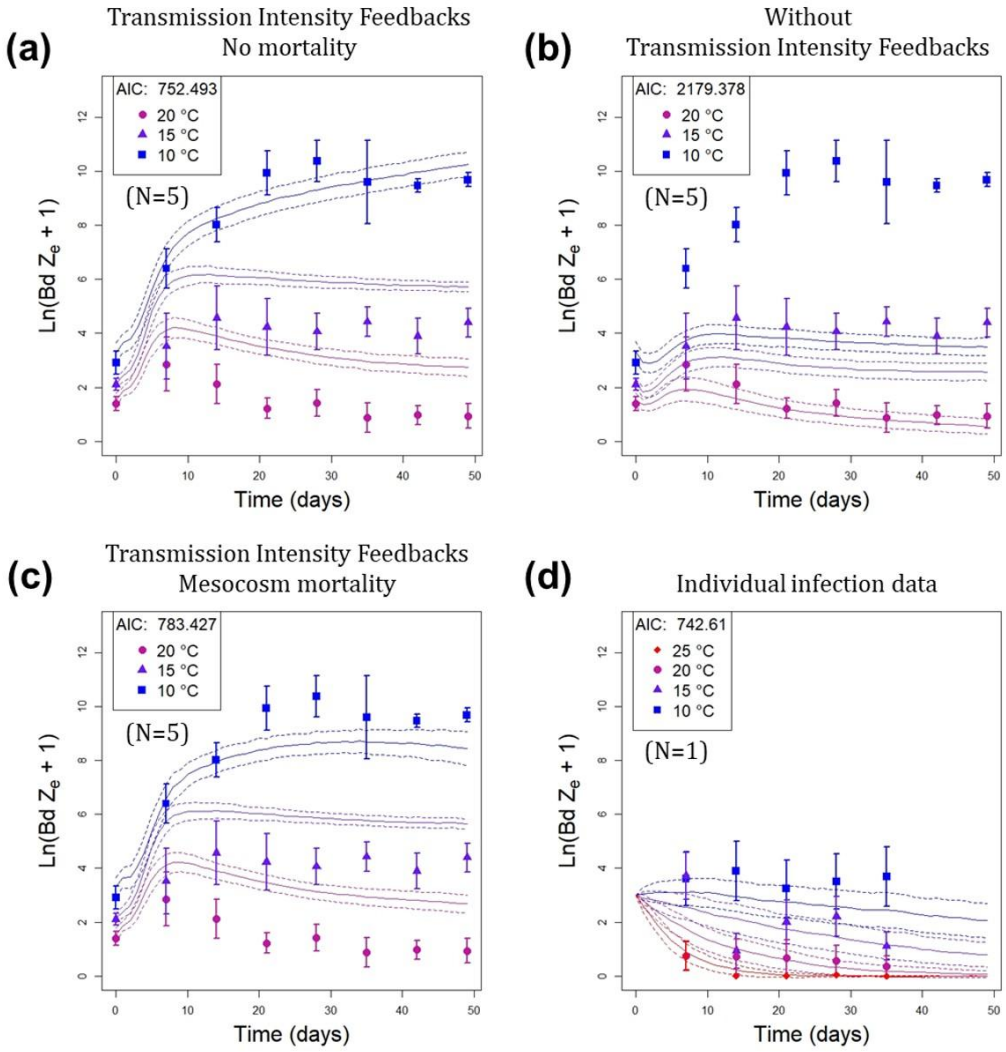

Figure 7.5: IBM model based on the nested thermal mismatch model that uses Bd zoospore maximum velocity (BA) and host O_2 consumption outputs overlayed onto constant temperature treatment mesocosm data. (a) Transmission intensity feedbacks allow continued transmission between infected frogs. (b) The same IBM where transmission stops after infection. (c) The IBM with a single α parameter estimated from the mesocosm experiment. (d) The IBM with n = 1 overlayed on individual infection data. Simulations = 1500.

APPENDIX A

IACUC APPROVAL DOCUMENTS

Oakland University
Institutional Animal Care and Use Committee
Committee Action Record

January 16, 2018	4405
Committee Review Date	**RAM Number**

PROJECT TITLE

A Metabolic Theory Approach to the Thermal Biology of Parasitism

Approved [X] Disapproved [ ]

NEW PROJECT

[X] 18011 — **IACUC Project Approval Number**

Thomas Raffel, Ph.D. — **Principal Investigator**

REVISED PROJECT

Your Request for Revision of your Application for Use of Vertebrate Animals has been reviewed by IACUC and given full approval.

[ ] _____ — **New IACUC Project Approval Number***

_____ — **Principal Investigator**

*** Please use this new approval number, with the revision number indicated, in all future activities.**

Authorization for Project Commencement

Keith Williams — **IACUC Chairperson: Keith Williams, PhD**

1/20/2018 — **Date**

Approval Period: **February 1, 2018 through January 31, 2021**

Annual Review Dates: **February 1, 2019 and February 1, 2020**

Project Completion Summary Due Date: **January 31, 2021**

Memorandum

To: Rebecca Sandborg, Ph.D., Director of Regulatory Support

From: Amy Banes-Berceli, Ph.D.,

RE: Tom Raffel's NSF and IACUC Congruency Review

Date: January 19, 2018

After reviewing Dr. Tom Raffel's new IACUC protocol 18011 I find that he has addressed all the previous issues noted and has brought his grant and the IACUC protocol into congruency.

Oakland University
Institutional Animal Care and Use Committee
Committee Action Record

January 20, 2021	4582
Committee Review Date	RAM Number

PROJECT TITLE

A Metabolic Theory Approach to the Thermal Biology of Parasitism

Approved [X] Disapproved [ ]

NEW PROJECT

[ ] _____ _____

IACUC Project Approval Number — Principal Investigator

REVISED PROJECT

Your Request for Revision of your Application for Use of Vertebrate Animals has been reviewed by IACUC and given full approval.

[X] **21011-R1** — Thomas Raffel, Ph.D.

New IACUC Project Approval Number* — Principal Investigator

*** Please use this new approval number, with the revision number indicated, in all future activities.**

Authorization for Project Commencement

Keith Williams — 4/20/2021

IACUC Chairperson: Keith Williams, PhD — **Date**

Approval Period:	**February 1, 2021 through January 31, 2024**
Annual Review Dates:	**February 1, 2022 and February 1, 2023**
Project Completion Summary Due Date:	**January 31, 2024**

Oakland University
Institutional Animal Care and Use Committee
Committee Action Record

May 20, 2021	4607
Committee Review Date	**RAM Number**

PROJECT TITLE

A Metabolic Theory Approach to the Thermal Biology of Parasitism

Approved [X] Disapproved [ ]

NEW PROJECT

[ ] | | |
|---|---|
| **IACUC Project Approval Number** | **Principal Investigator** |

REVISED PROJECT

Your Request for Revision of your Application for Use of Vertebrate Animals has been reviewed by IACUC and given full approval.

[X]	**21011-R2**	**Thomas Raffel, Ph.D.**
New IACUC Project Approval Number*	**Principal Investigator**

*** Please use this new approval number, with the revision number indicated, in all future activities.**

Authorization for Project Commencement

Keith L Williams	5/24/2021
IACUC Chairperson: Keith Williams, PhD	**Date**

Approval Period:	**February 1, 2021 through January 31, 2024**
Annual Review Dates:	**February 1, 2022 and February 1, 2023**
Project Completion Summary Due Date:	**January 31, 2024**

OAKLAND UNIVERSITY
Powered by Google

Thomas Raffel <raffel@oakland.edu>

Fwd: Committee Action Record – New or De Novo IACUC Protocol # 2022-1193 Approval

1 message

Janet Schofding <schofdin@oakland.edu> Wed, Sep 20, 2023 at 12:36 PM
To: Thomas Raffel <raffel@oakland.edu>

Janet R. Schofding, BS, LVT, RLATg
BRSF Manager / IACUC Administrator
Oakland University **<:3)))~~~**
104 BRSF
126 Library Drive
Rochester, MI 48309-4479
248-370-4440
schofdin@oakland.edu

---------- Forwarded message ---------
From: **eSirius3GWebServer** <no-reply@esirius.cayuse.com>
Date: Fri, Jun 2, 2023 at 3:58 PM
Subject: Committee Action Record – New or De Novo IACUC Protocol # 2022-1193 Approval
To: <raffel@oakland.edu>

cayuse Animal Oversight

Reference: IACUC Protocol # 2022-1193

Protocol Title: Amphibian comparative thermal biology

Principal Investigator: Raffel, Thomas

Approval Period: 06/02/2023 - 06/02/2026

Dear Professor Raffel, Thomas:

The Institutional Animal Care and Use Committee (IACUC) has reviewed the original proposal, noted the required modifications provided by you upon committee's request (if applicable), and approved the project referenced above.

The proposed activities are approved for a period of three years, starting 06/02/2023 and ending 06/02/2026, and assigned the approval # IACUC-2022-1193. This is your formal approval notice; please save it for your records. Be aware that protocols expire at 12:01 AM on the expiration date. Ninety (90) days before the protocol approval expires, Cayuse will send you an alert email prompting you to submit a De Novo application to renew the project, if desired.

Any unanticipated problems, changes in, or halting of the activities proposed in the project, as described, must be promptly reported to the IACUC Administrator.

In addition, all faculty, staff, and students involved in the project must be trained and qualified to conduct the project in a responsible manner. Please note, in this regard, that you, the Principal Investigator, are fully responsible at all times.

Please let me know if you have any questions.

Sincerely,

Janet Schofding
Animal Research Facility Manager and IACUC Administrator

(email ID #400004)

*** THIS IS AN EMAIL NOTIFICATION ONLY. PLEASE DO NOT REPLY ***

APPENDIX B

IBC APPROVAL DOCUMENT

OAKLAND UNIVERSITY

Institutional Biosafety Committee

March 13, 2018

Professor Thomas Raffel
Assistant Professor
Department of Biological Sciences

Reference: IBC Application # 2759, "A Metabolic Theory Approach to the Thermal Biology of Parasitism"

Dear Professor Raffel:

The Institutional Biosafety Committee (IBC), responsible for the review of research involving materials of human origin, recombinant DNA, and biohazardous, infectious or toxic materials, has reviewed the original proposal, noted the revisions provided by you upon committee's request, and approved the revised project referenced above.

The proposed activities were approved at BSL-2 for a period of five years starting, March 13, 2018 and ending, March 12, 2023. It has been assigned the approval number 2759-13.

Any unanticipated problems, changes in, or halting of the activities proposed in the project, as described, must be promptly reported to the IBC or the biosafety officer.

In addition, all faculty, staff and students involved in the project must be trained and qualified to conduct the project in a responsible manner. Please note, in this regard, that you, the principal investigator, are fully responsible at all times for limiting or restricting access to laboratories and for assessing, in each circumstances, who may enter or work in a laboratory when biohazardous materials are in use.

Please let me know if you have any questions. Thank you.

Sincerely,

Domenic Luongo, CHMM
Laboratory Compliance Manager

Office of Research Administration

371 Wilson Blvd, Rochester, MI 48309-4486
(248) 370-4898 | Fax: (248) 370-2973 | oakland.edu

OAKLAND UNIVERSITY

Institutional Biosafety Committee

May 19, 2021

Professor Thomas Raffel
Assistant Professor
Department of Biological Sciences

Reference: Addendum to IBC Application # 2759-13, "A Metabolic Theory Approach to the Thermal Biology of Parasitism"

Dear Professor Raffel:

The Institutional Biosafety Committee (IBC), responsible for the review of research involving materials of human origin, recombinant DNA, and biohazardous, infectious or toxic materials, has reviewed the original proposal, noted the revisions provided by you upon committee's request, and approved the revised project referenced above.

The proposed addendum to include a new procedure for treating chytridiomycosis-infected frogs with the drug itraconazole has been approved. The BSL-2 biosafety level and approval period of March 13, 2018 through March 12, 2023 has not changed.

Any unanticipated problems, changes in, or halting of the activities proposed in the project, as described, must be promptly reported to the IBC or the biosafety officer.

In addition, all faculty, staff and students involved in the project must be trained and qualified to conduct the project in a responsible manner. Please note, in this regard, that you, the principal investigator, are fully responsible at all times for limiting or restricting access to laboratories and for assessing, in each circumstance, who may enter or work in a laboratory when biohazardous materials are in use.

Please let me know if you have any questions. Thank you.

Sincerely,

Domenic Luongo, CHMM
Laboratory Compliance Manager

Office of Research Administration

371 Wilson Blvd, Rochester, MI 48309-4486
(248) 370-4898 | Fax: (248) 370-2973 | oakland.edu

APPENDIX C

SUPPLEMENTAL MATERIAL FOR CHAPTER THREE

APPENDIX C TABLES

Table C.1: Interactive effects of acclimation temperature and performance temperature treatments on log Bd load (SwabBd) at each time point following exposure, for frogs exposed on the day of the temperature switch (Day 0). Variable abbreviations are defined in Table 3.1. Statistical tests were based on Kenward-Rogers degrees of freedom (*df*), which may be non-integers in mixed effects models.

Experiment	*Days since exposure*	*Predictor*	*F value*	*df*	*P*
1A	7	**AccTemp**	**10.1**	**1, 17.3**	**0.005**
		PerfTemp	**26.6**	**1, 24.1**	**< 0.001**
		AccTemp × PerfTemp	**4.6**	**1, 24.1**	**0.043**
	14	**AccTemp**	**5.7**	**1, 16.8**	**0.029**
		PerfTemp	**17.8**	**1, 29.4**	**< 0.001**
		AccTemp × PerfTemp	**11.5**	**1, 29.4**	**0.002**
	21	AccTemp	< 0.1	1, 17.1	0.922
		PerfTemp	**10.9**	**1, 29.7**	**0.003**
		AccTemp × PerfTemp	2.9	1, 29.7	0.097
	28	AccTemp	3.3	1, 17.1	0.085
		PerfTemp	**19.1**	**1, 29.7**	**< 0.001**
		AccTemp × PerfTemp	**10.2**	**1, 29.7**	**0.003**
	35	AccTemp	1.5	1, 17.1	0.236
		PerfTemp	**17.2**	**1, 29.6**	**< 0.001**
		AccTemp × PerfTemp	**4.6**	**1, 29.6**	**0.040**
2	7	AccTemp	4.2	1, 18.4	0.055
		PerfTemp	**15.2**	**1, 22.8**	**< 0.001**
		AccTemp × PerfTemp	**12.0**	**1, 51.5**	**0.001**
	14	AccTemp	2.7	1, 18.8	0.116
		PerfTemp	**9.2**	**1, 21.1**	**0.006**
		AccTemp × PerfTemp	**10.4**	**1, 51.6**	**0.002**
	21	**AccTemp**	**4.9**	**1, 19.4**	**0.039**
		PerfTemp	3.6	1, 22.0	0.069
		AccTemp × PerfTemp	**12.1**	**1, 53.4**	**0.001**
	28	AccTemp	3.1	1, 19.4	0.094
		PerfTemp	3.8	1, 20.9	0.064
		AccTemp × PerfTemp	**8.8**	**1, 53.0**	**0.004**
	35	AccTemp	1.8	1, 20.3	0.194
		PerfTemp	1.9	1, 19.7	0.188
		AccTemp × PerfTemp	3.9	1, 58.8	0.054

Table C.2: Interactive effects of acclimation temperature and performance temperature treatments on log Bd load (SwabBd) in Experiment 1B, for the first two time points following exposure (7 days and 14 days), for each exposure time treatment (−7, 0, or +7). Variable abbreviations are defined in Table 3.1. Statistical tests were based on Kenward-Rogers degrees of freedom (*df*), which may be non-integers in mixed effects models.

Day of exposure	***Days since exposure***	***Predictor***	***F value***	***Df***	***P***
−7	7	**AccTemp***	**60.9**	**1, 18**	**< 0.001**
	14	AccTemp	2.2	1, 16	0.156
		PerfTemp	2.7	1, 16	0.122
		AccTemp × PerfTemp	1.2	1, 16	0.288
0	7	**AccTemp**	**9.7**	**1, 10.5**	**0.010**
		PerfTemp	**10.3**	**1, 10.2**	**0.009**
		AccTemp × PerfTemp	3.5	1, 10.5	0.089
	14	**AccTemp**	**5.8**	**1, 10.5**	**0.036**
		PerfTemp	**11.3**	**1, 10.2**	**0.007**
		AccTemp × PerfTemp	**12.8**	**1, 10.5**	**0.005**
7	7	AccTemp	< 0.1	1, 16	0.889
		PerfTemp	2.3	1, 16	0.152
		AccTemp × PerfTemp	0.2	1, 16	0.666
	14	AccTemp	< 0.1	1, 16	0.840
		PerfTemp	**16.8**	**1, 16**	**0.001**
		AccTemp × PerfTemp	< 0.1	1, 16	0.840

*PerfTemp was not included in this model because frogs had not yet experienced this treatment

Table C.3: Outputs from binomial versions of the mixed effects models presented in Table 3.2, using Bd infection status (+/−) as the response variable instead of LnSwabBd. Each model included interactive effects of performance temperature (PerfTemp), acclimation temperature (AccTemp), and time since exposure (TimeSinceExposure), only for frogs exposed to Bd immediately after the temperature shift ("Day 0" exposure day). Random effects structures were the same as for the primary models presented in Table 3.2. All degrees of freedom are 1. Variable abbreviations are defined in Table 3.1.

Experiment	***Response***	***Predictor***	X^2	***P***
1A	Bd status	Acclimation temperature	2.38	0.123
		Performance temperature	**14.62**	**< 0.001**
		Time since exposure	1.29	0.255
		AccTemp × PerfTemp	**4.07**	**0.044**
		AccTemp × TimeSinceExposure	**5.91**	**0.015**
		PerfTemp × TimeSinceExposure	2.68	0.102
		AccTemp × PerfTemp × TimeSinceExposure	0.24	0.625
2	Bd status	Acclimation temperature	0.76	0.382
		Performance temperature	**6.63**	**0.010**
		Time since exposure	**17.38**	**< 0.001**
		AccTemp × PerfTemp	**10.77**	**0.001**
		AccTemp ×TimeSinceExpo	2.17	0.141
		PerfTemp × TimeSinceExposure	**7.87**	**0.005**
		AccTemp × PerfTemp × TimeSinceExposure	0.13	0.722

APPENDIX C FIGURES

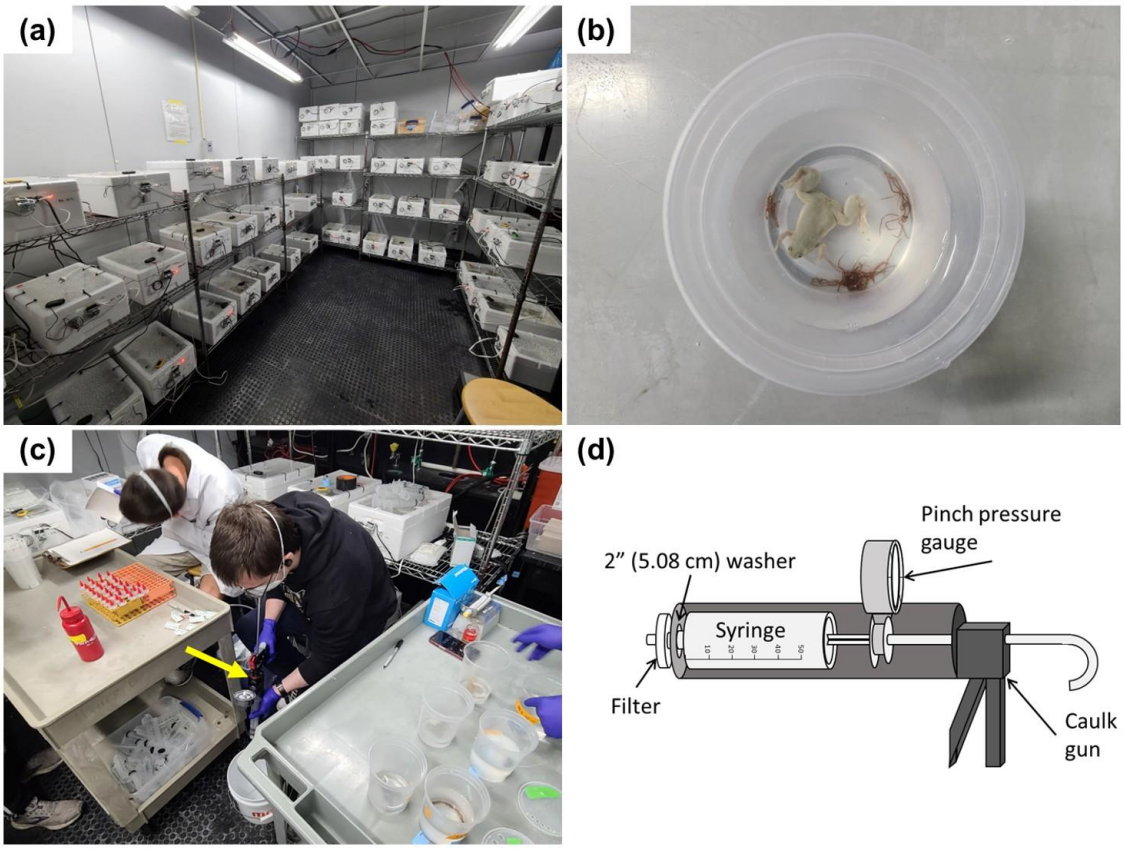

Figure C.1: Pictures of our experimental procedures from Experiments 1 and 2. (a) the cold room setup where we conducted the individual infection experiments to investigate the acclimation effects and performance effects of temperature on individual frog infections. (b) frogs were housed in 1 liter deli cups and fed blackworms during the acclimation and performance periods. (c) photograph of researchers conducting the swabbing procedure (left) and the filtering (right) using our filtering device (yellow arrow). (d) schematic of the filtering device we designed using a modified caulk gun and pinch pressure gauge for filtering water samples from exposed *X. laevis* to decrease the processing time for each animal. Photo credit: James E. Noelker (a, b, d) and Lutfi Abu-Shanab (c).

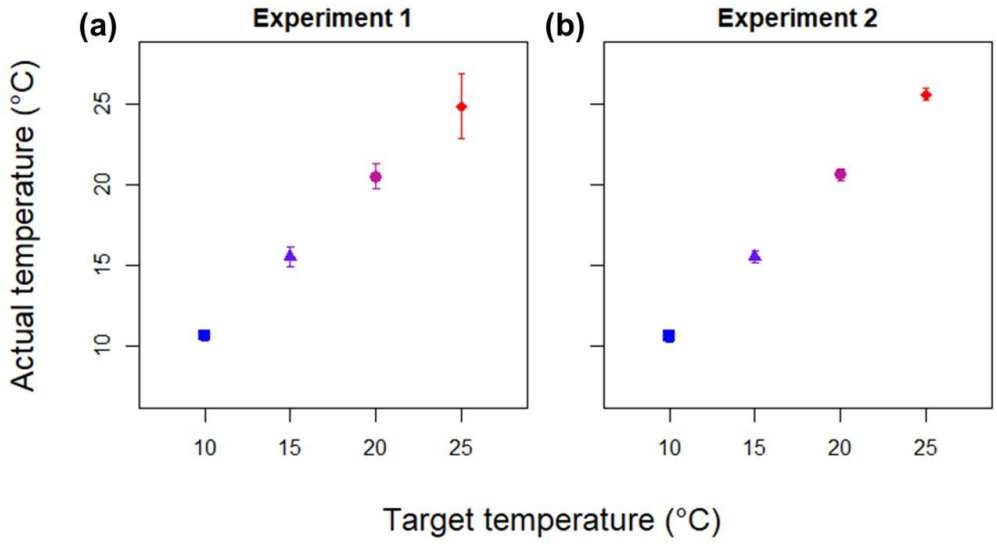

Figure C.2: Actual versus target temperatures (10 °C [blue squares], 15 °C [purple triangles], 20 °C [magenta circles], 25 °C [red diamonds]) for the two *X. laevis* Bd infection experiments: (a) Experiment 1 (2021) and (b) Experiment 2 (2022). We tracked temperatures throughout the experiments using HOBO temperature loggers (Onset, Bourne, Massachusetts, USA). Symbols indicate the mean +/- standard deviation across incubators within each temperature treatment (i.e., the mean of the mean). Error bars indicate standard deviation rather than standard error, to better communicate the full distribution of incubator temperatures in each treatment.

REFERENCES

Abreu Ruozzi, V. (2021). *Effects of current and past temperatures on chytridiomycosis infection in the African clawed frog.* (Theses and Dissertations - 105 KL (non-circulating) QL668.E265 A27 2021 LC) [*Unpublished masters thesis*, Oakland University]. Oakland University Catalog.

Allen, A. P., & Gillooly, J. F. (2007). The mechanistic basis of the Metabolic Theory of Ecology. *Oikos*, *116*(6), 1073–1077. JSTOR.

Altman, K. A. (2018). *Thermal biology of amphibian parasitism* [PhD Dissertation]. Oakland University.

Altman, K. A., Paull, S. H., Johnson, P. T. J., Golembieski, M. N., Stephens, J. P., LaFonte, B. E., & Raffel, T. R. (2016). Host and parasite thermal acclimation responses depend on the stage of infection. *Journal of Animal Ecology*, *85*(4), 1014–1024. https://doi.org/10.1111/1365-2656.12510

Altman, K. A., & Raffel, T. R. (2019). Thermal acclimation has little effect on tadpole resistance to *Batrachochytrium dendrobatidis*. *Diseases of Aquatic Organisms*, *133*(3), 207–216. https://doi.org/10.3354/dao03347

Anderson, R. M., Jackson, H. C., May, R. M., & Smith, A. M. (1981). Population dynamics of fox rabies in Europe. *Nature*, *289*(5800), 765–771. https://doi.org/10.1038/289765a0

Anderson, R. M., & May, R. M. (1979). Population biology of infectious diseases: Part I. *Nature*, *280*(5721), 361–367. https://doi.org/10.1038/280361a0

Andre, S. E., Parker, J., & Briggs, C. J. (2008). Effect of temperature on host response to *Batrachochytrium dendrobatidis* infection in the Mountain Yellow-legged frog (*Rana muscosa*). *Journal of Wildlife Diseases*, *44*(3), 716–720. https://doi.org/10.7589/0090-3558-44.3.716

Angilletta, M. J. (2006). Estimating and comparing thermal performance curves. *Journal of Thermal Biology*, *31*(7), 541–545. https://doi.org/10.1016/j.jtherbio.2006.06.002

Arrhenius, S. (1889). Uber die reaktionsgeschwindigkeit bei der inversion von rohrzucker durch sauren. *Zeitschrift Fur Physik Chemique*, *4*, 226–248.

Atkins, P. W., & De Paula, J. (2010). *Physical chemistry* (9th ed). W.H. Freeman.

Bates, D., Mächler, M., Bolker, B., & Walker, S. (2015). Fitting linear mixed-effects models using **lme4**. *Journal of Statistical Software*, *67*(1). https://doi.org/10.18637/jss.v067.i01

Becker, M. H., & Gratwicke, B. (2017). Minimum lethal concentration of sodium hypochlorite for the amphibian pathogen *Batrachochytrium dendrobatidis*. *PLOS ONE*, *12*(4), e0176439. https://doi.org/10.1371/journal.pone.0176439

Berger, L., Hyatt, A., Speare, R., & Longcore, J. (2005). Life cycle stages of the amphibian chytrid *Batrachochytrium dendrobatidis*. *Diseases of Aquatic Organisms*, *68*, 51–63. https://doi.org/10.3354/dao068051

Bivand, R., & Lewin-Koh, N. (2022). ***maptools****: Tools for handling spatial objects* (Version 1.1-3) [R]. CRAN.R-project.org/package=maptools

Blaustein, A., Urbina, J., Snyder, P., Reynolds, E., Dang, T., Hoverman, J., Han, B., Olson, D., Searle, C., & Hambalek, N. (2018). Effects of emerging infectious diseases on amphibians: A review of experimental studies. *Diversity*, *10*(3), 81. https://doi.org/10.3390/d10030081

Blem, C. R., Ragan, C. A., & Scott, L. S. (1986). The thermal physiology of two sympatric treefrogs *Hyla cinerea* and *Hyla chrysoscelis* (Anura; Hylidae). *Comparative Biochemistry and Physiology Part A: Physiology*, *85*(3), 563–570. https://doi.org/10.1016/0300-9629(86)90447-0

Bly, J. E., & Clem, L. W. (1991). Temperature-mediated processes in teleost immunity: In vitro immunosuppression induced by in vivo low temperature in channel catfish. *Veterinary Immunology and Immunopathology*, *28*(3–4), 365–377. MEDLINE. https://doi.org/10.1016/0165-2427(91)90127-x

Bosch, J., Carrascal, L. M., Durán, L., Walker, S., & Fisher, M. C. (2007). Climate change and outbreaks of amphibian chytridiomycosis in a montane area of Central Spain; is there a link? *Proceedings of the Royal Society B: Biological Sciences*, *274*(1607), 253–260. https://doi.org/10.1098/rspb.2006.3713

Bower, D. S., Brannelly, L. A., McDonald, C. A., Webb, R. J., Greenspan, S. E., Vickers, M., Gardner, M. G., & Greenlees, M. J. (2019). A review of the role of parasites in the ecology of reptiles and amphibians. *Austral Ecology*, *44*(3), 433–448. https://doi.org/10.1111/aec.12695

Bower, D. S., Lips, K. R., Schwarzkopf, L., Georges, A., & Clulow, S. (2017). Amphibians on the brink. *Science*, *357*(6350), 454–455. https://doi.org/10.1126/science.aao0500

Boyle, D., Boyle, D., Olsen, V., Morgan, J., & Hyatt, A. (2004). Rapid quantitative detection of chytridiomycosis (*Batrachochytrium dendrobatidis*) in amphibian samples using real-time Taqman PCR assay. *Diseases of Aquatic Organisms, 60,* 141–148. https://doi.org/10.3354/dao060141

Boyle, D., Hyatt, A., Daszak, P., Berger, L., Longcore, J., Porter, D., Hengstberger, S., & Olsen, V. (2003). Cryo-archiving of *Batrachochytrium dendrobatidis* and other chytridiomycetes. *Diseases of Aquatic Organisms, 56,* 59–64. https://doi.org/10.3354/dao056059

Bradley, P. W., Brawner, M. D., Raffel, T. R., Rohr, J. R., Olson, D. H., & Blaustein, A. R. (2019). Shifts in temperature influence how *Batrachochytrium dendrobatidis* infects amphibian larvae. *PLOS ONE, 14*(9), e0222237. https://doi.org/10.1371/journal.pone.0222237

Brady, S. P. (2019). *Thermal acclimation and energetics influence metabolic performance in the Mexican axolotl,* Ambystoma mexicanum (Theses and Dissertations - 105 KL (non-circulating) QL668 .C23 B73 2019 LC) [Master's Thesis, Oakland University]. Oakland University Catalog. https://search.ebscohost.com/login.aspx?direct=true&AuthType=sso&db=cat09721a&AN=ouc.oai.edge.oakland.folio.ebsco.com.fs00001142.f900fd51.e520.5667.9286.815da622c123&site=eds-live&scope=site&authtype=sso&custid=s9275379

Brannelly, L. A. (2014). Reduced itraconazole concentration and durations are successful in treating *Batrachochytrium dendrobatidis* infection in amphibians. *Journal of Visualized Experiments, 85,* 51166. https://doi.org/10.3791/51166

Brattstrom, B. H., & Lawrence, P. (1962). The rate of thermal acclimation in anuran amphibians. *Physiological Zoology, 35*(2), 148–156.

Breckling, B. (2002). Individual-based modelling potentials and limitations. *The Scientific World JOURNAL, 2,* 1044–1062. https://doi.org/10.1100/tsw.2002.179

Briggs, C. J., Knapp, R. A., & Vredenburg, V. T. (2010). Enzootic and epizootic dynamics of the chytrid fungal pathogen of amphibians. *Proceedings of the National Academy of Sciences, 107*(21), 9695–9700. https://doi.org/10.1073/pnas.0912886107

Briggs, C. J., Vredenburg, V. T., Knapp, R. A., & Rachowicz, L. J. (2005). Investigating the population-level effects of chytridiomycosis: An emerging infectious disease of amphibians. *Ecology, 86*(12), 3149–3159. https://doi.org/10.1890/04-1428

Brooks, M., E., Kristensen, K., Benthem, K., J. ,van, Magnusson, A., Berg, C., W., Nielsen, A., Skaug, H., J., Mächler, M., & Bolker, B., M. (2017). **glmmTMB** Balances speed and flexibility among packages for zero-inflated generalized linear mixed modeling. *The R Journal*, *9*(2), 378. https://doi.org/10.32614/RJ-2017-066

Brown, J. H., Gillooly, J. F., Allen, A. P., Savage, V. M., & West, G. B. (2004). Toward a metabolic theory of ecology. *Ecology*, *85*(7), 1771–1789. https://doi.org/10.1890/03-9000

Brown, P. T., Ming, Y., Li, W., & Hill, S. A. (2017). Change in the magnitude and mechanisms of global temperature variability with warming. *Nature Climate Change*, *7*(10), 743–748. https://doi.org/10.1038/nclimate3381

Carter, M. J., Cortes, P. A., & Rezende, E. L. (2023). Temperature variability and metabolic adaptation in terrestrial and aquatic ectotherms. *Journal of Thermal Biology*, *115*, 103565. https://doi.org/10.1016/j.jtherbio.2023.103565

Carvalho, T., Medina, D., Rebouças, R., Becker, C. G., & Toledo, L. F. (2024). Thermal mismatch explains fungal disease dynamics in Brazilian frogs. *Perspectives in Ecology and Conservation*, *22*(1), 72–78. https://doi.org/10.1016/j.pecon.2024.01.001

Cashins, S. D., Alford, R. A., & Skerratt, L. F. (2008). Lethal effect of latex, nitrile, and vinyl gloves on tadpoles. *Herpetological Review*, *39*(3), 298–301.

Cashins, S., Skerratt, L., & Alford, R. (2008). Sodium hypochlorite denatures the DNA of the amphibian chytrid fungus *Batrachochytrium dendrobatidis*. *Diseases of Aquatic Organisms*, *80*, 63–67. https://doi.org/10.3354/dao01919

Clare, F., Daniel, O., Garner, T., & Fisher, M. (2016). Assessing the ability of swab data to determine the true burden of infection for the amphibian pathogen *Batrachochytrium dendrobatidis*. *EcoHealth*, *13*(2), 360–367. https://doi.org/10.1007/s10393-016-1114-z

Codling, E. A., & Dumbrell, A. J. (2012). Mathematical and theoretical ecology: Linking models with ecological processes. *Interface Focus*, *2*(2), 144–149. https://doi.org/10.1098/rsfs.2012.0008

Cohen, J. M., McMahon, T. A., Ramsay, C., Roznik, E. A., Sauer, E. L., Bessler, S., Civitello, D. J., Delius, B. K., Halstead, N., Knutie, S. A., Nguyen, K. H., Ortega, N., Sears, B., Venesky, M. D., Young, S., & Rohr, J. R. (2019). Impacts of thermal mismatches on chytrid fungus *Batrachochytrium dendrobatidis* prevalence are moderated by life stage, body size, elevation and latitude. *Ecology Letters*, *22*(5), 817–825. https://doi.org/10.1111/ele.13239

Cohen, J. M., Sauer, E. L., Santiago, O., Spencer, S., & Rohr, J. R. (2020). Divergent impacts of warming weather on wildlife disease risk across climates. *Science*, *370*(6519), eabb1702. https://doi.org/10.1126/science.abb1702

Cohen, J. M., Venesky, M. D., Sauer, E. L., Civitello, D. J., McMahon, T. A., Roznik, E. A., & Rohr, J. R. (2017). The thermal mismatch hypothesis explains host susceptibility to an emerging infectious disease. *Ecology Letters*, *20*(2), 184–193. https://doi.org/10.1111/ele.12720

Coulson, T. (2012). Integral projections models, their construction and use in posing hypotheses in ecology. *Oikos*, *121*(9), 1337–1350. https://doi.org/10.1111/j.1600-0706.2012.00035.x

Craig, H. M. (2024). *Thermal biology of parasites and their hosts in the laboratory and classroom* [PhD Dissertation]. Oakland University.

Craig, H., Stepanian, R., Spengler, K., Altman, K., Sckrabulis, J., & Raffel, T. (2024). Testing for thermal acclimation in zoospores of an amphibian pathogen. *Diseases of Aquatic Organisms*, *160*, 101–114. https://doi.org/10.3354/dao03828

Curran, K. L., LaRue, S., Bronson, B., Solis, J., Trow, A., Sarver, N., & Zhu, H. (2008). Circadian genes are expressed during early development in *Xenopus laevis*. *PLoS ONE*, *3*(7), e2749. https://doi.org/10.1371/journal.pone.0002749

Danielson, J. J., & Gesch, D. B. (2011). *Global Multi-resolution Terrain Elevation Data 2010 (GMTED2010)* (U.S. Geological Survey Open-File Report Nos. 2011–1073; p. 26). U.S. Geological Survey. https://www.usgs.gov/coastal-changes-and-impacts/gmted2010

Dell, A. I., Pawar, S., & Savage, V. M. (2011). Systematic variation in the temperature dependence of physiological and ecological traits. *Proceedings of the National Academy of Sciences*, *108*(26), 10591–10596. https://doi.org/10.1073/pnas.1015178108

Dell, A. I., Pawar, S., & Savage, V. M. (2013). The thermal dependence of biological traits: *Ecological Archives* E094-108. *Ecology*, *94*(5), 1205–1206. https://doi.org/10.1890/12-2060.1

Dell, A. I., Pawar, S., & Savage, V. M. (2014). Temperature dependence of trophic interactions are driven by asymmetry of species responses and foraging strategy. *Journal of Animal Ecology*, *83*(1), 70–84. https://doi.org/10.1111/1365-2656.12081

DeLong, J. P., Bachman, G., Gibert, J. P., Luhring, T. M., Montooth, K. L., Neyer, A., & Reed, B. (2018). Habitat, latitude and body mass influence the temperature dependence of metabolic rate. *Biology Letters*, *14*(8), 20180442. https://doi.org/10.1098/rsbl.2018.0442

DeLong, J. P., Gibert, J. P., Luhring, T. M., Bachman, G., Reed, B., Neyer, A., & Montooth, K. L. (2017). The combined effects of reactant kinetics and enzyme stability explain the temperature dependence of metabolic rates. *Ecology and Evolution*, *7*(11), 3940–3950. https://doi.org/10.1002/ece3.2955

Deluen, M., Blanchet, S., Aubret, F., Trochet, A., Gangloff, E. J., Guillaume, O., Le Chevalier, H., Calvez, O., Carle, C., Genty, L., Arrondeau, G., Cazale, L., Kouyoumdjian, L., Ribéron, A., & Bertrand, R. (2022). Impacts of temperature on O_2 consumption of the Pyrenean brook newt (*Calotriton asper*) from populations along an elevational gradient. *Journal of Thermal Biology*, *103*, 103166. https://doi.org/10.1016/j.jtherbio.2021.103166

Denny, M. (2017). The fallacy of the average: On the ubiquity, utility and continuing novelty of Jensen's inequality. *Journal of Experimental Biology*, *220*(2), 139–146. https://doi.org/10.1242/jeb.140368

Denny, M., & Benedetti-Cecchi, L. (2012). Scaling up in ecology: Mechanistic approaches. *Annual Review of Ecology, Evolution, and Systematics*, *43*(1), 1–22. https://doi.org/10.1146/annurev-ecolsys-102710-145103

DeVore, J. L., Shine, R., & Ducatez, S. (2020). Urbanization and translocation disrupt the relationship between host density and parasite abundance. *Journal of Animal Ecology*, *89*(4), 1122–1133. https://doi.org/10.1111/1365-2656.13175

Dewenter, B. S., Shah, A. A., Hughes, J., Poff, N. L., Thompson, R., & Kefford, B. J. (2024). The thermal breadth of temperate and tropical freshwater insects supports the climate variability hypothesis. *Ecology and Evolution*, *14*(2), e10937. https://doi.org/10.1002/ece3.10937

DiRenzo, G. V., Langhammer, P. F., Zamudio, K. R., & Lips, K. R. (2014). Fungal infection intensity and zoospore output of *Atelopus zeteki*, a potential acute chytrid supershedder. *PLOS ONE*, *9*(3), e93356. https://doi.org/10.1371/journal.pone.0093356

DiRenzo, G. V., Tunstall, T. S., Ibáñez, R., deVries, M. S., Longo, A. V., Zamudio, K. R., & Lips, K. R. (2018). External reinfection of a fungal pathogen does not contribute to pathogen growth. *EcoHealth*, *15*(4), 815–826. https://doi.org/10.1007/s10393-018-1358-x

Dowell, S. F. (2001). Seasonal variation in host susceptibility and cycles of certain infectious diseases. *Emerging Infectious Diseases*, *7*(3).

Duellman, W. E., & Trueb, L. (1986). *Biology of amphibians*. McGraw Hill.

Dunlap, D. G. (1969). Influence of temperature and duration of acclimation, time of day, sex and body weight on metabolic rates in the hylid frog, *Acris crepitans*. *Comparative Biochemistry and Physiology*, *31*(4), 555–570. https://doi.org/10.1016/0010-406X(69)90057-7

Eisenlord, M. E., Agnew, M. V., Winningham, M., Lobo, O. J., Vompe, A. D., Wippel, B., Friedman, C. S., Harvell, C. D., & Burge, C. A. (2024). High infectivity and waterborne transmission of seagrass wasting disease. *Royal Society Open Science*, *11*(8), 240663. https://doi.org/10.1098/rsos.240663

Elzhov, T. V., Mullen, K. M., Spiess, A.-N., & Bolker, B. (2023). ***minpack.lm****: R Interface to the Levenberg-Marquardt Nonlinear Least-Squares Algorithm Found in MINPACK, Plus Support for Bounds* (Version 1.2-4) [R]. https://CRAN.R-project.org/package=minpack.lm

Epstein, P. R. (2001). Climate change and emerging infectious diseases. *Microbes and Infection*.

Esmizadeh, E., Chang, B. P., Jubinville, D., Seto, C., Ojogbo, E., Tzoganakis, C., & Mekonnen, T. H. (2021). Stability of nitrile and vinyl latex gloves under repeated disinfection cycles. *Materials Today Sustainability*, *11–12*, 100067. https://doi.org/10.1016/j.mtsust.2021.100067

Farrer, R. A., Weinert, L. A., Bielby, J., Garner, T. W. J., Balloux, F., Clare, F., Bosch, J., Cunningham, A. A., Weldon, C., Du Preez, L. H., Anderson, L., Pond, S. L. K., Shahar-Golan, R., Henk, D. A., & Fisher, M. C. (2011). Multiple emergences of genetically diverse amphibian-infecting chytrids include a globalized hypervirulent recombinant lineage. *Proceedings of the National Academy of Sciences*, *108*(46), 18732–18736. https://doi.org/10.1073/pnas.1111915108

Feder, M. E. (1985). Acclimation to constant and variable temperatures in Plethodontid salamanders—I. Rates of oxygen consumption. *Comparative Biochemistry and Physiology Part A: Physiology*, *81*(3), 673–682. https://doi.org/10.1016/0300-9629(85)91046-1

Feder, M. E., & Burggren, W. W. (Eds.). (1992). *Environmental physiology of the amphibians*. University of Chicago Press.

Fick, S. E., & Hijmans, R. J. (2017). WorldClim 2: New 1-km spatial resolution climate surfaces for global land areas. *International Journal of Climatology*, *37*(12), 4302–4315. https://doi.org/10.1002/joc.5086

Fisher, M. C., & Garner, T. W. J. (2007). The relationship between the emergence of *Batrachochytrium dendrobatidis*, the international trade in amphibians and introduced amphibian species. *Fungal Biology Reviews*, *21*(1), 2–9. https://doi.org/10.1016/j.fbr.2007.02.002

Fisher, M. C., & Garner, T. W. J. (2020). Chytrid fungi and global amphibian declines. *Nature Reviews Microbiology*, *18*(6), 332–343. https://doi.org/10.1038/s41579-020-0335-x

Fisher, M. C., Garner, T. W. J., & Walker, S. F. (2009). Global emergence of *Batrachochytrium dendrobatidis* and amphibian chytridiomycosis in space, time, and host. *Annual Review of Microbiology*, *63*(1), 291–310. https://doi.org/10.1146/annurev.micro.091208.073435

Fites, J. S., Ramsey, J. P., Holden, W. M., Collier, S. P., Sutherland, D. M., Reinert, L. K., Gayek, A. S., Dermody, T. S., Aune, T. M., Oswald-Richter, K., & Rollins-Smith, L. A. (2013). The invasive chytrid fungus of amphibians paralyzes lymphocyte responses. *Science*, *342*(6156), 366–369. https://doi.org/10.1126/science.1243316

Forrest, M. J., & Schlaepfer, M. A. (2011). Nothing a hot bath won't cure: Infection rates of amphibian chytrid fungus correlate negatively with water temperature under natural field settings. *PLoS ONE*, *6*(12), e28444. https://doi.org/10.1371/journal.pone.0028444

Foufopoulos, J., Wobeser, G. A., & McCallum, H. (2022). *Infectious disease ecology and conservation*. Oxford University Press.

Fox, J., & Weisberg, S. (2019). *An R companion to applied regression.* (3rd ed. / John Fox, Sanford Weisberg.). SAGE Publications.

Francis-Floyd, R., Yanong, R., & Pouder, D. (2016). *Ichthyophthirius multifiliis* (White Spot) infections in fish. *EDIS*, *2016*(10). https://doi.org/10.32473/edis-fa006-1991

Gatten, Jr., R. E., Miller, K., & Full, R. J. (1992). Energetics at rest and during locomotion. In M. E. Feder & W. W. Burggren (Eds.), *Environmental Physiology of the Amphibians* (pp. 314–377). The University of Chicago Press, Ltd; JSTOR.

GBIF. (2024). https://www.gbif.org/

Gehman, A.-L. M., Hall, R. J., & Byers, J. E. (2018). Host and parasite thermal ecology jointly determine the effect of climate warming on epidemic dynamics. *Proceedings of the National Academy of Sciences*, *115*(4), 744–749. https://doi.org/10.1073/pnas.1705067115

Gillooly, J. F., Brown, J. H., West, G. B., Savage, V. M., & Charnov, E. L. (2001). Effects of size and temperature on metabolic rate. *Science*, *293*(5538), 2248–2251. https://doi.org/10.1126/science.1061967

Gillooly, James. F., Charnov, E. L., West, G. B., Savage, V. M., & Brown, J. H. (2002). Effects of size and temperature on developmental time. *Nature*, *417*(6884), 70–73. https://doi.org/10.1038/417070a

Glasser, J. W., & Feng, Z. (2025). Mechanistic models are hypotheses: A perspective. *Mathematical Biosciences*, 109419. https://doi.org/10.1016/j.mbs.2025.109419

Gotelli, N. J., & Ellison, A. M. (2013). *A primer of ecological statistics* (2. ed). Sinauer Associates.

Gray, M. J., Duffus, A. L. J., Haman, K. H., Harris, R. N., Allender, M. C., Thompson, T. A., Christman, M. R., Sacerdote-Velat, A., Sprague, L. A., Williams, J. M., & Miller, D. L. (2017). Pathogen surveillance in herpetofaunal populations: Guidance on study design, sample collection, biosecurity, and intervention strategies. *Herpetological Review*, *48*(2), 334–351.

Gray, M. J., Spatz, J. A., Carter, E. D., Yarber, C. M., Wilkes, R. P., & Miller, D. L. (2018). Poor biosecurity could lead to disease outbreaks in animal populations. *PLOS ONE*, *13*(3), e0193243. https://doi.org/10.1371/journal.pone.0193243

Green, S. L. (2009). *The laboratory Xenopus sp.* (1st ed.). CRC Press.

Greener, M. S., Verbrugghe, E., Kelly, M., Blooi, M., Beukema, W., Canessa, S., Carranza, S., Croubels, S., De Troyer, N., Fernandez-Giberteau, D., Goethals, P., Lens, L., Li, Z., Stegen, G., Strubbe, D., Van Leeuwenberg, R., Van Praet, S., Vila-Escale, M., Vervaeke, M., … Martel, A. (2020). Presence of low virulence chytrid fungi could protect European amphibians from more deadly strains. *Nature Communications*, *11*(1), 5393. https://doi.org/10.1038/s41467-020-19241-7

Greenspan, S. E., Bower, D. S., Webb, R. J., Berger, L., Rudd, D., Schwarzkopf, L., & Alford, R. A. (2017). White blood cell profiles in amphibians help to explain disease susceptibility following temperature shifts. *Developmental & Comparative Immunology*, *77*, 280–286. https://doi.org/10.1016/j.dci.2017.08.018

Greenspan, S., Longcore, J., & Calhoun, A. (2012). Host invasion by *Batrachochytrium dendrobatidis*: Fungal and epidermal ultrastructure in model anurans. *Diseases of Aquatic Organisms*, *100*(3), 201–210. https://doi.org/10.3354/dao02483

Grogan, L. F., Robert, J., Berger, L., Skerratt, L. F., Scheele, B. C., Castley, J. G., Newell, D. A., & McCallum, H. I. (2018). Review of the amphibian immune response to chytridiomycosis, and future directions. *Frontiers in Immunology, 9*, 2536. https://doi.org/10.3389/fimmu.2018.02536

Gutleb, A. C., Bronkhorst, M., van den Berg, J. H. J., & Murk, A. J. (2001). Latex laboratory-gloves: An unexpected pitfall in amphibian toxicity assays with tadpoles. *Environmental Toxicology and Pharmacology*, *10*(3), 119–121. https://doi.org/10.1016/S1382-6689(01)00091-6

Hamilton, P. T., Richardson, J. M. L., Govindarajulu, P., & Anholt, B. R. (2012). Higher temperature variability increases the impact of *Batrachochytrium dendrobatidis* and shifts interspecific interactions in tadpole mesocosms. *Ecology and Evolution*, *2*(10), 2450–2459. https://doi.org/10.1002/ece3.369

Harrell, F. E., Jr, & Dupont, C. (2022). ***Hmisc****: Harrell Miscellaneous* (Version 4.7-2) [R]. https://CRAN.R-project.org/package=Hmisc

Havlíková, B., Havlíková, B., Baláž, V., Havlíková, B., Baláž, V., & Vojar, J. (2015). First systematic monitoring of *Batrachochytrium dendrobatidis* in collections of captive amphibians in the Czech Republic. *Amphibia-Reptilia*, *36*(1), 27–35. https://doi.org/10.1163/15685381-00002972

Hijmans, R. J. (2023). ***raster****: Geographic Data Analysis and Modeling* (Version 3.6-20) [R]. CRAN.R-project.org/package=raster

Hijmans, R. J., Phillips, S., Leathwick, J., & Elith, J. (2022). ***dismo****: Species Distribution Modeling* (Version 1.3-9) [R]. CRAN.R-project.org/package=dismo

Horsberg, T. E. (1994). Experimental methods for pharmacokinetic studies in salmonids. *Annual Review of Fish Diseases*, *4*, 345–358. https://doi.org/10.1016/0959-8030(94)90034-5

Hoyt, J. R., Kilpatrick, A. M., & Langwig, K. E. (2021). Ecology and impacts of white-nose syndrome on bats. *Nature Reviews Microbiology*, *19*(3), 196–210. https://doi.org/10.1038/s41579-020-00493-5

Hudson, P. J., Annapaola Rizzoli, Grenfell, B. T., Heesterbeek, H., & Dobson, A. P. (2009). *The Ecology of Wildlife Diseases*. Oxford University Press.

Huey, R. B., & Kingsolver, J. G. (1989). Evolution of thermal sensitivity of ectotherm performance. *Trends in Ecology & Evolution*, *4*(5), 131–135. https://doi.org/10.1016/0169-5347(89)90211-5

Hutchison, V. H. (1961). Critical thermal maxima in salamanders. *Physiological Zoology*, *34*(2), 92–125.

Hutchison, V. H., & Maness, J. D. (1979). The role of behavior in temperature acclimation and tolerance in ectotherms. *American Zoologist*, *19*(1), 367–384.

Hutchison, V. H. & Michael R. Ferrance. (1970). Thermal tolerances of *Rana pipiens* acclimated to daily temperature cycles. *Herpetologica*, *26*(1), 1–8. JSTOR.

Hyatt, A., Boyle, D., Olsen, V., Boyle, D., Berger, L., Obendorf, D., Dalton, A., Kriger, K., Hero, M., Hines, H., Phillott, R., Campbell, R., Marantelli, G., Gleason, F., & Colling, A. (2007). Diagnostic assays and sampling protocols for the detection of *Batrachochytrium dendrobatidis*. *Diseases of Aquatic Organisms*, *73*, 175–192. https://doi.org/10.3354/dao073175

Isidoro-Ayza, M., Lorch, J. M., & Klein, B. S. (2024). The skin I live in: Pathogenesis of white-nose syndrome of bats. *PLOS Pathogens*, *20*(8), e1012342. https://doi.org/10.1371/journal.ppat.1012342

Jackson, C. (2016). **flexsurv**: A Platform for Parametric Survival Modeling in *R*. *Journal of Statistical Software*, *70*(8). https://doi.org/10.18637/jss.v070.i08

Jensen, J. L. W. V. (1906). Sur les fonctions convexes et les inégalités entre les valeurs moyennes. *Acta Mathematica*, *30*(1), 175–193. https://doi.org/10.1007/BF02418571

Johnson, M., Berger, L., Philips, L., & Speare, R. (2003). Fungicidal effects of chemical disinfectants, UV light, desiccation and heat on the amphibian chytrid *Batrachochytrium dendrobatidis*. *Diseases of Aquatic Organisms*, *57*, 255–260. https://doi.org/10.3354/dao057255

Johnson, M. L., & Speare, R. (2003). Survival of *Batrachochytrium dendrobatidis* in water: Quarantine and disease control implications. *Emerging Infectious Diseases*, *9*(8), 915–921. https://doi.org/10.3201/eid0908.030145

Kinney, V. C., Heemeyer, J. L., Pessier, A. P., & Lannoo, M. J. (2011). Seasonal pattern of *Batrachochytrium dendrobatidis* infection and mortality in *Lithobates areolatus*: Affirmation of Vredenburg's "10,000 zoospore rule." *PLOS ONE*, *6*(3), e16708. https://doi.org/10.1371/journal.pone.0016708

Kirk, D., Jones, N., Peacock, S., Phillips, J., Molnár, P. K., Krkošek, M., & Luijckx, P. (2018). Empirical evidence that metabolic theory describes the temperature dependency of within-host parasite dynamics. *PLOS Biology*, *16*(2), e2004608. https://doi.org/10.1371/journal.pbio.2004608

Kirk, D., O'Connor, M. I., & Mordecai, E. A. (2022). Scaling effects of temperature on parasitism from individuals to populations. *Journal of Animal Ecology*, *91*(10), 2087–2102. https://doi.org/10.1111/1365-2656.13786

Koo, M. S., Vredenburg, V. T., Deck, J. B., Olson, D. H., Ronnenberg, K. L., & Wake, D. B. (2021). Tracking, synthesizing, and sharing global *Batrachochytrium* data at AmphibianDisease.org. *Frontiers in Veterinary Science*, *8*, 728232. https://doi.org/10.3389/fvets.2021.728232

Krichel, L., Kirk, D., Pencer, C., Hönig, M., Wadhawan, K., & Krkošek, M. (2023). Short-term temperature fluctuations increase disease in a Daphnia-parasite infectious disease system. *PLOS Biology*, *21*(9), e3002260. https://doi.org/10.1371/journal.pbio.3002260

Kriger, K., Hero, J., & Ashton, K. (2006). Cost efficiency in the detection of chytridiomycosis using PCR assay. *Diseases of Aquatic Organisms*, *71*, 149–154. https://doi.org/10.3354/dao071149

Kriger, K. M., Pereoglou, F., & Hero, J.-M. (2007). Latitudinal variation in the prevalence and intensity of chytrid (*Batrachochytrium dendrobatidis*) infection in eastern Australia. *Conservation Biology*, *21*(5), 1280–1290. https://doi.org/10.1111/j.1523-1739.2007.00777.x

Kupferberg, S. J., Moidu, H., Adams, A. J., Catenazzi, A., Grefsrud, M., Bobzien, S., Leidy, R., & Carlson, S. M. (2022). Seasonal drought and its effects on frog population dynamics and amphibian disease in intermittent streams. *Ecohydrology*, *15*(5), e2395. https://doi.org/10.1002/eco.2395

Lafferty, K. D. (2009). The ecology of climate change and infectious diseases. *Ecology*, *90*(4), 888–900. https://doi.org/10.1890/08-0079.1

Li, J., Guttmann, N., Drew, G. C., Hector, T. E., Wolinska, J., & King, K. C. (2024). Excess mortality of infected ectotherms induced by warming depends on pathogen kingdom and evolutionary history. *PLOS Biology*, *22*(11), e3002900. https://doi.org/10.1371/journal.pbio.3002900

Li, Z., Wang, Q., Sun, K., & Feng, J. (2021). Prevalence of *Batrachochytrium dendrobatidis* in amphibians from 2000 to 2021: A global systematic review and meta-analysis. *Frontiers in Veterinary Science*, *8*, 791237. https://doi.org/10.3389/fvets.2021.791237

Lincoln, G. (2019). A brief history of circannual time. *Journal of Neuroendocrinology*, *31*(3), e12694. https://doi.org/10.1111/jne.12694

Longcore, J. E., Pessier, A. P., & Nichols, D. K. (1999). *Batrachochytrium dendrobatidis* gen. Et sp. Nov., a chytrid pathogenic to amphibians. *Mycologia*, *91*(2), 219. https://doi.org/10.2307/3761366

Lorch, J. M., Knowles, S., Lankton, J. S., Michell, K., Edwards, J. L., Kapfer, J. M., Staffen, R. A., Wild, E. R., Schmidt, K. Z., Ballmann, A. E., Blodgett, D., Farrell, T. M., Glorioso, B. M., Last, L. A., Price, S. J., Schuler, K. L., Smith, C. E., Wellehan, J. F. X., & Blehert, D. S. (2016). Snake fungal disease: An emerging threat to wild snakes. *Philosophical Transactions of the Royal Society B: Biological Sciences*, *371*(1709), 20150457. https://doi.org/10.1098/rstb.2015.0457

Maguire, C., DiRenzo, G., Tunstall, T., Muletz, C., Zamudio, K., & Lips, K. (2016). Dead or alive? Viability of chytrid zoospores shed from live amphibian hosts. *Diseases of Aquatic Organisms*, *119*(3), 179–187. https://doi.org/10.3354/dao02991

Malagon, D. A., Melara, L. A., Prosper, O. F., Lenhart, S., Carter, E. D., Fordyce, J. A., Peterson, A. C., Miller, D. L., & Gray, M. J. (2020). Host density and habitat structure influence host contact rates and *Batrachochytrium salamandrivorans* transmission. *Scientific Reports*, *10*(1), 5584. https://doi.org/10.1038/s41598-020-62351-x

Maniero, G. D., & Carey, C. (1997). Changes in selected aspects of immune function in the leopard frog, *Rana pipiens*, associated with exposure to cold. *Journal of Comparative Physiology B: Biochemical, Systemic, and Environmental Physiology*, *167*(4), 256–263. https://doi.org/10.1007/s003600050072

Martel, A., Spitzen-van Der Sluijs, A., Blooi, M., Bert, W., Ducatelle, R., Fisher, M. C., Woeltjes, A., Bosman, W., Chiers, K., Bossuyt, F., & Pasmans, F. (2013). *Batrachochytrium salamandrivorans* sp. Nov. Causes lethal chytridiomycosis in amphibians. *Proceedings of the National Academy of Sciences*, *110*(38), 15325–15329. https://doi.org/10.1073/pnas.1307356110

Martin, T. L., & Huey, R. B. (2008). Why "suboptimal" is optimal: Jensen's inequality and ectotherm thermal preferences. *The American Naturalist*, *171*(3), E102–E118. https://doi.org/10.1086/527502

May, R. M., & Anderson, R. M. (1979). Population biology of infectious diseases: Part II. *Nature*, *280*(5722), 455–461. https://doi.org/10.1038/280455a0

McCoy, C. M., Lind, C. M., & Farrell, T. M. (2017). Environmental and physiological correlates of the severity of clinical signs of snake fungal disease in a population of pigmy rattlesnakes, *Sistrurus miliarius*. *Conservation Physiology*, *5*(1), cow077. https://doi.org/10.1093/conphys/cow077

McGill, B. (2003). Strong and weak tests of macroecological theory. *Oikos*, *102*(3), 679–685. https://doi.org/10.1034/j.1600-0706.2003.12617.x

McMahon, T. A., Sears, B. F., Venesky, M. D., Bessler, S. M., Brown, J. M., Deutsch, K., Halstead, N. T., Lentz, G., Tenouri, N., Young, S., Civitello, D. J., Ortega, N., Fites, J. S., Reinert, L. K., Rollins-Smith, L. A., Raffel, T. R., & Rohr, J. R. (2014). Amphibians acquire resistance to live and dead fungus overcoming fungal immunosuppression. *Nature*, *511*(7508), 224–227. https://doi.org/10.1038/nature13491

McWhinnie, R. B., Sckrabulis, J. P., & Raffel, T. R. (2021). Temperature and mass scaling affect cutaneous and pulmonary respiratory performance in a diving frog. *Integrative Zoology*, *16*(5), 712–728. https://doi.org/10.1111/1749-4877.12551

Melbourne, B. A., & Chesson, P. (2005). Scaling up population dynamics: Integrating theory and data. *Oecologia*, *145*(2), 178–186. https://doi.org/10.1007/s00442-005-0058-8

Mendez, D., Webb, R., Berger, L., & Speare, R. (2008). Survival of the amphibian chytrid fungus *Batrachochytrium dendrobatidis* on bare hands and gloves: Hygiene implications for amphibian handling. *Diseases of Aquatic Organisms*, *82*, 97–104. https://doi.org/10.3354/dao01975

Metcalf, C. J. E., Graham, A. L., Martinez-Bakker, M., & Childs, D. Z. (2016). Opportunities and challenges of Integral Projection Models for modelling host-parasite dynamics. *Journal of Animal Ecology*, *85*(2), 343–355. https://doi.org/10.1111/1365-2656.12456

Mideo, N., Alizon, S., & Day, T. (2008). Linking within- and between-host dynamics in the evolutionary epidemiology of infectious diseases. *Trends in Ecology & Evolution*, *23*(9), 511–517. https://doi.org/10.1016/j.tree.2008.05.009

Milner, F. A., & Patton, C. A. (2003). A diffusion model for host–parasite interaction. *Journal of Computational and Applied Mathematics*, *154*(2), 273–302. https://doi.org/10.1016/S0377-0427(02)00826-9

Mineo, P. M., & Schaeffer, P. J. (2015). The thermal plasticity of locomotor performance has diverged between northern and southern populations of the eastern newt (*Notophthalmus viridescens*). *Journal of Comparative Physiology B*, *185*(1), 103–110. https://doi.org/10.1007/s00360-014-0869-1

Molnár, P. K., Kutz, S. J., Hoar, B. M., & Dobson, A. P. (2013). Metabolic approaches to understanding climate change impacts on seasonal host-macroparasite dynamics. *Ecology Letters*, *16*(1), 9–21. https://doi.org/10.1111/ele.12022

Molnár, P. K., Sckrabulis, J. P., Altman, K. A., & Raffel, T. R. (2017). Thermal performance curves and the metabolic theory of ecology—A practical guide to models and experiments for parasitologists. *Journal of Parasitology*, *103*(5), 423. https://doi.org/10.1645/16-148

Mordecai, E. A., Caldwell, J. M., Grossman, M. K., Lippi, C. A., Johnson, L. R., Neira, M., Rohr, J. R., Ryan, S. J., Savage, V., Shocket, M. S., Sippy, R., Stewart Ibarra, A. M., Thomas, M. B., & Villena, O. (2019). Thermal biology of mosquito-borne disease. *Ecology Letters, 22*(10), 1690–1708. https://doi.org/10.1111/ele.13335

Mordecai, E. A., Paaijmans, K. P., Johnson, L. R., Balzer, C., Ben-Horin, T., de Moor, E., McNally, A., Pawar, S., Ryan, S. J., Smith, T. C., & Lafferty, K. D. (2013). Optimal temperature for malaria transmission is dramatically lower than previously predicted. *Ecology Letters*, *16*(1), 22–30. https://doi.org/10.1111/ele.12015

Neely, W. J., Greenspan, S. E., Ribeiro, L. P., Carvalho, T., Martins, R. A., Rodriguez, D., Rohr, J. R., Haddad, C. F. B., Toledo, L. F., & Becker, C. G. (2020). Synergistic effects of warming and disease linked to high mortality in cool-adapted terrestrial frogs. *Biological Conservation*, *245*, 108521. https://doi.org/10.1016/j.biocon.2020.108521

Nguyen, K. H., Boersch-Supan, P. H., Hartman, R. B., Mendiola, S. Y., Harwood, V. J., Civitello, D. J., & Rohr, J. R. (2021). Interventions can shift the thermal optimum for parasitic disease transmission. *Proceedings of the National Academy of Sciences, 118*(11), e2017537118. https://doi.org/10.1073/pnas.2017537118

Nietfeldt, J. W., Jones, S. M., Droge, D. L., & Ballinger, R. E. (1980). Rate of thermal acclimation in larval *Ambystoma tigrinum*. *Journal of Herpetology*, *14*(3), 209. https://doi.org/10.2307/1563541

Noelker, J., Abreu Ruozzi, V., Spengler, K., Craig, H., & Raffel, T. (2024). *Data from: Dynamic effects of thermal acclimation on chytridiomycosis infection intensity and transmission potential in Xenopus laevis* (Version 9, p. 110682 bytes) [Dataset]. Dryad. https://doi.org/10.5061/DRYAD.K3J9KD5GV

Noelker, J. E., Abreu Ruozzi, V., Craig, H. M., Sckrabulis, J. P., & Raffel, T. R. (2024). Glove decontamination procedures to prevent pathogen and DNA cross-contamination among frogs. *Diseases of Aquatic Organisms*, *158*, 173–178. https://doi.org/10.3354/dao03793

Noelker, J. E., Abreu Ruozzi, V., Spengler, K. D., Craig, H. M., & Raffel, T. R. (2024). Dynamic effects of thermal acclimation on chytridiomycosis infection intensity and transmission potential in *Xenopus laevis*. *Royal Society Open Science*, *11*(9), 240789. https://doi.org/10.1098/rsos.240789

Nowakowski, A. J., Watling, J. I., Whitfield, S. M., Todd, B. D., Kurz, D. J., & Donnelly, M. A. (2017). Tropical amphibians in shifting thermal landscapes under land-use and climate change. *Conservation Biology*, *31*(1), 96–105. https://doi.org/10.1111/cobi.12769

O'Connor, M. I., & Bernhardt, J. R. (2018). The metabolic theory of ecology and the cost of parasitism. *PLOS Biology*, *16*(4), e2005628. https://doi.org/10.1371/journal.pbio.2005628

O'Connor, M. P., Kemp, S. J., Agosta, S. J., Hansen, F., Sieg, A. E., Wallace, B. P., McNair, J. N., & Dunham, A. E. (2007). Reconsidering the mechanistic basis of the Metabolic Theory of Ecology. *Oikos*, *116*(6), 1058–1072. JSTOR.

Overgaard, J., Andersen, J. L., Findsen, A., Pedersen, P. B. M., Hansen, K., Ozolina, K., & Wang, T. (2012). Aerobic scope and cardiovascular oxygen transport is not compromised at high temperatures in the toad *Rhinella marina*. *Journal of Experimental Biology*, jeb.070110. https://doi.org/10.1242/jeb.070110

Paaijmans, K. P., Blanford, S., Bell, A. S., Blanford, J. I., Read, A. F., & Thomas, M. B. (2010). Influence of climate on malaria transmission depends on daily temperature variation. *Proceedings of the National Academy of Sciences*, *107*(34), 15135–15139. https://doi.org/10.1073/pnas.1006422107

Palmer-Young, E. C., Raffel, T. R., & McFrederick, Q. S. (2018). *Temperature-mediated inhibition of a bumblebee parasite by an intestinal symbiont*. 9.

Palmer-Young, E. C., Ryabov, E. V., Markowitz, L. M., Boncristiani, D. L., Grubbs, K., Pawar, A., Peterson, R., & Evans, J. D. (2023). Host-driven temperature dependence of Deformed wing virus infection in honey bee pupae. *Communications Biology*, *6*(1), 333. https://doi.org/10.1038/s42003-023-04704-6

Pebesma, E. (2018). Simple Features for R: Standardized Support for Spatial Vector Data. *The R Journal*, *10*(1), 439. https://doi.org/10.32614/RJ-2018-009

Petersen, J. E., & Englund, G. (2005). Dimensional approaches to designing better experimental ecosystems: A practitioners guide with examples. *Oecologia*, *145*(2), 215–223. https://doi.org/10.1007/s00442-005-0062-z

Petranka, J. W. (1998). *Salamanders of the United States and Canada*. Smithsonian Institution Press.

Petzoldt, T., & Rinke, K. (2007). **simecol**: An object-oriented framework for ecological modeling in *R*. *Journal of Statistical Software*, *22*(9). https://doi.org/10.18637/jss.v022.i09

Porco, D., Purnomo, C. A., Glesener, L., Proess, R., Lippert, S., Jans, K., Colling, G., Schneider, S., Stassen, R., & Frantz, A. C. (2024). eDNA-based monitoring of *Batrachochytrium dendrobatidis* and *Batrachochytrium salamandrivorans* with ddPCR in Luxembourg ponds: Taking signals below the Limit of Detection (LOD) into account. *BMC Ecology and Evolution*, *24*(1), 4. https://doi.org/10.1186/s12862-023-02189-9

R Core Team. (2022). *R: a language and environment for statistical computing* (Version 4.1.3) [R]. R Foundation for Statistical Computing. https://www.R-project.org/

Raffel, T. R., Halstead, N. T., McMahon, T. A., Davis, A. K., & Rohr, J. R. (2015). Temperature variability and moisture synergistically interact to exacerbate an epizootic disease. *Proceedings of the Royal Society B: Biological Sciences*, *282*(1801), 20142039. https://doi.org/10.1098/rspb.2014.2039

Raffel, T. R., Rohr, J. R., Kiesecker, J. M., & Hudson, P. J. (2006). Negative effects of changing temperature on amphibian immunity under field conditions. *Functional Ecology*, *20*(5), 819–828. https://doi.org/10.1111/j.1365-2435.2006.01159.x

Raffel, T. R., Romansic, J. M., Halstead, N. T., McMahon, T. A., Venesky, M. D., & Rohr, J. R. (2013). Disease and thermal acclimation in a more variable and unpredictable climate. *Nature Climate Change*, *3*(2), 146–151. https://doi.org/10.1038/nclimate1659

Räisänen, J. (2002). CO_2 -Induced changes in interannual temperature and precipitation variability in 19 CMIP2 experiments. *Journal of Climate*, *15*(17), 2395–2411. https://doi.org/10.1175/1520-0442(2002)015<2395:CICIIT>2.0.CO;2

Reddy, A. B., & Rey, G. (2014). Metabolic and nontranscriptional circadian clocks: Eukaryotes. *Annual Review of Biochemistry*, *83*(1), 165–189. https://doi.org/10.1146/annurev-biochem-060713-035623

Reed, B. T. (2005). *Guidance on the housing and care of the African clawed frog* Xenopus laevis. Royal Society for the Prevention of Cruelty to Animals (RSPCA).

Reeder, N. M. M., Pessier, A. P., & Vredenburg, V. T. (2012). A reservoir species for the emerging amphibian pathogen *Batrachochytrium dendrobatidis* thrives in a landscape decimated by disease. *PLoS ONE*, *7*(3), e33567. https://doi.org/10.1371/journal.pone.0033567

Rohr, J. R., Civitello, D. J., Cohen, J. M., Roznik, E. A., Sinervo, B., & Dell, A. I. (2018). The complex drivers of thermal acclimation and breadth in ectotherms. *Ecology Letters*, *21*(9), 1425–1439. https://doi.org/10.1111/ele.13107

Rohr, J. R., & Cohen, J. M. (2020). Understanding how temperature shifts could impact infectious disease. *PLOS Biology*, *18*(11), e3000938. https://doi.org/10.1371/journal.pbio.3000938

Rohr, J. R., & Raffel, T. R. (2010). Linking global climate and temperature variability to widespread amphibian declines putatively caused by disease. *Proceedings of the National Academy of Sciences*, *107*(18), 8269–8274. https://doi.org/10.1073/pnas.0912883107

Rohr, J. R., Raffel, T. R., Blaustein, A. R., Johnson, P. T. J., Paull, S. H., & Young, S. (2013). Using physiology to understand climate-driven changes in disease and their implications for conservation. *Conservation Physiology*, *1*(1), cot022–cot022. https://doi.org/10.1093/conphys/cot022

Rollins-Smith, L. A. (2009). Immune defenses of *Xenopus laevis* against *Batrachochytrium dendrobatidis*. *Frontiers in Bioscience*, *S1*(1), 68–91. https://doi.org/10.2741/s8

Rollins-Smith, L. A., & Le Sage, E. H. (2021). *Batrachochytrium* fungi: Stealth invaders in amphibian skin. *Current Opinion in Microbiology*, *61*, 124–132. https://doi.org/10.1016/j.mib.2021.04.002

Savage, V. M., Gillooly, J. F., Brown, J. H., West, G. B., & Charnov, E. L. (2004). Effects of body size and temperature on population growth. *The American Naturalist*, *163*(3), 429–441. https://doi.org/10.1086/381872

Schoolfield, R. M., Sharpe, P. J. H., & Magnuson, C. E. (1981). Non-linear regression of biological temperature-dependent rate models based on absolute reaction-rate theory. *Journal of Theoretical Biology*, *88*(4), 719–731. https://doi.org/10.1016/0022-5193(81)90246-0

Sckrabulis, J. P., Altman, K. A., & Raffel, T. R. (2022). Using metabolic theory to describe temperature and thermal acclimation effects on parasitic infection. *The American Naturalist*, 719409. https://doi.org/10.1086/719409

Searle, C. L., Gervasi, S. S., Hua, J., Hammond, J. I., Relyea, R. A., Olson, D. H., & Blaustein, A. R. (2011). Differential host susceptibility to *Batrachochytrium dendrobatidis*, an emerging amphibian pathogen: Differential host susceptibility. *Conservation Biology*, *25*(5), 965–974. https://doi.org/10.1111/j.1523-1739.2011.01708.x

Sheets, C. N., Schmidt, D. R., Hurtado, P. J., Byrne, A. Q., Rosenblum, E. B., Richards-Zawacki, C. L., & Voyles, J. (2021). Thermal Performance Curves of Multiple Isolates of Batrachochytrium dendrobatidis, a Lethal Pathogen of Amphibians. *Frontiers in Veterinary Science*, *8*, 687084. https://doi.org/10.3389/fvets.2021.687084

Shin, J., Bataille, A., Kosch, T. A., & Waldman, B. (2014). Swabbing often fails to detect amphibian chytridiomycosis under conditions of low infection load. *PLoS ONE*, *9*(10), e111091. https://doi.org/10.1371/journal.pone.0111091

Shocket, M. S., Bernhardt, J. R., Miazgowicz, K. L., Orakzai, A., Savage, V. M., Hall, R. J., Ryan, S. J., & Murdock, C. C. (2024). Mean daily temperatures can predict the thermal limits of malaria transmission better than rate summation. *bioRxiv*, 2024.09.20.614098. https://doi.org/10.1101/2024.09.20.614098

Shore, A., & Caldwell, J. M. (2019). Modes of coral disease transmission: How do diseases spread between individuals and among populations? *Marine Biology*, *166*(4), 45. https://doi.org/10.1007/s00227-019-3490-8

Sinclair, B. J., Marshall, K. E., Sewell, M. A., Levesque, D. L., Willett, C. S., Slotsbo, S., Dong, Y., Harley, C. D. G., Marshall, D. J., Helmuth, B. S., & Huey, R. B. (2016). Can we predict ectotherm responses to climate change using thermal performance curves and body temperatures? *Ecology Letters*, *19*(11), 1372–1385. https://doi.org/10.1111/ele.12686

Soetaert, K., Petzoldt, T., & Setzer, R. W. (2010). Solving Differential Equations in *R*: Package **deSolve**. *Journal of Statistical Software*, *33*(9). https://doi.org/10.18637/jss.v033.i09

Stark, K. A., Clegg, T., Bernhardt, J. R., Grainger, T. N., Kempes, C. P., Savage, V., O'Connor, M. I., & Pawar, S. (2024). Towards a more dynamic metabolic theory of ecology to predict climate change effects on biological systems. *The American Naturalist*, 733197. https://doi.org/10.1086/733197

Stark, K. A., Clegg, T., Bernhardt, J. R., Grainger, T. N., Kempes, C. P., Savage, V., O'Connor, M. I., & Pawar, S. (2025). Toward a more dynamic metabolic theory of ecology to predict climate change effects on biological systems. *The American Naturalist*, 000–000. https://doi.org/10.1086/733197

Stuart, S. N., Chanson, J. S., Cox, N. A., Young, B. E., Rodrigues, A. S. L., Fischman, D. L., & Waller, R. W. (2004). Status and trends of amphibian declines and extinctions worldwide. *Science*, *306*(5702), 1783–1786. https://doi.org/10.1126/science.1103538

Sunday, J. M., Bates, A. E., & Dulvy, N. K. (2011). Global analysis of thermal tolerance and latitude in ectotherms. *Proceedings of the Royal Society B: Biological Sciences*, *278*(1713), 1823–1830. https://doi.org/10.1098/rspb.2010.1295

Svendsen, M. B. S., Bushnell, P. G., & Steffensen, J. F. (2016). Design and setup of intermittent-flow respirometry system for aquatic organisms. *Journal of Fish Biology*, *88*(1), 26–50. https://doi.org/10.1111/jfb.12797

Szapudi, I. (2020). Heterogeneity in SIR epidemics modeling: Superspreaders and herd immunity. *Applied Network Science*, *5*(1), 93. https://doi.org/10.1007/s41109-020-00336-5

Tadiri, C. P., Kong, J. D., Fussmann, G. F., Scott, M. E., & Wang, H. (2019). A data-validated host-parasite model for infectious disease outbreaks. *Frontiers in Ecology and Evolution*, *7*, 307. https://doi.org/10.3389/fevo.2019.00307

Tao, Y., Hite, J. L., Lafferty, K. D., Earn, D. J. D., & Bharti, N. (2021). Transient disease dynamics across ecological scales. *Theoretical Ecology*, *14*(4), 625–640. https://doi.org/10.1007/s12080-021-00514-w

The IUCN Red List of Threatened Species. (2024). IUCN Red List of Threatened Species. https://www.iucnredlist.org/en

Therneau, T. M. (2022). ***coxme****: Mixed Effects Cox Models* (Version 2.2-18.1) [R]. doi.org/10.32614/CRAN.package.coxme

Therneau, T. M., & Grambsch, P. M. (2000). *Modeling survival data: Extending the Cox model.* (Books - 3rd Floor R853 .S7 T47 2000 LC). Springer; Oakland University Catalog. https://search.ebscohost.com/login.aspx?direct=true&AuthType=sso&db=cat09721a&AN=ouc.oai.edge.oakland.folio.ebsco.com.fs00001142.507edfd8.e177.5e39.92ac.9c043e870b04&site=eds-live&scope=site&authtype=sso&custid=s9275379

Thomas, V., Van Rooij, P., Meerpoel, C., Stegen, G., Wauters, J., Vanhaecke, L., Martel, A., & Pasmans, F. (2020). Instant killing of pathogenic chytrid fungi by disposable nitrile gloves prevents disease transmission between amphibians. *PLOS ONE*, *15*(10), e0241048. https://doi.org/10.1371/journal.pone.0241048

Torchiano, M. (2020). ***Effsize****—A package for efficient effect size computation* (Version 0.8.1) [R]. Zenodo. https://doi.org/10.5281/zenodo.1480624

Turner, A., Wassens, S., Heard, G., & Peters, A. (2021). Temperature as a driver of the pathogenicity and virulence of amphibian chytrid fungus *Batrachochytrium dendrobatidis*: A systematic review. *Journal of Wildlife Diseases*, *57*(3). https://doi.org/10.7589/JWD-D-20-00105

Underwood, N., Hambäck, P., & Inouye, B. D. (2005). Large-scale questions and small-scale data: Empirical and theoretical methods for scaling up in ecology. *Oecologia*, *145*(2), 176–177. https://doi.org/10.1007/s00442-005-0057-9

Van Drunen, S. G., McCune, J. L., & Husband, B. C. (2018). Distribution and environmental correlates of fungal infection and host tree health in the endangered American chestnut in Canada. *Forest Ecology and Management*, *427*, 60–69. https://doi.org/10.1016/j.foreco.2018.05.051

Van Rooij, P., Martel, A., D'Herde, K., Brutyn, M., Croubels, S., Ducatelle, R., Haesebrouck, F., & Pasmans, F. (2012). Germ tube mediated invasion of *Batrachochytrium dendrobatidis* in amphibian skin is host dependent. *PLOS ONE*, *7*(7), e41481. https://doi.org/10.1371/journal.pone.0041481

Van Rooij, P., Martel, A., Haesebrouck, F., & Pasmans, F. (2015). Amphibian chytridiomycosis: A review with focus on fungus-host interactions. *Veterinary Research*, *46*(1), 137. https://doi.org/10.1186/s13567-015-0266-0

Van Rooij, P., Pasmans, F., Coen, Y., & Martel, A. (2017). Efficacy of chemical disinfectants for the containment of the salamander chytrid fungus *Batrachochytrium salamandrivorans*. *PLOS ONE*, *12*(10), e0186269. https://doi.org/10.1371/journal.pone.0186269

Vasseur, D. A., DeLong, J. P., Gilbert, B., Greig, H. S., Harley, C. D. G., McCann, K. S., Savage, V., Tunney, T. D., & O'Connor, M. I. (2014). Increased temperature variation poses a greater risk to species than climate warming. *Proceedings of the Royal Society B: Biological Sciences*, *281*(1779), 20132612. https://doi.org/10.1098/rspb.2013.2612

Venesky, M. D., DeMarchi, J., Hickerson, C., & Anthony, C. D. (2022). Does the thermal mismatch hypothesis predict disease outcomes in different morphs of a terrestrial salamander? *Journal of Experimental Zoology Part A: Ecological and Integrative Physiology*, *337*(5), 467–476. https://doi.org/10.1002/jez.2581

Visher, E., & Boots, M. (2020). The problem of mediocre generalists: Population genetics and eco-evolutionary perspectives on host breadth evolution in pathogens. *Proceedings of the Royal Society B: Biological Sciences*, *287*(1933), 20201230. https://doi.org/10.1098/rspb.2020.1230

Voyles, J., Young, S., Berger, L., Campbell, C., Voyles, W. F., Dinudom, A., Cook, D., Webb, R., Alford, R. A., Skerratt, L. F., & Speare, R. (2009). Pathogenesis of chytridiomycosis, a cause of catastrophic amphibian declines. *Science*, *326*(5952), 582–585. https://doi.org/10.1126/science.1176765

Vredenburg, V. T., Knapp, R. A., Tunstall, T. S., & Briggs, C. J. (2010). Dynamics of an emerging disease drive large-scale amphibian population extinctions. *Proceedings of the National Academy of Sciences*, *107*(21), 9689–9694. https://doi.org/10.1073/pnas.0914111107

Webb, R., Mendez, D., Berger, L., & Speare, R. (2007). Additional disinfectants effective against the amphibian chytrid fungus *Batrachochytrium dendrobatidis*. *Diseases of Aquatic Organisms*, *74*, 13–16. https://doi.org/10.3354/dao074013

Weldon, C., Du Preez, L. H., Hyatt, A. D., Muller, R., & Speare, R. (2004). Origin of the amphibian chytrid fungus. *Emerging Infectious Diseases*, *10*(12), 2100–2105. https://doi.org/10.3201/eid1012.030804

Wells, K. D., Taigen, T. L., & O'Brien, J. A. (1996). The effect of temperature on calling energetics of the spring peeper (*Pseudacris crucifer*). *Amphibia-Reptilia*, *17*, 149:158.

Wickham, H. (2016). ***ggplot2****: Elegant Graphics for Data Analysis*. Springer-Verlag New York. https://ggplot2.tidyverse.org

Wilber, M. Q., Knapp, R. A., Toothman, M., & Briggs, C. J. (2017). Resistance, tolerance and environmental transmission dynamics determine host extinction risk in a load-dependent amphibian disease. *Ecology Letters*, *20*(9), 1169–1181. https://doi.org/10.1111/ele.12814

Wilber, M. Q., Langwig, K. E., Kilpatrick, A. M., McCallum, H. I., & Briggs, C. J. (2016). Integral Projection Models for host–parasite systems with an application to amphibian chytrid fungus. *Methods in Ecology and Evolution*, *7*(10), 1182–1194. https://doi.org/10.1111/2041-210X.12561

Wilber, M. Q., Pfab, F., Ohmer, M. E., & Briggs, C. J. (2021). Integrating infection intensity into within- and between-host pathogen dynamics: Implications for invasion and virulence evolution. *The American Naturalist*, *198*(6), 661–677. https://doi.org/10.1086/716914

Wilson, R. S., & Franklin, C. E. (2002). Testing the beneficial acclimation hypothesis. *Trends in Ecology & Evolution*, *17*(2), 66–70. https://doi.org/10.1016/S0169-5347(01)02384-9

Woodhams, D. C., Alford, R. A., Briggs, C. J., Johnson, M., & Rollins-Smith, L. A. (2008). Life-history trade-offs influence disease in changing climates: Strategies of an amphibian pathogen. *Ecology*, *89*(6), 1627–1639. https://doi.org/10.1890/06-1842.1

Woodhams, D. C., LaBumbard, B. C., Barnhart, K. L., Becker, M. H., Bletz, M. C., Escobar, L. A., Flechas, S. V., Forman, M. E., Iannetta, A. A., Joyce, M. D., Rabemananjara, F., Gratwicke, B., Vences, M., & Minbiole, K. P. C. (2018). Prodigiosin, Violacein, and Volatile Organic Compounds Produced by Widespread Cutaneous Bacteria of Amphibians Can Inhibit Two Batrachochytrium Fungal Pathogens. *Microbial Ecology*, *75*(4), 1049–1062. https://doi.org/10.1007/s00248-017-1095-7

WorldClim. (2024). https://www.worldclim.org/

Xiao, X., White, E. P., Hooten, M. B., & Durham, S. L. (2011). On the use of log-transformation vs. Nonlinear regression for analyzing biological power laws. *Ecology*, *92*(10), 1887–1894. https://doi.org/10.1890/11-0538.1

Yvon-Durocher, G., Montoya, J. M., Trimmer, M., & Woodward, G. (2011). Warming alters the size spectrum and shifts the distribution of biomass in freshwater ecosystems. *Global Change Biology*, *17*(4), 1681–1694. https://doi.org/10.1111/j.1365-2486.2010.02321.x

Zipkin, E. F., Jennelle, C. S., & Cooch, E. G. (2010). A primer on the application of Markov chains to the study of wildlife disease dynamics. *Methods in Ecology and Evolution, 1*(2), 192–198. https://doi.org/10.1111/j.2041-210X.2010.00018.x

Zumbado-Ulate, H., García-Rodríguez, A., & Searle, C. L. (2021). Species distribution models predict the geographic expansion of an enzootic amphibian pathogen. *Biotropica*, *53*(1), 221–231. https://doi.org/10.1111/btp.12863